

L. Sors

Fatigue
of design
machine
components

Akadémiai Kiadó, Budapest

**FATIGUE DESIGN
OF MACHINE COMPONENTS**

FATIGUE DESIGN
OF
MACHINE COMPONENTS

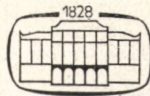
BY

L. SORS

Consultant Mechanical Engineer

English translation editor

S. E. MITCHELL



AKADÉMIAI KIADÓ · BUDAPEST 1971

The original edition

GÉPELEMEK MÉRETEZÉSE KIFÁRADÁSRA
was published by Műszaki Kiadó, Budapest

© Akadémiai Kiadó, Budapest 1971

Joint edition published by Akadémiai Kiadó, Budapest and Pergamon Press, London · Oxford

Printed in Hungary

Contents

Editor's Note	ix
Preface	xi
Introduction	xiii

Part I. Theoretical Basis

1. Fatigue Diagrams	1
1.1 Wöhler tests	1
1.2 Types of cyclic stress	2
1.3 Load spectrum	4
1.4 $S-N$ curves, and an outline of the metal-physics aspects of fatigue	5
1.5 The equations of the $S-N$ curves	6
1.6 Determination of fatigue limit	16
1.6.1 "Staircase" method of determining fatigue limit	16
1.6.2 Rapid method of determining fatigue limit: the Locati method	18
1.7 Fatigue diagrams	21
1.7.1 Smith diagrams	21
1.7.2 Haigh diagrams	24
1.7.3 Moore-Kommers-Jasper diagrams	25
1.7.4 Use of data in literature	26
1.8 Fatigue fractures: their causes and appearance	26
1.8.1 Causes	26
1.8.2 Appearance	27
2. Fatigue Diagrams of Various Materials	32
2.1 Steel	32
2.2 Cast iron	37
2.3 Malleable cast iron	37
2.4 Light alloys	38
2.5 Non-ferrous metals	39
2.6 Plastics	39
3. Effect of Various Factors on Fatigue Strength	40
3.1 Surface finish	40
3.2 Shape and dimensions	42
3.3 Temperature	44
3.3.1 Elevated temperatures	44
(a) Steels	44
(b) Non-ferrous metals and light alloys	45
3.3.2 Low temperatures	46
3.4 Surface treatment	46
3.4.1 Surface hardening	46
3.4.2 Surface rolling	48

3.4.3 Electrolytic deposits	48
3.4.4 Metal spraying	49
3.5 Corrosion	50
3.5.1 Composition of materials	50
3.5.2 Liquids producing corrosion	51
3.5.3 Number of load cycles	51
3.5.4 Loading frequency	51
3.5.5 Type of stress	51
3.5.6 Mean stress	51
3.6 Fretting corrosion	52
3.7 Previous history	52
3.7.1 Occasional stresses above yield	52
3.7.2 Cumulative damage	53
3.7.3 "Coaxing" of steels	53
4. Theoretical Stress Concentration Factor	55
4.1 The Neuber nomogram	55
4.1.1 Application of the basic nomogram	55
4.2 Tables of stress concentration factor	56
4.3 Multiple stress raisers	57
4.3.1 Effect of multiple stress raisers closely spaced in the line of action of the stress	58
4.3.2 Effect of multiple stress raisers in a line perpendicular to the line of action of the stress	59
4.3.3 Intersecting stress raisers	60
5. Fatigue Strength Reduction Factors	62
5.1 Fatigue strength reduction factors according to the conservative theory	62
5.2 The Bollenrath-Troost method	64
5.3 The Siebel method	65
6. Factor of Safety	67
6.1 Uniaxial stresses	67
6.1.1 Soderberg's proposal	67
6.1.2 The VDI proposal	68
6.1.3 Kimmelmann's proposal	68
6.1.4 Factor of safety in finite-life fatigue	68
6.2 Complex and combined stresses	69
6.3 Numerical values of the factor of safety	70
7. Fatigue Design	72
7.1 Conservative design	72
7.2 Design using the Harris notch sensitivity factor	73
7.3 Design by the Bollenrath-Troost theory	73
7.4 Design by the Siebel theory	74
7.5 Example	74
7.5.1 Conservative method	74
7.5.2 Determination of K_f according to Harris	76
7.5.3 The Bollenrath-Troost method	77
7.5.4 The Siebel method	77
8. Fatigue Design of Some Machine Components	79
8.1 Shafts and journals	79
8.2 Shrink-fit and keyed joints	81
8.3 Ball and roller bearings	81
8.4 Bolts	82
8.5 Springs	84

8.6 Welded joints	86
8.7 Plates with holes at each end	87
8.8 Points to remember in designing for increased life of machine components	87
Summary	89
List of Symbols	90
References and Sources of Further Information	93

Part II. Tables and Diagrams

General Summary of Fatigue Design (as described in Section 7 of Part I)	2
Conservative method	2
Fatigue strength reduction factor q_H by Harris theory	3
Bollenrath-Troost theory	3
Siebel theory	4

Chapter or section number of Part I

1. Fatigue Diagrams	6
1.5 The equations of the $S-N$ curves	6
Table 1. Weibull formula constants	6
2. Fatigue Diagrams of Various Materials	9
Table 2. Rotating-bending fatigue strength of some plastics	19
Table 3. Rotating-bending fatigue strength of some light alloys	21
Table 4. Fatigue strength of light alloys with $N=50 \times 10^6$	22
Table 5. Fatigue strength of copper and some of its alloys	26
3. Effect of Various Factors on Fatigue Strength	28
3.1 Surface finish	28
3.2 Shape and dimensions	29
3.3 Temperature	30
3.5 Corrosion	32
Table 6. Effect of corrosion on cast steel parts	34
Table 7. Effect of corrosion on the fatigue strength of cast iron	34
Table 8. Effect of corrosion on the fatigue strength of some metals and alloys	35
Table 9. Bending fatigue strength of steels in various kinds of water	35
Table 10. Bending fatigue strength of steels in steam	36
Table 11. Effect of the number of load cycles on fatigue strength	36
4. Theoretical Stress Concentration Factor	37
Table 12. Theoretical stress concentration factors	39
5. Fatigue Strength Reduction Factors	58
6. Factor of Safety	86
Table 13. Factor of safety	86
Table 14. Multiplying coefficients for the factor of safety	86
8. Fatigue Design of some Machine Components	88
8.1 Shafts and journals	88
Table 15. Fatigue strength reduction factor K_f for flanged shafts	88
8.2 Shrink-fit and keyed joints	90
Table 16. Fatigue strength reduction factor K_f for splined shaft in torsion	90
Table 17. Nomenclature for the materials used in the determination of the fatigue strength reduction factor of the various wheel hubs	91
Table 18. Summary of the results of tests carried out by A. Thum to determine the fatigue strength reduction factors of wheel hubs	92
8.3 Ball and roller bearings	94

8.4 Bolts	98
Table 19. Fatigue strength reduction factor K_t for bolts	98
8.5 Springs	98
Table 20. Fluctuating torsion fatigue strength of piano wires of various sizes	98
Table 21. Factors of various endurances for some spring materials	99
8.6 Welded joints	102
Table 22. Formulae for the determination of nominal stress for various types of welded joints	102
Table 23. "z to s" lines for welded joints	103
Table 24. Values of Φ_k for steels St 37 (0.15% C steel) and St 52 (En 7 approx.)	104
8.7 Plates with holes at each end	108
Table 25. Fatigue strength reduction factors of bars and various shapes, drilled at both ends	108

Editor's Note

THE following pages contain an abundance of the data and procedures needed for fatigue design of machine components. Since, however, the boundaries of knowledge in this field are continually advancing, the designer wishing to keep abreast of the latest developments is strongly recommended to supplement his reading of the book by studying the Design Data Sheets on fatigue which are published from time to time by the Engineering Sciences Data Unit, 251-259 Regent Street, London W1R 7AD.

Preface

THE reader will find in this work a practical aid to the design of machine components subjected to cyclic stresses.

A short review (Part I) of the methods of calculation used in current theoretical investigations, which are being continually broadened by the acquisition of new knowledge, is followed by numerical data derived from research, contained in tables and diagrams (Part II), without which the theory would not be utilizable in practice, for most of the results of the very extensive and ramified research work are scattered over a wide range of periodicals.

The book deals with the fatigue strength of various materials of construction (steels, other metals, plastics) and the factors by which it is mostly affected (surface finish, surface treatment, size of workpiece, corrosion, heat treatment, thermal effects, life, overload, etc.).

The determination of the theoretical stress concentration factor and the fatigue strength reduction factor is greatly simplified by a series of special nomograms. Instructions are given for the calculation procedure and the determination of safety factors.

Designers can effect considerable economies in size and savings in material with the help of this book. In addition, it offers research workers a valuable survey of the field (particularly in the comprehensive bibliography). It will also be of great service as a textbook in universities and colleges of technology.

Introduction

MOST machines and appliances have to withstand frequent load variations. To take only a few examples, the load on vehicles and transport equipment, power generators and converters, machine tools and agricultural machinery, is perpetually changing.

Variation of the load on machines involves variation of the load on their components, and in fact the load (or the direction of the load) on individual components very often varies even when the load on the machine as a whole remains unchanged — a typical example being a rotating shaft subject to bending.

As long ago as the beginning of the nineteenth century it was established that the stress which a material could resist was much higher if it was held at a steady value than if it was repeatedly reversed, say a million or more times. After a certain number of loading cycles fracture takes place at stresses which would be harmless if applied statically.

It was BACH who, on the evidence of WÖHLER's tests, first divided the permissible stresses for steels into three categories, viz. those for (i) static, (ii) reversed, and (iii) fluctuating stress. This classification was in general use for a long time, and it is still applicable in cases when special accuracy is not required.

Consideration of the yield point and the safety factor led to the assignment of the ratio 3 : 2 : 1 to the permissible stresses in these three categories in order.

Development in engineering, more especially in transport and aviation, and the striving for economical design, called for a careful re-appraisal of all methods of calculation, for the factors of safety in common use were being shown to be on the whole too large — though in quite a number of cases too small. Too large a factor of safety results in overdimensioning and increased weight and power consumption. Too small a factor of safety, on the other hand, causes premature fracture, operating troubles, accidents or even, in some circumstances, danger to life.

Understanding the behaviour of a material under fluctuating load is not a simple matter. Under static load the permissible stress in a material depends on the cross-section, the type of stress, and the composition of the material. Under fluctuating load, however, other factors, such as surface finish, number of stress cycles, and, in some cases, corrosion, also have an effect. Investigation has been adversely affected by the fact that the theoretical and practical principles of the measurement of surface roughness were not established until recently, added to which the necessary measuring instruments were not available. This partly explains the frequent very considerable differences or even contradictions in results of investigations.

It can be stated without hesitation that the whole former concept of design for fatigue conditions has needed rethinking. Thus, for example, if calculation by the methods hitherto used indicated a high stress, a high-strength alloy would be selected. Recent

researches have shown that this is not always correct, because in the presence of a notch steels of higher strength show a vulnerability not exhibited by plain carbon steels, and it can thus happen that they withstand a smaller instead of a greater number of cycles. The specifying of surface roughness not only serves aesthetic ends but is very important in regard to the endurance of the workpiece. Deciding on the fillet radius at the end of a shaft (which used to be drawn routine-fashion using any template to hand) has proved to be just as important as a proper choice of material.

Designers have so far made relatively little use of the modern methods of fatigue design. This is due to the lack not so much of theoretical treatment — which is already sufficiently provided in textbooks — as of actual numerical values.

The present work, then, can most effectively help to make the new methods known if in conjunction with a short explanatory summary of the theory, followed by appropriate critical comments, it offers designers all the relevant data now available or to be extracted from the literature. This has been attempted in the following pages.

PART I

THEORETICAL BASIS

CHAPTER 1

Fatigue Diagrams

1.1 Wöhler tests

It was about a hundred years ago (1870) that WÖHLER's classic paper *On Mechanical Tests with Iron and Steel* (*Über die Festigkeitsversuche mit Eisen und Stahl – Zeitschrift für Bauwesen*) appeared – based on twelve years' laboratory experiments. In this paper WÖHLER showed quantitatively that railway-wagon axles broke when repeatedly subjected to a load that they could carry quite safely if it were applied statically. Despite fairly general acquaintance with this fact, the beginnings of the design of engineering components in relation to "fatigue strength" have been only recent. C. BACH made a systematic summary of WÖHLER's results, and his important work *Engineering Components – their Design and Construction* (*Die Maschinenelemente, ihre Berechnung und Konstruktion*, Stuttgart, 1880) was the first book on this subject.

Since then the effect of cyclic loading – "fatigue" of materials – has become one of the most frequently and variously treated chapters of the strength of materials. Yet even now it cannot be said that every aspect of the problem has been clarified.

For years or even decades the test results obtained were sometimes contradictory, for the effects of certain factors on the fatigue strength of materials became clear only later – like the surface finish of the test piece or the component, for instance. Only in the last decade or so has it been possible to express this latter quantitatively and to achieve precise repeatability in production, thus making the study of the effect of surface finish on fatigue strength practicable. Inconsistencies in the results of earlier tests carried out without proper precautions in this respect are not surprising. As another example, even today there is no suitable means of measuring degree of corrosion, and yet this too is a factor that has a considerable influence on fatigue strength.

The laws of fatigue, and the aim of increasing the life of materials as much as possible, have greatly altered the outlook of designers. The carefree sketching-in of the radius joining the different diameters of a shaft which prevailed in former times has been replaced by an exhaustive consideration from the fatigue point of view. Previously no one worried over using a high-alloy material for a component in which the loading produced a high stress. In fatigue, however, these materials are very sensitive to stress concentrations, and it can easily happen that a component made from high-alloy material will withstand fewer load cycles than one made from plain carbon steel.

Accurate knowledge of fatigue phenomena is of the greatest importance in economical dimensioning of machines and components. It often happens that because of the variability in fatigue endurance, components that are still sound are rejected along with one that has come to the end of its safe life. If endurances were definitely known, it would in most cases be possible to reduce manufacturing costs by reducing the dimensions of those components that had an unnecessarily high endurance, or by changing the material used.

Dimensioning in relation to fatigue is of particular importance in the motor industry, where the vehicle weight exerts a telling influence on the fuel consumption and so on the running costs.

1.2 Types of cyclic stress

In studying the fatigue strength of materials or components the first thing to do is to classify the different types of stress fluctuation. Fluctuation implies an upper and a lower limit of load, and consequently an upper and a lower limit of the stress produced in the component. Denote the former by σ_u and the latter by σ_l . The fluctuation can be considered as a stress of amplitude $\pm \sigma_a$ superimposed on a steady average stress σ_m . Thus

$$\sigma_l = \sigma_m - \sigma_a$$

and

$$\sigma_u = \sigma_m + \sigma_a$$

The stress fluctuation, with its amplitude σ_a , may take place in a continuously increasing and decreasing fashion; the stress at any instant then varies according to the well-known sine curve (see Fig. 1.1). On the other hand the fluctuation may be abrupt (discontinuous),¹ and then the stress at any instant is represented by a square-cornered pattern

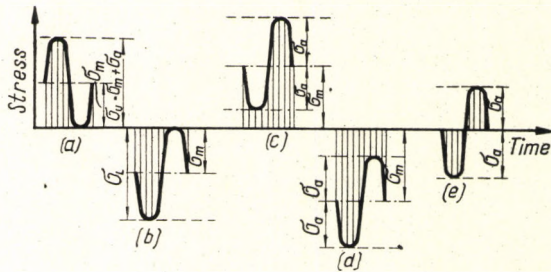


FIG. 1.1. Continuously varying cyclic stress

- (a) — Fluctuating tensile stress between 0 and σ_u
- (b) — Fluctuating compressive stress between 0 and $-\sigma_u$
- (c) — Fluctuating tensile stress between $+\sigma_l$ and $+\sigma_u$
- (d) — Fluctuating compressive stress between $-\sigma_l$ and $-\sigma_u$
- (e) — Reversed symmetrical stress between $+\sigma_u$ and $\sigma_l = -\sigma_u$

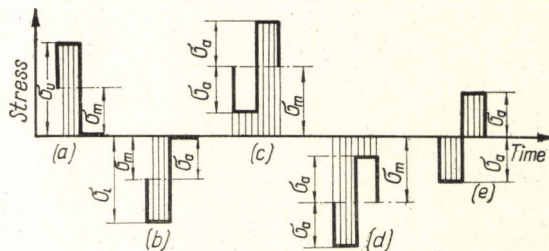


FIG. 1.2. Abruptly varying cyclic stress

- (a), (b), (c), (d) — Fluctuating stresses
- (e) — Reversed symmetrical stress

of lines (see Fig. 1.2). The special but frequently occurring case in which $\sigma_m = 0$, i.e. $\sigma_l = -\sigma_u$, is given the name of *reversed (symmetrical)* stress, and that in which $\sigma_l = 0$, i.e. $\sigma_u = 2\sigma_a$, *repeated* stress.

The quotient $R = \sigma_l/\sigma_u$ is termed the "stress ratio". Its value is:

- 1 when $\sigma_m = 0$
- 0 when $\sigma_l = 0$
- 1 when $\sigma_l = \sigma_u$

for which reason the first case is usually denoted in the literature by

$$\sigma_{-1},$$

the second by

$$\sigma_0,$$

and the third by

$$\sigma_{+1}.$$

The number of load cycles is usually denoted by N and the frequency by n (i.e. $N=nt$).

The above is also fully valid when torsional or shear stresses occur in the component instead of tensile-compressive or bending stresses.

From the series of experiments already mentioned, WÖHLER established that the fatigue strength of components depends not only on the maximum stress σ_u , but also on the minimum stress σ_l , and thus also on σ_m . Originally he presented his results in tables, but later, for practical utility, he gave them in the form of graphs, with the logarithm of the number N of stress cycles as abscissa and the value of σ as ordinate. One of his tables of results is reproduced below, and the σ - N (or, as commonly known, "S-N") curve plotted from them is shown in Fig. 1.3.

Railway-wagon axle, machined.

Material: "Phoenix" steel, tensile strength $\sigma_T = 3\ 250\ \text{kgf/cm}^2$.

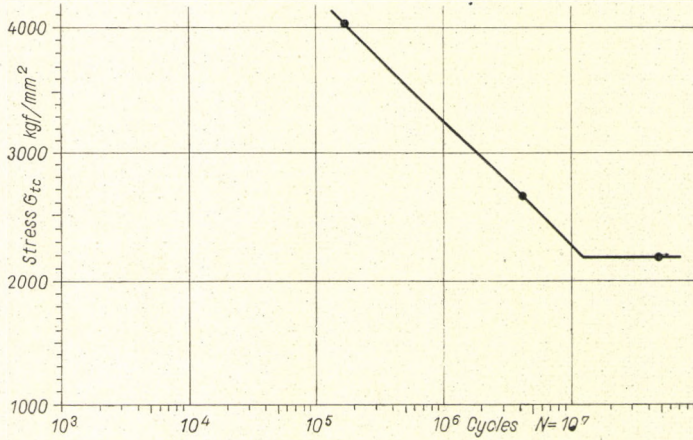
Type of loading: tensile.

σ_l	σ_u kgf/cm ²	N
0	4 010	169 750
0	2 630	4 035 400
0	2 190	48 200 020 (unbroken)

On the basis of this test the "fatigue limit" (or "fatigue strength") σ_{ref} of the axle was determined as 2 190 kgf/cm². This means that the test piece (or component) would sustain without fracture a tensile stress of 2 190 kgf/cm² repeated "any desired number" of times — which in practice may amount to many millions of cycles.

To shorten the testing time, it is usual with steels to carry out fatigue tests only as far as $N = 1$ to 2, or exceptionally 5 million cycles, as may be agreed; for experience shows that if a test piece will sustain this number of cycles it will not break however many similar cycles are applied to it.

WÖHLER's results mentioned above are, however, applicable only to a very limited extent in practice, because they are valid (1) only for tensile loading, and then (2) only

FIG. 1.3. S - N curve for railway-wagon axle

if $\sigma_l = 0$. For practical application a diagram is needed from which fatigue limits can be read off not only for $\sigma_l = 0$ but for any other loading conditions (any tension-compression fatigue limit). This purpose is best served by the diagrams known as the SMITH, HAIGH and MOORE-KOMMERS diagrams, which we will come back to later.

1.3 Load spectrum

The variation of stress amplitude in components with changing load in the machines of which they form part has already been discussed in the Introduction, and need not be gone into further here. It is evident that the stress in the connecting-rod of a car engine will have different values at running speeds of, for example, 20 and 60 miles per hour. Again, there will be little stress when the car is running on a level road, but when it is going uphill the stress will be high.

The endurance of machine components is, of course, considerably affected by variation of stress amplitude. For a reasonable prediction of endurance, the stress variation must be imitated in fatigue tests.

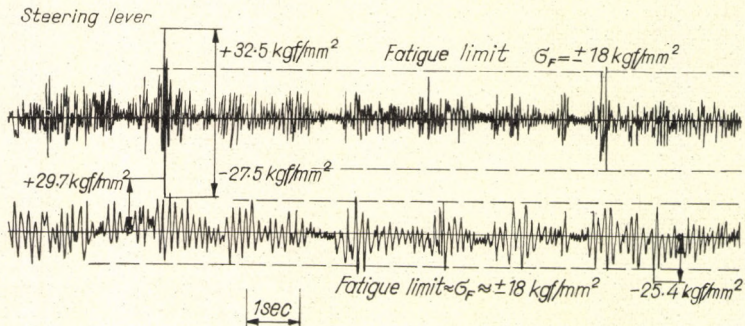


FIG. 1.4. Record of stress variation

With this in view, fatigue tests not long ago used to be preceded by a determination of the spectrum (distribution) of loading. This was effected by fitting strain gauges or magnetostriction sensing elements, photographing the traces which they gave on oscilloscope screens, and stating the frequency of given stress levels (Figs. 1.4 and 1.5). Owing to the vast amount of work required to evaluate the film records, preference has recently been shown for devices which automatically count the frequency of the individual stress levels. The structure and operation of a portable device of this kind, called a histometer, is described by RUDNAI [79].

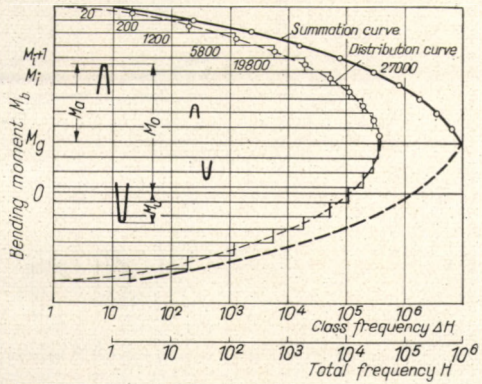


FIG. 1.5. Bending moment (and stress) frequency distribution

When the frequency of the various stress levels is known a programme-controlled fatigue testing machine can be used to reproduce very closely in a specimen the actual stress in the machine component concerned. This is an essential condition for reliable prediction of endurance.

1.4 S-N curves, and an outline of the metal-physics aspects of fatigue

If S-N curves obtained from fatigue tests on various steels are studied, a great deal of similarity will be noticed. Up to a few hundred or thousand cycles the test pieces sustain a stress only slightly lower than they would in the familiar static tensile test. At an endurance of several thousand cycles, however, their load-carrying capacity rapidly diminishes, i.e. the S-N curve begins to drop sharply. But ultimately all types of steel reach a limiting stress which the test piece will withstand without fracture, even at many millions of cycles. Thus three phases of the S-N curve can be distinguished (Fig. 1.6). Phase I is the low-cycle fatigue phase, Phase II is that of high-range fatigue' and Phase III that of low-range fatigue. The mechanism of fatigue of the material is quite different in these three phases.

Phase I – the phase of static or low-cycle loading – occurs comparatively rarely in practice, for there are very few machine components whose loading, at least during their actual working lives, is completely or almost completely static. The properties of the material determined on ordinary static testing machines are usually, therefore, not really significant. If the loading varies (or even changes direction) a few hundred times, then, as tests have shown, “damage” occurs in the interior of the material, though it does not appear at the surface until later.

Phase II is of greater practical importance. If the surface of the test piece is viewed under high magnification, bands of lines at an angle with the length of the test piece can be observed. They reveal the slip planes at the surface. Slip planes occur at places where dislocations are present in the crystallites. Slip beginning at these places will sooner or later, under the influence of repeated loading, reach the surface of the test piece, appearing as microcracks.

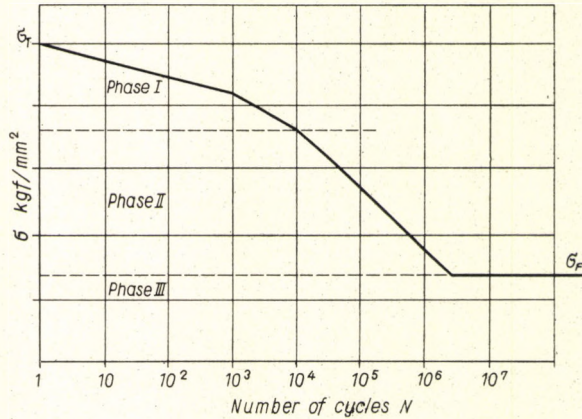


FIG. 1.6. Features of the $S-N$ curve

If the loading is sufficiently high, these microcracks develop into macrocracks, and finally fracture occurs. It can happen, however, that the dislocation is blocked if any obstruction lies in the path of the microcrack and the stress caused by the loading is not high enough to overcome the obstruction. In this way Phase III, the low-range fatigue phase, comes into operation below a certain level of stress.

According to LEBEDYEV [45], an effective obstruction in the path of the dislocation is formed only by those stray atoms that penetrate into the lattice of the steel atoms. For this reason "blocking of microcracks" and a "fatigue limit" can be spoken of only for those metals in which stray atoms can be incorporated in the lattice. Such are, for example, the various steels, but not light alloys, which are known not to comply with the necessary condition and for which, therefore, it is not possible to have a fatigue limit in the proper sense. With light alloys the $S-N$ curve tends to fall even in Phase III. For these metals, therefore, the "fatigue limit" is taken, for want of a better criterion, as the stress at which they withstand ten million cycles.

As in Phase II and Phase III the position of the slip planes and the occurrence of dislocations are entirely "random" phenomena, modern investigations are based on probability theory, which treats random events mathematically.

1.5 The equations of the $S-N$ curves

As $S-N$ curves are all very similar, and straight lines in the $\sigma-\log N$ coordinate system approximate quite closely to their individual parts, attempts have been made to represent them by a mathematical equation. The aim is readily understandable. If the equation of the $S-N$ curves (straight lines) can be successfully put into mathematical form, then deductions about the behaviour of a material — even at different stress levels — can be drawn from extremely few measured values.

On the basis of calculations and tests, Stüssi [89] formulated an equation for the $S-N$ curve as follows:

$$\sigma_E = \frac{\sigma_T + CN^p \sigma_F}{1 + CN^p} \quad (\text{kgf/mm}^2). \quad (1)$$

Here C and p denote constants depending upon the material. Thus, when the tensile strength σ_T and the fatigue limit σ_F of the material are known, the endurance limit σ_E for fatigue failure at a given number of cycles N may be calculated. The value σ_F may relate to repeated, fluctuating or reversed stress, and σ_E will relate to the same type of stress.

For practical purposes it is best to transform equation (1) as follows:

$$\sigma_E = \frac{\sigma_T + CN^p \sigma_F}{1 + CN^p}$$

whence

$$\sigma_E + \sigma_E CN^p = \sigma_T + CN^p \sigma_F$$

or

$$\sigma_T - \sigma_E = N^p C (\sigma_E - \sigma_F)$$

and thus we have

$$\frac{\sigma_T - \sigma_E}{\sigma_E - \sigma_F} = N^p C$$

or

$$\log \frac{\sigma_T - \sigma_E}{\sigma_E - \sigma_F} = p \log N + \log C$$

and denoting $\log N$ by i ,

$$\log \frac{\sigma_T - \sigma_E}{\sigma_E - \sigma_F} = pi + \log C.$$

To determine the constants p and C , a trial-and-error method is used to find the value of σ_F which gives a straight-line relationship between $\log \frac{\sigma_T - \sigma_E}{\sigma_E - \sigma_F}$ and $\log N$.

EXAMPLE. The following experimental results were obtained:

$$\sigma_T = 39 \text{ kgf/mm}^2$$

Test No.	σ_E	N	$\log N$
1	$\sigma_{E1} = 27 \text{ kgf/mm}^2$	$N_1 = 255\,000$	$\log N_1 = 5.407$
2	$\sigma_{E2} = 21 \text{ kgf/mm}^2$	$N_2 = 408\,000$	$\log N_2 = 5.611$
3	$\sigma_{E3} = 18 \text{ kgf/mm}^2$	$N_3 = 970\,000$	$\log N_3 = 5.987$

First trial value: $\sigma_F = 15 \text{ kgf/mm}^2$. This gives

$$\log \frac{\sigma_T - \sigma_{E1}}{\sigma_{E1} - \sigma_F} = \log \frac{39 - 27}{27 - 15} = \log \frac{12}{12} = 0$$

$$\log \frac{\sigma_T - \sigma_{E2}}{\sigma_{E2} - \sigma_F} = \log \frac{39 - 21}{21 - 15} = \log \frac{18}{6} = 0.477$$

$$\log \frac{\sigma_T - \sigma_{E3}}{\sigma_{E3} - \sigma_F} = \log \frac{39 - 18}{18 - 15} = \log \frac{21}{3} = 0.845.$$

When the three values of $\log \frac{\sigma_T - \sigma_E}{\sigma_E - \sigma_F}$ are plotted against the corresponding values of $\log N$, the points do not lie on a straight line, and another value of σ_F must be tried. Second trial value: $\sigma_F = 17.5 \text{ kgf/mm}^2$. This gives

$$\log \frac{\sigma_T - \sigma_{E1}}{\sigma_{E1} - \sigma_F} = 0.102$$

$$\log \frac{\sigma_T - \sigma_{E2}}{\sigma_{E2} - \sigma_F} = 0.711$$

$$\log \frac{\sigma_T - \sigma_{E3}}{\sigma_{E3} - \sigma_F} = 1.623.$$

When these values are plotted, the points lie, to a close approximation, on a straight line; so the value $\sigma_F = 17.5 \text{ kgf/mm}^2$ is adopted (Fig. 1.7).

If $\log \frac{\sigma_T - \sigma_E}{\sigma_E - \sigma_F}$ is denoted by y and $\log N$ by x , the equation of the straight line can be obtained from the well-known formula

$$y - y_1 = \frac{y_3 - y_1}{x_3 - x_1} (x - x_1).$$

From Fig. 1.7 we have

$$x_1 = 5.407 \quad x_3 = 5.987$$

$$y_1 = 0.102 \quad y_3 = 1.623$$

whence

$$y = 2.62x - 14.08.$$

The equation of the straight line then reads

$$\log \frac{39 - \sigma_E}{\sigma_E - 17.5} = 2.62 \log N - 14.08$$

$$\log N = 5.40 + 0.382 \log \frac{39 - \sigma_E}{\sigma_E - 17.5}.$$

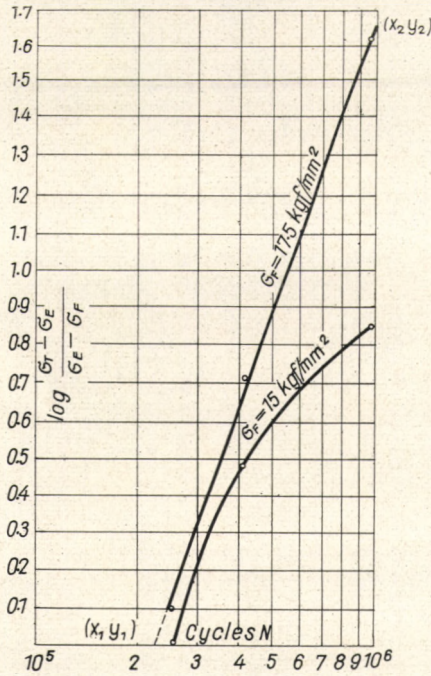


FIG. 1.7. Determination of constants in Strüssi's equation

WEIBULL [111] assumed that the $\log \sigma - \log N$ curve approximates closely to a straight line, and stated the following relationship:

$$\log N = \log k - m \log (\sigma_E - \sigma_F).$$

With steels, for endurances between 10^5 and 2 to 4×10^6 cycles, the above formula gives a close approximation to experimental values. The constants k and m can be found from experimentally determined values of σ_E and N , as follows:

Three specimens are tested in fatigue to fracture at different stresses. The endurances and associated stresses are denoted respectively by:

$$\begin{array}{ll} N_1 & \sigma_{E1} \\ N_2 & \sigma_{E2} \\ N_3 & \sigma_{E3} \end{array}$$

$$(N_1 < N_2 < N_3; \sigma_{E1} > \sigma_{E2} > \sigma_{E3}).$$

The WEIBULL formula may be written:

$$N = k(\sigma_E - \sigma_F)^{-m}$$

or

$$N(\sigma_E - \sigma_F)^m = k.$$

Thus:

$$N_1(\sigma_{E1} - \sigma_F)^m = k$$

$$N_2(\sigma_{E2} - \sigma_F)^m = k$$

$$N_3(\sigma_{E3} - \sigma_F)^m = k$$

or, by substitution:

$$N_1(\sigma_{E1} - \sigma_F)^m = N_2(\sigma_{E2} - \sigma_F)^m$$

$$N_1(\sigma_{E1} - \sigma_F)^m = N_3(\sigma_{E3} - \sigma_F)^m,$$

giving

$$\frac{N_1}{N_2} = \left(\frac{\sigma_{E2} - \sigma_F}{\sigma_{E1} - \sigma_F} \right)^m \quad \frac{N_1}{N_3} = \left(\frac{\sigma_{E3} - \sigma_F}{\sigma_{E1} - \sigma_F} \right)^m$$

Taking logarithms,

$$\log \frac{N_1}{N_2} = m \log \left(\frac{\sigma_{E2} - \sigma_F}{\sigma_{E1} - \sigma_F} \right)$$

$$\log \frac{N_1}{N_3} = m \log \left(\frac{\sigma_{E3} - \sigma_F}{\sigma_{E1} - \sigma_F} \right),$$

whence

$$\frac{\log \frac{N_1}{N_2}}{\log \frac{N_1}{N_3}} = \frac{\log \left(\frac{\sigma_{E2} - \sigma_F}{\sigma_{E1} - \sigma_F} \right)}{\log \left(\frac{\sigma_{E3} - \sigma_F}{\sigma_{E1} - \sigma_F} \right)},$$

$$\text{i.e. } \frac{\log N_1 - \log N_2}{\log N_1 - \log N_3} = \frac{\log(\sigma_{E2} - \sigma_F) - \log(\sigma_{E1} - \sigma_F)}{\log(\sigma_{E3} - \sigma_F) - \log(\sigma_{E1} - \sigma_F)}.$$

A few values of σ_F are now assumed. The corresponding values of the right-hand side of the equation are plotted against σ_F . A curve is drawn through the resulting points, and the point on the curve which gives the value of the left-hand side of the equation corresponds to the required value of σ_F .

Let us calculate σ_F in this way, using the data of the example given above.

Test No.	N_n	σ_{En}
1	255 000	27 kgf/mm ²
2	408 000	21 kgf/mm ²
3	970 000	18 kgf/mm ²

Assuming that $\sigma_F = 17$ kgf/mm²,

$$\frac{\log \left(\frac{21 - 17}{27 - 17} \right)}{\log \left(\frac{18 - 17}{27 - 17} \right)} = \frac{\log 0.4}{\log 0.1} = \frac{0.602 - 1}{0 - 1} = 0.398.$$

If $\sigma_F = 16 \text{ kgf/mm}^2$,

$$\frac{\log \left(\frac{21 - 16}{27 - 16} \right)}{\log \left(\frac{18 - 16}{27 - 16} \right)} = \log \frac{0.455}{0.182} = \frac{0.658 - 1}{0.260 - 1} = 0.462.$$

Finally, if $\sigma_F = 15 \text{ kgf/mm}^2$,

$$\frac{\log \left(\frac{21 - 15}{27 - 15} \right)}{\log \left(\frac{18 - 15}{27 - 15} \right)} = \frac{\log 0.500}{\log 0.250} = \frac{0.699 - 1}{0.398 - 1} = 0.500.$$

The left-hand side of the equation is

$$\frac{\log \frac{N_1}{N_2}}{\log \frac{N_1}{N_3}} = \frac{\log \frac{255\,000}{408\,000}}{\log \frac{255\,000}{970\,000}} = \frac{\log 0.625}{\log 0.263} = \frac{0.796 - 1}{0.420 - 1} = 0.352.$$

Plotting the calculated values of the right-hand side against σ_F , the graph shown in Fig. 1.8 is obtained. Taking the point 0.352 at which the right-hand side is equal to the left-hand side of the equation, we read off the required value of the fatigue strength σ_F as 17.5 kgf/mm^2 .

Knowing that $\sigma_F = 17.5 \text{ kgf/mm}^2$, we can determine the value of m :

$$m = \frac{\log \frac{N_1}{N_2}}{\log \left(\frac{\sigma_{E2} - \sigma_F}{\sigma_{E1} - \sigma_F} \right)} = \frac{\log \frac{255\,000}{408\,000}}{\log \left(\frac{21 - 17.5}{27 - 17.5} \right)} = \frac{\log 0.635}{\log 0.369} = \frac{0.803 - 1}{0.567 - 1} = 0.455.$$

For k , we have

$$\begin{aligned} \log k &= \log N_1 + m \log(\sigma_{E1} - \sigma_F) \\ &= 5.407 + 0.455 \log 9.5 \\ &= 5.852. \end{aligned}$$

Thus the equation of the $S-N$ curve will read:

$$\log N = 5.852 - 0.455 \log(\sigma_E - 17.5).$$

The WEIBULL formula constants for a number of materials can be found in Table 1 of Part II.

Tests carried out to determine $S-N$ curves have shown that the $\sigma-\log N$ relationship is not a rigid one — in other words, if several specimens are tested at the same stress, they do not all fracture at exactly the same number of cycles. This phenomenon is in full accord with that mentioned in connection with Phases II and III of the $S-N$ curve. It cannot be definitely asserted that, for example, a particular steel specimen under tension-compression loading with $\sigma_{tcf} = 45 \text{ kgf/mm}^2$ will break at an endurance

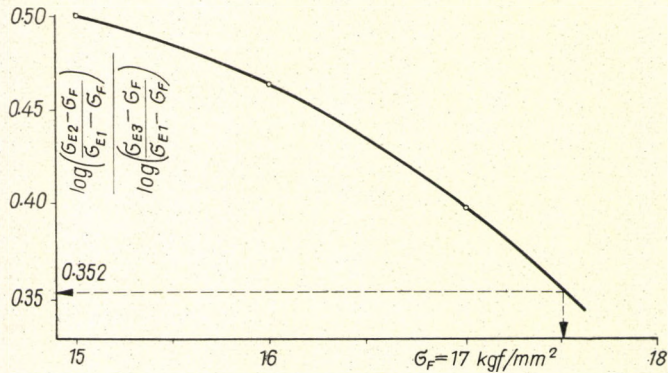


FIG. 1.8. Determination of fatigue limit by WEIBULL'S method

$N = 10^6$. There is only a certain *probability* that fracture will occur. Such an assertion is thus only technically accurate if the probability of fracture, e.g. 1 per cent, is coupled with it. The meaning of this is that if a large number of specimens are fatigue tested at the given stress, only 1 per cent of them will fracture within the given endurance.

Table 1.1 shows the results obtained by various laboratories in fatigue tests that were very carefully planned and carried out on specimens of similar material, similarly prepared.

As can be seen from the table, fracture at each stress level occurred at widely varying endurances. It is only by the application of statistics that the expected value for the

TABLE 1.1
SUMMARY OF RESULTS OF FATIGUE TESTS

Laboratory	Stress (kgf/mm ²)	Endurance, 10 ³ cycles										
NEL (U.K.)	55	226	264	265	293	324	342	391	461	647		
J. Lucas (U.K.)		113	114	196	240	268	354	400	505	810		
MPI Darmstadt (Germany)		236	284	301	323	381	385	638	672	809		
NEL (U.K.)	60	109	119	119	129	135	157	197	201	204		
J. Lucas (U.K.)		137	142	231	233	243	266	270	278	291		
MPI Darmstadt (Germany)		137	158	163	181	211	215	229	235	265		
NEL (U.K.)	65	8	11	12	27	34	35	36	39	39		
J. Lucas (U.K.)		45	48	53	60	82	88	104	137	230		
MPI Darmstadt (Germany)		20	24	32	38	42	51	53	59	64		

Material composition: 0.35 % C, 0.32 % Si, 0.60 % Mn, 0.006 % S,
0.016 % P, 0.20 % Ni, 1.16 % Cr, 0.020 % Mo

Heat treatment: 850°C, 45 min; quenched in oil. Afterwards 590°C,
4 h; cooled in air.

$\sigma_T = 100$ kgf/mm²

$\varepsilon = 14$ to 16 per cent.

Stress: Tension-compression.

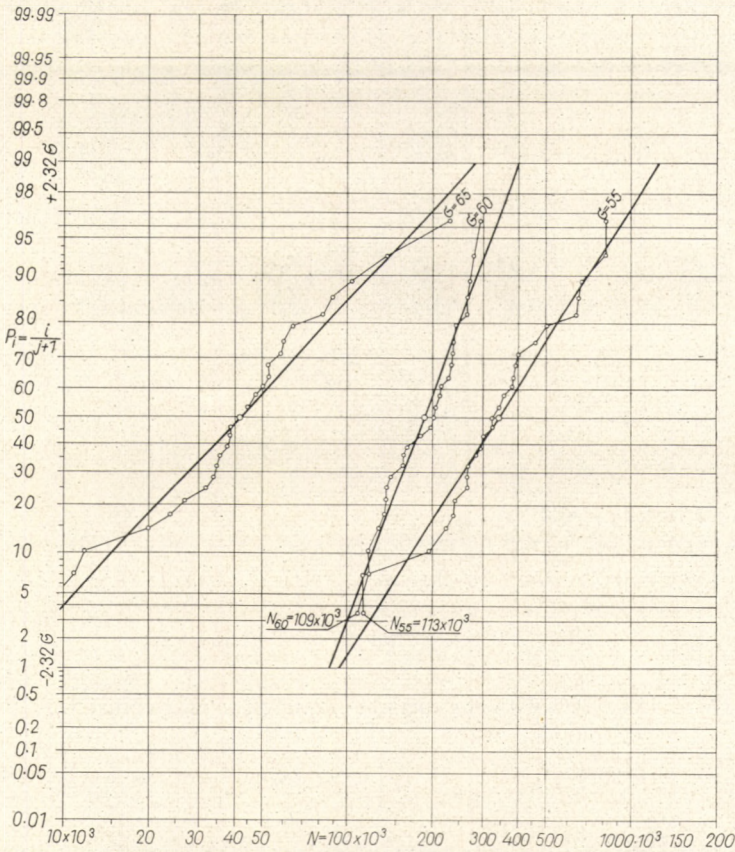


FIG. 1.9. Log-normal distribution for probability of fracture

endurance of any further specimen and the scatter — and thus at the same time the probability of fracture — can be given.

A simple but effective method of obtaining a “complete” $S-N$ curve from the test results in Table 1.1 is given below.

As with all statistical treatments, the first task is to determine how the values — the population, in mathematical parlance — are distributed. Investigations have shown that the two best assumptions in regard to distribution are the log-normal distribution and the WEIBULL distribution. The WEIBULL distribution, with three parameters, undoubtedly gives a better fit to the test results, yet just because of its three parameters it is difficult to handle. In most cases the assumption of the log-normal distribution seems best. To determine whether the available results actually correspond to a log-normal distribution, either the χ^2 test [110] or a graphical method will serve. As the χ^2 test is lengthy to apply, we describe the graphical method below. Its essential feature is that the results are plotted with $\log N$ as abscissa and the cumulative probability of fracture as ordinate. If the distribution of the population does correspond to a log-normal distribution, the points will fall on a straight line. Suitable log-normal/probability graph

paper is obtainable to simplify the work. It is shown in Fig. 1.9. In order to plot the graph it is first necessary to arrange the values in ascending order, and then the relative frequency of the results (i.e. probability of fracture) has to be determined by means of the formula

$$p = \frac{i}{j+1},$$

where i = the number in order (1, 2, 3, . . . , j) of the individual result,
and j = the total number of results.

If the results obtained in the three laboratories are considered as a single population, the values for $\sigma_{tc} = 55 \text{ kgf/mm}^2$ arranged in ascending order are as follows:

$N =$	113	114	196	226	236	240	264	265	268
	284	293	301	323	324	342	354	381	385
	391	400	461	505	638	647	672	809	810

thousand cycles.

Number of results $j = 27$.

Thus the first point — that for the lowest endurance ($N = 113 \times 10^3$) — is plotted with the ordinate equal to a probability of

$$\frac{1}{27+1} = \frac{1}{28} = 0.0357 = 3.57 \text{ per cent};$$

the second ($N = 114 \times 10^3$) with the ordinate equal to a probability of

$$\frac{2}{28} = 7.14 \text{ per cent};$$

and so on.

Repeating the process for $\sigma_{tc} = 60 \text{ kgf/mm}^2$ and $\sigma_{tc} = 65 \text{ kgf/mm}^2$ we obtain the points shown on Fig. 1.9 and joined by the thin lines. It can be seen that between 1 per cent and 99 per cent probability a straight line can be drawn through the points with reasonable approximation, so that the assumption of a log-normal distribution appears to be correct.

We shall now regard these straight lines as the idealized experimental results, assuming that with an increasing number of values a closer and closer approximation to the straight lines would be shown. Care must be taken, however, to draw the lines so as to get the best possible fit to the points, that is to say so that the points on the two sides of the line lie at equal distances from it. It often happens — as can be seen in our example, particularly for $\sigma_{tc} = 65 \text{ kgf/mm}^2$ — that the deviations of the points from the straight line tend to be greater for both very low (10 per cent and less) and very high (90 per cent and greater) probabilities. This only indicates that the statistical population of results departs a little from the assumed log-normal distribution, and that special care is required in interpreting the behaviour patterns in these ranges of probability.

If computer facilities are available it is desirable to position the straight lines by the method of least squares. As any computer will be provided with a programme for this purpose, there is no need to go into further detail here.

Even if computer facilities are not available, it is highly desirable to determine the point corresponding to the 50 per cent probability — which is termed the expected

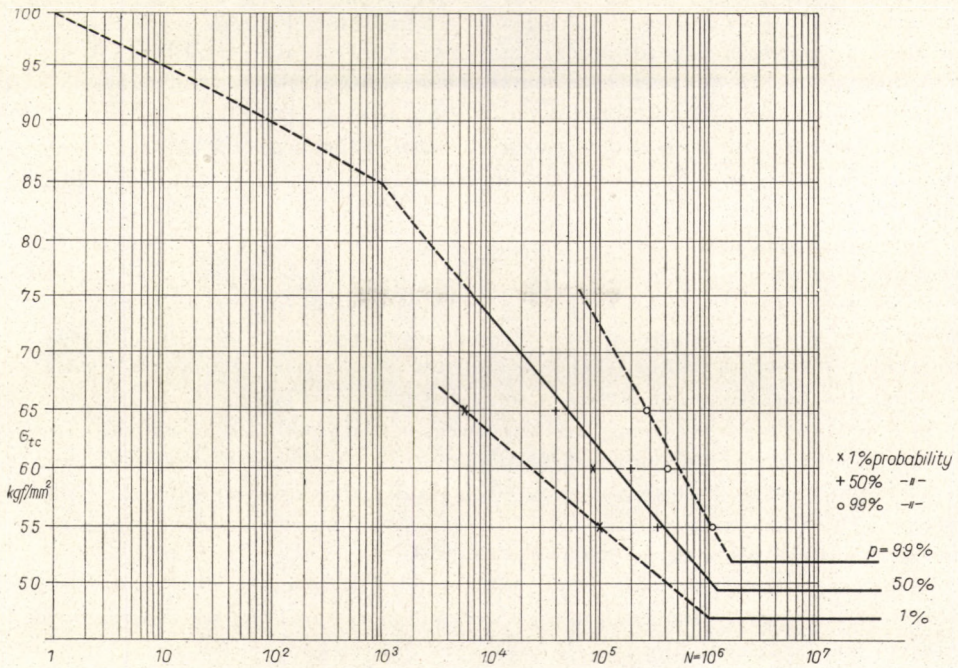


FIG. 1.10. Prediction of endurance for given probability of fracture at any stress

value, mean value, or value of greatest frequency – for each stress. This is the mathematical average of the logarithms of the endurance. For example, with $\sigma_{tc} = 55 \text{ kgf/mm}^2$, the average, μ , is given by

$$\mu = \frac{\Sigma \log N}{j} = \frac{149 \cdot 2711}{27} = 5 \cdot 5285,$$

and $N_{50} = 338 \times 10^3$,

where

N = endurance, and
 j = number of values.

This point must be plotted at the ordinate for 50 per cent probability, and the straight line must pass through it. In this way it is easier to find the line giving the best fit to the plotted points; it should be drawn as far as the 1 per cent and 99 per cent ordinates.

The slope of the line indicates the scatter of the results; a steep slope indicates little scatter, and a lesser slope a greater scatter. The scatter constant can be determined by dividing the endurance for 50 per cent probability by that for 15.8 per cent probability:

$$S = \frac{N_{50\%}}{N_{15.8\%}}.$$

Since, in the design of machine components, it is generally the small probabilities of fracture (1 per cent or less) that are of interest, the diagram shows clearly that not only the “most frequent” (the mathematical average) endurance – usually depending on the

chemical composition and heat treatment — governs the behaviour of the material, but also the scatter, which depends on care in manufacture and heat treatment. A specimen of medium-alloy but homogeneous material may have a greater endurance for 1 per cent probability than one of a high-alloy material that has been less carefully manufactured and heat-treated. In the former case, because of the smaller scatter, the endurance for 1 per cent probability is higher than where there is a higher average value but greater scatter.

Not only the endurance for 1 per cent or 99 per cent probability of fracture but also that for any intermediate probability can be read off from the diagram. If such endurances are plotted on the $S-N$ diagram at various stresses for the same probability of fracture and straight lines are drawn through the points, the endurance for any given probability of fracture can be predicted not only for the particular stresses used in the tests, but also for any other stresses (Fig. 1.10).

In practice it may be found that the three or more points for, say, the 1 per cent probability of fracture (in our example at stresses of 55, 60 and 65 kgf/mm²) do not lie on a straight line. In the interests of safety it is advisable always to join the points corresponding to the lowest endurances. The line thus obtained should be regarded as the limiting line for 1 per cent probability of fracture.

In the case, which occurs only very rarely in practice, when the 99 per cent probability of fracture is required, the line joining the points corresponding to the greatest endurances should be accepted.

1.6 Determination of fatigue limit

In Phase III of the $S-N$ curve — which, for steels, runs approximately parallel to the log- N axis — difficulties arise about fatigue tests carried out at the same stress level. It can easily be understood from the general character of the curve that the endurances shown by specimens vary considerably for even small differences in applied stress. This means that the “accuracy” of the testing machine, i.e. the uniformity of the stress amplitude, has a considerable influence on the results. The technical problem of ensuring a strictly uniform stress amplitude is a very difficult one to solve, especially when the cycling frequency is high (as is very desirable in order to shorten the time required for testing as much as possible).

A further difficulty arises — when either the graphical method here described, or the mathematical method, is used — in incorporating in the calculation of the “average” (= 50 per cent probability of fracture) the result from a specimen which does not break within the ordinary maximum endurance of from 1 to 2×10^6 cycles. Continuation of the test to 10, 50 or 100×10^6 cycles takes an extremely long time, and is also very expensive, and consequently is to be avoided if possible. For “infinite” endurance it is impossible to calculate the mathematical average either graphically or arithmetically. In the neighbourhood of the fatigue limit, therefore, what is termed the “staircase” method is employed.

1.6.1 “Staircase” method of determining fatigue limit

The essence of the method [5] is to test a specimen in fatigue at a stress near what is estimated to be the fatigue limit. If it breaks at less than the “limiting” endurance decided upon beforehand (e.g. $N = 2 \times 10^6$), the stress is lowered a step and the test is

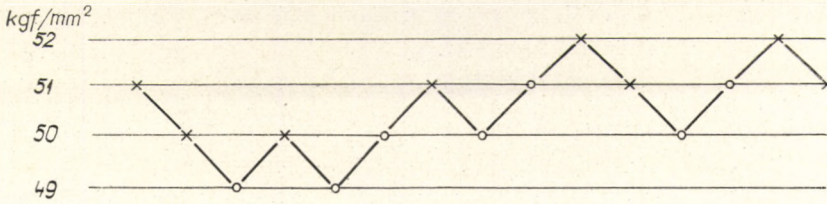


FIG. 1.11. "Staircase" method

repeated on another specimen. If it withstands the limiting endurance without fracture, the stress is raised a step. Upward and downward steps are equal. An example will assist in describing the method.

The material already referred to was tested by the National Engineering Laboratory, East Kilbride, to a maximum of 10×10^6 cycles with the results shown in Fig. 1.11.

The results are summarized in Table 1.2. The expected value (corresponding to 50 per cent probability of fracture) of the fatigue limit can be calculated [5] from the following formula:

$$\sigma_F = \sigma_{F0} + \Delta\sigma \left(\frac{A}{F} \pm \frac{1}{2} \right) \tag{2}$$

where σ_F denotes the fatigue limit, and the significance of the other symbols is as shown in the bottom row of Table 1.2. The ranking number for stress level entered in the table denotes each applied stress level (step) in order; the number 0 is always assigned to the stress level at which the *less frequent occurrence* first appears. (In the example it is at a stress of 49 kgf/mm^2 that for the first time no fracture of a specimen occurs.)

The plus sign has to be used in the formula if the less frequent occurrence is "fractured", and the minus sign if (as in the example) it is "not fractured". Thus:

$$\sigma_F = 49 + 1 \left(\frac{7}{7} - \frac{1}{2} \right) = 49.5 \text{ kgf/mm}^2.$$

TABLE 1.2
"STAIRCASE" METHOD

Stress (kgf/mm ²)	Ranking number of stress level <i>i</i>	Number of test pieces	Number of occurrences of the less frequent type* <i>f_i</i>	<i>if_i</i>	<i>i²f_i</i>
52	3	2	0	0	0
51	2	6	2	4	8
50	1	5	3	3	3
49	0	2	2	0	0
= σ_{F0}					
$\Delta\sigma = 1 \text{ kgf/mm}^2$		$\Sigma = 15$	$F = \Sigma f_i = 7$	$A = \Sigma if_i = 7$	$B = \Sigma i^2 f_i = 11$

* In this example, the number of unbroken test pieces.

The expected scatter in the average value is determined from the formula:

$$S = 1.620 \Delta\sigma \left(\frac{FB - A^2}{F^2} + 0.029 \right)$$

which for the example becomes

$$\begin{aligned} S &= 1.620 \times 1 \left(\frac{7 \times 11 - 7^2}{7^2} + 0.029 \right) \\ &= 1.620 \left(\frac{28}{49} + 0.029 \right) \\ &= 0.97 \text{ kgf/mm}^2. \end{aligned}$$

This is the standard deviation of the values, and it is a well-known fact of statistics that the 1 per cent and 99 per cent probability limits are situated at $\mu \pm 2.34 S$; thus specimens stressed at $49.5 - 2.34 \times 0.97 = 47.2 \text{ kgf/mm}^2$ have a 1 per cent probability of fracture, and those stressed at $49.5 + 2.34 \times 0.97 = 51.8 \text{ kgf/mm}^2$ a 99 per cent probability of fracture.

The method gives reliable results only if the distribution is normal or log-normal.

It is desirable that the number of specimens tested should be at least forty. This condition was not fulfilled in our example, but the aim there was to illustrate the method in simplified fashion. The advantage of the method is that the fatigue limit can be determined using relatively few specimens and that not only the expected value (mathematical average) but also the scatter is obtained, so that the probability of fracture can also be given.

On the other hand the disadvantage of the method is that the specimens must be tested one after the other, so that the complete test takes up a considerable amount of time.

The above-indicated supplementary treatment permits the construction of an "amplified" $S-N$ curve including any given probabilities of fracture (Fig. 1.10 shows 1 per cent, 50 per cent and 90 per cent).

It should be noted that the form of the $S-N$ curve shown in Fig. 1.10 is not typical, because in most cases the scatter increases near the fatigue limit, instead of decreasing as in the figure.

1.6.2 Rapid method of determining fatigue limit: the Locati method

Determination of the $S-N$ curve calls for fatigue tests on several specimens or components. This is not practicable, however, in certain cases when only a single sample or prototype is available or the testing is restricted by shortage of time or by financial considerations. In such circumstances the use of the method recommended by LOCATI [51], which in most cases gives results accurate enough for practical use, is suggested.

LOCATI started from MINER's principle, according to which

$$\Sigma \frac{n_m}{N_m} = 1.$$

MINER assumed that fatigue failure appeared at different stress levels after the same amount of deformation work. Thus if a specimen fractures after N_1 cycles under a

stress σ_1 , and the work of deformation in a single cycle is a_1 , then if A_t is the total work of deformation to fracture,

$$a_1 N_1 = A_t, \text{ i.e. } a_1 = \frac{A_t}{N_1}.$$

If a specimen fractures after N_2 cycles under a stress σ_2 , we have

$$a_2 N_2 = A_t, \text{ i.e. } a_2 = \frac{A_t}{N_2},$$

and at any stress level σ_m ,

$$a_m N_m = A_t, \text{ i.e. } a_m = \frac{A_t}{N_m}.$$

Suppose now that a specimen is subjected to only n_1 cycles at the stress σ_1 , n_2 at σ_2 , and n_m at σ_m , after which it fractures; then, according to MINER, the total work of deformation is still A_t , so that

$$a_1 n_1 + a_2 n_2 + \dots + a_m n_m = A_t.$$

Substituting for a_1 , a_2 and a_m we have

$$\frac{n_1}{N_1} A_t + \frac{n_2}{N_2} A_t + \dots + \frac{n_m}{N_m} A_t = A_t$$

or

$$\frac{n_1}{N_1} + \frac{n_2}{N_2} + \dots + \frac{n_m}{N_m} = 1$$

or in a short form

$$\Sigma \frac{n_m}{N_m} = 1.$$

Tests have not fully confirmed MINER's principle. Different results are obtained according as the successive stresses are applied with increasing or decreasing magnitude; for increasing stresses $\Sigma \frac{n}{N} > 1$, and for decreasing stresses $\Sigma \frac{n}{N} < 1$.

For mild steel KOMMERS [39] obtained $\frac{n}{N} = 1.71$ to 2.35 ; RICHART and NEWMARK [78] found 1.46 to 1.56 for NiCrMo steel. These values were for increasing stresses. For decreasing stresses, REYLENCE found 0.75 to 1.1 for mild steel and DILTER, HERNE and MEHL 0.91 to 1.01 for NiCrMo steel. WÄLLGREN [109] proposed a correction factor. According to his results,

$$\Sigma \frac{n_m}{N_m} = X,$$

where X is a constant, depending upon the material, which has to be evaluated from test results.

The LOCATI method consists in testing a single specimen, the stress being raised by equal increments, and the same number of cycles being applied at each level, until finally the specimen breaks.

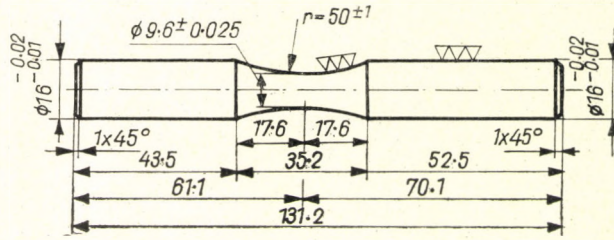


FIG. 1.12. Rotating-bending fatigue test specimen

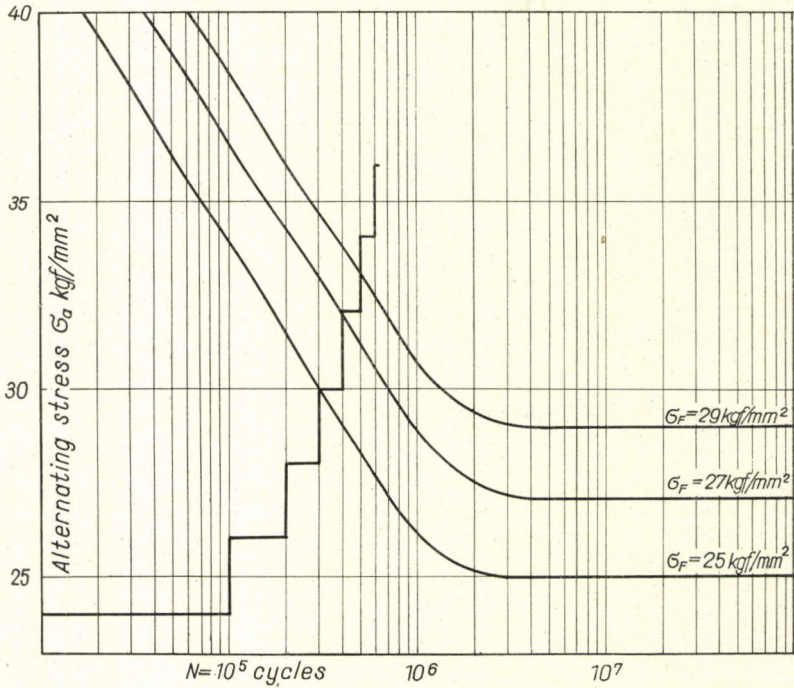


FIG. 1.13. Graph for LOCATI method

Three different $S-N$ curves and fatigue limits are then assumed, and the value of $\Sigma \frac{n}{N}$ is determined using each of them. Thus there are three values of $\Sigma \frac{n}{N}$ corresponding respectively to three values of σ . These are plotted and a curve is drawn through the three points. The required value of σ_F is the one corresponding to $\Sigma \frac{n}{N} = 1$.

The procedure is illustrated by the following example:

A specimen as shown in Fig. 1.12 was stressed at levels beginning with 24 kgf/mm² and increasing in steps of 2 kgf/mm²; 100 000 cycles were applied at each level until the stress was reached at which fracture took place in less than 100 000 cycles. Three different $S-N$ curves were then assumed, with fatigue limits σ_F of 25, 27 and 29 kgf/mm² respectively (Fig. 1.13). Table 1.3 was drawn up from the test results and the assumed curves.

Ordinary or logarithmic coordinates may be used for plotting $\Sigma \frac{n}{N}$ against σ_F . In Fig. 1.14 the ordinate scale is logarithmic and the abscissa scale is plain. At $\Sigma \frac{n}{N} = 1$, $\sigma_F =$ about 27.5 kgf/mm², which is taken as the expected fatigue limit.

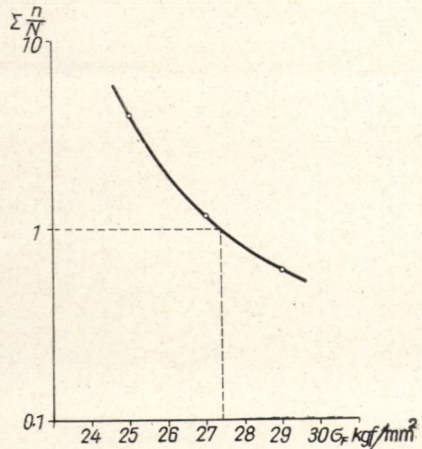


FIG. 1.14. Graph for LOCATI method

The value of the fatigue limit σ_F given by the LOCATI method has been found by experience to be accurate enough for practical use, although, as mentioned already, experiments have shown that in many cases the relation $\Sigma \frac{n}{N} = 1$ is not correct. Nevertheless, the method has the important advantage that a single specimen or machine component is sufficient to estimate the fatigue limit.

It should be mentioned, however, that the method applies only to steels, and that it does not indicate the probability of failure which has been discussed above.

TABLE 1.3

ROTATING-BENDING FATIGUE TEST OF THE SPECIMEN SHOWN IN FIG. 1.12

Stress (kgf/mm ²)	n	$\sigma_F = 25$		$\sigma_F = 27$		$\sigma_F = 29$	
		N	n/N	N	n/N	N	n/N
24	100 000	∞	0				
26	100 000	900 000	0.111	∞	0		
28	100 000	485 000	0.206	1 300 000	0.077	∞	0
30	100 000	260 000	0.385	660 000	0.151	1 300 000	0.077
32	100 000	150 000	0.666	380 000	0.260	680 000	0.147
34	100 000	80 000	1.250	215 000	0.460	390 000	0.256
36	31 000	45 000	0.689	130 000	0.238	225 000	0.138
	631 000		3.307		1.186		0.618

1.7 Fatigue diagrams

1.7.1 Smith diagrams

The fatigue limit varies with mean stress. Separate tests must therefore be made not only for each kind of stress, such as tension-compression and bending, but also for each mean stress, and separate S-N curves must of course be plotted. When calculations are carried out it is thus necessary to select the appropriate S-N curves from the group of curves for various mean stresses. It is for this reason that the fatigue diagrams devised by SMITH and HAIGH are used in computation instead of the S-N curves.

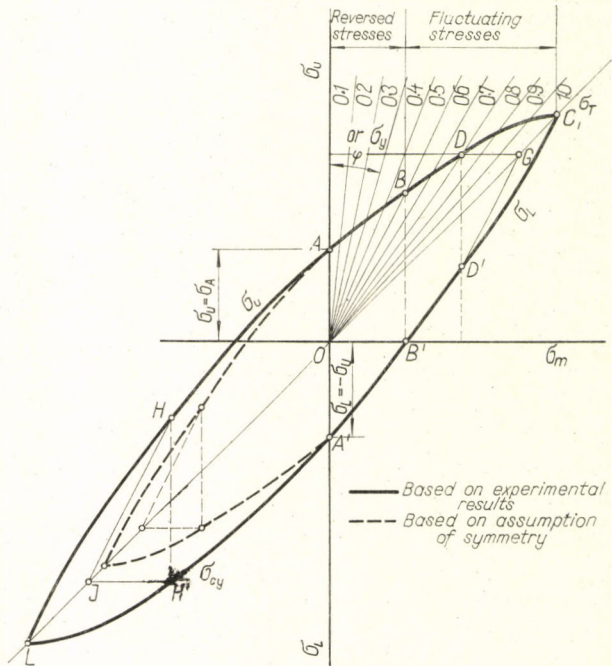


FIG. 1.15. Smith diagram

SMITH suggested representing the results in a diagram having the mean stress σ_M as abscissa and the maximum and minimum stresses, σ_U and σ_L respectively, plotted on the ordinate scale.

The symmetrical reversed-stress amplitude $\sigma_a (= \sigma_U = -\sigma_L)$ which the material will just withstand without fracture (even at an infinite number of cycles) must be plotted on the ordinate axis, as the mean stress $\sigma_m = 0$. The upper value of stress, $\sigma_U = +\sigma_a$, must be plotted in the positive direction, while the lower value $\sigma_L = -\sigma_U$ will be plotted at the same distance from the origin but in the negative direction (A and A' in Fig. 1.15).

The upper value of the repeated stress, varying between 0 and a maximum ($\sigma_L = 0$ and $\sigma_U = \sigma_{\max}$), which the material will withstand for an infinite number of cycles has to be plotted with abscissa $+\sigma_U/2$, since in these conditions this is, of course, the value of σ_m . Thus σ_U and σ_L become respectively B and B' in Fig. 1.15. By plotting test results for other values of σ_m in a similar way, curves of σ_U and σ_L are obtained.

A straight line at 45 degrees to the coordinate axes completes a diagram in which the values of σ_U , σ_m , and σ_L at any point are given by the intersections with the curves and the 45-degree line of a straight line parallel to the ordinate axis. The curves of σ_U and σ_L will intersect on this straight line at points C and L . At these points $\sigma_L = \sigma_U = \sigma_m$, giving the static strength in tension or compression.

In practice, Smith diagrams are terminated at the yield point σ_y , for beyond this point the stress pattern is altered because of permanent deformations in the material under test. The curve of σ_U stops in practice at D , where $\sigma_U = \sigma_y$. The point D is projected on to the curve of σ_L at D' , and the straight line of the yield point σ_y is extended

as DG to the point of intersection G with the 45-degree line. Similarly for the part of the diagram representing compressive stresses, the curve of σ_L stops at H' . The point H' is projected on to the curve of σ_U at H , and the straight line of the yield point in compression is extended as $H'J$ to the point of intersection J with the 45-degree line. The behaviour under any stress may be determined from the Smith diagram obtained in this way. If the maximum and minimum stresses lie between the curves of σ_U and σ_L , the material in question will not break even at an indefinite number of load cycles. On the other hand if the maximum and minimum stresses lie outside the curves, but the value of σ_U does not exceed the yield point σ_y , failure will take place in all cases, but only after a given number of load cycles or period of duty. If σ_U exceeds the yield point σ_y , permanent deformation will occur.

The straight lines subtending the following angles with the σ_U axis are often added to the diagram:

- $\phi = 5^\circ 40'$ ($\tan 5^\circ 40' = 0.1$)
- $\phi = 11^\circ 20'$ ($\tan 11^\circ 20' = 0.2$)
- $\phi = 16^\circ 42'$ ($\tan 16^\circ 42' = 0.3$)
- $\phi = 21^\circ 50'$ ($\tan 21^\circ 50' = 0.4$)
- $\phi = 26^\circ 40'$ ($\tan 26^\circ 40' = 0.5$)
- $\phi = 30^\circ 55'$ ($\tan 30^\circ 55' = 0.6$)
- $\phi = 34^\circ 55'$ ($\tan 34^\circ 55' = 0.7$)
- $\phi = 38^\circ 40'$ ($\tan 38^\circ 40' = 0.8$)
- $\phi = 41^\circ 55'$ ($\tan 41^\circ 55' = 0.9$).

The straight lines marked 0.1, 0.2, . . . , 0.9 intersect the Smith diagram in the points in which the ratio of the mean stress to the maximum stress $\sigma_m/\sigma_U = \tan \phi$ (Fig. 1.15).

For the sake of simplicity, the above discussion has been restricted to tensile and compressive stress. The Smith diagram for fatigue in bending, torsion, and shear, and in combinations of these modes, and the problem of determining an unknown fatigue strength from a known one, are discussed in section 2.1.

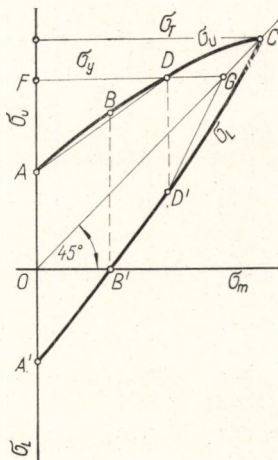


FIG. 1.16. Simplified Smith diagram

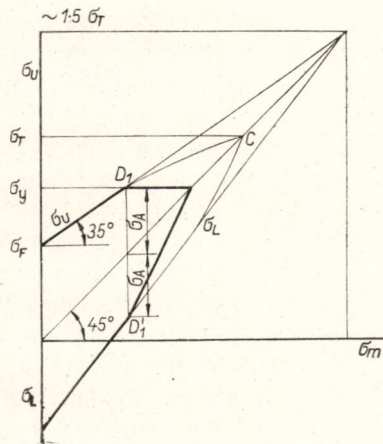


FIG. 1.17. Simplified Smith diagram bounded by straight lines

Since most materials have a considerably lower fatigue strength in tension than in compression, their Smith diagrams will not be symmetrical. For steels, however, the difference between the fatigue strengths in tension and compression is ignored in practice, and the fatigue strength in compression is assumed to be equal to the fatigue strength in tension. On this assumption the Smith diagram becomes symmetrical, and the left-hand side need not be plotted from actual observations.¹

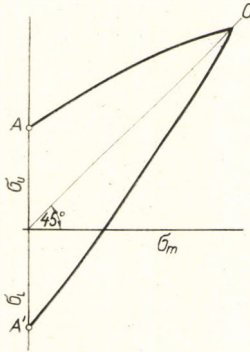


FIG. 1.18. Smith diagram of brittle materials

A further simplification used in practice is to connect points A and A' with D and D' respectively by straight lines instead of curves (Figs. 1.15 and 1.16).

Both of these simplifications are permissible because any error they introduce will be on the safe side.

A useful approximation to the curve of σ_U has been found to be a straight line drawn from the point A in Fig. 1.16 (σ_U for $\sigma_m = 0$) at an angle of 35 degrees to the horizontal as in Fig. 1.17. To avoid permanent deformations, the upper peak of the diagram is cut off at the level of the yield stress σ_y with a horizontal line. From the point of intersection of this line with the 45-degree line another straight line is drawn to the point D_1' (Fig. 1.17) which is at the same vertical distance below the 45-degree line as D_1 is above it. Below D_1' the curve of σ_L is the straight line on which each point is the same vertical distance below the 45-degree line as the corresponding point for σ_U is above it.

For brittle materials such as hardened steel and cast iron, when fracture takes place without yielding, the curves σ_L and σ_U intersect at the point representing the static breaking strength (Fig. 1.18). Thus the cut-off form of the Smith diagram applies to tough materials, while for brittle materials it has a pointed shape.

1.7.2 Haigh diagrams

In the Haigh diagram the stress amplitude σ_A is the ordinate and the mean stress σ_M is the abscissa. This eliminates the dual appearance of the mean stress σ_M , once as abscissa and again as ordinate to the 45-degree line, which is a feature of the Smith diagram. The Haigh diagram may in fact be considered as an alternative representation of the part of the Smith diagram lying between the ordinate axis and the 45-degree line, with axes at 90° instead of 45° (Fig. 1.19).

The straight line indicating the yield point, which is parallel to the abscissa axis in the Smith diagram, makes an angle of 135° with it in the Haigh diagram. It is the straight line DG in Fig. 1.19. The point of intersection C (Fig. 1.15) of the σ_U , σ_m , and σ_L lines on the Smith diagram, corresponding to the static strength, lies on the abscissa axis in the Haigh diagram (point C in Fig. 1.19). In the Smith diagram (Fig. 1.15) any fluctuating stress conditions which when plotted fall within the area $ABDGD'B'A'$ will not cause fracture even in an infinite number of cycles. In the Haigh diagram

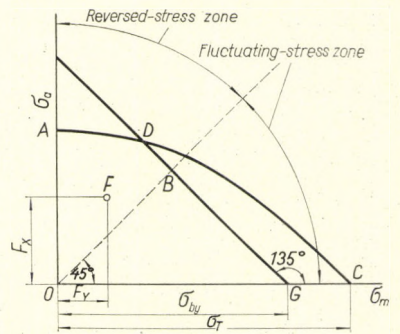


FIG. 1.19. Haigh diagram

the corresponding area is $OADBG$ (Fig. 1.19). In the Smith diagram, stresses appearing in the area $DGD'C$ will cause permanent deformation, and the corresponding area in the Haigh diagram is DCG .

For both diagrams, fracture takes place sooner or later without permanent deformation under any fluctuating stress with a maximum appearing in the area ADF (Fig. 1.16).

The area of reversed stress in the Smith diagram is $AOA'B'B$, while the area of fluctuating stress is $BB'D'GD$. In the Haigh diagram the corresponding areas are $OADB$ and BOG respectively. The construction of the Smith diagram from the Haigh diagram is shown in Fig. 1.20.

Any point F on the Haigh diagram can be transferred to the Smith diagram by using the same abscissa F_x and marking the ordinate F_y upwards and downwards from the 45-degree line (Fig. 1.20).

Although the Smith and Haigh diagrams are completely equivalent, the first gives a clearer picture of the fatigue-stress conditions, and it is preferable to use it to show the values of fatigue strength of materials. The Haigh diagram, on the other hand, is more suitable when safety factors are being considered.

STRÜSSI [89] formulated the following equation for the Haigh diagram:

$$\sigma_A = \sigma_F \frac{\sigma_T(\sigma_T - \sigma_m)}{\sigma_T(\sigma_T - \sigma_m) + \sigma_F \sigma_m} \tag{3}$$

With $\sigma_m = 0$, the equation gives

$$\sigma_A = \sigma_F,$$

and with $\sigma_A = 0$, it gives

$$\sigma_T = \sigma_m,$$

as would be expected.

The $S-N$ diagram shows that each arbitrary number of stress cycles N is associated with a different endurance limit σ_F . Consequently each number of stress cycles N requires a different Haigh diagram. The relationship of all the three variables (σ_m , σ_U and N) is illustrated in Fig. 1.21.

1.7.3 Moore-Kommers-Jasper diagrams

The fatigue-limit diagram developed by MOORE, KOMMERS and JASPER takes the stress ratio R as abscissa and the corresponding fatigue limit as ordinate. The stress ratio $R = \sigma_L/\sigma_U$ can vary from -1 to $+1$. $R = +1$ signifies static stressing, and the corresponding stress is σ_T . $R = 0$ signifies repeated stressing, and finally, $R = -1$

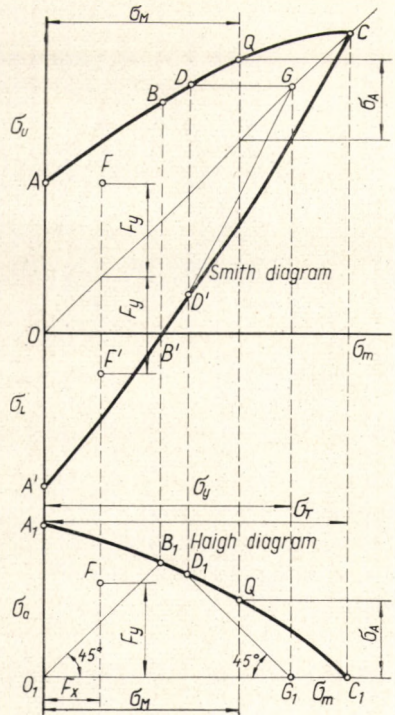


FIG. 1.20. Construction of the Smith diagram from the Haigh diagram

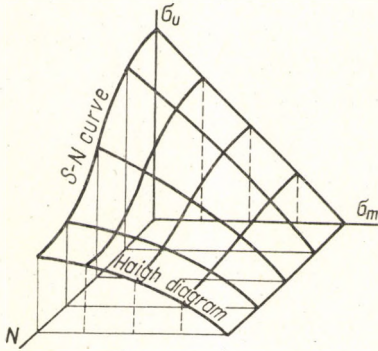


FIG. 1.21. Three-dimensional relationship between the S - N curve and the Haigh diagram

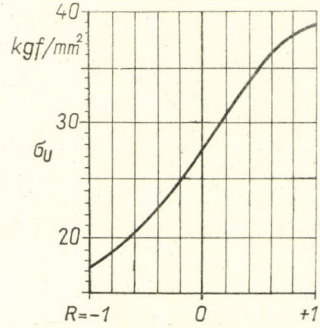


FIG. 1.22. Moore-Kommers-Jasper fatigue-limit diagram (MKJ diagram)

signifies reversed symmetrical stressing. If the Smith and Haigh diagrams are known, the Moore-Kommers-Jasper (MKJ) diagram can be easily plotted (Fig. 1.22). These diagrams have a major importance for the calculation of the fatigue strength of welded joints.

1.7.4 Use of data in literature

Note that in the above-described construction of Smith and Haigh diagrams the fatigue limit of the test pieces has been involved. In Part II we give, for practical use, Smith diagrams based on numerous tests reported in the literature. As, however, these diagrams were prepared at a time when the statistical treatment of fatigue was not yet known, it is also not known to what probability of fracture the diagrams relate.

The descriptions of the tests show, however, that the authors prepared the diagrams very carefully, using the lowest results obtained, so that the diagrams can be considered to correspond to a very low (0.1 to 1 per cent) probability of fracture.

The data found in the literature can in fact be used as reference values, except in critical cases when it is impossible to dispense with the preparation of the S - N curves or, when necessary, the Smith or Haigh diagrams.

1.8 Fatigue fractures: their causes and appearance

1.8.1 Causes

The precise cause of fatigue fractures is not known, despite the efforts of numerous investigators to discover it. Various suggestions have been made. According to E. OROWAN [68], hair cracks, preceding fracture, result from insufficient deformability of the crystal structure. H. F. MOORE and J. B. KOMMERS [61] regard the cause as lying in the stress-raising effect between the individual crystals, whereas E. HOUDREMONT [32] attributes it to local heating. On the evidence of radiographic examination H. MÖLLER and M. HEMPEL [59] maintain that with repeated stressing above the fatigue limit a

few particularly unfavourably oriented grains of the material undergo bending or distortion. This seems the more probable in that it can be demonstrated by microscopical examination that edges and corners providing stress-raising effects exist locally between the grains of metals. Should the stress-raising effect gain ascendancy over the deformability of the grains, these latter will undergo displacement, and hair cracks will appear. These, however — as all the investigators agree — give rise to further stress-raising effects, which hasten the propagation of the cracks. According to HEMPEL [21], the speed of propagation is approximately proportional to the square of the crack depth. When a crack becomes so deep that the remaining cross-section is insufficient to sustain the load, a sudden fracture occurs.

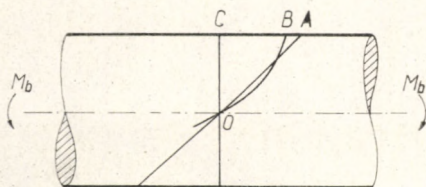


FIG. 1.23. Actual stress distribution in bending ("supporting effect")

The theory of "impeded displacements" developed by BOLLENRATH and TROOST must also be mentioned. This theory starts from the hypothesis that the mechanical properties of materials depend upon the characteristic directions of crystals. In the direction of the so-called slip planes, permanent displacements occur under even relatively low shear stresses, while crystals in the perpendicular direction are able to resist quite large tensile or compressive stresses without permanent deformation. If the stress exceeds a certain value, permanent displacement will occur in one of the unfavourably oriented crystals (one with its slip plane parallel to the local shear stress) even if the average stress over the whole cross-section is below the elastic limit. It may be mentioned here that most materials have no definite elastic limit; the initial portion of the stress-strain diagram is not really straight, and appears to be so only because the instruments available are not sensitive enough to reveal its curvature.

If the stress distribution in the cross-section is not uniform (as, for example, in bending), the stress at the outer fibres will not be as indicated by CA in Fig. 1.23, but smaller, as indicated by CB . The stress distribution corresponds not to the straight line OA , with uniform slope across the section, but to the curve OB . It is as if the fibres more remote from the surface take more than their proportionate share of the load, and thus in a sense "support" those nearer the surface. Thus in the experimentally determined Smith diagrams shown in Figs. 1 to 17 of Part II (pp. 9–13) the fatigue strength in bending is greater than that in tension.

1.8.2 Appearance

The appearance of the surfaces of fatigue fractures is of two kinds:

(a) The surfaces of cracks, which start from notches, corners, edges, or defects in the material, and penetrate inwards from the outside surface of the workpiece, get discoloured and blackened by external impurities or by the oxygen of the air. The opposing surfaces gradually wear, however small their relative movement, as is evident from the loss of the brightness of their grains.

(b) The fracture surface of the rest of the cross-section, on the other hand, does possess brightness of the familiar kind regularly displayed in specimens broken in static testing machines, because this part of the fracture occurs quite abruptly.



FIG. 1.24. Grain structure of a 12 per cent manganese steel showing distortion under fatigue

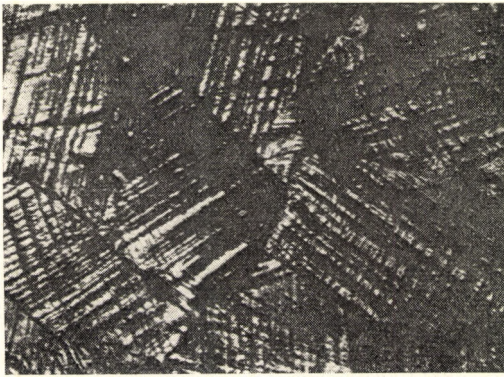


FIG. 1.25. Hair cracks occurring in consequence of grain distortion

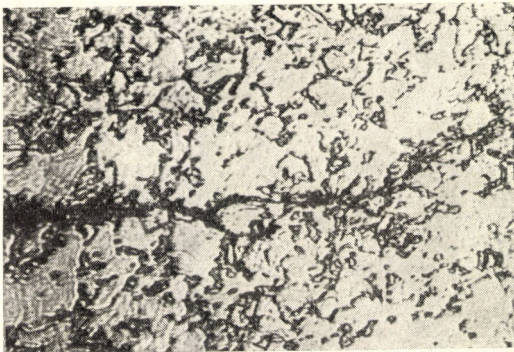


FIG. 1.26. Growth of hair cracks

The distortion of the grains of a 12 per cent manganese steel is shown in Fig. 1.24, and the hair cracks between the grains, due to fatigue, in Fig. 1.25. Figure 1.26 shows the course of propagation of hair cracks, and the whole fracture surface is shown in Fig. 1.27.

It is clear from Fig. 1.27 that fatigue was due to the alternating bending stress on the shaft and started from both sides. Since the surface of the fatigue fracture is smaller than that of the final fracture, it is evident that the shaft was designed with too low a factor of safety. From investigation of numerous fatigue fractures under repeated bending, F. BACON [1] drew the following conclusions (Fig. 1.28):

Under fluctuating bending stress, in the absence of a stress raiser, a fatigue fracture advances in clearly visible steps, similar to annual rings in the trunk of a tree. The ratio between the area of the fatigue fracture and that of the fracture due to the eventual insufficient cross-sectional area is a pointer to the stress: the greater the area of the fatigue fracture, the lower the stress, and vice versa.

Under reversed bending stress, however, the rings appear on both sides, as the specimen is stressed on each side alternately, and the surface of the final fracture is shown at the middle of the cross-section by a strip having the form of a concave lens. With combined reversed bending and torsion, the axis of symmetry of the residual fracture area makes an acute angle with that of the fatigue-fracture rings, because of the shear stresses.

If a severe stress-raising effect is present, fatigue occurs, under fluctuating bending stress, earlier in the areas away from the neutral zone (where the stresses are higher) and propagates more rapidly than in the interior of the workpiece. For this reason the



FIG. 1.27. Surface of fracture occurring under reversed bending stress. Failure started on both sides at the positions marked by arrows

	No stress concentration		Slight stress concentration		Severe stress concentration	
	Relatively low stress	Relatively high stress	Relatively low stress	Relatively high stress	Relatively low stress	Relatively high stress
Fluctuating bending stress						
Reversed bending stress						
Reversed bending and torsional stresses						

FIG. 1.28. Diagrammatic representation of various fatigue-fracture surfaces

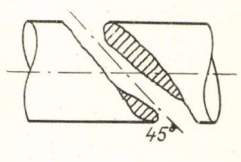
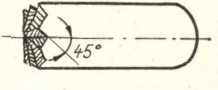
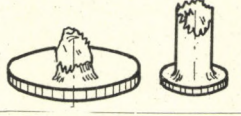
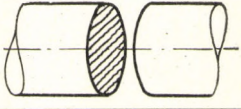
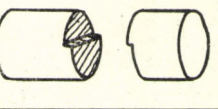
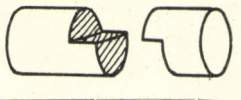
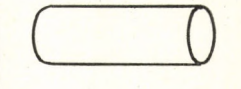
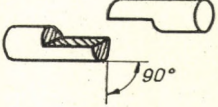
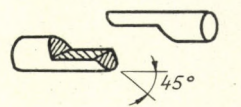
Cause of fracture	Basic form of fracture	Types of fractures	
		a	b
Tensile stress		Star-like fracture surface 	Saw-like fracture surface caused by stress concentration 
Perpendicular shear stress			
Longitudinal shear stress			

FIG. 1.29. Diagrammatic representation of various shear fatigue-fracture surfaces

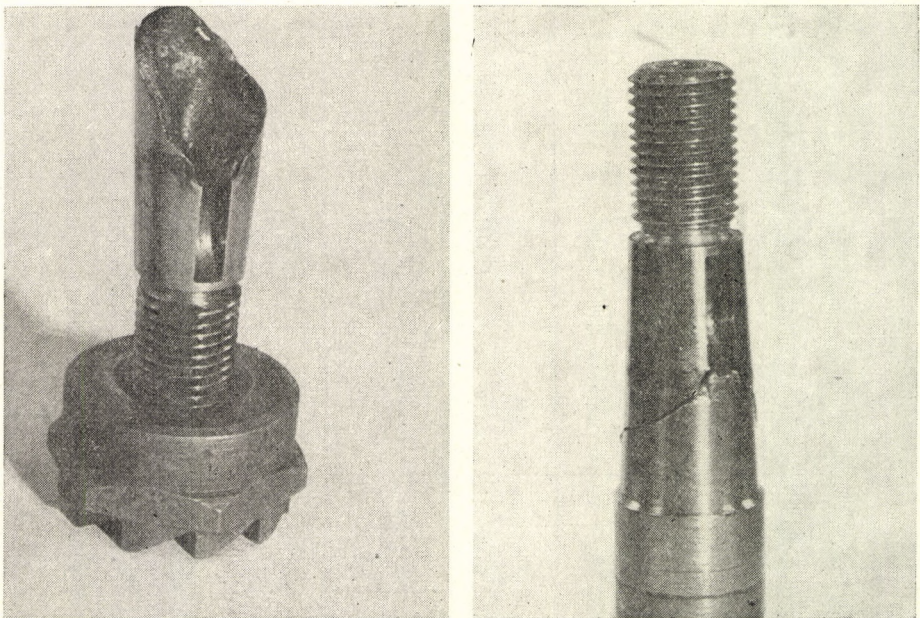


FIG. 1.30. Typical form of fatigue fracture caused by torsional stress

“annual rings” “stretch”, frequently even to the extent of reversing their curvature. The residual fracture area is then no longer of crescent shape, as in the absence of stress-raising effect, but in the form of a convex lens. Here too the relative size of the two different fracture areas is an indication of the stress in the workpiece.

Under reversed bending stress, fracture again begins at both sides.

With combined reversed bending and torsion, the reversal of curvature of the growth lines and the displacement of the axis of symmetry can both be observed. Under high stresses, the cracks starting from both sides may leave the residual fracture area surrounded like an island in the middle of the fatigue-fracture area.

With a less severe stress-raising effect, the same phenomena can be observed, but to a less pronounced extent.

In Fig. 1.28 the hatched parts of the fracture areas give a diagrammatic representation of the residual fractures, and the lined parts do the same for the fatigue-fracture areas.

There are three well-known categories of torsional fatigue fractures, which may occur singly or in combination, viz.:

- fractures at approximately 45 degrees to the torsion axis;
- fractures perpendicular to the torsion axis;
- fractures in longitudinal planes parallel to the torsion axis (see Fig. 1.29).

The first type is brought about by tensile stresses concomitant with the torsion, while fractures of the two other types are caused by shear stresses. As the tensile strength of steels is considerably higher than their shear strength, fractures caused by tensile stresses can only occur at points of stress concentration, which may sometimes result from a defect discernible only under the microscope, or an irregularity (e.g. a scratch) in the machining of the surface.

A typical fracture surface for a shaft failing under repeated torsion is shown in Fig. 1.30. Figure 1.31 shows diagrammatically the typical form of fatigue fracture of a splined shaft.

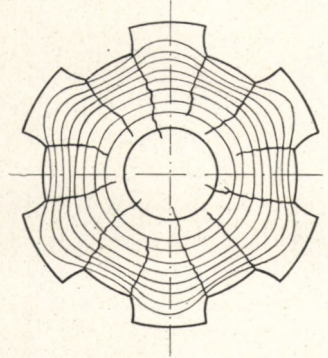


FIG. 1.31. Typical form of fatigue fracture in splined shafts

CHAPTER 2

Fatigue Diagrams of Various Materials

THE methods for carrying out fatigue tests and the requirements for specimen form and preparation have been specified in standards.

Fatigue diagrams for certain materials, based on data given in the literature, are commented on below.

2.1 Steel

Part II gives the Smith diagrams of various standardized carbon steels (Figs. 1 to 5, pp. 9–10), nickel–chromium steels (Figs. 6 to 12, pp. 10–11), nickel–chromium–tungsten steel, often used for crankshafts (Fig. 13, p. 12), and cast steel (Figs. 14 to 17, pp. 12–13).

The relationships between the fatigue limits in bending, tension, and torsion obtained from these diagrams are shown in Table 2.1.

Although there is a considerable theoretical (and also physical) difference between fatigue phenomena and the process of fatigue, on the one hand, and simple tension and tensile strength on the other, the relationships between the two – between bending

TABLE 2.1
RATIOS ξ and η OF THE TORSIONAL AND TENSILE FATIGUE STRENGTHS
RESPECTIVELY TO THE BENDING FATIGUE STRENGTH FOR VARIOUS STEELS

Material	$\xi = \tau_F/\sigma_{bF}$	$\eta = \sigma_{tCF}/\sigma_{bF}$
St 37.11 (0.15% C)	0.588	0.706
St 42.11 (0.25% C)	0.579	0.710
St 50.11 (0.35% C)	0.583	0.750
St 60.11 (0.45% C)	0.571	0.714
St 70.11 (0.60% C)	0.594	0.719
VCN 15.69 w (En 111)	0.594	0.719
VCN 15.69 h (En 111)	0.610	0.722
VCN 25.69 w (En 25)	0.617	0.735
VCN 25.69 h (En 25 T)	0.605	0.736
VCN 35.69 w (En 23 S)	0.582	0.750
VCN 35.69 h (En 23 T)	0.572	0.714
VCN 45.69 (En 30 B)	0.608	0.761
Average	$0.592 \pm 4.2\%$	$0.728 \pm 4.5\%$
LEHR [47] determined the above ratios for a further large number of materials, with the results shown here:	$0.59 \pm 14.0\%$	$0.70 \begin{matrix} + 11 \\ - 7 \end{matrix} \%$

fatigue strength and tensile strength – have received abundant attention in the literature. Some relationships which find useful application – at least in practice if not in theory – are listed below.

Keeping the symbols already used, we have the following formulae:

MAILÄNDER's formula: $\sigma_{bF} = 0.49 \sigma_T \pm 20\%$ (4)

$\sigma_{bF} = 0.65 \sigma_{by} \pm 30\%$ (5)

STRIEBECK's formula: $\sigma_{bF} = 0.285 (\sigma_T + \sigma_{by}) \pm 20\%$ (6)

ROGER's formula: $\sigma_{bF} = 0.4 \sigma_{by} + 0.25 \sigma_T$ (7)

HOUDREMONT-MAILÄNDER formula: $\sigma_{bF} = 0.245 (\sigma_{by} + \sigma_T) + 5$ (8)

JUNGEN's formula: $\sigma_{bF} = 0.2 (\sigma_T + \lambda_{by})$ (9)

where λ_{by} is the percentage reduction of area at fracture;

LEGUIR, BUCHHOLZ, and SCHULTZ formula: $\sigma_{bF} = 0.175 (\sigma_T + \sigma_{by} - \varepsilon + 100)$ (10)

where ε is the percentage elongation in the tensile test;

FRY, KRESSNER, and OETTEL formula: $\sigma_{bF} = C_1 \sigma_T + C_2 \sigma_{by}$ (11)

where for

$\sigma_T =$	40	60	80	100	120	140	160
$C_1 =$	0.15	0.20	0.25	0.32	0.38	0.42	0.48
$C_2 =$	0.57	0.46	0.35	0.22	0.12	0	-0.10

Some authors have also examined the relationship between fatigue strength and tensile strength of materials in relation to their microstructure. The results are given in Table 2.2.

To elucidate the above, the tensile strength σ_T of each material and its reversed bending fatigue strength σ_{bF} have been plotted as abscissa and ordinate respectively in Fig. 2.1. As may be seen, the points for carbon steels, nickel-chromium steels, and cast steels all lie approximately on the same straight line.

This fact is extremely important, for it means that the bending fatigue strength of any kind of steel can be easily determined without direct observation provided that its

TABLE 2.2
RATIO σ_{bF}/σ_T FOR STEELS WITH VARIOUS MICROSTRUCTURES

Type	Ratio σ_{bF}/σ_T				
	Ferrite	Pearlite	Austenite	Martensite	Sorbite
Carbon steel	0.57-0.63	0.38-0.41	—	0.25	0.56
Alloy steel	—	—	0.35-0.45	0.23-0.47	0.57-0.60

tensile strength is known, and further, the tensile, compressive, and torsion fatigue strengths can also be determined with good approximation.

The Smith diagrams for the chromium–molybdenum and nickel–chromium–molybdenum case-hardened steels and the quenched and tempered nickel–chromium–molybdenum structural steels included in Figs. 2.2 and 2.3 have not been given, for, as can be seen, a large number of test results were obtained and the Smith diagrams for all of them would have occupied a very considerable space. Therefore only the relationship between tensile strength and bending fatigue strength has been given. In practice it is found that the relevant points lie only approximately on a straight line, and a scatter range has been shown instead of a single line in Figs. 2.2 and 2.3. As the upper and lower limits of the range are situated at a distance of only ± 5 per cent from the centre line drawn in each figure, the diagrams are sufficient for practical requirements.

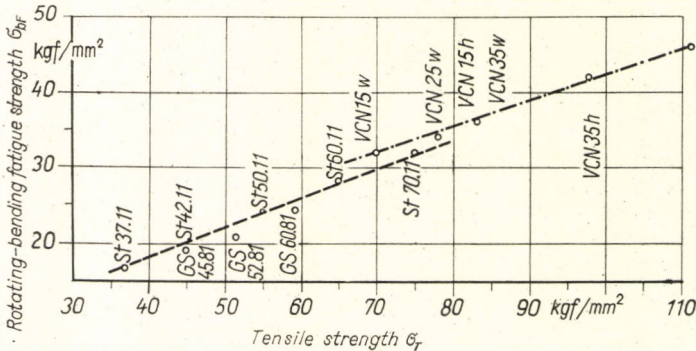


FIG. 2.1. Relationship between tensile strength and rotating-bending fatigue strength of carbon steels, cast steels, and nickel–chromium steels

In Fig. 18 of Part II (p. 13) the results from Figs. 2.1, 2.2, and 2.3 are collected, and supplemented by data from numerous authors. The chain-dotted curve indicates the relationship between tensile strength and bending fatigue strength for steels. As according to certain authors the values for high-strength alloy steels deviate somewhat from the straight lines drawn in Fig. 2.2, the top part had to be replaced by a curve in the interests of safety. The relationships between tensile strength and reversed torsion fatigue strength, and between tensile strength and reversed tension-compression fatigue strength, will also be found in Fig. 18 of Part II.

It should be emphasized, however, that the determination of the fatigue limit from the tensile strength can give only a general indication. In critical cases, or for high-alloy steels, actual testing, or, possibly, examination of the dispersion of the fatigue limit, may be unavoidable.

If necessary, the Smith diagram may be plotted entirely from theoretical data for any given steel provided that the yield stress is known. As, however, this latter depends on a number of factors, amongst them not only the composition but also the heat treatment of the material, it has no close relationship to the tensile strength. The diagram in Fig. 19 of Part II (p. 14), plotted from data given by PATTON [70] and the ASM Handbook [119], may, however, be used for practical purposes. This diagram enables the yield stress in tension to be read off when the tensile strength is known.

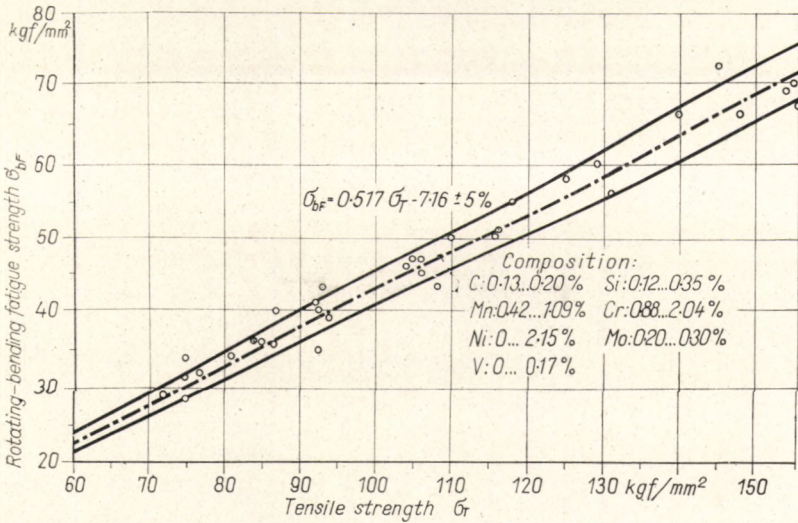


FIG. 2.2. Rotating-bending fatigue strength of chromium-molybdenum and nickel-chromium-molybdenum case-hardened steels

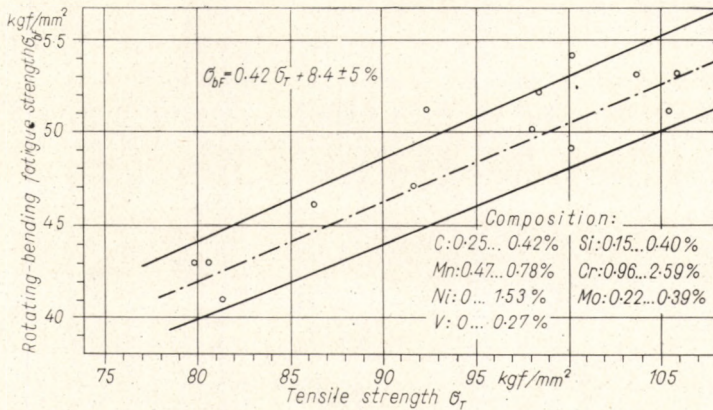


FIG. 2.3. Relationship between rotating-bending fatigue strength and tensile strength for quenched and tempered nickel-chromium-molybdenum structural steels

There is not much in the literature about the yield stress in bending. We therefore have to content ourselves with the values given in the Smith diagrams in Figs. 1 to 17 of Part II (pp. 9-13). These values are collected in Fig. 20 of Part II (p. 14). Although great caution must be exercised in deducing a relationship from the data available, the following values may be assumed for practical purposes for the yield stress in bending until more reliable data become available.

$$\text{For carbon steel} \quad \sigma_{by} = 0.57\sigma_T - 5.5 \text{ kgf/mm}^2 \quad (12)$$

$$\text{For alloy steels} \quad \sigma_{by} = 1.09\sigma_T - 37.6 \text{ kgf/mm}^2 \quad (13)$$

The above data correspond to the straight lines in Fig. 20.

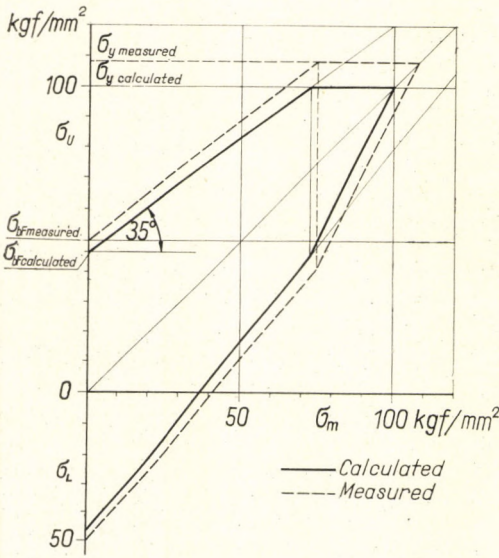


FIG. 2.4. Comparison of Smith diagrams drawn by applying Figs. 18, 19 and 20 of Part II and experimental results

Smith diagram. Afterwards draw a straight line from the point σ_U at an angle of 35° to the horizontal. If the yield stress is not known, determine it from Fig. 19 of Part II (p. 14). Cut off the 35° line at the yield stress. Then draw in the lower part of the dia-

The yield stress in shear and torsion may also be determined theoretically if its value in tension is known, for it has been proved [83] that the value of the yield stress in shear and torsion is equal to $1/\sqrt{3} = 0.577$ of its value in tension, in accordance with the HUBER-VON MISES-HENCKY shear-strain-energy theory.

Thus if the tensile strength of the material is known, the simplified Smith diagram can be plotted with sufficient accuracy with the help of calculations and diagrams. The method is as follows:

Locate the value corresponding to tensile strength on the abscissa axis in Fig. 18 of Part II (p. 13), draw a vertical line from this point to the appropriate curve, and then project the point of intersection on to the ordinate axis. This gives the fatigue limit for reversed stress ($\sigma_M = 0$). Plot this value, positive for σ_U and negative for σ_L , on the ordinate axis of the

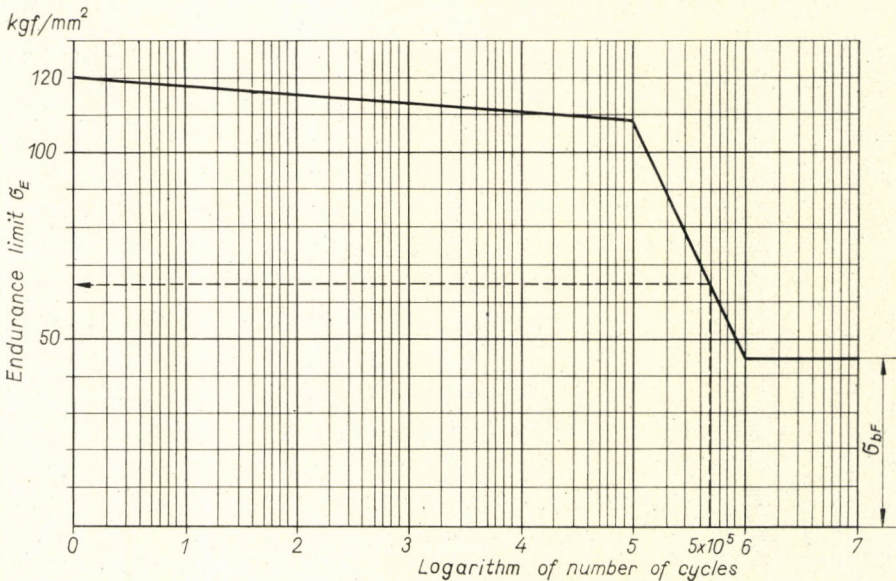


FIG. 2.5. Determination of the endurance limit of a steel ($\sigma_T = 120 \text{ kgf/mm}^2$) with endurance $N = 5 \times 10^5$ cycles using the simplified $S-N$ curve

gram in such a way that it is symmetrical with the upper part about a straight line starting from the origin and at 45° to the horizontal.

EXAMPLE. Required to plot the simplified Smith diagram of a nickel-chromium-tungsten steel (crankshaft material), $\sigma_T = 120 \text{ kgf/mm}^2$, for bending fatigue.

Figure 18 of Part II (p. 13) shows the bending fatigue strength of the material as $\sigma_{bF} = 47 \text{ kgf/mm}^2$, and Fig. 20 of Part II shows the yield point as $\sigma_{by} = 100 \text{ kgf/mm}^2$. Figure 2.4 shows the Smith diagram plotted on the basis of these data, and reproduces, for the purpose of comparison, the other Smith diagram drawn on the basis of experimental observations and already given in Fig. 13 of Part II (p. 12). There is not a great deal of difference between the two diagrams. The maximum deviation is 9 per cent, and is, moreover, on the safe side.

Finally, let us determine the permissible alternating stress if the crankshaft is required to have an endurance N of only 500 000 cycles.

Mark seven equal values of $\log N = 0, 1, 2, \dots, 7$ on the abscissa axis of a coordinate system, corresponding to values of endurance. With $\log N = 0$, plot to a suitable scale the value $\sigma_T = 120 \text{ kgf/mm}^2$ as ordinate. Then for $\log N = 5$, plot as ordinate 90 per cent of the value of σ_T , i.e. 108 kgf/mm^2 , and for $\log N = 6$, plot $\sigma_{bF} = 47 \text{ kgf/mm}^2$. By connecting the points the simplified S - N curve will be obtained. For the required endurance $N = 5 \times 10^5$, the bending fatigue stress is read off as $\sigma_{bF} = 67 \text{ kgf/mm}^2$ (Fig. 2.5).

2.2 Cast iron

The Smith diagram for cast iron differs from that for steel. The most pronounced difference is that the diagram ends in a point corresponding to the static tensile strength, for since cast iron does not elongate or yield before fracture, there is no cutting-off of the diagram as there is for steel at the yield stress. There is a further difference resulting from the fact that the compressive strength of cast iron is considerably higher than its tensile strength. In view of this, it would be a gross mistake to simplify the diagram for cast iron in the way that is permissible for steels. Figures 21 and 22 of Part II¹ (p. 15) show the Smith diagrams for two cast irons, BS 1452 : 1961 Grade 10 and Grade 14, according to POMP and HEMPEL [76]. In Fig. 23 of Part II part of the Smith diagram is shown enlarged for BS 1452 : 1961 Grade 10, Grade 12, Grade 14 and Grade 17. An empirical relationship between tensile strength and fatigue strength in bending, tension-compression, and torsion has been established from the results of tests, and is shown in Fig. 24 of Part II.

The compressive strength of cast iron of known tensile strength is easily determined from the ratio of compressive strength to tensile strength given in Fig. 25 of Part II.

2.3 Malleable cast iron

Very few data on malleable cast iron are available. Data given by POMP and HEMPEL [76] on the fatigue limit of malleable cast iron BS 310 : 1958 Grade B 22/14 have been used to prepare Fig. 26 of Part II for tension and compression, and on that of BS 310 : 1958 Grade W 24/8 to prepare Fig. 27 of Part II for torsion. The data relate to specimens with a machined surface.

The observations indicate that the fatigue limit of malleable cast iron in compression is 1.5 times that in tension.

2.4 Light alloys

The $S-N$ curves of a few light alloys are shown in Fig. 2.6. It can be seen that these $S-N$ curves, contrary to those for steels, indicate a continual decrease of the permissible stress with an increasing number of cycles. While the $S-N$ curves of steels become horizontal at a value of N between 1 and 2×10^6 , those of light alloys are still descending even beyond $N = 500 \times 10^6$. Magnesium alloys, however, are an exception; the rate of descent at high endurance becomes so small as to be negligible in practice.

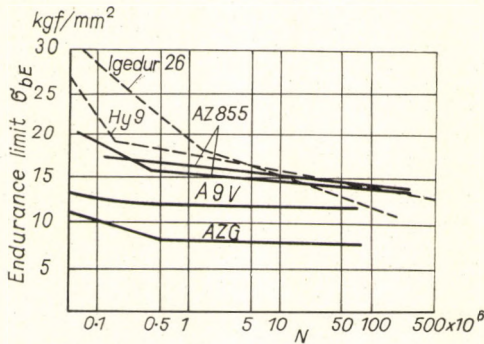


FIG. 2.6. $S-N$ curves of aluminium alloys
 AZG and A9V casting "Elektron"
 AZ 855 "Elektron"
 Hy 9 Al-Mg alloy
 Igedur 26 Al-Cu-Mg alloy
 Specimen 7.5 mm dia.

Thus one cannot properly speak of a fatigue limit in light alloys. In practice, however, the fatigue limit is taken to be the stress that the material can withstand without failure at 50×10^6 cycles. The Smith diagrams shown in Figs. 28 to 31 of Part II (pp. 16-17) have been plotted on this basis.

The fatigue strength, of course, depends very greatly upon the composition of the material. Figure 32 of Part II shows the relationship between the tensile strength and the bending fatigue strength of various magnesium alloys. The relationship between the tensile strength and the bending fatigue strength of some aluminium alloys is shown in Fig. 33 of Part II. As, however, the bending fatigue strength has a fairly large scatter (± 25 per cent), the figures serve only to provide a general indication when more precise data are not available. Tables 3 and 4 of Part II (pp. 21-25) give values of the fatigue strength of a number of light alloys.

If the fatigue strength in bending is known, it is possible to determine the fatigue strengths in tension and torsion respectively with fairly good approximation. According to W. BUCHMANN [4], the ratio of the fatigue strength in tension-compression to that in bending is

$$\eta_b = \sigma_{tcF} / \sigma_{bF} = 0.63$$

for wrought alloys (AZM and AZ855) and Al-Cu-Mg and Al-Mg alloys.

For the casting alloys AZG and A9V the ratio is

$$\eta_b = 0.48 \text{ to } 0.56.$$

Finally, the ratio of the fatigue strength in torsion to that in bending for "Elektron" (magnesium) casting alloy is

$$\tau_F / \sigma_{bF} = \eta_t = 0.55 \text{ to } 0.60$$

2.5 Non-ferrous metals

(See Table 5 of Part II, pp. 26-27.)

2.6 Plastics

Some $S-N$ curves are shown in Fig. 35 of Part II for phenolic resins, in Fig. 36 for cellulose acetate, and in Fig. 37 for some reinforced glass-fibre plastics (Part 2, p. 18).

It is clear from these figures that it is absolutely necessary to carry out tests on phenolic resins up to $N = 10 \times 10^6$ and advantageous to continue them to $N = 20 \times 10^6$. Table 2 of Part II (pp. 19-20) gives values of the fatigue strength of certain plastics.

CHAPTER 3

Effect of Various Factors on Fatigue Strength

THE data analysed in the preceding sections are from the results of fatigue tests carried out on polished specimens of standardized dimensions (mostly 10 mm in diameter) at a temperature of 20°C.

The effects on fatigue strength observed when there is a departure from these conditions are dealt with below.

3.1 Surface finish

Fatigue failures always start from points of maximum stress. During roughing-out, the turning tool digs into the material from time to time as it removes the chips, giving rise to fine cracks in the surface, which cause stress concentration and reduce fatigue strength. If this layer is removed by fine machining and grinding, stress concentration will be reduced, and consequently fatigue strength will be increased.

Numerous tests have been carried out to establish relationships between surface roughness and fatigue strength. As, however, there was for a long time no consensus of opinion regarding the measurement of surface roughness, and in addition there was a lack of suitable instruments, a large proportion of the results hitherto obtained have to be treated with reserve. According to MOORE and KOMMERS [62], the proportional decrease of fatigue strength, in relation to that of a ground and polished specimen, is as follows:

specimen turned only	12 per cent
specimen coarse-filed	18 to 20 per cent
specimen fine-filed	14 per cent
specimen polished with No. 3 emery cloth	6 per cent
specimen polished with No. 1 emery cloth	4 per cent
specimen polished with No. 0 emery cloth	2 to 3 per cent
specimen scratched at several places	16 per cent.

MAILÄNDER [53] found that the fatigue strength of steels was increased by improvement in surface finish as indicated in Table 3.1.

If the fatigue strength obtained after a long polishing time is taken as 100 per cent, the proportional reduction caused by using only a short polishing time is as follows for different tensile strengths:

$\sigma_T = 60 \text{ kgf/mm}^2$	3 per cent
$\sigma_T = 85 \text{ kgf/mm}^2$	10 per cent
$\sigma_T = 107 \text{ kgf/mm}^2$	17 per cent
$\sigma_T = 185 \text{ kgf/mm}^2$	23 per cent
$\sigma_T = 216 \text{ kgf/mm}^2$	24 per cent

TABLE 3.1

RELATIONSHIP BETWEEN MECHANICAL TREATMENT OF THE SURFACE AND BENDING FATIGUE STRENGTH FOR VARIOUS STEELS

Tensile strength, σ_T (kgf/mm ²)	Bending fatigue strength, σ_{bF} (kgf/mm ²)	
	short polishing time	long polishing time
60	31	32
85	46	51
108	50	60
216 (Ni-Cr-Mo steel)	78	102

Figure 3.1 shows the reduction factor b for bending fatigue strength corresponding to different degrees of surface finish in relation to tensile strength, as given by SIEBEL [85]. For a micropolished specimen the factor b is equal to 1 (line A corresponds to a value R of the maximum surface irregularity — roughness depth — of $1 \mu\text{m}$).

For a fine-polished surface ($R = 1.5$ to $2 \mu\text{m}$) curve B is applicable; for a precision-ground surface ($R = 2.5$ to $6 \mu\text{m}$), curve C ; for a fine-ground or smooth-finished surface ($R = 6$ to $16 \mu\text{m}$), curve D ; for a rough-machined surface, curve E ; and for an as-rolled surface (with rolling skin), curve F .

The values agree completely with MAILÄNDER's results. High-strength materials exhibit a considerably lower value of the factor b than do those of lower strength.

The correctness of the values in this diagram has been confirmed by the observations of NIEMANN and GLAUBITZ [67] in 1952, according to which

$$b = \sigma_{bF1} / \sigma_{bF2} = (R_2 / R_1)^n \quad (14)$$

where

σ_{bF1} denotes the fatigue strength of a steel with a surface finish identified as "1";

σ_{bF2} denotes the fatigue strength of the same steel with a surface finish identified as "2";

R_1 denotes the maximum roughness depth in surface finish "1" (μm);

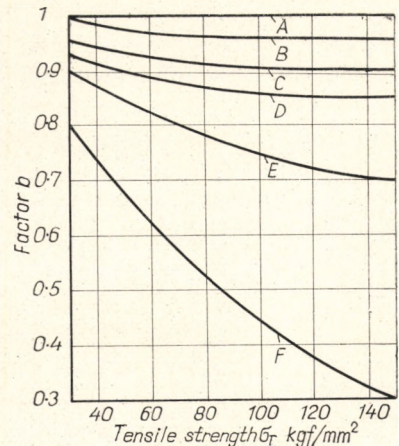


FIG. 3.1. Bending fatigue strength reduction factor b shown as a function of tensile strength and surface finish (for steels)

- A very highly polished surface
- B finely polished surface
- C precision-ground surface
- D smooth-finished surface
- E rough-machined surface
- F rolling skin left on

- R_2 denotes the maximum roughness depth in surface finish "2" (μm);
 n is a constant depending on the material.

These authors determined the values of n for two materials, viz. St 70.11 (0.60% C) with $\sigma_T = 70 \text{ kgf/mm}^2$ and VCMo 140.63 (En 19A) with $\sigma_T = 100 \text{ kgf/mm}^2$, and found $n = 0.079$ for St 70 and $n = 0.102$ for VCMo 140.63 (En 19A).

The above constants were applied to plot the graph in Fig. 38 of Part II (p. 28), from which the factor b may be read off for any given tensile strength and surface roughness.

Recent measurements have led SIEBEL and GAIER [86] to recommend the application of the factors plotted in Fig. 39 of Part II for fluctuating tensile stress and those in Fig. 40 for tension-compression and rotating-bending stress.

For cast iron Fig. 41 (Part II) was plotted on the basis of the very few data available; it shows clearly that the bending fatigue strength of cast iron is much lower for a rough surface than for a polished surface (cf. POMP and HEMPEL [76]). The factor b for cast iron in the higher strength range is so low when the casting skin is left on that, in some cases, it is questionable whether the material should be used. Cast iron in the higher strength range should therefore be used with a machined surface when at all possible.

For malleable cast iron (BS 310 : 1958 Grade B 22/14) POMP and HEMPEL [76] found the value of b to lie between 0.82 and 0.84.

3.2 Shape and dimensions

The data on fatigue strength dealt with above come from tests carried out on standardized test pieces (usually 10 mm, but in exceptional cases 7.5 or 12.5 mm, in diameter). For machine components of fairly large size or of non-circular cross-section, however, the fatigue strength, being influenced by shape and dimensions, never comes up to the values observed with the test pieces. But as tests with large-size specimens and those of varying shapes call for testing machines and apparatus of unusual capacity, which are extremely expensive, they have been carried out only on isolated occasions. This is not enough to establish a basis of assessment.

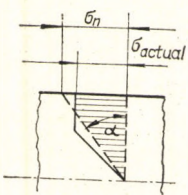


FIG. 3.2. Ideal and actual stress distribution (supporting effect)

The most modern theory of the effect of dimensions and shape, and one that shows good agreement with experience, is that of VON PHILIPP [74]. It is similar to that of BOLLENRATH and TROOST, which has already been discussed (p. 27), for he too maintains that displacements which occur when the stress distribution is not uniform — which, by the way, must not be confused with permanent deformations — are probably somewhat delayed by the grains in the inner zones, subjected to a lower stress and therefore suffering less displacement and providing support to the outer grains; but that the displacements of the latter are not completely eliminated. For this reason, the stress distribution in a specimen subjected to bending fatigue does not follow the laws of elementary theory as indicated

by the broken line in Fig. 3.2, but instead is represented by the solid line.

VON PHILIPP determined the ratios of σ_{bF} to σ_{tCF} and of τ_F to τ_{sF} for several cross-sections (Tables 3.2 and 3.3). He proved that the relationship between dimensions and

TABLE 3.2

RATIO σ_{bF}/σ_{tCF} FOR VARIOUS PROFILES

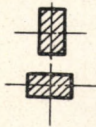
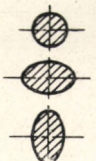
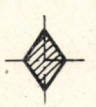

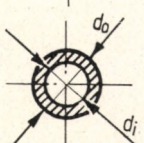
Profile	σ_{bF}/σ_{tCF}
 rectangle { upright flat	1.5
 circle ellipse	$16/3\pi = 1.695$
 vertical rhomb	2

TABLE 3.3

RATIO τ_F/τ_{Fs} OF THE TORSIONAL TO THE SHEAR FATIGUE STRENGTH FOR VARIOUS PROFILES

Profile	τ_F/τ_{Fs}
 circle	1.33
 annulus	$\frac{4}{3} \left\{ \frac{1 - (d_i/d_o)^3}{1 - (d_i/d_o)^4} \right\}$

bending or torsion fatigue strength could be represented by a unilateral hyperbola (Fig. 3.3) whose position depended on the shape of the cross-section of the test piece or component being tested. He also showed — a remarkable observation — that the thickness of the outer layer s_{Ph} , within which the displacements which he postulated took place, was a constant for the material, its value being:

$$\begin{array}{ll} \text{for steel} & s_{Ph\text{st}} = 3.1 \text{ mm} \\ \text{for light alloys} & s_{Ph\text{la}} = 1.0 \text{ mm.} \end{array}$$

A factor k_b to be used in determining the bending fatigue strength of components of various shapes and dimensions can be obtained from Fig. 42 of Part II (p. 29); the

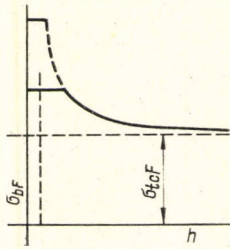


FIG. 3.3. Relation-ship between dimensions and bending fatigue strength according to VON PHILIPP

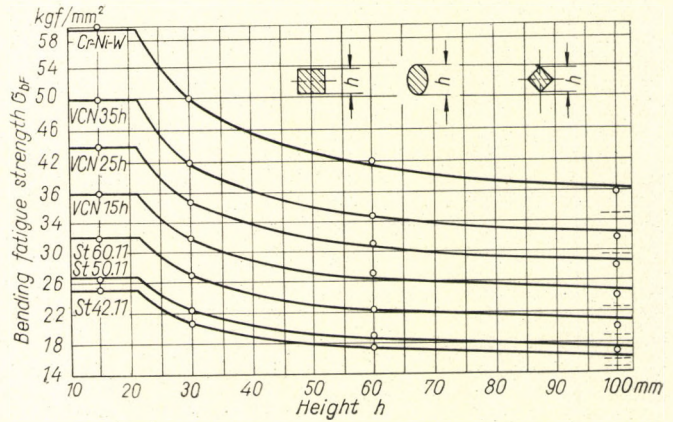


FIG. 3.4. Comparison of the values of bending fatigue strength established by tests and those calculated using the size factor b

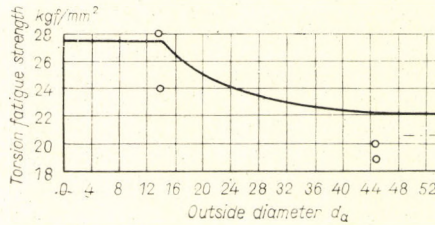


FIG. 3.5. Comparison of the values of torsion fatigue strength established by tests and those calculated using the size factor b

values of bending fatigue strength given earlier in this book have to be multiplied by this factor. For example, for a circular profile 10 mm in diameter (a standard size for test pieces) k_b for steel is equal to 1. Figure 43 of Part II gives the corresponding size factor in torsion, k_t , applicable to components of circular solid and annular cross-section.

The VON PHILIPP theory has been confirmed by experiment. Results obtained by LEHR [47] on seven types of steel, and by MAILÄNDER and BAUERSFELD [54], are plotted for comparison with VON PHILIPP's theoretical results in Figs. 3.4 and 3.5.

3.3 Temperature

The results given so far refer to room temperature, i.e. +20°C. Increase or decrease of temperature has a great effect, however, upon the strength of materials under both static and cyclic loading.

3.3.1 Elevated temperatures

a) Steels

The effect of elevated temperature upon the strength of materials depends on the duration of static and cyclic stress [43].

Under static load, inadmissible strains, changes of shape, or even "time-yield" phenomena and failures take place after a certain time at a temperature which depends

on the quality and quantity of alloying elements. According to WHITE-CLARK and WILSON, the tensile strength of a steel with 0.15 % C, 0.5 % Mn, 0.23 % Si, 0.019 % P, and 0.021 % S was 25.6 kgf/mm² at 538°C; the same material fractured at a stress of

8.4 kgf/mm ²	after	1 552 hours;
7.0 kgf/mm ²	after	3 650 hours;
6.35 kgf/mm ²	after	4 788 hours;
4.2 kgf/mm ²	after	13 950 hours.

Different definitions for the "creep limiting stress" can be found in the literature. According to the DIN standard, it is to be understood as the maximum stress (kgf/mm²) at which the rate of strain between the 25th and 35th hours of loading does not exceed 10×10^{-4} per cent per hour and the maximum permanent elongation in the 45th hour of loading does not exceed 0.2 per cent.

Under cyclic loading also, particularly at higher temperatures (above about 400°C) phenomena similar to that of "time-yield" appear. In Fig. 44 of Part II (p. 30) the Smith diagram of a chromium-molybdenum steel is plotted for temperatures of 20°, 100°, 200°, and 300°C. Within these limits the properties do not fall off to any marked extent; the diagram shows, in fact, that for symmetrical reversed stress, with $\sigma_m = 0$, the tension-compression fatigue strength increases somewhat (from 36 to 40 kgf/mm²). If the temperature of the component is below 200°C, therefore, values determined at room temperature or calculated by the methods already explained can be used under reversed-stress conditions.

Figure 45 of Part II (p. 30) shows the variation with temperature of the tension-compression fatigue limit and of the creep limiting stress for three different steels. Curve *a* (LEA and BUGDEN) is for a steel of 0.14 % C, 0.19 % Si, and 0.68 % Mn; curve *b* (WIBERG) is for a carbon steel with 0.15 % C; curve *c* (WIBERG) is for a steel with 0.35 % C and 13.5 % Cr, hardened in oil at a temperature of 925°C and then tempered at 610°C. It must be emphasized, however, that (at a temperature above 200°C) the fatigue strength alone, without reference to elongation and permanent deformation, does not give a proper idea of the adequacy of a material. HEMPEL and ARDELT [22] have plotted the Smith diagram for three steels, viz. an ordinary carbon steel, a molybdenum steel, and a nickel-chromium-tungsten steel, for temperatures of 20° and 500°C (Figs. 46, 47 and 48 of Part II, pp. 30-31). It can be seen that the reversed-symmetrical-stress ($\sigma_m = 0$) tension-compression fatigue limit does not decrease appreciably even at the high temperature; in fact in a few exceptional cases, e.g. that of molybdenum steel, it increases slightly. The creep limiting stress, however, falls considerably. To avoid a gross permanent deformation the Smith diagram for any temperature at which the creep limiting stress is below the fatigue strength (Fig. 45, Part II, p. 30) is cut off not at the room-temperature yield stress but at the creep limiting stress.

(b) *Non-ferrous metals and light alloys*

Although even fewer data are available for non-ferrous metals and light alloys than for steels, the statements made for steels may reasonably be assumed to apply here also, i.e. that at temperatures at which the creep limiting stress is below the fatigue strength, the former must be taken as the upper limit of stress. Figures 49 and 50 of Part II (p. 31) show, in relation to temperature, values of the fatigue strength of some light alloys and, in one case, the creep limiting stress; Fig. 51 shows values for a 99.5 % aluminium-copper alloy [18].

3.3.2 Low temperatures

At low temperatures the tensile strength, yield stress, and fatigue strength of steels increase. Brittleness, however, also increases, and consequently materials will be more sensitive to grooves, holes, and changes in cross-section. Figure 52 of Part II (p. 32) shows the increase of fatigue strength with decreasing temperature; the diagram was prepared by interpolation of the data in references [23] and [82]. The tension-compression and bending fatigue strengths in kgf/mm^2 are plotted as abscissae and the temperature factor K_T , by which the values of fatigue strength at $+20^\circ\text{C}$ have to be multiplied to arrive at the values for the lower temperatures, as ordinates. The increase in fatigue strength between -20° and -40°C , i.e. in the range most common in practice, is insignificant.

Down to -40°C copper behaves in a similar way to steel. The increase of fatigue strength of aluminium and its alloys is even less than for steel, and can therefore be ignored in practice.

3.4 Surface treatment

Fatigue fracture surfaces show clearly that the crack forming the beginning of the fracture always starts from the surface of the specimen or component. Surface finish is therefore of the utmost importance. With a brittle surface, e.g. a chromium-plated one, the first hair-cracks appear at once, causing stress concentration and so facilitating the propagation of the cracks into the deeper layers.

Surface treatments such as rolling, shot-peening, carburizing, nitriding, etc., produce residual compressive stresses in the surface of the workpieces, and increase the fatigue strength if the applied stress is in the opposite direction.

3.4.1 Surface hardening

In surface hardening, a martensitic or nitrided layer is formed. As its specific space requirement is greater than that of the original material, compressive stresses will occur at the surface. If the loading is such as to produce a tensile stress at the surface, as for example on the outside of a bend, the compressive stress already present will greatly reduce the magnitude of the net tensile stress. Although there will be a proportionate increase in compressive stress at the inside of the bend, the total effect of surface hardening or nitriding will be to increase the strength of the specimen or component considerably, for steels are much stronger in compression than in tension (Fig. 3.6).

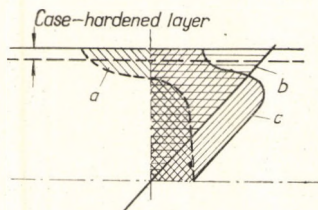


FIG. 3.6. Stress distribution in a case-hardened material
a: internal stress due to hardening; *b*: internal stress due to external forces; *c*: resultant of internal stresses

When case-hardening is used, the whole surface of the workpiece must be hardened, since fatigue strength decreases sharply at the boundaries of the unhardened surfaces [113] (see Table 3.4).

According to WILSON [116], the fatigue strength of a six-cranked aircraft crankshaft (tensile strength 100 to 116 kgf/mm^2) fell by 33 per cent because the crankpins were ground down to the base material at the ends after the surface hardening.

TABLE 3.4
DECREASE OF FATIGUE STRENGTH RESULTING FROM DISCONTINUITY OF
A HARDENED LAYER

Material composition: 0.5% C, 0.3% Si, 0.5% Mn, 0.035% P, 0.002% S,
1.92% Cr, 2.15% Ni, 0.22% Mo
Specimens 14 mm in diameter.

Condition	Surface treatment	σ_{bF}	τ_F
		kgf/mm ²	
1. Smooth cylindrical surface	Oil quenched 820° to 840°C, tempered 2 hours 200°C	62	25
2. Smooth cylindrical surface	Carburized layer reduced in thick- ness from 0.4 mm to 0.2 mm by grinding	80	31.5
3. With transverse hole 2 mm in diameter	Heat treatment as for No. 1	34	12
4. With transverse hole 2 mm in diameter	Case-hardened as for No. 2; trans- verse hole drilled subsequently	21	10
5. With transverse hole 2 mm in diameter	Case-hardened as for No. 2 after drilling of transverse hole	44	29
6. With conical case-hardened layer	Case-hardened as for No. 2; hardened layer then ground away down to the material beneath	57	—

TABLE 3.5

TENSION-COMPRESSION FATIGUE STRENGTH OF QUENCHED AND TEMPERED STEEL
AFTER NITRIDING

Condition			σ_{icF}	
			kgf/mm ²	per cent
Quenched and tempered			34.5	100
Conditions of preliminary nitriding				
Temperature (°C)	Time (h)	Layer thickness (mm)		
480	30	0.15	38	110
520	30	0.32	43.5	126
520	30	0.52	47	136
520	6	0.34	45	130
570	10			
480	14			

Good results are obtainable with nitriding also; the bending fatigue strength increases by from 20 to 35 per cent according to the thickness of the nitrided layer [114].

For a steel containing 0.34% C, 0.45% Mn, 0.25% Si, 1.60% Cr, 0.47% Ni, and 0.83% Al, J. E. KONTOROVIC and E. J. ARANOVIC [40] observed a tensile strength of 100 kgf/mm² and a bending fatigue strength of 49 kgf/mm² after oil quenching at 950°C and suitable annealing. By nitriding for 10 hours at 500° to 650°C it was possible to increase the bending fatigue strength by 12 to 23 per cent, while by nitriding for 30 to 50 hours the increase obtained was as high as 29 per cent.

Torsion fatigue strength can also be increased to a small extent by nitriding; after 10 hours' treatment the increase was from 3 to 10 per cent, but it was only 17 per cent after 30 to 50 hours [40].

N. V. PINESZ observed an increase of the tension-compression fatigue strength with nitriding of a steel containing 0.32% C, 1.46% Cr, 0.22% Mo, and 0.96% Al, oil quenched at 950°C and oil tempered at 650°C (Table 3.5).

Even better results can be achieved by induction surface hardening. According to I. V. KUDRYAVTSEV [44], the fatigue strength of a steel containing 0.38% C, 0.2% Si, 0.54% Mn, 0.013% P, 0.07% Cr, and 0.24% Ni was increased from 24.5 to 42.5 kgf/mm² (by 173 per cent) by induction hardening. It is also interesting to note that a high-frequency induction-hardened specimen suffered no great reduction of fatigue strength by subsequent turning of a groove in the hardened layer [44]. The explanation probably lies in the compressive stress at the surface produced by the cutting pressure.

3.4.2 Surface rolling

Rolling causes residual compressive stresses at the surface of a workpiece, and increases the fatigue strength just as does thermal hardening of the surface. According to KUDRYAVTSEV the increase is between 27 and 33 per cent.

HORGER and MAULBETSCH [31] observed that after a rolling treatment under a pressure of about 2000 kgf applied through rolls 2.92 inches in diameter and 0.63 inch wide at a feed rate of 60 steps per inch, the fatigue strength of a shaft 2 inches in diameter increased by 41 per cent.

The relationship between the percentage increase of the Vickers hardness number at the surface and the bending fatigue strength is as follows:

Increase of Vickers hardness number HV (per cent)	10	20	30	40	50
Increase of σ_{bF} (per cent)	10	15	20	22	25

Similar results were reported by HORGER [29].

3.4.3 Electrolytic deposits

It is well known that chromium-plating gives protection from wear and corrosion; but it has an unfavourable effect on fatigue strength.

H. WIEGAND and R. SCHEINOST do not support the view that in chromium-plating hydrogen "in statu nascendi" (atomic) penetrates partly into the gaps between the grains and the slag inclusions and partly between the base material and the chromium layer, thus provoking a disintegration of the grains which reduces the fatigue strength. In their opinion, the only reason for the decrease of fatigue strength is the brittleness of

the chromium layer. The bubbles of hydrogen penetrating between the base material and the chromium merely accelerate the decrease of fatigue strength, especially if the chromium layer is fairly thick.

Chromium-plating has a particularly deleterious effect at positions of stress concentration such as at the edges of holes, in grooves, etc. The decrease of bending fatigue strength caused by chromium layers of various thicknesses is as follows:

- 7 to 15 per cent for chromium 0.04 mm thick;
- approximately 35 per cent for chromium 0.15 mm thick;
- approximately 50 per cent for chromium 0.20 mm thick.

This holds even with a two-hour annealing at 250°C in the last two cases.

KUDRYAVTSEV [44] finds that nickel-plating, owing to the residual tensile stress in the nickel layer, reduces the bending fatigue strength of mild steels with low carbon content (e.g. StC 10.61 with 0.08% C) by about 9 per cent, but that of steels with higher carbon content (e.g. St 50.11 with 0.63% C) by 30 to 34 per cent. An electro-deposited copper layer reduces the bending fatigue strength by about 13 per cent [44]. Electro-deposited zinc does not affect the bending fatigue strength.

The variation of the bending fatigue strength of light alloys with an anodic oxidation was investigated by H. WIEGAND [114] (Table 3.6).

3.4.4 Metal spraying

Voids (interstices) occurring in the amalgamation of incandescent metal particles are sources of hair cracks, reducing the fatigue strength of the specimens or components. According to THUM and LANGE, the bending fatigue strength of a metal-sprayed specimen of an Al-Cu-Mg alloy known as "Heddur" was about 14 per cent less than that of an unsprayed test piece.

TABLE 3.6

CHANGE IN FATIGUE STRENGTH OF LIGHT ALLOYS WITH ANODIC OXIDATION

Material	Surface treatment	σ_{bF}		τ_F	
		kgf/mm ²	per cent	kgf/mm ²	per cent
AZM Elektron $N = 10^7$ $\sigma_T = 27$ kgf/mm ²	Original condition with finish-machined surface	11	100	3.5	100
	As above, anodized*	9	82	—	—
	As above, seomagized**	8	73	4	114
	As above, chromatized***	8	73	3.5	100
A9V Elektron $N = 10^7$ $\sigma_T = 11$ to 15 kgf/mm ²	Original condition with finish-machined surface	6.5	100	3.5	100
	As above, seomagized**	4.5	69	4	114
	As above, chromatized***	4	61.5	4	114

* Regarding anodization, see SCHMIDT, JENNEY and EISLER, ZVDI 1934, p. 1499.

** Seomagization means anodic oxidation of magnesium alloys by the Siemens-Halske Company's process.

*** Chromatization means the pickling of magnesium alloys, e.g. in sodium bichromate.

3.5 Corrosion

The surface of metals coming into contact with water, particularly sea water, is covered with a thin deposit as a result of corrosion. If the deposit is insoluble in water, it forms a protection against further corrosion and the metal becomes "rust-proof", while in the opposite case it develops "rust spots". Under repeated loading such a deposit provides rust protection only if it is elastic enough; otherwise it gradually cracks and breaks away.

In consequence of corrosion, pitting of metals occurs, first on the surface, where it is often visible to the naked eye, then penetrating deeper and deeper, causing stress concentration under repeated stress and initiating fatigue fracture.

It follows that corroded metals have a much lower fatigue strength than those that are not corroded, and that the reduction in fatigue strength depends on the degree of corrosion. The reduction in fatigue strength also depends on, amongst other things, the composition of the liquid causing corrosion (rainwater, sea water, acid or alkaline spring water) and on the duration of exposure. Tests are carried out either by exposing a specimen or component to the corroding medium for a given time (some days or months) and then performing the fatigue test, or by subjecting the specimen immersed in the liquid to repeated loading. In the latter case the liquid will penetrate into the fatigue hair-cracks, where its damaging effect will continue. It was from results obtained under such conditions that MCADAM plotted the curve f shown in Fig. 53 of Part II (p. 32), where the exceedingly rapid decrease in fatigue strength is clearly visible.

The fatigue strength of metals exposed to corrosion is influenced by the following factors:

3.5.1 Composition of materials

Figure 54 of Part II (p. 33) is a summary diagram based on MCADAM's investigations. It is clear from Fig. 18 of Part II (p. 13) that the relationship between tensile strength and bending fatigue strength is approximately linear. The relationship between the tensile strength and the bending fatigue strength of steels exposed to corrosion by tap water is likewise linear. It is noteworthy, however, that while the fatigue strength of uncorroded steels increases considerably with increase of tensile strength (see Fig. 54), that of corroded steels remains almost unchanged, i.e. 16 to 18 kgf/mm².

The influence of corrosion on cast steel and cast iron is shown in Tables 6 and 7 of Part II.

Pure nickel suffers a reduction in fatigue strength of 30 to 50 per cent under corrosion in tap water and 40 to 60 per cent in sea water. Monel metal (about 25% to 30% Cu and 65% to 70% Ni) shows a similar reduction in fatigue strength; if the copper content of the alloy is higher, the reduction is rather less — about 16 to 40 per cent in tap water.

The fatigue strength of pure electrolytic copper shows no reduction.

The fatigue strength of Cu-Zn alloys (brass) is reduced by from 8 to 30 per cent in tap water and 23 to 45 per cent in salt water. The reduction is inversely proportional to the copper content.

The fatigue strength of Cu-Zn-Sn alloys (bronze) is reduced by about 25 per cent in salt water; for Cu-Sn alloys the reduction is 4 to 20 per cent in salt water, but only 4 to 10 per cent in tap water.

There is no reduction at all in the fatigue strength of Cr-Ni alloys in tap water, but in sea water there is a reduction of 8 to 50 per cent.

The reduction in the fatigue strength of pure aluminium is approximately 50 per cent in both tap water and sea water. For duralumins it is 17 to 50 per cent in tap water and 30 to 60 per cent in sea water. Silumin alloys exhibit no reduction in fatigue strength in tap water and only a 10 to 25 per cent reduction in sea water. The fatigue strength of "Elektron" and other magnesium alloys is reduced by about 50 per cent in tap water and about 70 per cent in sea water. (Table 8 of Part II.)

3.5.2 Liquids producing corrosion

The effect of the liquid corrosive medium is shown in Fig. 55 of Part II (p. 33). Information on the effect of various kinds of water is given in Table 9 of Part II, and on that of steam, and of steam and air in Table 10.

3.5.3 Number of load cycles

The continuing progress of corrosion reduces the fatigue strength of steels very considerably. Since, for example, the time required to complete 50×10^6 cycles is ten times that required to complete 5×10^6 cycles (if the frequency is the same), the fatigue strength will be lower in the first than in the second case. Some results obtained with VCN 35.62 mild steel in tap water are given in Table 11 of Part II.

3.5.4 Loading frequency

The progress of corrosion is influenced by the loading frequency (n cycles per minute). Figure 56 of Part II (p. 33) shows the reduction of the fatigue strength of a hardened and tempered Cr-Si-Ni steel in relation to the frequency n and the total number of cycles N . The tensile strength of the material was 176 kgf/mm².

3.5.5 Type of stress

Tests carried out by MCADAM indicated that under the influence of corrosion the torsion fatigue strength of metals was reduced more than was the bending fatigue strength (Fig. 57 of Part II, p. 33). The tests were carried out on a steel containing 0.46% C, 0.88% Cr, 0.34% V; its tensile strength was 68.4 kgf/mm² in the annealed and 103 kgf/mm² in the quenched and tempered condition. It can be seen that in both conditions whilst specimens subjected to corrosion in tap water had a bending fatigue strength at $N = 10^7$, for example, of about 65 per cent of that of an uncorroded specimen, the torsion fatigue strength was only 40 to 50 per cent of that of the uncorroded specimen.

3.5.6 Mean stress

Thin corrosion coatings resist compression better than tension, so that the greater the mean compressive stress, the greater is the fatigue strength of corroded metals. Investigations by THUM and OCHS [99] showed that in relation to the uncorroded material the reduction of the fatigue strength of spring steel in repeated compression ($\sigma_U = 0$) was only 5 per cent, while in repeated tension it was 90 per cent. Even though the data for individual steels and other metals show some scatter, they clearly demonstrate the effect of mean stress on the fatigue strength of corroded metals.

3.6 Fretting corrosion

Phenomena similar to corrosion appear in bolted joints, wheel hubs, or, in general, at places where two materials are in contact with each other under pressure. First discolorations, and then small pits, appear on the surface of the softer metal, and eventually fatigue failure occurs at a considerably lower endurance than in smooth test specimens.

The phenomenon has been investigated by several authors. Amongst them mention should be made of TOMLINSON et al. [104], who published the following observations:

(a) Fretting corrosion always appears in places in which metals in close contact undergo relative displacement brought about by elastic deformation, even if the displacement is extremely small. Such a displacement occurs, for example, between a shaft and a wheel hub keyed on to it, due to the elastic torsion of the shaft.

(b) Fretting corrosion is greatest if both elements in contact are completely dry. Thus the rate of corrosion decreases with increasing humidity of the atmosphere.

(c) The degree of fretting corrosion depends upon the specific pressure between the two metals concerned.

(d) In general, less fretting corrosion is evident in softer than in harder materials.

HEYWOOD [28] made 250 tests to investigate fretting corrosion of pin joints in aluminium alloy plates using steel fasteners such as bolts and rivets. His results showed that the plates clamped with close-fitting fasteners, i.e. where the size of the hole exceeds that of the bolt by only 0.07 to 0.08 per cent, had approximately 3.3 times as long a life as plates with loose-fitting fasteners, i.e. with clearances of 0.5 to 1 per cent. Furthermore, the life was increased 2.9 times by lubricating the joint with molybdenum disulphide (MoS_2).

MCDOWELL [52] found that fretting corrosion appeared very easily between light alloys and either steels or chromium-plated surfaces, but that combinations of hardened steel and high-alloy tool steels, plain cast iron and cast iron with a phosphate surface coating, and metals coated with molybdenum or tungsten disulphide, proved to be highly resistant.

Several authors consider that fretting corrosion reduces fatigue strength to 25 to 30 per cent of that of a smooth specimen. Some tests have indicated, however, that the reduction amounts to only 5 per cent.

3.7 Previous history

Besides the factors already dealt with, the previous history of a specimen or machine component, involving all kinds of influences, abuse, hardening, etc., also affects the fatigue strength. From a practical point of view investigation of these influences gives information on the effect of a few loadings (e.g. an occasional exceeding of the yield point) departing from the exact and regularly repeated load of the fatigue testing machine.

3.7.1 Occasional stresses above yield

With materials having a yield point (i.e. a permanent deformation at a certain stress prior to fracture) the fatigue strength is not reduced by occasional stressing beyond yield as long as cracks do not occur in the yielding, and may in fact be increased.

Of the numerous investigations in this field we mention only those of A. THUM and A. ERKER [96]. Their tests were carried out on St 52 steel welded with heavily coated electrodes. The steel was of the following composition: 0.14% C, 0.36% Si, 1.49% Mn, 0.02% P, 0.019% S, and 0.37% Cu. Figures 3.7 and 3.8 show the stress-strain diagrams of butt-welded and fillet-welded test pieces. After welding, the joints were loaded beyond the yield to the points V_1 , V_2 , and V_3 respectively. The $S-N$ curves were then obtained (Figs. 3.9 and 3.10).

Both diagrams demonstrated that as long as there was no cracking in the welds (see the curves corresponding to points V_1 and V_2), the fatigue strength was either not reduced at all or reduced only slightly. After loading to the point V_3 , however, which was just below the fracture load, cracks, clearly visible in the test piece to the naked eye, caused a substantial reduction in the fatigue strength of the butt-welded test piece.

From the results of their own and other researches, KÖRBER and HEMPEL [41] observed that if low-alloy steels are strained 5 to 10 per cent, and then left for from 2 to 20 days or aged for one hour at 250° to 260°C, the fatigue strength increases by 10 per cent; but for more highly alloyed steels the increase is only about 5 per cent.

3.7.2 Cumulative damage

MINER's hypothesis of cumulative damage has been explained in section 1.6.2 (p. 18) in connection with the LOCATI method.

3.7.3 "Coaxing" of steels

Among factors influencing fatigue strength, what is known as "coaxing" must be noted; it occurs in certain circumstances in some materials, particularly in steels, under cyclic stress. It has been observed that an increase in fatigue strength of 20 to 30 or even 60 per cent can be obtained if specimens are stressed for 4 to 10×10^6 cycles at 10 to 15 per cent less than the fatigue limit and the process is then repeated several times, increasing the applied stress by 2 to 5 per cent each time. This explains the fact that in many cases new (and thus not "coaxed") replacements for machine components (e.g. shafts) fracture under a moderate overload, although made from the same material as the original component, which had been used for a long time and thus "coaxed" in service.

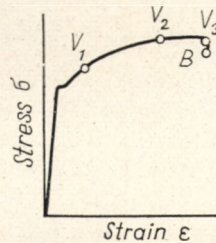


FIG. 3.7. Stress-strain diagram of a butt-welded joint

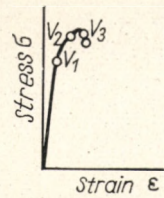


FIG. 3.8. Stress-strain diagram of a fillet-welded joint

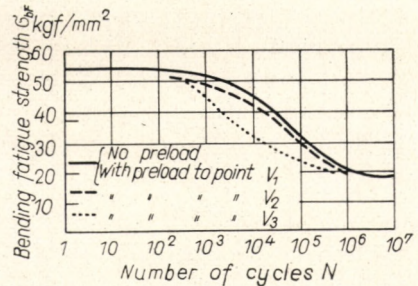


FIG. 3.9. $S-N$ curves of a butt-welded joint, $\sigma_1 = 2 \text{ kgf/mm}^2$, after preloads V_1 , V_2 , and V_3 (Fig. 3.7)

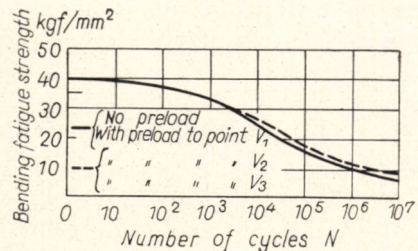


FIG. 3.10. $S-N$ curves of a fillet-welded joint after preloads V_1 , V_2 , and V_3 (Fig. 3.8)

TABLE 3.7

SERIES OF TESTS FOR "COAXING" OF STEELS
(HEROLD [24])

Stress (kgf/mm ²)	Number of cycles (millions)	Cumulative total of cycles (millions)
26	3.515	3.515
28	12.494	16.009
30	7.875	23.884
32	5.605	29.489
33	6.115	35.604
35	0.230	35.834
36	5.490	41.324
38	11.840	53.164
40	5.886	59.050
42	1.845	60.895
		fracture

TABLE 3.8

SERIES OF TESTS FOR "COAXING" OF STEELS
(LEHR [47])

Stress (kgf/mm ²)	Number of cycles (millions)	Cumulative total of cycles (millions)
22	1.65	1.65
23	1.17	2.82
24.3	1.72	4.54
25	0.92	5.46
26.4	0.85	6.31
28	1.15	7.46
29.3	1.00	8.46
31	1.08	9.54
32.8	0.86	10.40
34	0.34	10.83
35.8	0.43	11.26
37.3	0.067	11.327
		broken

The results of two interesting "coaxing" tests are given below:

HEROLD's test [24], carried out on Cr-Ni-W steel (Table 3.7).

Composition 0.34% C, 1.06% Si, 0.52% Mn, 10.91% Ni, 11.96% Cr, 2% W.

Mechanical properties — yield stress σ_{by} 42.6 kgf/mm², tensile strength σ_T 82 kgf/mm², bending fatigue strength σ_{bF} 30 kgf/mm².

The increase of bending fatigue strength was about 40 per cent.

LEHR's test [47], carried out on a tool steel with 0.9% C and a lamellar pearlitic structure (Table 3.8).

Mechanical properties — yield stress σ_{by} 24.8 kgf/mm², tensile strength σ_T 71 kgf/mm², bending fatigue strength σ_{bF} 24 kgf/mm².

The increase of bending fatigue strength was about 56 per cent.

As, however, very little is to be found about "coaxing" in the literature, and what there is confines itself mostly to description instead of explanation, it is best to take the degree of strengthening produced by "coaxing" from the results of actual tests carried out on the appropriate specimen.

CHAPTER 4

Theoretical Stress Concentration Factor

THE preceding sections have dealt with the factors that affect the fatigue strength of materials. It is clear that if failure is to be avoided, machine components must be dimensioned with such a factor of safety that the stresses occurring are always less than the fatigue limit (or in some cases the appropriate endurance limit) of the material concerned.

It has been demonstrated by experience, by calculations and by measurements, however, that local stresses considerably higher than those given by elementary theory often occur. It was shown by SAINT VENANT that the elementary formulae $\sigma_{tc} = F/A$ for tensile and compressive stresses and $\sigma_b = M_b/W$ for bending stresses are only valid when the cross-section concerned is uniform and far enough away from the point of application of the load. In practice, however, there are cross-sections with holes, steps, grooves, etc., where local stresses exceed the calculated values.

It is therefore necessary to study the extent to which changes in cross-section, grooves, notches, etc., occasion an increase in stress, and by how much the local stress exceeds the calculated nominal stress. The ratio of the two, which depends on the shape of the component or workpiece, is called the stress concentration factor, K_t ; thus

$$K_t = \sigma_{\max} / \sigma_{\text{nom}} .$$

The stress concentration factor can be determined theoretically (NEUBER [64]).

To avoid the necessity of using the rather complicated formulae applicable, appropriate nomograms are given in Part II.

4.1 The Neuber nomogram

The Neuber nomogram [64] consists of two parts, the first being a table (Fig. 58 of Part II, p. 37) showing the curve and scale of the nomogram to be used in the different cases of stress concentration, and the second being the nomogram proper. This latter consists of two parts, viz. the basic and the supplementary nomograms (Figs. 59 and 60 of Part II, p. 38), the latter being applied in cases of stress concentration in hollow workpieces.

4.1.1 Application of the basic nomogram

Find the value of $\sqrt{a/r}$ on the right-hand part of the abscissa, and then proceed from this point upwards parallel to the ordinate until the appropriate curve is reached. Project the point of intersection on to the ordinate scale and connect the resulting point by a straight line to the value $\sqrt{h/r}$ on the left-hand part of the abscissa. The circle

to which this straight line is a tangent indicates the value of the stress concentration factor K_t .

For hollow workpieces, find the value of $\sqrt{b/r}$ on the right-hand part of the abscissa (Fig. 60 of Part II, p. 38), and draw a line parallel to the ordinate up to the appropriate curve. Project the point of intersection on to the ordinate scale and connect the resulting point by a straight line to that value of K_t , on the left-hand part of the abscissa, which Fig. 59 gives as the stress concentration factor for solid workpieces. The circle to which this straight line is a tangent indicates the value of the required stress concentration factor K_t .

Although these nomograms are correct theoretically, their use in practice is limited, because, firstly, the curves are so close together near the beginning that it is difficult to distinguish between them, and secondly, it is necessary to draw a circle touching the line connecting two points and then to read off the value it gives on the scale. This makes it tedious to use the nomograms, and the values obtained are not precise. The Neuber nomogram thus relates only to particular examples of stress concentration, and does not cover all the cases which may occur.

4.2 Tables of stress concentration factor

Numerous investigations, using the most varied methods, have been made to determine the stress concentration factor. Extremely valuable results have been reported by FROCHT, HETÉNYI, NÁDAI, HEYWOOD, and others, using photoelastic techniques, while others have reported tests carried out with electric resistance strain gauges (e.g. GIBBONS) or using electrical models (THUM). Their results were plotted on diagrams. Except for a few cases it is more convenient, however, to give the values (shown in Table 12 of Part II, pp. 39–56) in place of the diagrams, because any required values can be obtained from them quickly, and with sufficient accuracy, by interpolation. The accuracy will at least be better than is attainable with small-scale diagrams, showing only a few curves, as reproduced in books or periodicals.

If the required value of K_t cannot be read directly from the table, the stress concentration factors for one or two lower and one or two higher values should be plotted to a suitable scale on millimetre paper and the required value interpolated graphically.

Mathematical interpolation may sometimes be quicker. In that case the well-known interpolation formula

$$K_{t\text{req}} = K_{t1} + \frac{K_{t2} - K_{t1}}{(D/d)_2 - (D/d)_1} \{(D/d)_{\text{req}} - (D/d)_1\} \quad (15)$$

should be applied.

It is necessary, however, that

$$K_{t1} < K_{t\text{req}} < K_{t2} \text{ and } (D/d)_1 < (D/d)_{\text{req}} < (D/d)_2.$$

If the parameter does not happen to be (D/d) , the formula has to be modified as reason indicates.

The calculation is simplified by the nomogram shown in Fig. 61 of Part II (p. 41). It is used as follows:

Let $(D/d)_2$ be the next higher and $(D/d)_1$ the next lower value in Table 12 of Part II, to $(D/d)_{\text{req}}$, and K_{t2} and K_{t1} the respective stress concentration factors.

Join the difference $K_{t2} - K_{t1}$ on the left-hand scale to $(D/d)_{\text{req}} - (D/d)_1$ on the right-hand scale by a straight line. Then join the point of intersection of this line and the central line with the point $(D/d)_2 - (D/d)_1$ on the right-hand scale. The second straight line will intersect the left-hand scale at the point $K_{t\text{req}}$, i.e. the required value $K_{t\text{req}}$ will be given by adding K_{t1} to the value obtained on the left-hand scale.

For the sake of completeness it should be mentioned that interpolation must sometimes be done in two directions, i.e. first between values of D/d and then between values of r/d .

EXAMPLE. What is the stress concentration factor to be applied for a stepped shaft with $D = 60$ mm, $d = 52$ mm, and $r = 4$ mm, under bending stress?

The dimensions give $D/d = 60/52 = 1.153$ and $r/d = 4/52 = 0.077$. These values cannot be found, however, in Table 12, sub-table No. 23, so that interpolation becomes necessary. It is first made between values of D/d .

With $r/d = 0.04$ and $D/d = 1.10$ we have $K_t = 2.00$, and with $D/d = 1.20$ we have $K_t = 2.09$.

Interpolating for $D/d = 1.153$,

$$K_t = 2.0 + \frac{2.09 - 2.0}{1.20 - 1.10} (1.153 - 1.100) = 2.048.$$

Likewise for $r/d = 0.10$: with $D/d = 1.10$ we have $K_t = 1.59$, and with $D/d = 1.20$ we have $K_t = 1.62$. Interpolating for $D/d = 1.153$, we have

$$K_t = 1.59 + \frac{1.62 - 1.59}{1.20 - 1.10} (1.153 - 1.100) = 1.606$$

And now interpolating between values of $\frac{r}{d}$

$$\text{if } \frac{r}{d} = 0.04 \quad K_t = 2.048$$

$$\frac{r}{d} = 0.10 \quad K_t = 1.606$$

$$\text{for } \frac{r}{d} = 0.077$$

$$K_t = 1.606 + \frac{2.048 - 1.606}{0.10 - 0.04} (0.100 - 0.077) = 1.776 \approx 1.78$$

4.3 Multiple stress raisers

Stress concentrations arising from more than one groove are not always greater than those produced by a single groove. It can indeed be an advantage to form additional grooves close to the one necessary in the design, the stress being reduced as a result. Again, the grooves may exert no influence whatever on one another, yet it is equally possible that the presence of several grooves will considerably increase the stress concentration. What determines whether one case or the other prevails?

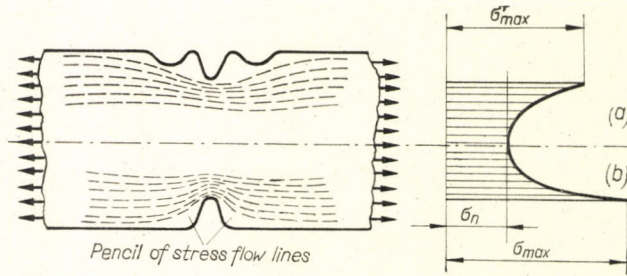


FIG. 4.1. Stress flow lines of a machine component stressed in tension
 (a) concentration is reduced by smaller notches in the pencil of stress flow lines in front of and behind the notch
 (b) high concentration of stress flow lines at root of notch

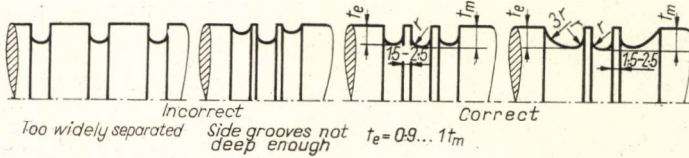


FIG. 4.2. Correct and incorrect formation of stress-relieving grooves

4.3.1 Effect of multiple stress raisers closely spaced in the line of action of the stress

Figure 4.1b shows one side of a beam which is notched on both sides and stressed in tension. The broken lines in the diagram represent the lines of stress flow. There is a pencil of stress flow lines immediately in front of the notch, but a sudden crowding of the lines at the root of the notch. The maximum stress is K_t times as great as for uniform stress distribution (see section 4.1). If a similar notch, or one a little smaller but of the same shape, is cut in the pencil of stress flow lines (Fig. 4.1a), the lines will not exhibit

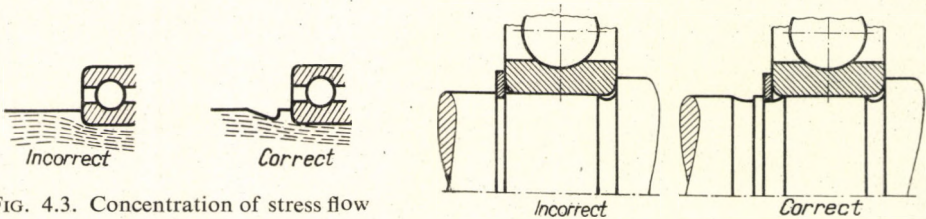


FIG. 4.3. Concentration of stress flow lines where shaft diameter alters. Concentration can be reduced by means of stress-relieving grooves

FIG. 4.4. Correct and incorrect formation of a shaft for ball bearings

the sudden crowding but will be disposed as if the notch had a larger radius, or, what amounts to the same thing, as if the stress concentration factor were lower. Figure 4.2 shows some correct and incorrect forms of stress-relieving notches.

This also holds for a plate with a central hole. Holes of equal or smaller size provided in front of and behind the first hole required by the design decrease the stress peaks.

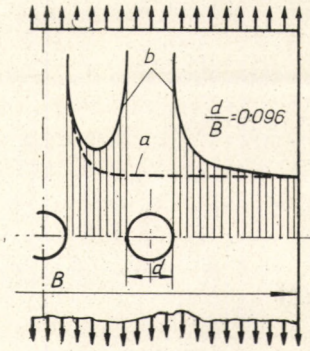


FIG. 4.5. Stress distribution in a drilled plate.
a—one central hole, $K_t = 2.75$
b—with an additional hole drilled on each side, $K_t = 2.28$

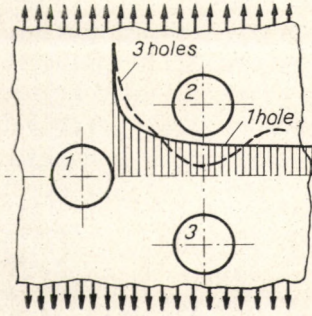


FIG. 4.6. Plate stressed in tension with holes drilled in more than one row. Holes 2 and 3 are situated in opposite stress-flow-line pencils, so that the stress increase sat the edges

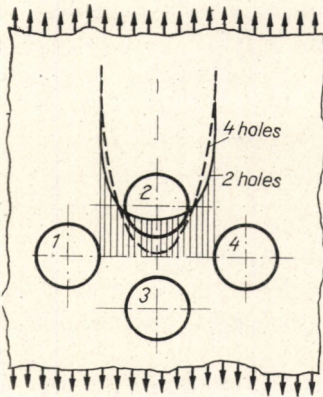


FIG. 4.7. Since holes 2 and 3 are closer together than in Fig. 4.6, stress concentration is higher.
 $K_t = 2.07$ for holes 1 and 4
 $K_t = 3.83$ for holes 1, 2, 3 and 4

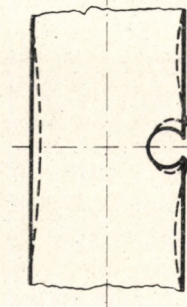


FIG. 4.8. If a hole is very close to the edge of the plate, the stresses increase considerably on account of bending moments

This is also why a thread always has a lower stress concentration factor than a single groove of the same dimensions, and why it is advantageous to cut a groove close to the shoulder required on a shaft when a ball or roller bearing is to be fitted (Figs. 4.3. and 4.4).

4.3.2 Effect of multiple stress raisers in a line perpendicular to the line of action of the stress

(a) If the spacing is great enough (e.g. when the ligament width is not less than twice the radius of the hole for rivet holes) the stress concentration factor remains unchanged, and the several sources of stress concentration have no effect on one another.

(b) With close spacing, the concentration of stress in relation to the uniform stress (e.g. under tensile loading) in the unpierced cross-section is higher.

The broken line in Fig. 4.5 represents the stress distribution in a flat beam, with a central hole, loaded in tension. If a further hole is drilled symmetrically at each side of the central hole (one side of the beam only is shown in Fig. 4.5), the stress concentration will give the distribution represented by the full line. The increase in stress concentration may, however, be less than the decrease in cross-section, so that in the end the resultant stress concentration factor, calculated on the reduced cross-section, is lower.

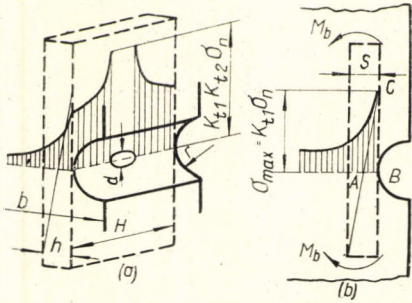


FIG. 4.9. Theoretical stress concentration factor of a beam notched through the full thickness on both sides and with a hole in the centre of the notch

(c) When the holes are not in a single cross-section but in more than one row (Fig. 4.6), there is no fundamental change from the conditions described above; the only difference is that the pencil of stress flow lines changes according to the distance apart of holes 2 and 3, and the stress around them will be higher the closer they are to each other (Fig. 4.7).

(d) The increase of stress is particularly great if the holes are not symmetrical or if the first row of holes is very close to the edge of the plate (Fig. 4.8). In that case the bending moment acting at the innermost edge of the hole increases the stress considerably.

4.3.3 Intersecting stress raisers

The best way to explain the method to be followed with intersecting stress raisers is to give an example. Figure 4.9a represents a beam with a notch at each side and a central transverse hole d . The question is: what is the stress concentration factor in tension?

Initially, we ignore the transverse hole. The stress distribution in the beam notched at each side is shown in Fig. 4.9b. As we know, the stress at the root of the notch is

$$\sigma_{\text{notch}} = K_t \sigma_{n1}$$

where K_t is the stress concentration factor, and σ_{n1} the nominal stress in the beam.

The same stress would act, however—with a uniform distribution of reversed stress — if the plate of thickness s shown by the dashed lines in Fig. 4.9b were bent by a bending moment M_b as indicated in the figure. If the angle of inclination of the stress distribution for the transverse bending coincides with that of the tangent to the stress that occurs at the root of the notch, the two cases can be regarded as identical at the critical point, i.e. at the root of the notch. With this approximation the original problem is reduced to the transverse bending of a beam drilled at its centre, and thus the maximum stress occurring is expressed as

$$\sigma_{\text{max}} = K_{t2} \sigma_{n2} = K_{t2} K_{t1} \sigma_{n1}$$

where K_{t2} denotes the stress concentration factor applicable to the transverse bending of the plate drilled at its centre. The stress σ_{notch} already determined has to be regarded as the nominal stress for the transverse bending, so $\sigma_{\text{notch}} = \sigma_{n2}$.

Now, however, we have to determine the thickness s of the imaginary plate, for we need it to determine the stress concentration factor K_{t2} .

According to SIEBEL (section 5.3, p. 65),

$$X = \left(\frac{d\sigma}{dx} \right)_{\sigma_{\max}} \times \frac{1}{\sigma_{\max}} = \tan \alpha \times \frac{1}{\sigma_{\max}}$$

From the triangle ABC (Fig. 4.9b), however,

$$\tan \alpha = \frac{2\sigma_{\max}}{s} \quad \text{and thus} \quad s = \frac{2}{X}$$

According to Fig. 94 of Part II (p. 85),

$$X = \frac{2}{r}$$

in a beam notched on both sides, r being the notch radius. Substituting this, we have

$$s = r.$$

Thus if in Fig. 4.9 $r = 5$ mm, $b = 24$ mm, $h = 16.5$ mm, and $d = 6$ mm, we find from Table 12 of Part II, sub-table no. 1 (p. 42), using our symbols instead of the corresponding ones in the table,

$$\frac{b}{b-2r} = \frac{24}{14} = 1.71 \quad \text{and} \quad \frac{r}{b-2r} = \frac{5}{14} = 0.357.$$

Now with

$$\frac{d}{s} = \frac{6}{5} = 1.2 \quad \text{and} \quad \frac{d}{h} = \frac{6}{16.5} = 0.363$$

we find from Table 12 of Part II, sub-table no. 29 (p. 51) that $K_{t2} = 1.68$.

The stress concentration factor for transverse notches, then, will be $K_t = K_{t1} \times K_{t2} = 1.78 \times 1.68 = 3.0$.

Measurements by THUM and SVENSON [101] gave $K_t = 3.23$, a difference of -7 per cent.

Fatigue Strength Reduction Factors

5.1 Fatigue strength reduction factors according to the conservative theory

EXPERIENCE shows that at stress concentrations the peak stresses are often less than σ_{\max} , the nominal stress multiplied by the stress concentration factor. It is reasonable to assume that the material grains are displaced at such positions, which is why the peak stress is reduced. The magnitude of this displacement depends on the material; it is much less – if it occurs at all – in a hard, brittle material than in a ductile one, and the reduction of stress in a brittle material likewise differs from that in a ductile one.

Because of this displacement, according to A. THUM and W. BUCHMANN [95], the actual stress increase is only a certain fraction of the increase indicated by calculating σ_{\max} from the theoretical stress concentration factor K_t .

Since the theoretical stress increase is

$$\sigma_{\max} - \sigma_n = K_t \sigma_n - \sigma_n = \sigma_n (K_t - 1)$$

and the actual stress increase is

$$\sigma_{\text{act}} - \sigma_n = \sigma_n (K_f - 1),$$

we have

$$q \sigma_n (K_t - 1) = \sigma_n (K_f - 1),$$

whence

$$q = \frac{K_f - 1}{K_t - 1}, \quad (16)$$

where

q denotes the notch sensitivity factor and K_f the fatigue strength reduction factor.

THUM and BUCHMANN supposed q to be a material constant, and consequently the value of K_f , giving the actual stress increase, could be calculated from K_t by means of the following equation:

$$K_f = q(K_t - 1) + 1.$$

The notch sensitivity factor q expresses the sensitivity of the material to stress raisers. If $q = 1$, we have $K_f = K_t$, i.e. there is no stress decrease as a consequence of grain displacement in the material; it is very brittle, and sensitive to grooves, changes in cross-section, etc. If $q = 0$, the stress occurring at what would normally constitute stress raisers does not rise above the nominal stress, so $\sigma_n = \sigma_{\text{act}}$. The displacements are so large that no stress peak is produced; the material is ideally plastic. In practice, these are limiting values; q always lies between 1 and 0.

HEROLD [25] makes the rather sweeping statement that the factor q "is to be regarded as a material constant in stepped shafts of the dimensions investigated". It has become clear, however, that his supposition is not correct, because q depends not only on the material but on the form of the stress-raising groove, and also, though to a lesser extent, on other factors.

From data given by MOORE, JORDAN, MORKOVIN, GOGH and others, R. E. PETERSON [71] produced the diagrams shown in Figs. 5.1 and 5.2, in which the notch sensitivity factor q is shown in relation not only to the composition of the material, but also to the degree of rounding of the groove, hole, etc. Using these data, a nomogram (Fig. 66 of Part II, p. 59) was prepared to enable the notch sensitivity factor q to be determined for materials of various tensile strengths for a given radius. When K_t is known, q can be found from the nomogram.

HARRIS [20], formulated an expression for q , agreeing closely with experiment, viz.

$$q = \{1 - \exp(-r/\rho_H)\}$$

where

$$\sqrt{\rho_H} = \frac{33.5}{\sigma_T}$$

In the above formula,

r = radius of notch root in mm;
 σ_T = tensile strength of the material in kgf/mm².

By combining the above two equations the following relationship is obtained:

$$r \left\{ \frac{\sigma_T}{50.8} \right\}^2 = \log \frac{1}{1 - q}$$

This last equation is very suitable for the nomographic determination of the value of q (Fig. 67 of Part II, p. 60). To use the nomogram, join the value of r , the notch radius, to the point giving the tensile strength of the material, and the resulting straight line gives the required value of q on the middle scale.

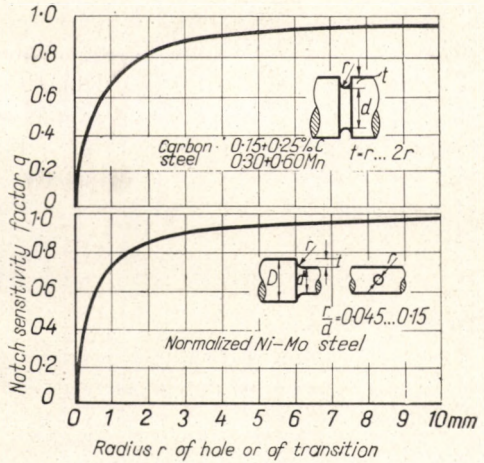


FIG. 5.1. Relationship between notch-sensitivity factor q of normalized steels and size of hole or radius of transition (JORDAN and MORKOVIN)

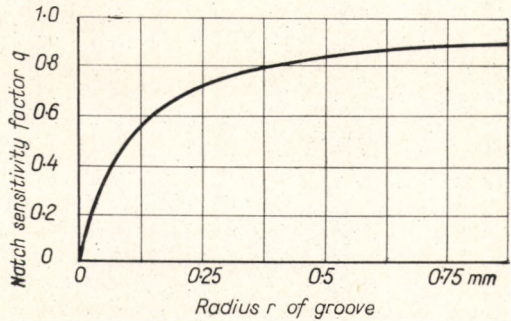


FIG. 5.2. Relationship between notch-sensitivity factor q of hardened and tempered steels and size of hole or radius of transition (GOGH)

5.2 The Bollenrath-Troost method

The theoretical formula of F. BOLLENRATH and A. TROOST is at present the most suitable for determining the value of the fatigue strength reduction factor.

They consider that fatigue fracture occurs in a material under frequently repeated stress when the elastic strain component at the most highly stressed positions exceeds a certain critical limit. All their calculations are based on the fatigue strength in tension. They also show that the bending and torsion fatigue strengths differ from the tension fatigue strength only because of the "supporting effect". In their theoretical derivation they use the fatigue strength reduction factor K_{fB} , which is the ratio of the fatigue strength of a notched specimen to that of a smooth specimen.

$$K_{fB} = \frac{\sigma_{FN}}{\sigma_{icFt}}$$

Here

σ_{FN} = fatigue strength of notched specimen;

σ_{icFt} = tension-compression fatigue strength of smooth specimen.

It must be emphasized that the size factor and the difference existing between the fatigue strengths for tensile and for other stresses are included in the value of K_{fB} .

These authors derived theoretically the following formula for the determination of K_{fB} for stepped and grooved round steel shafts under reversed symmetrical tensile or bending stress. We omit the derivation, and give only the formula itself:

$$\frac{K_{fB}}{K_t} = 1 - \frac{\frac{1540}{\sigma_T}}{\left\{ \frac{1}{1 + \frac{\sigma_T}{13700}} \right\} + r} \quad (17)$$

where

K_t = σ_{\max}/σ_n , the theoretical stress concentration factor;

K_{fB} = $\sigma_{FN}/\sigma_{icFt}$, the fatigue strength reduction factor;

σ_T = tensile strength in kgf/mm²;

r = groove radius in mm.

To facilitate the application of the rather complicated formula, a diagram has been drawn (Fig. 65 of Part II, p. 58). The values of K_{fB} from this diagram have been compared with the experimental results obtained by F. KÖRBER and M. HEMPEL [42] for drilled shafts and by W. HEROLD [25] for stepped shafts, respectively, and it is found that the differences vary from -20 to +5 per cent; the formula can therefore be used also to calculate K_{fB} for stepped and drilled shafts, but in this case the value obtained must be multiplied by 1.2. It should be noted, however, that even after the multiplication the value of K_{fB} must not be greater than K_t .

The fatigue strength σ_{FN} of a notched workpiece is determined in three stages. First the stress concentration factor K_t is determined from Table 12 of Part II by selecting the appropriate sub-table and interpolating; next this value is multiplied by the value of K_{fB}/K_t obtained from Fig. 65 of Part II (p. 58), and finally the result is multiplied by the tension-compression fatigue strength of a smooth specimen (above 2).

The determination of K_{fB} is simplified by the nomograms in Figs. 68 to 87 of Part II (pp. 61 to 80). First take the nomogram corresponding to the given loading conditions, locate the value of r/d on the left-hand side, and join it to the appropriate point in the middle (D/d) curve or straight line. The resulting straight line when produced will intersect the right-hand scale at the applicable value of K_r . Then place at this intersection the point marked with an arrow in Fig. 88 of Part II (in pocket inside cover) corresponding to the form of the workpiece; the arrow may point either to the right or to the left. Locate the point on the abscissa axis of the movable part of the nomogram which gives the value r , and move vertically to the straight line for the appropriate tensile strength. From here project to the left-hand or right-hand edge of the movable part of the nomogram, adjoining which the value of K_{fB} can be read off on the fixed part. As already mentioned, however, the value of K_{fB} cannot be greater than K_r , so that whenever the movable part of the nomogram gives a value greater than K_r , a value equal to K_r should actually be used.

It should be noted that nomogram values differ in some cases by between 15 and 20 per cent from the theoretical and the experimental values of the fatigue strength reduction or the theoretical stress concentration factor. This accuracy is usually sufficient in practice, however, the more so because the larger differences tend to occur only in extreme cases.

5.3 The Siebel method

SIEBEL [84] has developed a method for the determination of the fatigue strength of machine components containing stress raisers which is completely different from previous methods. Although the details published in the literature are far from complete, the method is worth discussing because of its novelty. SIEBEL made the basis of design the permanent equivalent strain occurring at the most highly stressed point, and he proposed taking the uniform value of $\epsilon = 0.2$ per cent. He demonstrated that, for a non-uniform stress distribution, the fatigue strength of machine components depends on the ratio of the stress gradient to the maximum stress. He introduced the variable X , defined as follows:

$$X = \left(\frac{d\sigma}{dx} \right)_{\sigma_{\max}} \frac{1}{\sigma_{\max}} \tag{18}$$

In the above equation $\frac{d\sigma}{dx}$ denotes the slope of the curve representing the stress distribution produced by the grooves, etc., where the stress is highest (σ_{\max} , Fig. 5.3). The value of this slope has to be divided by σ_{\max} in order to obtain X .

Experimental values of X have been plotted as abscissae in Fig. 93 of Part II (p. 85) against the ordinate δ_F , which is the ratio of the fatigue strength of a grooved machine component to the tension-compression fatigue strength of a smooth (i.e. not grooved) specimen. Hence

$$\delta_F = \frac{\sigma_{FN}}{\sigma_{tcFt}} \tag{19}$$

A separate curve is given for each material.

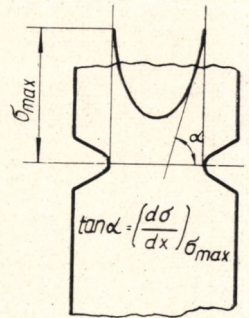


FIG. 5.3. Tensile stress distribution in a notched plate

To determine the fatigue strength of a machine component made from a known material and containing stress raisers, first calculate the value of X and then determine the value of δ_F from Fig. 93, using the appropriate material curve. Multiply the value of the tension-compression fatigue strength determined as in section 5.2 by δ_F and by the surface-roughness factor b (Fig. 38 of Part II, p. 28); the result is the required fatigue strength of the machine component containing stress raisers.

The values of X for different types of notch can be taken from Fig. 94 of Part II (p. 85).

The SIEBEL method has the disadvantage that the values of δ_F corresponding to small values of X can be read off only with very poor accuracy, and further, that the calculation of X is simple only for the few cases given in Fig. 94; for other cases it is somewhat complicated.

CHAPTER 6

Factor of Safety

6.1 Uniaxial stresses

THE extent to which different materials can be stressed under given conditions was discussed in Chapter 2. In Chapter 5 information was given on the actual stresses arising in a machine component in consequence of notch effects. In regard to both the load capacity of a material and the determination of the stresses occurring, we have to be satisfied with a limited accuracy owing on the one hand to microscopic inhomogeneity and general uncertainty about material quality, and on the other to the way in which some factors have to be simplified and others neglected in the mathematical treatment of problems in the theory of strength of materials. We must also bear in mind that in practice, in addition to the postulated stresses which are provided for, there may be unexpected, unavoidable larger stresses.

The factor of safety covers all these uncertainties. It is important that this factor should be realistic, for if it is unjustifiably high, it brings to naught all the calculations aimed at a more economical use of material, and there is no point in carrying out the complicated calculations relating to fatigue strength; but if it is too low, there is a liability to fracture in the unfavourable cases which inevitably occur.

With static loads, the factor of safety indicates that the tensile strength or the yield point of the material is some multiple of the permissible stress, the first criterion relating to design against fracture and the second to design against permanent deformation. The first is customary for brittle, the second for ductile, materials. At temperatures above 500°C the creep limiting stress, and for boiler drums, the hot yield point, must be divided by the factor of safety in order to arrive at the permissible stress.

A cyclic alternating stress is composed of two elements, i.e. the mean stress σ_m and the stress amplitude σ_a . Since the fatigue of materials depends on both the mean stress and the amplitude, it is reasonable to ask to what the mean stress and the stress amplitude must be related in any given case. To this question the literature provides three answers, proposed respectively by SODERBERG, the *VDI*, and KIMMELMANN.

6.1.1 Soderberg's proposal

SODERBERG proposes that the mean stress σ_m and the stress amplitude σ_a should have the same ratio as those causing fatigue fracture, i.e.

$$\frac{\sigma_m}{\sigma_a} = \frac{\sigma_M}{\sigma_A}$$

In this case the factor of safety S is given by

$$S = \frac{\sigma_M}{\sigma_m} = \frac{\sigma_A}{\sigma_a}$$

Thus if the point P marks the mean stress and stress amplitude in the Haigh diagram (Fig. 6.1), point Q represents the criterion corresponding to the above condition, being the point of intersection of the straight line OP and the Haigh-diagram fatigue curve.

6.1.2 The VDI proposal

The VDI proposal is that the stress required to cause fatigue fracture with the given mean stress should be considered as the criterion ($\sigma_m = \sigma_M$). The factor of safety then becomes the ratio of the stress amplitude causing fatigue fracture to the stress amplitude actually applied (Fig. 6.2), i.e.

$$S = \frac{\sigma_A}{\sigma_a}$$

Thus if the point P on the Haigh diagram again denotes the mean stress and the stress amplitude, point T represents the criterion, being the point of intersection of the vertical straight line through point P and the Haigh-diagram fatigue curve.

The factor of safety proposed by the VDI is thus higher than that proposed by SODERBERG.

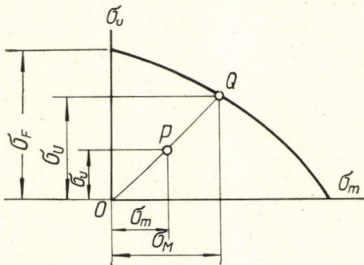


FIG. 6.1. SODERBERG factor of safety

6.1.3 Kimmelmann's proposal

KIMMELMANN [36] showed that both the above proposals were based on arbitrary assumptions, for nothing whatever corroborates the assumption either that mean stress and stress amplitude vary in proportion or that the mean stress remains constant and only the stress amplitude varies. KIMMELMANN considers that the increased mean stress and stress amplitude (points P_1, P_2 , etc., in Fig. 6.3) must be calculated from the changes of working stress. The factor of safety is the ratio of the stresses causing failure to the limiting value under actual working conditions.

As it is often very difficult to determine the stresses resulting from the working load, the SODERBERG factor of safety is generally used.

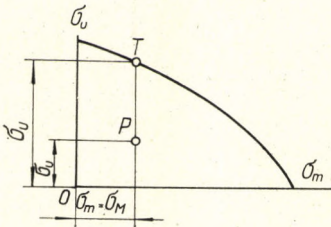


FIG. 6.2. VDI factor of safety

6.1.4 Factor of safety in finite-life fatigue

If the number of cycles N is such that $10^5 < N < 10^6$, the Haigh diagram for the stress and endurance in question is drawn, and used to determine the factor of safety. The Haigh diagrams so far show apply for infinite life (for practical purposes, 10^6 cycles with steels), and the same holds for everything that has so far been said about the factor of safety.

On a logarithmic scale, the $S-N$ curve is approximately a straight line between $N = 10^5$ and $N = 10^6$, starting, with $N = 10^5$, at the point corresponding to approximately 90 per cent of the tensile strength. This enables us, knowing the tensile strength and fatigue

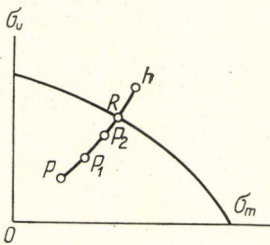


FIG. 6.3. KIMMELMANN factor of safety

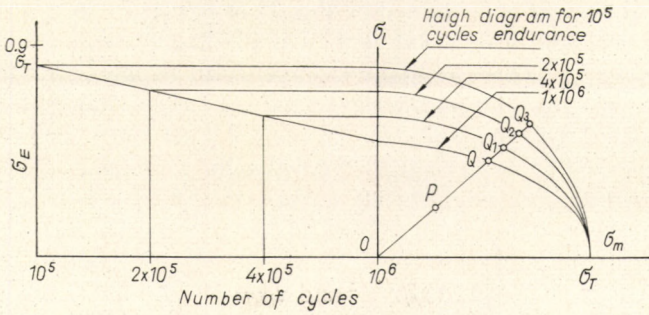


FIG. 6.4. Determination of the factor of safety when $N < 10^6$

limit, to draw, first, the $S-N$ curve, and then the Haigh diagram for the appropriate endurance (Fig. 6.4). After that the process is carried out by the method already known. For example, the ratio of Q_1O to PO in Fig. 6.4 gives the SODERBERG factor of safety when $N = 4 \times 10^5$.

6.2 Complex and combined stresses

Various explanations of the cause of fracture are to be found in the theory of the strength of materials. For steels, the MISES-HENCKY theory makes the nearest approach to practice. According to this theory, fracture under static load occurs when the part of the strain energy used for the change of shape (the work performed during the change of shape) equals or exceeds the critical value for the material. It can be deduced mathematically that the equivalent stress σ_e under plane stress conditions for static combined loading is given by:

$$\sigma_e = \sqrt{\sigma_x^2 - \sigma_x\sigma_y + \sigma_y^2 + 3\tau_{xy}^2}$$

For the very frequent case of

$$\sigma_x = \sigma_1, \sigma_y = 0, \text{ and } \tau_{xy} = \tau$$

the result will be

$$\sigma_e = \sqrt{\sigma^2 + 3\tau^2}$$

Here σ_x denotes the normal stress in the x direction;
 σ_y denotes the normal stress in the y direction;
 τ_{xy} denotes the shear stress in the xy plane.

With reversed plane stress the types of stress are frequently different for σ and τ ; σ , for example, may be reversed and τ fluctuating or static. In this case the equivalent stress σ'_e is given by

$$\sigma'_e = \sqrt{\sigma^2 + 3(\alpha_0\tau)^2}$$

with the stress ratio

$$\alpha_0 = \frac{1}{\sqrt{3}} \cdot \frac{\sigma_{bF}}{\tau_F}$$

The determination of σ'_e is facilitated by Fig. 95 of Part II (p. 87). Proceed from the value of τ on the left-hand scale as far as the straight line α_0 . Draw a straight line from the point of intersection upwards or downwards until it intersects the straight line corresponding to the value of σ on the right-hand scale. The (interpolated) value of the circle going through this point gives the value of σ'_e . All the scales have two numberings, one being distinguished by being ringed. Only values of τ , σ , and σ'_e belonging to corresponding scale markings (all ringed or all unringed) are to be related.

For example, if a shaft carrying a flywheel has to transmit a torque, the bending stress has to be regarded as reversed and the torsion stress as static. For 0.35% C steel (Fig. 3 of Part II, p. 9), $\sigma_{bF} = 24 \text{ kgf/mm}^2$ and $\tau_F = 19 \text{ kgf/mm}^2$, whence

$$\alpha_0 = \frac{24}{1.73 \times 19} = 0.73.$$

If the shaft works with a bending stress of

$$\sigma_b = 15 \text{ kgf/mm}^2$$

and a torsion stress of

$$\tau_t = 11 \text{ kgf/mm}^2,$$

the nomogram shows the equivalent stress to be

$$\sigma_e = 20.3 \text{ kgf/mm}^2.$$

To determine the factor of safety under combined plane stress, the equivalent mean stress σ_{mr} and amplitude σ_{ar} must be ascertained.

Since

$$\sigma = \sigma_m + \sigma_a \quad \text{and} \quad \tau = \tau_m + \tau_a,$$

we have

$$\begin{aligned} \sigma_{mr} &= \sqrt{\sigma_m^2 + 3\tau_m^2} \quad \text{or} \quad \sigma'_{mr} = \sqrt{\sigma_m^2 + 3(\alpha_0\tau_m)^2} \\ \sigma_{ar} &= \sqrt{\sigma_a^2 + 3\tau_a^2} \quad \text{or} \quad \sigma'_{ar} = \sqrt{\sigma_a^2 + 3(\alpha_0\tau_a)^2}. \end{aligned}$$

We proceed as if $\sigma_{mr} = \sigma_m$ and $\sigma_{ar} = \sigma_a$. Afterwards we use one of the methods discussed in section 6.1.

6.3 Numerical values of the factor of safety

As pointed out by VOLK [105], the factor of safety is "a function of space and time". The designer must give careful thought to the value to be assigned to it; he must take account of stress concentrations and reduction of strength resulting from lack of uniformity in the material, from surface machining, from corrosion, etc., and must also consider the consequences of any failure. Obviously, if failure may entail accidents, or gross material damage (e.g. to the machine itself, or to other parts of the plant), a higher degree of safety must be ensured than in other cases.

In the literature a factor of safety S , giving the permissible stress in relation to the reversed-stress or fluctuating-stress fatigue limit, of from 2 to 3 is proposed. This value,

TABLE 6.1

FACTOR OF SAFETY FOR SHOCK LOADING

Type of machine; magnitude and frequency of expected shocks	Factor
Steam and water centrifugal pumps, grinding machines, electric motors, with small shocks, occurring at most only on starting	1 to 1.1
Internal combustion engines, reciprocating machinery, slotting machines, and in general machines subject to only small shocks	1.2 to 1.5
Hot presses, section shearing machines, punching machines, and in general machines subject to shocks and impacts of medium frequency of occurrence	1.5 to 2.0
Hammers, rolling mills, stone crushers, and all machines subject to heavy and frequent impacts	2.0 to 3.0

however, may be regarded as excessive, for even with a factor of safety S of only 1.5 to 2.5 the stress is in most cases below the damage line discussed in section 3.7. If operating conditions can be controlled reliably enough, a safety factor $S = 1.2$ to 1.5 is sufficient, provided that the machine component is manufactured with due care and the material is selected under a proper approval procedure. For shock loading the factor of safety must be multiplied by the factors shown in Table 6.1. If failure could cause an accident — possibly even endangering life — the factor of safety must be increased by 20 to 50 per cent, and at the same time the material testing requirements must be made more stringent. Thus, in general, we should attempt to achieve safety not by overdimensioning, but by conscientious, deliberate and exact design, and above all by making sure of sound materials, limiting the stresses and suitably checking the machining, etc. There is no avoiding these measures, for without them no factor of safety, however high, can be adequate.

CHAPTER 7

Fatigue Design

THE fatigue limit can be calculated as indicated in the foregoing except for materials, profiles or loadings for which no data are yet available.

In the majority of practical cases what is required is either

- (a) to determine the dimensions of the machine component, or
- (b) to check the factor of safety in relation to the loading and the dimensions of the component.

The calculation can be carried out either by the earlier method or on the basis of more recent tests and theories. There are more literature references applying to the first method, but the second is theoretically more exact. It is very regrettable that the necessary data for the second method are not yet available in sufficient quantity, so that sometimes we are compelled to use the earlier one.

The essential difference between the two methods is that according to the more recent BOLLENRATH-TROOST theory only the tension-compression fatigue limit σ_{icF} and the theoretical stress concentration factor K_t are used, but the conservative method requires the tension-compression fatigue limit σ_{icF} , the bending and torsion fatigue limits σ_{bF} and σ_{tF} , the size factors k_b and k_t , and also, to determine the fatigue strength reduction factor K_f , the theoretical stress concentration factor K_t and the notch sensitivity factor q . The BOLLENRATH-TROOST method is thus simpler, but the formula is strictly applicable only to shouldered shafts of circular section and keyways. In all other cases a greater or lesser degree of approximation is involved.

Although the conservative method is the more complicated of the two, the application of the HARRIS formula (p. 63) is generally accepted.

SIEBEL's method, taking into account the supporting effect of the surrounding material, brings in the tension-compression fatigue limit σ_{icF} increased by the fatigue limit ratio σ_F . Notch effects are expressed by the theoretical stress concentration factor K_t .

Let us now consider the three methods of calculation in more detail.

7.1 Conservative design

The conservative method requires knowledge of the fatigue limit σ_{icF} , σ_{bF} , or τ_F which corresponds to the type of loading of the material. If this cannot be obtained from the literature, use Fig. 18 of Part II (p. 13).

If the stress is not of the reversed symmetrical type with $\sigma_m = 0$, plot the simplified Smith diagram with the aid of Figs. 18, 19 and 20, as detailed on pp. 13-14 of Part II. Also draw the straight line with slope $\tan \phi = F_u/F_m$ passing through the value of σ_u in

the Smith diagram. Then draw a straight line from this point corresponding to $\sigma_m = \text{constant}$ (parallel to the σ_a axis) which will then intersect the values of σ_M and σ_L . Next consider the factors affecting the fatigue limit and multiply the value of σ_u by the surface-finish factor b (Figs. 39 and 40 of Part II, p. 28, or for cast iron, Fig. 41) and by the factor k_b or k_t (Figs. 42 and 43), covering the effect of the form of the cross-section and the expected dimensions. If the working temperature of the component differs greatly from room temperature, modify the factors by means of the coefficients which can be read directly or indirectly from Figs. 44 to 52 of Part II (pp. 30–32). When calculation for finite life is required ($N < 10^6$), determine the endurance limit using the simplified $S-N$ diagram shown on p. 23.

Afterwards divide the value of fatigue limit modified by the application of all the above factors by the relevant factor of safety, thus finally obtaining the maximum permissible stress for the component. This stress must not be exceeded by that determined by the elementary method ($\sigma_{tc} = F/A$, $\sigma_b = M_b/W$, etc.) multiplied by the fatigue strength reduction factor K_f . This factor may be determined either from Table 12 (Part II, pp. 42–56) or from the theoretical stress concentration factor K_t , determined using the nomograms in Figs. 68 to 92 of Part II, applied in the nomogram in Fig. 66.

The fundamental formula for the calculation is

$$\frac{\sigma_f bk}{S} \leq \sigma_n K_f \quad (20)$$

where K_f is a function of K_t and r .

7.2 Design using the Harris notch sensitivity factor

The process is identical with that described in section 7.1 except that the fatigue strength reduction factor K_f must be determined by either the HARRIS formula (p. 63) or the corresponding nomogram (Fig. 67 of Part II).

The fundamental formula is then

$$\frac{\sigma_f bk}{S} \leq \sigma_n K_f$$

where K_f is a function of σ_T and r .

7.3 Design by the Bollenrath-Troost theory

When calculating according to the BOLLENRATH-TROOST theory, only the tension-compression fatigue limit has to be known; multiply it by the surface-finish factor b and, for elevated temperatures, by the temperature coefficient. The size factor need not be considered. If $\sigma_m \neq 0$, or if the calculation is to be made for an endurance of $N < 10^6$, use the procedure described in section 7.1.

The fatigue limit thus modified must then be divided, of course, by the factor of safety. The stress finally obtained must not be exceeded by the stress determined by the elementary method ($\sigma_{tc} = F/A$, $\sigma_b = M_b/W$, etc.) multiplied by the factor K_{fB} . This latter factor may be determined from Fig. 65 of Part II (p. 58) via the theoretical stress concentration factor K_t , obtained from Table 12 of Part II (pp. 42 to 56) or by applica-

tion of the nomograms in Figs. 68 to 87, using the movable nomogram in Fig. 88 (in pocket inside cover).

The fundamental formula for the calculation is

$$\frac{\sigma_{icF} b}{S} \leq \sigma_n K_{fB} \quad (21)$$

where K_{fB} is a function of σ_T and r .

7.4 Design by the Siebel theory

When calculating according to SIEBEL's theory, determine first the value X from Fig. 94 of Part II (p. 85). From this, using the appropriate material curve in Fig. 93, the fatigue-limit ratio δ_F can be obtained. Multiply the tension-compression fatigue limit σ_{icF} by this and by the surface-finish factor b (Figs. 39 and 40 of Part II, p. 28), and divide by the factor of safety S . The result is the permissible fatigue stress, and it must not be exceeded by the product of the stress in the component determined by the elementary method ($\sigma_n = F/A$, etc.) and the theoretical stress concentration factor K_t .

The fundamental formula for the calculation is

$$\frac{\sigma_{icF} \delta_F}{S} \leq \sigma_n K_t, \quad (22)$$

where δ_F is a function of X .

It should be noted that in the case of brittle materials such as cast iron and phenolic resins, K_t must be used instead of K_f or K_{fB} . In the case of soft, plastic materials, e.g. certain light metals, K_f or $K_{fB} \approx 1$.

If the problem is to check the safety factor S , the above equations must be solved for S . For the sake of simplicity we do not describe the process in detail.

7.5 Example

Let us illustrate the procedure by an example. The factor of safety in relation to fatigue strength of the transmission shaft of 0.35% C steel shown in Fig. 7.1 is to be checked. The required life is 10 000 hours, and the shaft is to transmit 15 HP at a speed of rotation $n = 365 \text{ min}^{-1}$.

Since the required number of cycles is $N = 10\,000 \times 60 \times 365 > 10^6$, the factor of safety for the given diameter must be checked in relation to the fatigue limit.

7.5.1 Conservative method

(1) According to Fig. 3 of Part II (p. 9), the bending fatigue limit σ_{bF} for 0.35% C steel is equal to 24 kgf/mm^2 .

(2) Since $N > 10^6$, this value of σ_{bF} is not to be increased.

(3) If we assume that $R_t = 4 \mu\text{m}$, Fig. 38 of Part II (p. 28) gives the surface-finish factor b as 0.93 (50 kgf/mm² tensile strength).

(4) From Fig. 42 of Part II (p. 29) the size factor k_b (40 mm diameter) is 0.76.

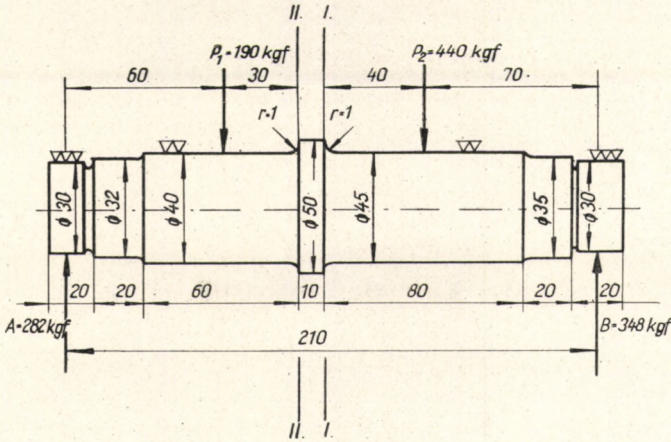


FIG. 7.1. Example of fatigue design of a shaft

No modification of the fatigue limit is called for on account of

- (5) temperature;
- (6) surface treatment;
- (7) corrosion;
- (8) previous history of the material.

(9) The calculated fatigue limit σ_{Fcalc} of the material is given by

$$\sigma_{Fcalc} = \sigma_{bF} \times b \times k_b = 24 \times 0.93 \times 0.76 = 17 \text{ kgf/mm}^2.$$

(10) The peak stresses as calculated according to the elementary theory of strength of materials occur at one or both of the points of load application. It is, however, not there but at the two sides of the central enlargement that we check the safety factors, because that is where the stress concentrations occur.

Moments of resistance:

- at position I (45 mm dia.) $W_I = 8.9 \text{ cm}^3$
- at position II (40 mm dia.) $W_{II} = 6.3 \text{ cm}^3$.

Moments of polar resistance:

- at position I (45 mm dia.) $W_{pI} = 17.8 \text{ cm}^3$
- at position II (40 mm dia.) $W_{pII} = 12.6 \text{ cm}^3$.

The bending moment at position I is:

$$M_{bI} = 348(3+4+4) - 440 \times 4 = 2068 \text{ kgf-cm,}$$

and at position II is:

$$M_{bII} = 348(3+4+4+1) - 440 \times 5 = 1976 \text{ kgf-cm.}$$

$$\sigma_{bI} = \frac{M_b}{W} = \frac{2068}{8.9} = 233 \text{ kgf/cm}^2 = 2.33 \text{ kgf/mm}^2$$

$$\sigma_{bII} = \frac{1976}{6.3} = 314 \text{ kgf/cm}^2 = 3.14 \text{ kgf/mm}^2.$$

The twisting moment at both positions is

$$M_t = 71\,620 \left(\frac{HP}{n} \right) = 71\,620 \left(\frac{15}{365} \right) = 2950 \text{ kgf-cm.}$$

The torsional stress at position I is:

$$\tau_{tI} = \frac{M_t}{W_{pt}} = \frac{2950}{17.8} = 166 \text{ kgf/cm}^2 = 1.66 \text{ kgf/mm}^2$$

and at position II is:

$$\tau_{tII} = \frac{2950}{12.6} = 234 \text{ kgf/cm}^2 = 2.34 \text{ kgf/mm}^2.$$

Assuming that $\alpha_0 \approx 0.7$, we have for the equivalent stress σ_e , from the nomogram in Fig. 95 of Part II (p. 87),

$$\sigma_{Ie} = 3.1 \text{ kgf/mm}^2 \quad \text{and} \quad \sigma_{IIe} = 4.2 \text{ kgf/mm}^2.$$

(11) The theoretical stress concentration factor K_t from the nomogram in Fig. 84 of Part II (p. 77), for $D/d = 50/40 = 1.25$, $L/D = 10/50 = 0.20$, $r/d = 1/45 = 0.02$, is equal to 2.15.

(12) With $r = 1$ mm we have, from the nomogram in Fig. 66 of Part II (p. 59), $q = 0.68$ and $K_f = 1.78$.

(13) The maximum stress to be expected at position I will be

$$\sigma_{Ie} \times K_f = 3.1 \times 1.78 = 5.5 \text{ kgf/mm}^2$$

and at position II will be

$$\sigma_{IIe} \times K_f = 4.2 \times 1.78 = 7.5 \text{ kgf/mm}^2.$$

(14) Finally, the factor of safety S at the position of maximum stress is given by

$$S = \frac{\sigma_{Fcalc}}{\sigma_{IIe}} = \frac{17 \text{ kgf/mm}^2}{7.5 \text{ kgf/mm}^2} = 2.2.$$

7.5.2 Determination of K_f according to Harris

Steps (12), (13) and (14) are modified as follows when K_f is determined by HARRIS'S method:

(12) From Fig. 67 of Part II (p. 60), with $\sigma_T = 50 \text{ kgf/mm}^2$ and $r = 1$ mm, we obtain $q = 0.89$. Hence, using THUM and BUCHMANN'S formula (p. 62),

$$K_f = 0.89(2.15 - 1) + 1 = 2.02.$$

(13) On this basis the maximum stress occurring (position II) will be

$$\sigma_{IIe} = 4.2 \times 2.02 = 8.5 \text{ kgf/mm}^2.$$

(14) Consequently the factor of safety at this position will be

$$S = \frac{\sigma_{Fcalc}}{\sigma_{IIe}} = \frac{17 \text{ kgf/mm}^2}{8.5 \text{ kgf/mm}^2} = 2,$$

i.e. less by about 10 per cent than the result obtained using the conservative method.

7.5.3 The Bollenrath-Troost method

(1) Figure 3 of Part II (p. 9) shows that the tension-compression fatigue limit σ_{icF} for 0.35% C steel under reversed symmetrical stress ($\sigma_M = 0$) is 18 kgf/mm².

(2) Since $N > 10^6$, the value of σ_{icF} is not to be increased.

(3) If we assume that $R_t = 4 \mu\text{m}$, Fig. 38 of Part II (p. 28) gives the surface-finish factor b as 0.93.

No modification of the fatigue limit is called for on account of

- (4) temperature;
 - (5) surface treatment;
 - (6) corrosion;
 - (7) previous history of the material.
- (8) The calculated fatigue limit σ_{Fcalc} is given by

$$\sigma_{Fcalc} = \sigma_{icF} \times b = 18 \times 0.93 = 16.8 \text{ kgf/mm}^2.$$

(9) The maximum equivalent stress, at position II, is $\sigma_{IIr} = 4.2 \text{ kgf/mm}^2$ as in item (10) of section 7.5.1.

(10) From the nomograms in Figs. 84 and 88 of Part II (pp. 77 and inside cover) mentioned earlier, with $L/D = 10/50 = 0.20$ and $r/d = 1/40 = 0.025$, and with $r = 1 \text{ mm}$ and $\sigma_T = 50 \text{ kgf/mm}^2$, we obtain $K_{fB} = 1.5$.

(11) Thus we have finally

$$\frac{16.8}{S} = 4.2 \times 1.5,$$

and hence

$$S = \frac{16.8}{4.2 \times 1.5} = 2.65.$$

According to the BOLLENRATH-TROOST theory, therefore, the safety factor is $2.65/2.20 = 1.20$ times (i.e. higher by about 20 per cent than) that given by the conservative method.

7.5.4 The Siebel method

(1) For a stepped shaft, we have for X by analogy with Fig. 94 of Part II (p. 85)

$$X = \frac{2}{r} + \frac{4}{D+d} = \frac{2}{1} + \frac{4}{45+40} = 2.04 \text{ with the dimensions shown in Fig. 7.1.}$$

(2) Using the curve for $\sigma_T = 50 \text{ kgf/mm}^2$ in Fig. 93 of Part II (p. 85), we have $\delta_F = 1.3$.

(3) Figure 4 shows that for the same value of σ_T , $\sigma_{icF} = 18 \text{ kgf/mm}^2$.

(4) For $R_t = 4 \mu\text{m}$, the surface-finish factor is $b = 0.93$.

(5) The equivalent stress σ_{IIr} at position II is 4.2 kgf/mm^2 .

(6) According to Fig. 84 of Part II (p. 77), $K_t = 2.15$ ($L/D = 10/50 = 0.2$ and $r/d = 1/40 = 0.025$).

Utilizing the above values, we have

$$S = \frac{\sigma_{tcF} \delta_F b}{\sigma_{IIr} K_t} = \frac{18 \times 1.30 \times 0.93}{4.2 \times 2.15} = 2.5.$$

Here the factor of safety is $2.5/2.2 = 1.14$ times (i.e. higher by 14 per cent than) that given by the conservative method.

CHAPTER 8

Fatigue Design of some Machine Components

THIS chapter contains a number of points of special relevance to the fatigue design of some frequently encountered machine components. In it certain matters are discussed which up till now have been dealt with only generally or not at all. But no design problems not related to fatigue will be discussed.

8.1 Shafts and journals

No difficulties should remain in the design of shafts and journals after the foregoing discussion. For the sake of completeness, the tests carried out by THUM and BRUDER [91] must be mentioned; they relate to the determination of the stress concentration due to the combined effect of ball or roller bearings and steps in shafts. Their results showed that the fatigue strength reduction factor K_f due to the combined effect was only 5 to 10 per cent higher than without the ball or roller bearing, i.e. due only to the change of shaft diameter.

The tests fully corroborated the effect of the stress-relieving groove (Fig. 4.3), showing an increase of about 15 per cent in fatigue strength, and also showed that it was possible to increase the fatigue strength by rolling, the increase being about 50 per cent when the rolling pressure was suitably chosen.

Correct shapes of shafts, from the stress-concentration point of view, are shown in Figs. 8.1 and 8.2.

Larger changes in diameter may be effected in several steps (Fig. 8.3). Conical transitions are also permissible; suitable details are shown in Fig. 8.4.

Figure 8.5 shows correct methods of fitting a hub on a shaft.

Figure 8.6 shows correct forms of grooves from the point of view of stress concentrations.

The fatigue strength reduction factors K_f , calculated by THUM and BRUDER [93] for flanged shafts and by HEROLD [25] for splined shafts, are given respectively in Tables 15 and 16 of Part II (pp. 88 and 90).

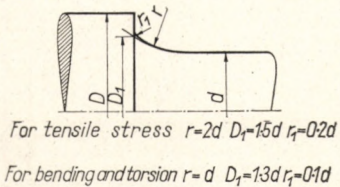


FIG. 8.1. Appropriate treatment for a step in a shaft

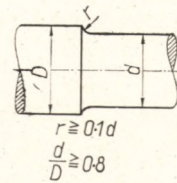


FIG. 8.2. Various correct forms of steps in shafts — I

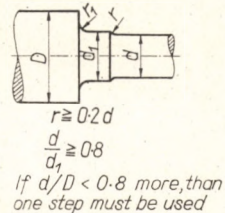


FIG. 8.3. Various correct forms of steps in shafts



FIG. 8.4. Conical steps in shafts

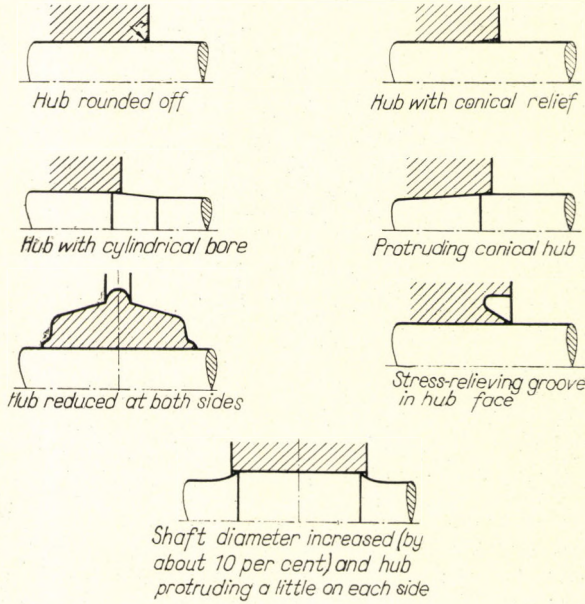


FIG. 8.5. Correct shaft-hub joints

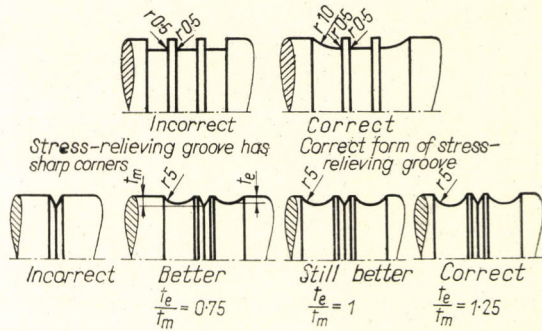


FIG. 8.6. Suitable arrangements of shaft grooves

8.2 Shrink-fit and keyed joints

The values of the "notched" fatigue strength and the fatigue strength reduction factors associated with keyed or shrunk-on hubs of various materials and forms have been investigated by A. THUM [94]. The results are summarized in Tables 17 and 18 of Part II (pp. 91-92).

The tests and measurements showed that as the surface pressure increased, the fatigue strength decreased until the stress at the wheel-hub surface reached the yield point. After that the fatigue strength did not change. The tests demonstrated the importance of the form of wheel hub. As keys and keyways reduce fatigue strength, it is better to use shrink fits. If the use of the former is unavoidable, however, surface hardening (rolling, flame hardening) is advantageous.

In torsion fatigue the importance of surface pressure and form of wheel hub is not so great. But here too keys and keyways very considerably reduce the fatigue strength. The fatigue strength of interference-fit hub joints differs from that of shrink-fit hub joints.

8.3 Ball and roller bearings

Ball and roller bearings are calculated for endurance, i.e. the required working life, by means of the formula

$$NP^m = K,$$

which is similar to the WEIBULL formula.

Here:

N = endurance (number of revolutions)

= $60 nL_h$, where n = revolutions per minute
and L_h = endurance in working hours;

P = "equivalent" load of the bearing (with loads acting in several directions, it is the vectorial sum of the loads), in kgf;

m = constant

= 3 for ball bearings and 10/3 for roller bearings;

K = constant depending on type of bearing.

The above formula may be found in bearing catalogues and elsewhere written as

$$NP^m = C^m \text{ or } N = (C/P)^m.$$

The value of C is indicated for all bearings in the relevant catalogue. The quantity C/P is called the load factor. When determining the value of P , all forces acting, dynamic factors, etc., must be taken into account.

When the load on a bearing is variable, the value of P used in calculating the endurance should be P_{mean} as given by the following formula:

$$P_{\text{mean}} = \left(\frac{\sum N_n P_n^3}{\sum N_n} \right)^{1/3},$$

where N_n is the number of revolutions at an individual load P_n .

If the required type of bearing has to be determined rapidly, the nomograms in Figs. 96 and 97 of Part II (pp. 94-96) may be used.

8.4 Bolts

Bolted joints occur in the most varied forms. Their fatigue design is not an easy problem, for a great many factors affect it: the bolt material, the thread profile, the type of machining, the surface roughness, and — to a very high degree — the amount of prestressing.

In essence a thread consists of several grooves following one behind the other in the direction of load. Its theoretical stress concentration factor K_t can be determined from the Neuber nomogram or from Table 12 of Part II (pp. 42–56). In addition the reduction of stress-raising effect brought about by the numerous turns of the thread (equivalent to grooves) must be taken into account, but there are no appropriate data available in this respect. The usual procedure is to make use, instead, of the values obtained from direct measurements which are given in Table 19 of Part II (p. 98). The surface-finish factor and size factor are already included in these values.

The stress concentration factor K_t also has a considerable influence on the choice of nut form. Measurements carried out by HETÉNYI [27] gave the value of K_t as 3.85 for a 1-inch bolt with a normal nut (Fig. 8.7). With a nut of the form shown in Fig. 8.8, however, the value of K_t fell to 3.

POMP and HEMPEL [75] and other authors have demonstrated that the fatigue strength is very much affected by the mean stress σ_m (which is the prestress). The Smith diagram for bolts is shown in Fig. 8.9. It indicates that bolts must be designed and fitted so that the sum of the prestress and the maximum tensile stress in fatigue should reach approximately the yield point, for in this case the specific load-carrying capacity of the bolt is a maximum. Further, care must be taken that the prestress does not fall off — or at least not appreciably — during service. Assembly — at least in the more critical cases — should be effected with the aid of a torque spanner, and compliance of the prestress with specification should be checked.

The interplay of forces in a bolted joint resulting from repeated stress is best seen in the loading diagram (elongation or compression diagram).

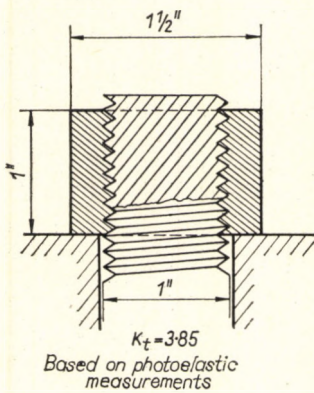


FIG. 8.7. Effect of form of nut on theoretical stress concentration factor of thread

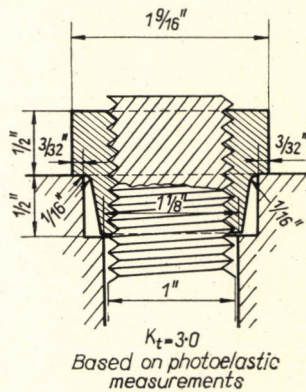


FIG. 8.8. Effect of form of nut on theoretical stress concentration factor of thread

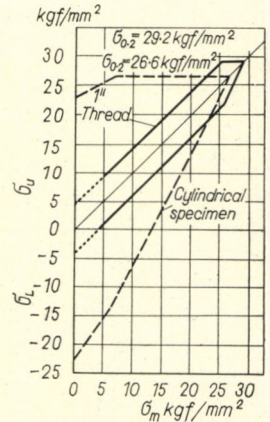


FIG. 8.9. Smith diagram for a 1-inch bolt

When a bolted joint presses two surfaces together, the bolt extends under tensile load, while both the joint elements are pressed together. As the elongation and compression usually take place below the yield point, however, the load-elongation diagram is a straight line. Figure 8.10a shows the elongation of the bolt, and Fig. 8.10b the compression of the two parts of the joint.

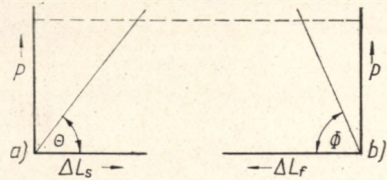


FIG. 8.10. Forces in bolted joints

As the elongation and the compression have opposite signs, it is convenient to draw them in opposite directions. Let ΔL_s be the elongation of the bolt due to the tensile load (notation as in Fig. 8.10) and ΔL_r the compression of the parts of the joint. To give a better representation, both diagrams are combined in Fig. 8.11.

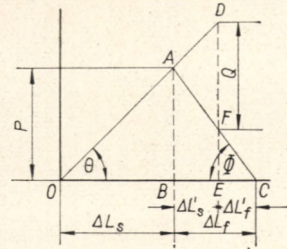


FIG. 8.11. Forces in bolted joints

It must be noted, however, that a suitable scale has to be chosen for P and ΔL , and that the angles Θ and Φ are indicative of the elasticity of the material. If the conditions are altered by the application of an external tensile force Q , the bolt will extend further, but not by the same amount as would a bolt without prestress under the same external tensile force Q . For the additional tensile force reduces the pressure on the parts of the joint so that the further elongation of the bolt is due only to the difference between these two forces; it corresponds to the length $BE = \Delta L'_s$. The tensile force $\overline{EF} = P'$ and the compression of the two joint elements $\overline{EC} = \Delta L'_r$, but the maximum tensile force in the bolt is $\overline{ED} = P_{max}$.

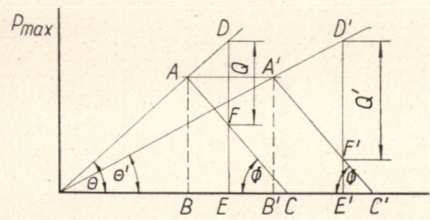


FIG. 8.12. With equal prestress, the useful load Q is greater for a tough bolt material than for a brittle one

Figure 8.12 shows two different cases for the same bolted joint, one with a softer and the other with a harder material. It can be seen that with the same prestress $\overline{AB} = \overline{A'B'}$ and the same load P_{max} , the useful load of a more ductile bolt is greater than that of a brittle one, i.e. $\overline{D'F'} > \overline{DF}$. This is the reason why the more ductile materials should be used for bolts. For the same reason, long bolts are preferable, when it is possible to use them, if necessary with thick washers or with shanks reduced to core diameter away from the threads.

It can also be seen from the figure that the external force Q increases the prestress to

$$P_{max} = P + Q \left(\frac{\tan \Theta}{\tan \Theta + \tan \Phi} \right)$$

but reduces the compression of the parts of the joint to

$$P_{min} = P - Q \left(\frac{\tan \Phi}{\tan \Theta + \tan \Phi} \right)$$

As the clamping force of bolted joints may fall to $P = 0$ in the extreme case, however, the required amount of prestress can be calculated from the last equation, for if $P_{\min} \geq 0$,

$$P \geq Q \left(\frac{\tan \Phi}{\tan \Theta + \tan \Phi} \right).$$

For highly stressed bolts the stress due to twisting must also be taken into account in design.

H. WIEGAND and B. HAAS [115] demonstrated that the torque M_t can be calculated, with the effect of friction included, from the equation

$$M_t = P \frac{d_2(h + \mu' \pi d_2)}{2(\pi d_2 - \mu' h)}$$

where M_t (kgf-cm) denotes the torque necessary to attain the required prestress P (kgf), d_2 (cm) the mean diameter of the bolt, h (cm) the pitch of the thread, and μ' its coefficient of friction.

Substituting now in the above equation the values

$$\begin{aligned} M_t &= \pi d_1^3 \tau / 16 \\ P &= \pi d_1^2 \sigma / 4 \\ d_2 &= 1.1 d_1 \\ h &= d_2 \pi \tan \gamma, \end{aligned}$$

we obtain

$$\frac{\tau}{\sigma} = 2.2 \frac{\tan \gamma + \mu}{1 - \mu' \tan \gamma}.$$

Since it may be assumed that $\mu' = 0.2$ and $\tan \gamma = 0.0033$ to 0.0053 , we have

$$\frac{\tau}{\sigma} = 0.53.$$

Hence, for the case of $\alpha_0 \approx 0.7$, the equivalent stress becomes

$$\sigma_c = \sqrt{\sigma^2 + 3\alpha^2\tau^2} = \sqrt{\sigma^2 + 3 \times 0.7^2 \times 0.53^2\sigma^2} = 1.2\sigma$$

and for the extreme case, when $\alpha = 1$, the result will be

$$\sigma_c = 1.35\sigma.$$

A. THUM and H. LORENZ [98] have demonstrated that toothed locking washers reduce fatigue strength but do not prevent the decrease of prestress. This is due to their compensating the unevenness of the bearing surfaces, and so reducing the resistance to loosening of the nuts. These authors consider that a decrease of prestress can be prevented only by systematic retightening of the bolts with measured torque.

8.5 Springs

To calculate helical springs the fatigue limits or the $S-N$ curves of the various spring materials must be known, and the results must then, as previously explained, be corrected by applying the size factor. As the diameter of the spring wire is often very small,

the effect of the size factor may be considerable; it is therefore more nearly correct to give the fatigue limit directly in relation to the dimensions. Table 20 of Part II (p. 98) gives the fatigue limit for various sizes of piano wire for the case $R = \sigma_1/\sigma_u = 0.5$ according to MAYERS [57]; in Table 21 can be found the factors to be applied for various endurance applicable to springs of which the wires were ground after hardening, the surface decarburized in the hardening process being removed if necessary, and which were wound cold with the contact surfaces ground flat.

Measurements carried out by POMP and HEMPEL [77] revealed that the fatigue limit of springs is considerably affected by surface finish. Scratches or other damage are very dangerous, particularly at the inside surfaces of wound springs, i.e. at the places of the highest stress concentrations, and especially if they run perpendicular to the axis of the wire. A depth of indentations or scratches greater than 0.03 mm is sufficient to reduce the endurance of springs. On the other hand, their fatigue strength is not reduced by heating below 300°C.

The stress occurring when a spring of circular cross-section is compressed or extended can be determined from the following formula:

$$\tau_{\max} = \frac{8FD}{\pi d^3} \left(\frac{4c-1}{4c-4} + \frac{0.615}{c} \right)$$

where τ_{\max} = maximum torsional stress in kgf/cm²;
 F = compressive (or tensile) force in kgf;
 D = mean coil diameter of the spring in cm;
 d = spring wire diameter in cm;
 c = ratio D/d .

The expression in brackets in the formula is the "Wahl factor", which allows for the stress concentrations at the inside diameter.

For a rectangular cross-section, τ_{\max} must be determined from the formula

$$\tau_{\max} = \frac{FD}{ab\sqrt{ab}} \psi$$

where a = width of spring material in cm;
 b = length of spring material in cm;
 ψ = a correction factor [50] (see also Fig. 98 of Part II, p. 100).

For torsion springs with a circular cross-section we have

$$\tau_{\max} = \beta_2 \frac{32M_t}{\pi d^3}$$

where M_t is the torque (kgf-cm). The value of the factor β_2 is obtained from Fig. 100 of Part II (p. 101).

With a rectangular cross-section,

$$\tau_{\max} = \beta_3 \frac{6M_t}{bh^2}$$

where b = width of spring material (perpendicular to axis of spring), in cm;
 h = height of spring material (parallel to axis of spring), in cm.

The value of the factor β_3 is obtained from Fig. 100 of Part II (p. 101).

Figures 101 to 104 of Part II (p. 101) give data from H. C. CARLSON [6] showing the permissible torsional stress of spring steels of various compositions and dimensions and for various endurance.

A diagram for the determination of the extension (or compression) of steel springs of rectangular cross-section is given in Fig. 99 of Part II (p. 100)

8.6 Welded joints

The design of welded joints is not possible on the lines so far indicated, for even with the highest quality of welding the welded joint is not always completely homogeneous. There are inclusions and slag islands which, of course, give rise to notch effects. The form of the weld, the base material, the electrode used, the internal stresses present, etc., also have a substantial effect on the fatigue strength. Proper expression cannot be given to all these factors in the methods that have been described above.

A number of tests relating to the fatigue design of welded joints are reported in the literature.

The method developed by NEUMANN [66] is in harmony with the above remarks, and it is briefly summarized below.

Essentially the NEUMANN method consists in plotting Smith diagrams for the parent metal and for the various welded joints, and investigating the behaviour of the ratio of one to the other for the various stress conditions ($-1 < R < +1$). The factor φ_k is introduced, defined by the formula

$$\varphi_k = \frac{\sigma_U \text{ welded joint}}{\sigma_U \text{ parent metal}}$$

When this factor is known for the various materials, forms of welded joints and welding processes, then if the Smith diagram of the material is known, the welded joint can be designed for fatigue.

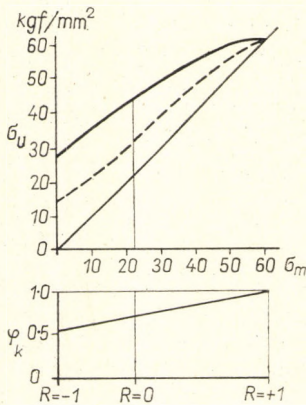


FIG. 8.13. Smith diagram of a welded joint drawn by the NEUMANN method, the straight line for the factor φ_k being given

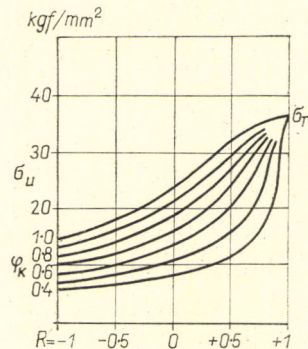


FIG. 8.14. Moore-Kommers-Jasper diagram drawn by the NEUMANN method, the curves for definite constant values of φ_k being given

NEUMANN demonstrated – in agreement with STÜSSI's theoretical work – that the factor φ_k bore a linear relationship to the mean stress σ_M and that it decreased uniformly from the value corresponding to static loading (at $R = 1$) to the value observed for reversed symmetrical loading ($R = -1$).

The heavy line in Fig. 8.13 represents the Smith diagram of a material, and the broken line below it that of a welded joint. The measurements of NEUMANN and STÜSSI showed that the value of the factor φ_k varies as indicated by the straight line drawn in the lower part of the figure.

As an extension of the method, NEUMANN also plotted the MOORE-KOMMERS-JASPER diagram, and gave the curves for various constant values of φ_k (Fig. 8.14).

Figure 105 of Part II (p. 104) gives the “z to s” lines for welded joints of St 37 (0.15% C) steel, and Fig. 106 those for St 52 (En 7) steel. Each constant value of φ_k is allotted one of the letter symbols, z to s, as indicated in Table 23 of Part II (p. 103).

The results for various welded joints are shown in Figs. 107 to 118 of Part II (pp. 105–108).

It can be seen that the MOORE-KOMMERS-JASPER diagram for each of the welded joints coincides with one of the “z to s” curves. Curves having the same letter identification have been collected to give the summary of results in Table 24 of Part II (p. 104).

Formulae for the determination of the nominal stresses for the different welded joints are given in Table 22 of Part II (p. 102).

8.7 Plates with holes at each end

The fatigue-strength reduction factors of plates with holes at each end (bush roller chain links), as given by THUM and BRUDER [94], are shown in Table 25 of Part II (p. 108).

8.8 Points to remember in designing for increased life of machine components

(1) Under fatigue conditions, and particularly when notches are present, high-tensile materials do not always possess an advantage over those of lower strength.

(2) Full homogeneity of the material is of the utmost importance. With homogeneous materials the $S-N$ curve for small probability of failure is usually higher than with more highly alloyed materials possessing higher strength as such but exhibiting greater scatter of results.

(3) Very stringent surface-finish requirements are necessary, and the utmost care must be exercised to comply with them. A good surface finish is very expensive, but a less satisfactory one considerably reduces the fatigue strength.

(4) It is essential to provide correct technological specifications. Care must be taken in grinding to prevent decarburization. Hardened layers must not be damaged. Surface hardening must be carried out with the utmost care. It is essential to ensure uniform pressure for surface rolling, and uniform speed, i.e. time of dispersion, in shot-peening.

(5) Resonant vibrations must be avoided.

(6) Corrosion must be prevented under all conditions. For the prevention of fretting corrosion appropriate fitting should be effected and molybdenum disulphide should be applied.

(7) The profiles of edges, corners, and transitions must receive careful attention. It is preferable to provide for "streamlined" load transmission both in the drawings and in actual manufacture.

(8) A high prestress, duly checked, is desirable in bolts. There should be small clearances between bolts and holes. Rolled threads are preferable.

(9) Safety has to be ensured by strict attention to technical parameters, and it should not be specified at an excessively high level to avoid the trouble of proper calculation. In any case a satisfactory degree of safety cannot be achieved without strict specifications and checking compliance with their requirements.

(10) It must be remembered that the weakest cross-section in fatigue is not always identical with the weakest under static load. Critical points should be checked by calculation.

Summary

THIS book has briefly summarized all that was available in the literature of the leading industrial countries regarding practical fatigue design. The collection and arrangement of the material was made more difficult by the need to evaluate the often contradictory results of various workers. In a few particular cases methods (e.g. SIEBEL'S) about which too little has yet been published have been included only for the sake of completeness.

Fatigue design is of immense importance for industry. Unfortunately it cannot yet be claimed that all details of the procedure are known. There are still very many unexplored regions, such as, for example, the behaviour of materials under torsional shear stresses at elevated temperatures; "coaxing" of materials; and many more.

If this book has given the reader an idea of the present position of fatigue design, and placed at his disposal data enabling him — at least in the simpler cases — to perform it himself, and if, in addition, it has stimulated the interest of research workers in the questions still to be investigated, then the author's aim will have been achieved.

List of Symbols

General

Symbol	Definition	Unit
A	cross-sectional area	cm ² , mm ²
b	surface-finish factor	—
C_W	constant depending on the material	—
d	smaller diameter	mm
D	larger diameter	mm
E	modulus of elasticity (Young's modulus)	kgf/mm ²
f	frequency	sec ⁻¹
F	force	kgf
G	shear modulus	kgf/mm ²
$i = \log N$	logarithm of number of cycles	—
I	moment of inertia, axial	cm ⁴
J	moment of inertia, polar	cm ⁴
k_b	size factor for workpieces stressed in bending	—
k_t	size factor for workpieces stressed in torsion	—
K_f	fatigue strength reduction factor according to the conservative method	—
K_{fB}	fatigue strength reduction factor according to the BOLLENRATH-TROOST theory	—
K_t	theoretical stress concentration factor	—
K_T	temperature coefficient	—
M_b	bending moment	kgf-cm
M_t	twisting moment	kgf-cm
n	number of load cycles (general)	—
N	endurance (number of load cycles to fracture)	—
p	constant depending on the material	—
q	notch sensitivity factor	—
q_H	HARRIS notch sensitivity factor	—
P, Q	load (force)	kgf
R	stress ratio	—
R_t	roughness depth, index of surface finish	μm
S	factor of safety	—
s_{Ph}	VON PHILIPP's [74] material constant	mm
t	thickness of notched workpiece	cm, mm
W	moment of resistance	cm ³

Symbol	Definition	Unit
W_p	polar moment of resistance	cm^3
X	SIEBEL'S relative stress gradient	mm^{-1}
α_0	stress ratio (for combined stress)	—
β_2	constants used for the calculation of helical springs	—
β_3		
δ_F	SIEBEL'S notched/smooth fatigue limit ratio	—
Δ_{L_s}	increase or decrease in length of a loaded bolt	mm
Δ_{L_f}	increase or decrease in length of a workpiece compressed by a bolted joint	mm
ε	ratio of elongation to original length	per cent
$\eta = \frac{\sigma_{tcF}}{\sigma_{bF}}$	ratio of tension-compression fatigue strength to bending fatigue strength	—
$\xi = \frac{\tau_F}{\sigma_{bF}}$	ratio of torsion fatigue strength to bending fatigue strength	—
λ_{by}	reduction of area at fracture	per cent
ϕ	angle in the Smith diagram	—

$$\left(\tan \phi = \frac{\sigma_M}{\sigma_U} \right)$$

ϕ_k	ratio of maximum stress (welded joint) to maximum stress (parent metal)	—
----------	---	---

Stresses (all expressed in kgf/cm^2 or kgf/mm^2)

$\sigma_0 = \sigma_{\text{fluct}}$	} symbols often used in the literature to denote the fluctuating-stress fatigue limit, reversed-stress fatigue limit, and static tensile strength respectively
$\sigma_{-1} = \sigma_F$	
$\sigma_{+1} = \sigma_T$	
$\sigma_{0.2}$	stress causing a permanent elongation of 0.2 per cent in a material
σ_a	stress amplitude
σ_A	stress amplitude causing fatigue fracture
σ_{adm}	permissible principal stress in a workpiece or test specimen
σ_b	static bending strength
σ_{bE}	bending endurance limit ($N < 10^6$)
σ_{bF}	bending fatigue limit
σ_{by}	yield stress in bending of a material
σ_{cy}	compressive yield stress
σ_c	static compressive strength
σ_e	equivalent stress according to the Mises-Hencky distortion energy hypothesis $\sigma_e = \sqrt{\sigma^2 + 3(\alpha_0\tau)^2}$
σ_{ea}	equivalent stress amplitude $\sigma_{ea} = \sqrt{\sigma_a^2 + 3(\alpha_0\tau_a)^2}$
σ_{em}	equivalent mean stress $\sigma_{em} = \sqrt{\sigma_m^2 + 3(\alpha_0\tau_m)^2}$
σ_D	"creep limiting stress"

σ_E	endurance limit of a material ($N < 10^6$)
σ_{full}	stress calculated on full cross-section
σ_F	fatigue strength in general
σ_{FN}	fatigue strength of a notched workpiece or specimen
σ_l	lower limit of range of cyclic stress
σ_L	lower limit of range of cyclic stress causing fatigue fracture
σ_m	mean value of cyclic stress
σ_M	mean value of cyclic stress causing fatigue fracture
σ_{max}	maximum stress produced by stress-raising effect
$\sigma_{max} = \sigma_m + \sigma_a$	maximum value of cyclic stress
$\sigma_{min} = \sigma_m - \sigma_a$	minimum value of cyclic stress
σ_n	principal stress according to elementary theory

$$\left(\sigma_n = \frac{P}{F} \text{ or } \frac{M_b}{W} \text{ etc.} \right)$$

σ_{fluct}	fluctuating-stress fatigue limit
σ_T	static tensile strength
σ_{icE}	tension-compression endurance limit ($N < 10^6$)
σ_{icF}	tension-compression fatigue strength
σ_{icFt}	tension-compression fatigue strength of specimen with smooth finish
σ_u	upper limit of range of cyclic stress
σ_U	upper limit of range of cyclic stress causing fatigue fracture
σ_y	tensile yield stress
τ_a	torsional stress amplitude
τ_A	torsional stress amplitude causing fatigue fracture
τ_{adm}	permissible shear stress in a workpiece or test specimen
τ_F	torsional fatigue strength
τ_{Fs}	shear fatigue strength
τ_l	lower limit of range of cyclic torsional stress
τ_L	lower limit of range of cyclic torsional stress causing fatigue fracture
τ_m	mean value of cyclic torsional stress
τ_M	mean value of cyclic torsional stress causing fatigue fracture
$\tau_{max} = \tau_m + \tau_a$	maximum value of cyclic torsional stress
$\tau_{min} = \tau_m - \tau_a$	minimum value of cyclic torsional stress
τ_n	static shear or torsional stress according to elementary theory
τ_u	upper limit of range of cyclic torsional stress
τ_U	upper limit of range of cyclic torsional stress causing fatigue fracture
τ_y	yield stress in torsion

References and Sources of Further Information

- [1] BACON, F.: The Rupture of Shafts by Fatigue. *Engineering* (1933).
- [2] BOLLENRATH, F. and TROOST, A.: Wechselbeziehungen zwischen Spannungs- und Verformungsgradient. *Arch. f. d. Eisenhüttenwesen* (1952).
- [3] BOLLER, K.: Fatigue Properties of Fibrous Glass-reinforced Plastic Laminates Subjected to Various Conditions. *Modern Plastics* (1957).
- [4] BUCHMANN, W.: Dauerfestigkeitseigenschaften der Magnesiumlegierungen. *VDI* (1941).
- [5] BÜHLER, H. and SCHREIBER, W.: Lösung einigen Aufgaben der Dauerschwingfestigkeit mit dem Treppenstufen-Verfahren. *Arch. f. d. Eisenhüttenwesen* (1957).
- [6] CARLSON: Properties of Spring Materials and Allowable Working Stresses. *Product Design Handbook* 1955.
- [7] CAZAUD, R.: Évaluation de la Limite de Fatigue à partir d'une seule Éprouvette, Pièce ou Élément d'Essai. *Conference of the Hungarian Academy of Sciences on Dimensioning and Strength Calculation*. Budapest, 1961.
- [8] CAZAUD, R. and DE LEIRIS, H.: Evaluation of the Fatigue Limit Using Only One Welded Specimen or Assembly. *Soudages et Techniques Connexes* (1962).
- [9] CHIH-BING LING: On the Stresses in a Plate containing Two Circular Holes. *J. Appl. Phys.* (1948).
- [10] DOLAN and BORGHAMER: A Photoelastic Study of Stresses in Gear Tooth Fillets. *Univ. Ill. Expt. Stn. Bull.* (1942).
- [11] ERKER: Festigkeitsversuche mit brenngeschrittenen Proben aus Cr-V-Stahl. *Schweissen und Schneiden* (1953).
- [12] FROCHT, M.: Factors of Stress Concentration Photoelastically Determined. *Trans. ASME* (1935).
- [13] FROCHT and HILL: Stress Concentration Factors around a Central Circular Hole in a Plate loaded through a Pin in the Hole. *Trans. ASME* (1940).
- [14] FROCHT and LANDSBERG: Factors of Stress Concentration on Bars with Deep Sharp Grooves and Fillets in Tension. *Proc. SESA* (1951).
- [15] FROCHT and LEVEN: Factors of Stress Concentration for Slotted Bars in Tension and Bending. *Trans. ASME* (1951).
- [16] FROCHT and LEVEN: Stress Concentration Factors for Single Notch in Flat Bar in Pure and Central Bending. *Trans. ASME* (1952).
- [17] GOODIER, J.: Influence of Circular and Elliptical Holes on Transverse Flexure of Elastic Plates. *Phil. Mag.* (1936).
- [18] GÜRTLER and SCHMID: Temperaturabhängigkeit der Dauerwährung metallischer Werkstoffe bei ruhender und wechselnder Beanspruchung. *VDI* (1939).
- [19] HÄNCHEN: Berechnung und Gestaltung der Maschinenteile auf Dauerhaltbarkeit. *Technische Fachbücher* 1950.
- [20] HARRIS, W. J.: *Metallic Fatigue*. Pergamon Press, London, 1961.
- [21] HEMPEL, M.: Zur Frage des Dauerbruches. Magnetpulverbild und Dauerbruchariss. *Mitt. d. Kaiser-Wilh.-Inst. Abhdlg.* 374, 1939.
- [22] HEMPEL and ARDELT: Verhalten des Stahles in der Wärme unter Zug-Druck-Wechselbeanspruchung. *Mitt. d. Kaiser-Wilh.-Inst.* (1939).
- [23] HEMPEL and LUCE: Verhalten von Stahl bei tiefen Temperaturen unter Zug-Druck-Wechselbeanspruchung. *Mitt. d. Kaiser-Wilh.-Inst.* (1941).
- [24] HEROLD, W.: Wechselfestigkeit metallischer Werkstoffe. 1934.

- [25] HEROLD, W.: Versuche über Drehschwingungsfestigkeit an Wellen. *VDI* (1937).
- [26] HETÉNYI, M.: Some Applications of Photoelasticity in Turbine-generator Design. *Trans. ASME* (1939).
- [27] HETÉNYI, M.: The Distribution of Stresses in Threaded Connections. *Proc. SESA* (1943).
- [28] HEYWOOD, R. B.: Correlated Fatigue Data for Aircraft Structure Joints. *Engineering* (1957).
- [29] HORGER, O.: Effect of Surface Rolling on the Fatigue Strength of Steel. *ASME* (1935).
- [30] HORGER and BRUCKWALTER: Photoelasticity as Applied to Design Problems. *Iron Age* (1940).
- [31] HORGER and MAULBETSCH: Increasing the Fatigue Strength of Press-fitted Axle Assemblies by Surface Rolling. *Trans. ASME* (1936).
- [32] HOUDREMONT, E.: Einige Gesichtspunkte zur Entwicklung der Forschung auf dem Gebiet der Dauerfestigkeit. *Lilienthal-Ges. f. Luftfahrtforschung*, Bericht 116, 1939.
- [33] HOWLAND, R.: On the Stress in the Neighbourhood of a Circular Hole in a Strip under Tension. *Phil. Trans. Roy. Soc. London* (1929-1930).
- [34] HUTH, J.: Torsional Stress Concentration in Angle and Square Tube Fillets. *Trans. ASME* (1950).
- [35] JACOBSEN, L.: Torsional Stress Concentrations in Shafts of Circular Cross-section and Variable Diameter. *Trans. ASME* (1925).
- [36] KIMMELMANN: *Gépkatrészek szilárdsági számításai ismételt igénybevételeknél.* (Mechanical design of machine components subject to repeated loading.) Nehézipari Könyvkiadó 1951.
- [37] KOLOSOFF, G.: *Thesis.* St. Petersburg, 1910.
- [38] KOMMERS, J. B.: *ASTM Technical Papers*, II (1938).
- [39] KOMMERS, J. B.: The Effect of Overstresses in Fatigue. *Proc. ASTM*, Vol. 45.
- [40] KONTOROVIC and ARANOVIC: *Tyechnika vozdušnovo flota.* 1934.
- [41] KÖRBER and HEMPEL: Einfluss von Recken und Altern auf das Verhalten von Stahl bei Schwingungsbeanspruchung. *Mitt. d. Kaiser-Wilh.-Inst.* (1935).
- [42] KÖRBER and HEMPEL: Zug-Druck-, Biege- und Verdrehwechselbeanspruchung an Stäben mit Querbohrungen und Kerben. *Mitt. d. Kaiser-Wilh.-Inst.* (1939).
- [43] KÖRBER and POMP: Zur Bestimmung der Warmstreckgrenze von Stahl. *Mitt. d. Kaiser-Wilh.-Inst.* (1930).
- [44] KUDRYAVTSEV, I. V.: *A belső feszültségek, mint a gépgyártás szilárdsági tartalékai.* (The inner stresses as strength factors of machine engineering.) Akadémiai Kiadó, 1954.
- [45] LEBEDYEV, T. A.: *Trudi Leningr. Polyt. Inst.* (1953) No. 4.
- [46] LEE, G.: The Influence of Hyperbolic Notches on the Transverse Flexure of Elastic Plates. *Trans. ASME* (1940).
- [47] LEHR, E.: Beitrag zur Berechnung dauerbeanspruchter Wellen. *Techn. Zentralbl. prakt. Metallbearb.* (1937).
- [48] LEVEN, M.: Stresses in Keyway by Photoelastic Methods and Comparison with Numerical Solution. *Proc. SESA* (1949).
- [49] LEVEN and HARTMANN: Factors of Stress Concentration for Flat Bars and Shafts with Centrally Enlarged Section. *Proc. SESA* (1951).
- [50] LIESECKE: Berechnung zylindrischer Schraubfedern mit rechteckigem Draht-querschnitt. *VDI* (1933), pp. 425, 892.
- [51] LOCATI, L.: Le Prove di Fatica come Ausilio alla Progettazione ed alla Produzione. *Metalurgia Italiana* (1955), No. 9.
- [52] MCDOWELL: Fretting Corrosion Tendencies of Several Combinations of Metals. Symposium on Fretting Corrosion. *ASTM Special Publication*, 1952.
- [53] MAILÄNDER: *Z. f. Metallkunde* (1928).
- [54] MAILÄNDER and BAUERSFELD: Einfluss der Probengröße und Probenform auf die Drehschwingungsfestigkeit von Stahl. *Techn. Mitt. Krupp* (1934).
- [55] MAKHULT, M.: *Acéltengelyek méretezése.* KGM Tervező Irodái, Tervezési segédlet. (Design of Steel Shafts. Auxiliary Design Tables.) Budapest, 1961.
- [56] MATLE and DOLAN: A Photoelastic Study of Stresses in U-shaped Members. *Proc. SESA* (1948).
- [57] MAYERS: Working Stresses for Helical Springs. *Machine Design* (1951).
- [58] MINER, M.: Estimation of Fatigue Life with Particular Emphasis on Cumulative Damage. *Metal Fatigue* (edited by Sines and Waisman). McGraw-Hill, 1959.
- [59] MÖLLER and HEMPEL: Wechselbeanspruchung und Kristallzustand, III. *Arch. f. d. Eisenhüttenw.* (1953).

- [60] MOORE, H.: *Metals and Alloys*. 1935.
- [61] MOORE and KOMMERS: An Investigation of the Fatigue of Metals. *Univ. Illinois Engng. Exp. Stn. Bull.* (1923).
- [62] MOORE and KOMMERS: *The Fatigue of Metals*. 1927.
- [63] MUTNYANSZKY, A.: *Szilárdságtan*. (Strength of Materials.) Tankönyvkiadó, Budapest, 1956.
- [64] NEUBER: *Kerbspannungslehre*. Springer Verlag, Berlin, 1958.
- [65] NEUMANN, A.: *Schweisstechnisches Handbuch*. Berlin: VEB Verlag Technik. 1960.
- [66] NEUMANN, A.: *Probleme der Dauerfestigkeit von Schweissverbindungen*. Berlin: VEB Verlag Technik. 1960.
- [67] NIEMANN and GLAUBITZ: Einfluss der Oberflächenrauheit auf die Biege-Wechselfestigkeit von ungehärtetem und vergütetem Stahl. *VDI* (1952).
- [68] OROWAN, E.: Theory of the Fatigue of Metals. *Proc. Roy. Soc. London* (1939).
- [69] OSTESPEY, I.: Spannungsverteilung in Stangenköpfen und Dauerhaltbarkeit. *Forschg. Ing.-Wesen* (1943), 14, H.3.
- [70] PATTON, W.: Mechanical Properties of NE, SAE and other Hardened Steels. *Metal Progress* (1943).
- [71] PETERSON, R.: *Stress Concentration Design Factors*. Wiley & Sons, Inc., New York 1953.
- [72] PETERSON, R.: Notch sensitivity. *Metal Fatigue* (edited by Sines and Waisman). McGraw-Hill 1959.
- [73] PETERSON and WAHL: Fatigue of Shafts and Fitted Members with Related Photoelastic Analysis. *Trans. ASME* (1935).
- [74] PHILIPP, H. VON: Einfluss von Querschnittgröße und Querschnittform auf die Dauerfestigkeit bei ungleichmässig verteilten Spannungen. *Thesis*, Munich, 1941. (*Forschg. a. d. Geb. d. Ing.-Wesens* (1942).)
- [75] POMP and HEMPEL: Dauerfestigkeit von gekerbten und kaltverformten Stählen sowie 1-inch und 1 1/8-inch Schrauben. *Mitt. d. Kaiser-Wilh.-Inst.* (1936).
- [76] POMP and HEMPEL: Über das Verhalten von Gusseisen und Temperguss unter wechselnder Beanspruchung. *Mitt. d. Kaiser-Wilh.-Inst.* (1940).
- [77] POMP and HEMPEL: Über die Dauerhaltbarkeit von Schraubenfedern mit und ohne Oberflächenverletzungen. *Mitt. d. Kaiser-Wilh.-Inst.* (1940).
- [78] RICHART, F. E. and NEWMARK, N. M.: An Hypothesis for the Determination of Cumulative Damage in Fatigue. *Proc. ASTM*, Vol. 48.
- [79] RUDNAI, G.: Recording the Load Spectra of Vehicles. *Conference of the Hungarian Academy of Sciences on Dimensioning and Strength Calculation*. Budapest, 1961.
- [80] SCHIMKE and HORN: *Praktisches Handbuch der gesamten Schweisstechnik*. III. Berechnen und Entwerfen der Schweisskonstruktionen. Springer Verlag, Berlin, 1950.
- [81] SCHOULZ, K.: Over den Spannungstoestand in doorborde Platen. *Thesis*, Technical University of Delft, 1941.
- [82] SCHWIMMING, W.: Festigkeit der Werkstoffe bei tiefen Temperaturen. *VDI* (1935).
- [83] SEELY and SMITH: *Advanced Mechanics of Materials*. J. Wiley, New York. 1952.
- [84] SIEBEL, E.: Ungleichförmige Spannungsverteilung bei schwingender Beanspruchung. *VDI* (1955).
- [85] SIEBEL, E.: *Handbuch der Werkstoffprüfung*, Vol. II. Springer Verlag, Berlin, 1955.
- [86] SIEBEL and GAIER: Untersuchungen über den Einfluss der Oberflächenbeschaffenheit. *VDI* (1956).
- [87] SJÖSTRÖM, S.: On the Stresses at the Edge of an Excentrically Located Circular Hole in a Strip under Tension. *Aeronaut. Res. Inst. of Sweden*. Stockholm, 1950.
- [88] SMITH, J.: The Effect of Range of Stresses in the Fatigue Strength of Metals. *Univ. Ill. Eng. Expt. Stn. Bull.* (1942, 334).
- [89] STÜSSI: *Theorie der Dauerfestigkeit und die Versuche von A. Wöhler*. Verlag VSB. Zürich. 1955.
- [90] TAUSCHER, H.: Berechnung der Dauerfestigkeit. Einfluss von Werkstoff und Gestalt. *Fachbuchverlag*, Leipzig, 1960.
- [91] THUM and BRUDER: Dauerbruchgefahr an Hohlkehlen von Wellen. *Deutsche Kraftfahrtforschung*. No. 11.
- [92] THUM and BRUDER: Gestaltung und Dauerhaltbarkeit von geschlossenen Stabköpfen und ähnlichen Bauteilen. *Deutsche Kraftfahrtforschung*. No. 20.

- [93] THUM and BRUDER: Flanschwellen-Dauerbrüche und ihre Ursachen. *Deutsche Kraftfahrtforsch.* No. 41.
- [94] THUM and BRUDER: Beanspruchungsmechanismus und Gestaltfestigkeit von Nabensitzen. *Deutsche Kraftfahrtforsch.* No. 73.
- [95] THUM and BUCHMANN: *Dauerfestigkeit und Konstruktion*. 1932.
- [96] THUM and ERKER: *Schweissen im Maschinenbau*. Part I: Festigkeit und Berechnung von Schweissverbindungen. 1943.
- [97] THUM and KIRMSE: Überlagerte Wechselbeanspruchungen, ihre Erzeugung und Einfluss auf die Dauerhaltbarkeit und Spannungsbildung quergebohrter Wellen. *VDI Forschungsheft* No. 419 (1943).
- [98] THUM and LORENZ: Dauerhaltbarkeit von Schraubenverbindungen. *VDI Forschungsheft*, (1941).
- [99] THUM and OCHS: *Korrosion und Dauerfestigkeit*. VDI Verlag, 1937.
- [100] THUM and SVENSON: Mehrfache Kerbwirkung. *VDI* (1950), p. 225.
- [101] THUM and SVENSON: Mehrfache Kerbwirkung. *VDI* (1950), p. 228.
- [102] TIMOSHENKO, S.: On the Distribution of Stresses in a Circular Ring compressed by Two Forces along a Diameter. *Phil. Mag.* (1922).
- [103] TIMOSHENKO, S.: On the Stresses in a Plate with a Circular Hole. *J. Franklin Inst.* 1924.
- [104] TOMLINSON, G. A., THORPE, P. L. and GOUGH, H. J.: An Investigation of the Fretting Corrosion of Closely Fitted Surfaces. *Proc. Inst. Mech. E.* (1939).
- [105] VOLK: Sicherheit und zulässige Spannung. *Elektroschweissung* (1937).
- [106] VÖRÖS, I.: *A Siebel-féle méretezési elmélet.* (Siebel's Design Theory.) Magyar Tudományos Akadémia, Budapest, 1958.
- [107] WAHL, A.: *Mechanical Springs*. Penton Publishing Co., Cleveland, Ohio. 1944.
- [108] WAHL, A.: Calculation of Stresses in Crane Hooks, *Trans. ASME* (1946) and *Design Data and Methods*, ASME, New York, 1953.
- [109] WÄLLGREN, G.: *Fatigue Tests with Cycles of Varying Amplitude*. FFA Sweden, 1949.
- [110] WEATHERBURN, C. E.: *A First Course in Mathematical Statistics*. Cambridge University Press, 1949.
- [111] WEIBULL, W.: Statistical Representation of Fatigue Failures in Solids. *Acta Polytechnica*, Stockholm (1949).
- [112] WEIBULL, W.: Scatter of Fatigue Life and Fatigue Strength in Aircraft Structural Materials and Parts. *Columbia Conference*, 1956.
- [113] WIEGAND, H.: Einsatzhärtung und Dauerfestigkeit. *VDI* (1939).
- [114] WIEGAND, H.: Oberflächengestaltung dauerbeanspruchter Maschinenteile. *VDI* (1940).
- [115] WIEGAND and ILLGNER: *Berechnung und Gestaltung von Schraubenverbindungen*. Springer Verlag, Berlin, 1962.
- [116] WILSON, W.: *Engineering* (1945).
- [117] *Design Data and Methods*. Booklet published by ASME, 1939, 1953, New York.
- [118] *Modern Plastics Encyclopedia*, Plastic Catalogue Corp. New York. 1947.
- [119] *Metals Handbook*. Published by American Society for Metals, 8th ed. Novelty, Ohio, 1961.
- [120] *Hütte des Ingenieurs*. Taschenbuch, 28th ed. W. Ernst & Sohn, Berlin.

PART II
TABLES AND DIAGRAMS

The numbering of the headings corresponds to the numbering of the chapters and sections of Part I.

General summary of fatigue design

(Section 7 of Part I)

Conservative method (Section 7.1)

Serial No.	Operation	Symbol	Feature	To be found in			Remarks
				Part I	Part II		
				pp.	pp.	Fig.	
1	Read off according to stress (tensile, bending, etc.) from the existing or plotted Smith diagram	$\sigma_{\theta F}$ σ_{icF} τ_F τ_{Fs}	Reversed or fluctuating fatigue strength of the material	21-36	9-28	1-37	
2	Determine graphically	σ_E	Endurance limit	36			Only if $N < 10^6$
3	Multiply by	b	Surface-finish factor	40-42	28	38-40	
4	Estimate modification required		For temperature	44-46	30-32	44-52	Negligible in range -40° to $+300^\circ\text{C}$
5			For surface treatment	46-50			These factors may be neglected in most cases in practice. Designers have to know, however, under what conditions this may be done
6			For corrosion	50-52	32-36	53-57	
7			For previous history of material	52-54			
8	Multiply by	k_b	Size factor	42-44	29	41-43	
9	Result	σ_{Fcalc}	Calculated fatigue strength of the material				
10	Divide by	K_f	Fatigue strength reduction factor	55-62	37-84	59-69	Interpolated using Fig. 61

Serial No.	Operation	Symbol	Feature	To be found in			Remarks
				Part I	Part II		
				pp.	pp.	Fig.	
11	Result	σ_{FN}	Fatigue strength of the machine component				
12	Determine from table, and divide by	S	Factor of safety	67-71	86		
13	Result	$\sigma_{adm\ calc}$	Permissible stress in the machine component				
14	Use the value of $\sigma_{adm\ calc}$ as if it were the value $\sigma_n(\tau_n)$ in elementary strength of materials theory. For complex or combined stresses consider $\sigma_{adm\ calc}$ as equivalent stress σ_e						

Fatigue strength reduction factor q_H by Harris theory (Section 7.2)

1 to 9	As for conservative method						
10	Divide by	q_H	Harris notch sensitivity factor	63	60	67	
11 to 14	As for conservative method						

Bollenrath-Troost theory (Section 7.3)

1	Read off as in conservative method	σ_{icF}	Reversed or fluctuating fatigue strength of the material				
2 to 7	As for conservative method						
8	Determine from graph, and divide by	K_{fB}	Fatigue strength reduction factor	64	58	65	K_{fB} from the graph in Fig. 65

Serial no.	Operation	Symbol	Feature	To be found in			Remarks
				Part I	Part II		
				pp.	pp.	Fig.	
9	Result	σ_{FN}	Fatigue strength of the machine component				
10	Determine from table, and divide by	S	Factor of safety	67-71	86		
11	Result	$\sigma_{adm \text{ calc}}$	Permissible stress in the machine component				
12	As No. 14 of conservative method						

Siebel theory (Section 7.4)

1	As for <i>Bollenrath-Troost</i> theory						
2	Calculate	X		65	85	94	
3	Multiply σ_{icf} by	δ_F	Factor depending on X and the material	65	85	93	Read δ_F from Fig. 93
4	Using the fatigue strength determined by means of Nos. 1 to 3, obtain graphically	σ_E	Endurance limit				Only if $N < 10^6$
5	Multiply by	b	Surface-finish factor	40-42	28	38-40	
6	Estimate modification required		For temperature	44-46	30-32	44-52	Negligible in range -40° to $+300^\circ\text{C}$

Serial No.	Operation	Symbol	Feature	To be found in			Remarks
				Part I	Part II		
				pp.	pp.	Fig.	
7	Estimate modification required		For surface treatment	46-50	32-36	53-57	These factors may be neglected in most cases in practice. Designers have to know, however, under what conditions this may be done
8			For corrosion	50-52			
9			For previous history of material	52-54			
10	Divide by	K_t	Theoretical stress concentration factor	55-61	37-57 61-84	68-87	Interpolated using Fig. 61
11	Determine from table, and divide by	S	Factor of safety	67-71	86		
12	As No. 14 of conservative method						

1. Fatigue diagrams

1.5 The equations of the $S-N$ curves

TABLE 1

WEIBULL FORMULA CONSTANTS (50 PER CENT PROBABILITY OF FRACTURE)

No.	Description of material in the literature	Corresponding British nomenclature	Type of stress	σ_F kgf/mm ²	k	m	Static loading kgf/mm ²	Literature reference
1	C 15	En 2B	b $R = -1$	25	7.146	0.557	$\sigma_T = 44.5$	STIELER: Untersuchungen über die Dauerfestigkeit metallischer Bauteile bei Raumtemperatur. Thesis, Stuttgart Technical University, 1954
2	C 15 (normalized)	En 2B	tc $R = -1$	22	6.301	0.540	$\sigma_T = 44.7$	ditto
3	C 15 (normalized)	En 2B	tc $R = 0$	36	7.000	0.400	$\sigma_T = 44.7$	ditto
4	C 15 (normalized)	En 2B	tc $R = -1$	22.5	7.176	0.364	$\sigma_T = 45.5$	ditto
5	C 15 (normalized)	En 2B	tc $R = -1$	23	7.097	0.276	$\sigma_T = 45.5$	ditto
6	C 15	En 2B	to $R = -1$	15	7.000	0.475	$\sigma_T = 44.5$	ditto
7	C 35 (quenched and tempered)	En 5	b $R = -1$	40	5.910	0.164	$\sigma_T = 71$	SCHRAIVOGEL: Dauerbiegeversuche mit Schraubenbolzen. Stahl und Eisen (1932)
8	C 45 (quenched and tempered)	En 6A	b $R = -1$	31	6.875	0.416	$\sigma_T = 66.5$	STIELER (as above)
9	C 45 (quenched and tempered)	En 6A	b $R = 0$	29	6.114	0.110	$\sigma_T = 85$	TAUSCHER and BUCHHOLZ: Biegedauerfestigkeit induktiv oberflächen gehärteter Vergütungsstähle. Inst. für Leichtbau, Dresden, 1964
10	C 45 (quenched and tempered)	En 6A	b $R = -1$	39	5.653	0.073	$\sigma_T = 85$	ditto
11	C 45 (normalized)	En 6A	tc $R = -1$	23.4	7.000	0.455	$\sigma_T = 60.5$	STIELER (as above)

12	C 45 (quenched and tempered)	En 6A	<i>tc</i> $R = -1$	29	6.079	0.345	$\sigma_T = 66.5$	ditto
13	C 60	En 9	<i>b</i> $R = -1$	38.5	5.858	0.091	$\sigma_T = 80.5$	RÉTI: Die Streuung der Ergebnisse von Dauerschwingversuchen. Materialprüfung (1964)
14	70 Si7 spring steel (quenched and tempered)	BS 970 En 45A BS 1429 En 45A	<i>tc</i> $R = -1$	58.4	5.700	0.086	$\sigma_T = 132$	STIELER (as above)
15	70 Si7 spring steel (quenched and tempered)	BS 970 En 45A BS 1429 En 45A	<i>t</i> $R = 0$	86	7.000	0.330	$\sigma_T = 132$	ditto
16	70 Si7 spring steel (quenched and tempered)	BS 970 En 45A BS 1429 En 45A	<i>to</i> $R = -1$	39	7.000	0.380	$\sigma_T = 132$	ditto
17	(Cr 135) 34 Cr 4	BS 970 En 18B	<i>t</i> $R = 0$	30	6.900	0.142	$\sigma_T = 66.3$	RÉTI: Einfluss einer Vorer-müdung auf die Festigkeitseigenschaften von Stählen. Materialprüfung (1965)
18	(Cr 135) 34 Cr 4	BS 970 En 18B	<i>tc</i> $R = -1$	17	6.740	0.190	$\sigma_T = 66.3$	ditto
19	(HB 304-313) 40 Cr 4	BS 970 En 18D	<i>to</i> $R = -1$	31.5	6.3010	0.250	$\sigma_T = 110$	LINKE and DEMKO: Zum Einfluss des Badnitrierens auf die Verdrehwechsel-festigkeit. Maschinenbau-techn. (1964)
20	20 MoCr5 920°C for 25 min, oil quenched, tempered 180°C	BS 3111 Type 5	<i>b</i> $R = -1$	42	5.9777	0.133	$\sigma_T = 95$	TAUSCHER and STECHER: Das Verhalten der Einsatzstähle bei Dauerschwingbeanspruchung. Maschinenbautechn. (1962)
21	20 MoCr5 920°C for 15 min, oil quenched, tempered 180°C	BS 3111 Type 5	<i>b</i> $R = -1$	59	6.3010	0.091	$\sigma_T = 135$	ditto

(TABLE 1, CONT.)

No.	Description of material in the literature	Corresponding British nomenclature	Type of stress	σ_F kgf/mm ²	k	m	Static loading kgf/mm ²	Literature reference
22	20 MoCr5 920°C for 8 h CN, quenched in oil, tempered 180°C	BS 3111 Type 5	b $R = -1$	74	6.4393	0.154	Edge hardness HRC = 61 to 62	TAUSCHER and STECHER (as above)
23	20 MoCr5 (as No. 20)	BS 3111 Type 5	tc $R = -1$	35	6.4393	0.142	$\sigma_T = 95$	ditto
24	20 MoCr5 (as No. 21)	BS 3111 Type 5	tc $R = -1$	51	6.3617	0.154	$\sigma_T = 135$	ditto
25	20 MoCr5 (as No. 22)	BS 3111 Type 5	tc $R = -1$	56	6.4771	0.330	Edge hardness HRC = 61 to 62	ditto
26	25 Cr Mo 4 with rolling skin	3T. 50	b $R = -1$	26	5.9542	0.118	$\sigma_T = 120$	TAUSCHER: Festigkeitseigenschaften von Schweissverbindungen. Inst. für Leichtbau, Dresden, Mittg. (1962)
27	GG 22		tc $R = -1$	8	5.6990	0.400	$\sigma_T = 23.5$	STIELER (as above)
28	GG 22		t $R = 0$	10.5	5.8451	0.370	$\sigma_T = 23.5$	STIELER (as above)
29	GG 22		c $R = 0$	11	5.6532	0.500	$\sigma_T = 23.5$	ditto
30	GG 22		to $R = -1$	8.5	6.3010	0.450	$\sigma_T = 23.5$	ditto

 tc = tension-compression b = bending t = tension to = torsion c = compression

2. Fatigue diagrams of various materials

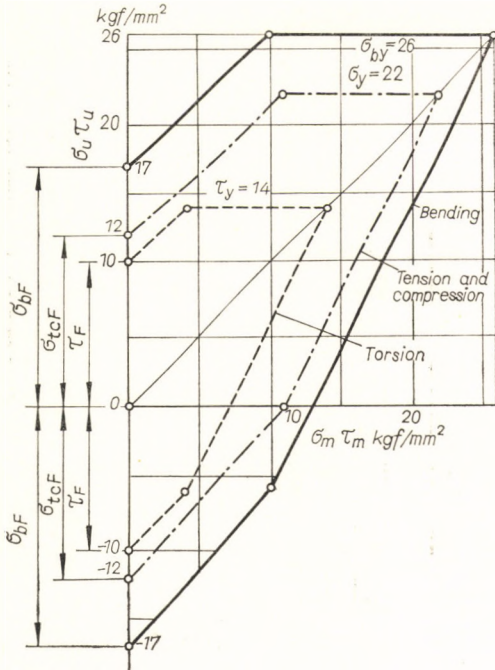


FIG. 1. Smith diagram of 0.15% C steel

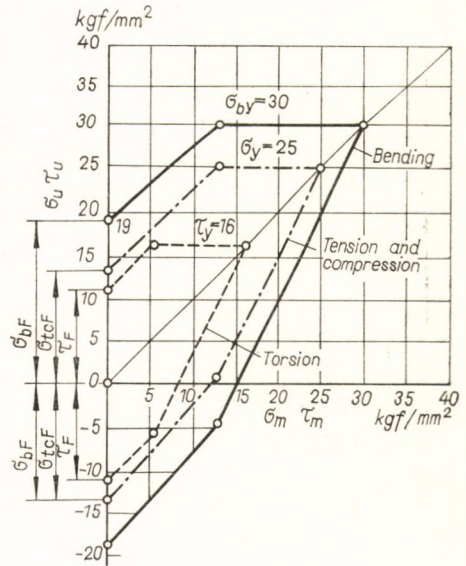


FIG. 2. Smith diagram of 0.25% C steel

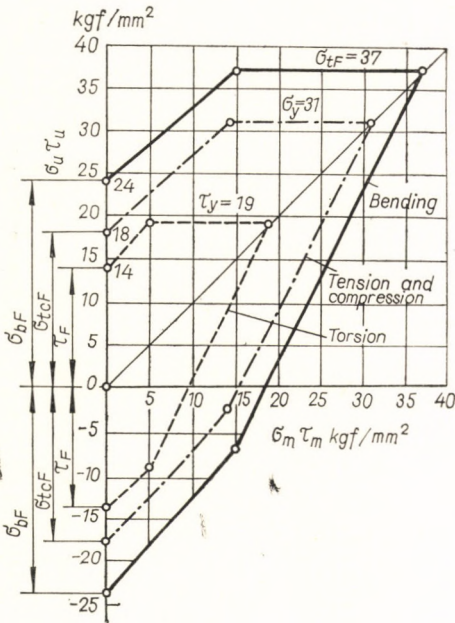


FIG. 3. Smith diagram of 0.35% C steel

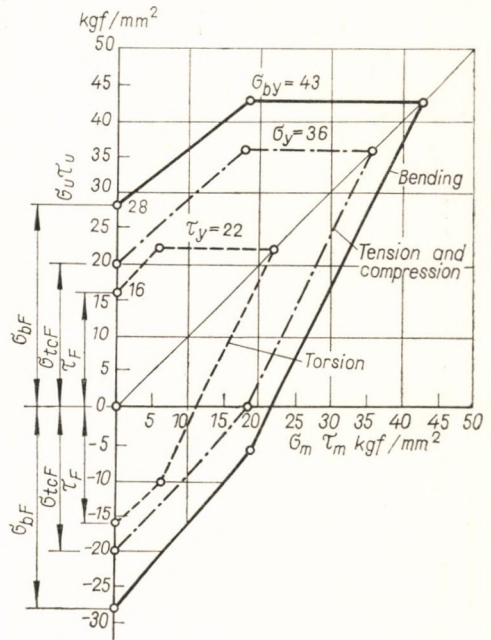


FIG. 4. Smith diagram of 0.45% C steel

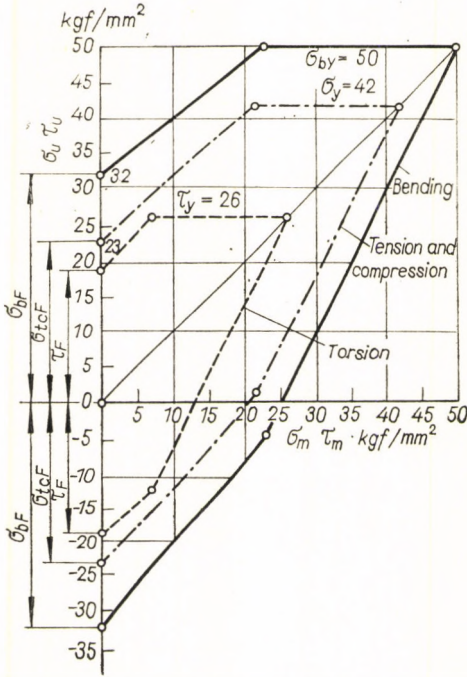


FIG. 5. Smith diagram of 0.60% C steel

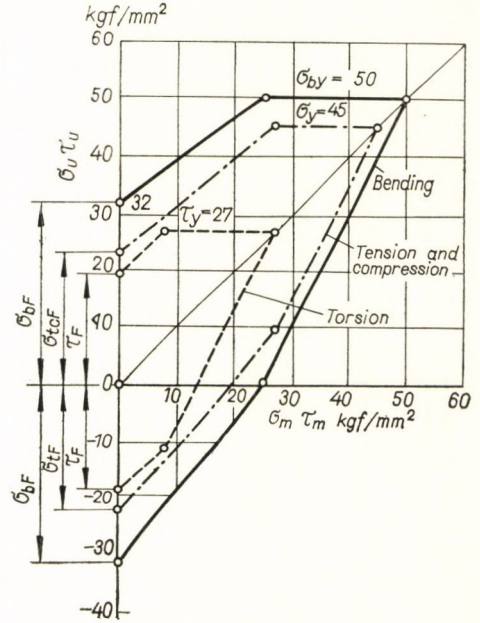


FIG. 6. Smith diagram of steel of composition 0.28% C, 0.25% Si, 0.60% Mn, 0.50% Cr, 1.50% Ni (En 111 approx.)

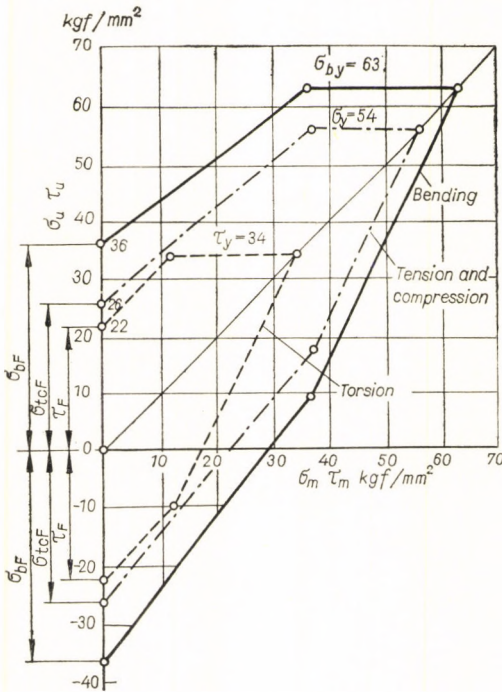


FIG. 7. Smith diagram of steel of composition 0.36% C, 0.25% Si, 0.60% Mn, 0.50% Cr, 1.50% Ni (En 111 approx.)

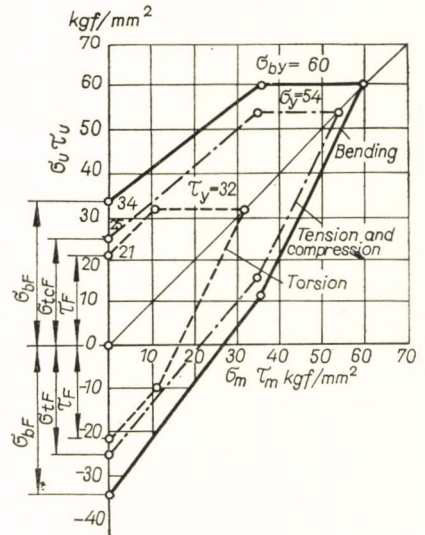


FIG. 8. Smith diagram of steel of composition 0.28% C, 0.25% Si, 0.60% Mn, 0.75% Cr, 2.50% Ni (En 25 approx.)

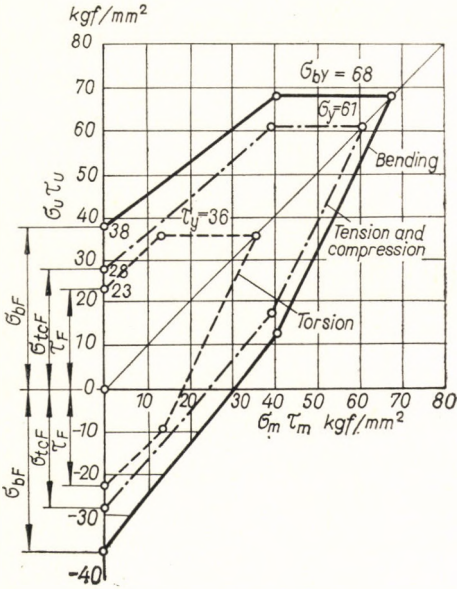


FIG. 9. Smith diagram of steel of composition 0.36% C, 0.25% Si, 0.60% Mn, 0.75% Cr, 2.50% Ni (En 25 T approx.)

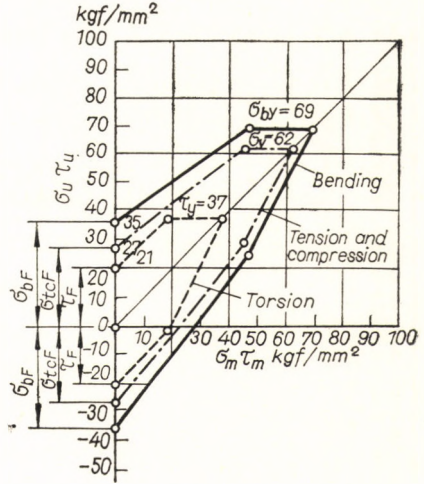


FIG. 10. Smith diagram of steel of composition 0.22% C, 0.25% Si, 0.60% Mn, 0.75% Cr, 3.50% Ni (En 23 S approx.)

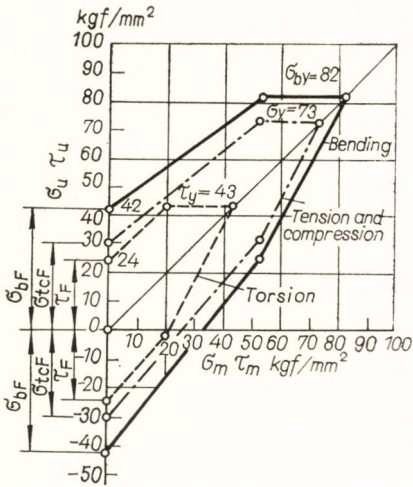


FIG. 11. Smith diagram of steel of composition 0.31% C, 0.25% Si, 0.60% Mn, 0.75% Cr, 3.50% Ni (En 23 T approx.)

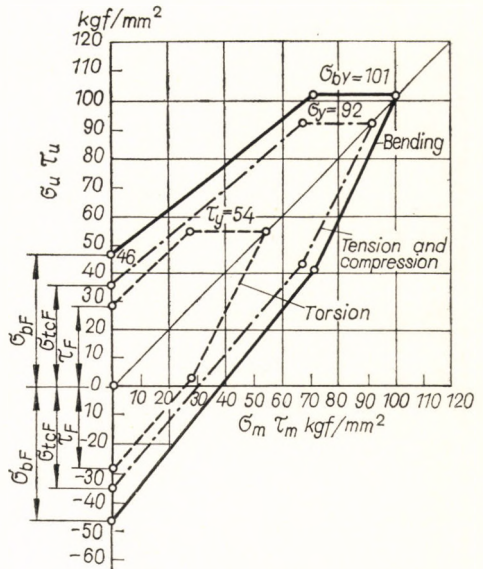


FIG. 12. Smith diagram of steel of composition 0.36% C, 0.25% Si, 0.60% Mn, 1.30% Cr, 4.50% Ni (En 30 B approx.)

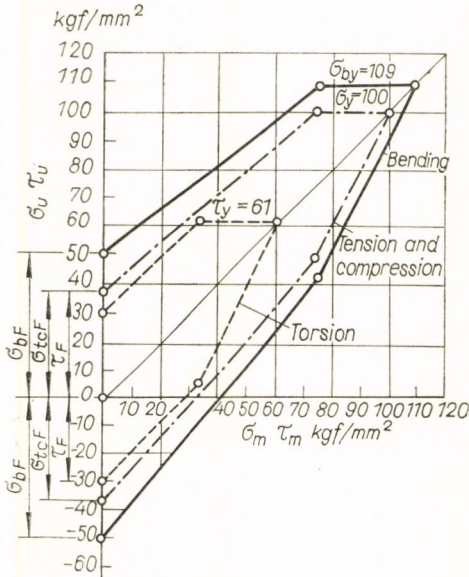


FIG. 13. Smith diagram of Ni-Cr-W steel of composition 0.3 to 0.5% C, 3.5 to 4.5% Ni, 0.9 to 1.2% Cr, 0.5 to 0.7% W, 0.3 to 0.5% Mn, 0.2 to 0.3% Si. Typical properties: $\sigma_T = 120 \text{ kgf/mm}^2$, $\sigma_y = 100 \text{ kgf/mm}^2$, ϵ on $11 \cdot \sqrt{\text{area}} = 10$ per cent

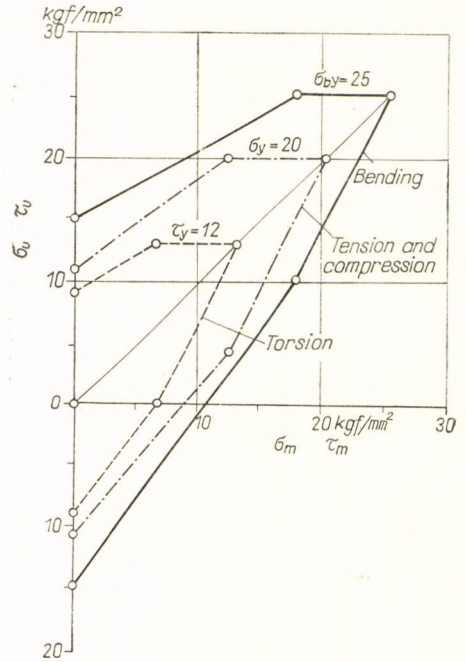


FIG. 14. Smith diagram of cast steel, 38 kgf/mm² tensile strength

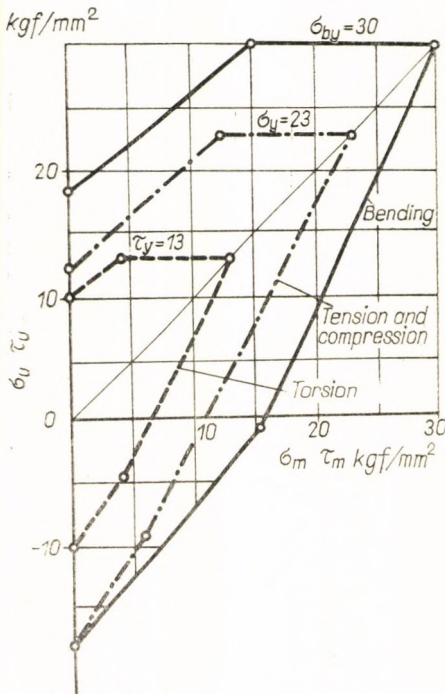


FIG. 15. Smith diagram of cast steel, 45 kgf/mm² tensile strength (approx. BS 592, Grade A)

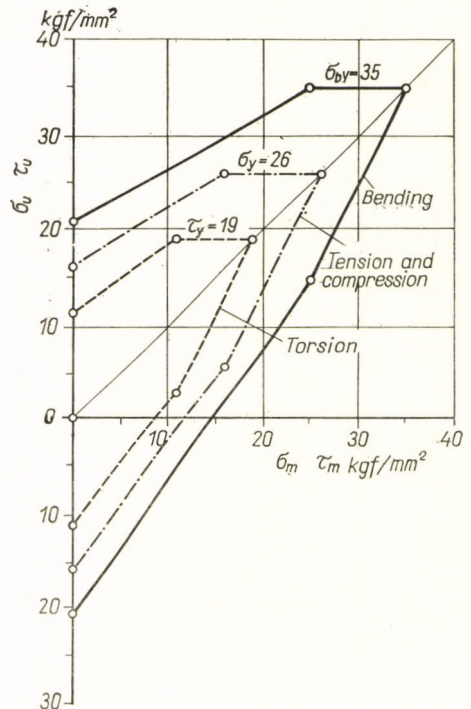


FIG. 16. Smith diagram of cast steel, 52 kgf/mm² tensile strength (approx. BS 592, Grade B)

FIG. 17. Smith diagram of cast steel, 60 kgf/mm² tensile strength (approx. BS 592, Grade C)

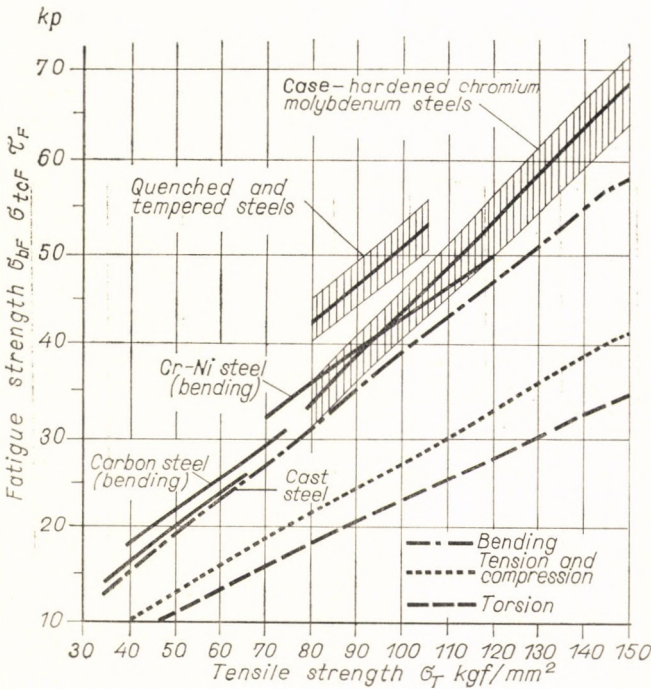
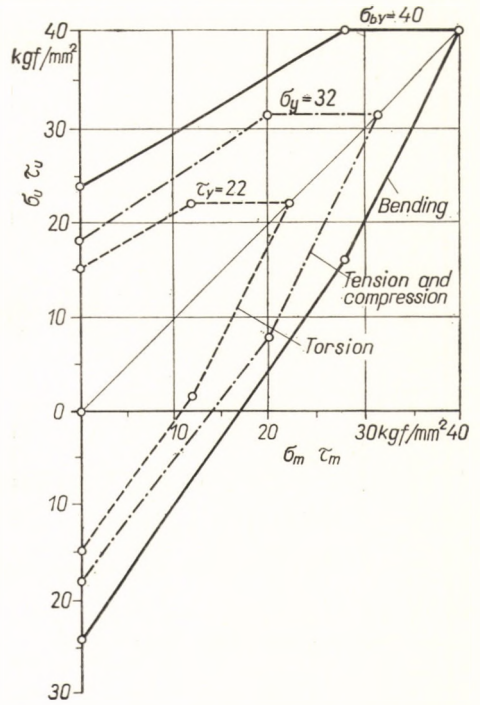


FIG. 18. Relationship between the bending, tensile, compressive, and torsional fatigue strength and the tensile strength of various steels and of cast steel

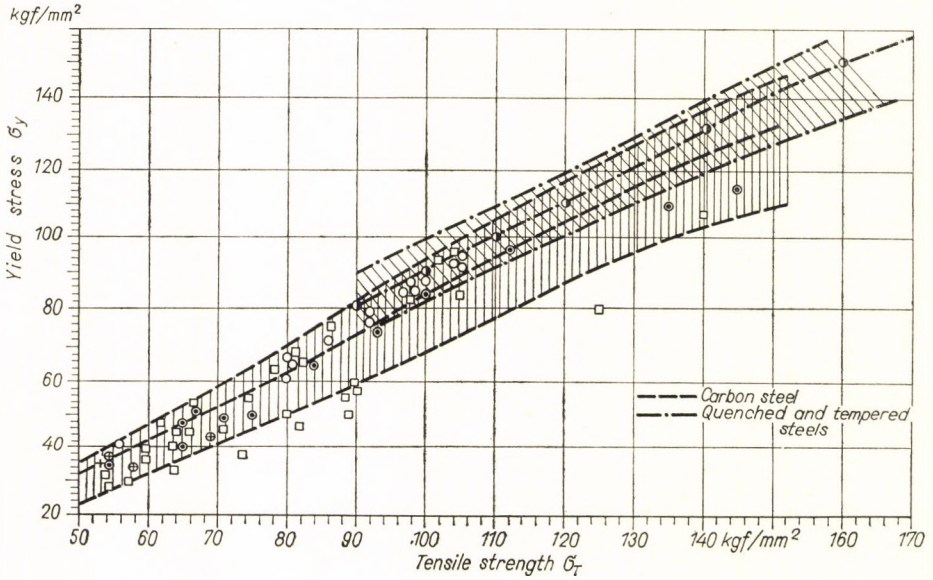


FIG. 19. Relationship between yield stress and tensile strength of steels as indicated by experimental values

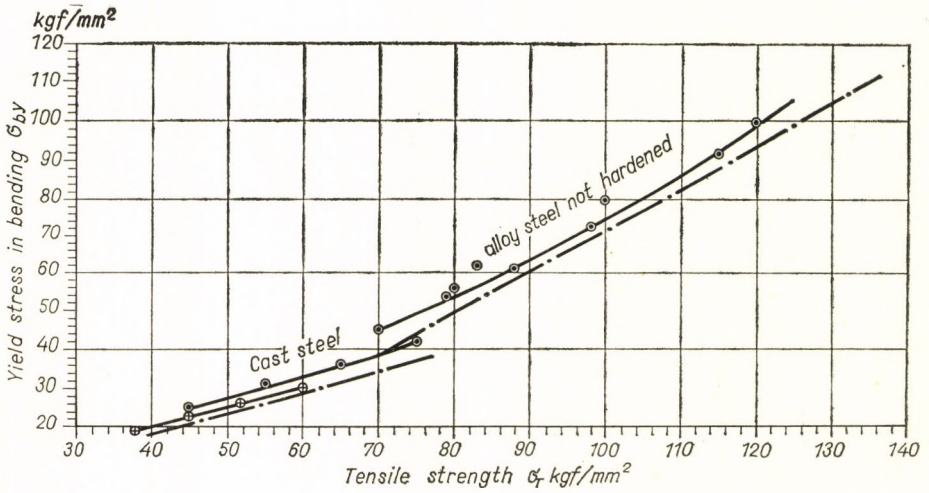


FIG. 20. Relationship between yield stress in bending and tensile strength of steels as indicated by experimental values

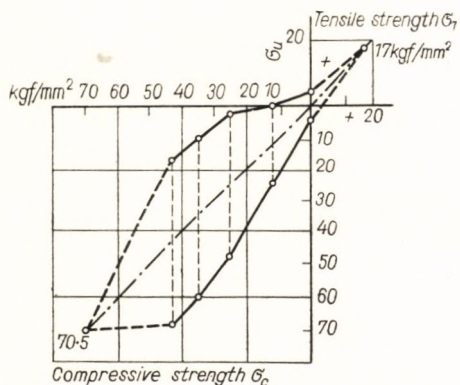


FIG. 21. Smith diagram of cast iron, BS 1452 : 1961, Grade 10

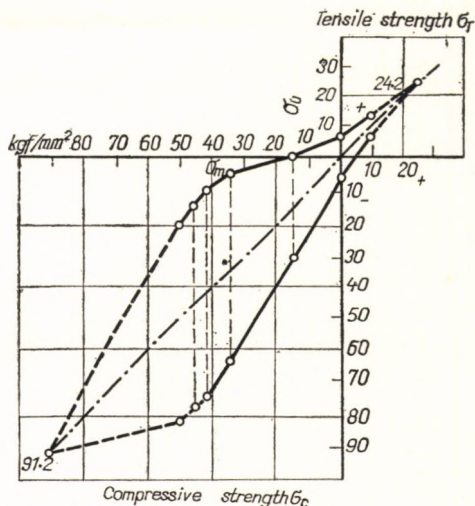
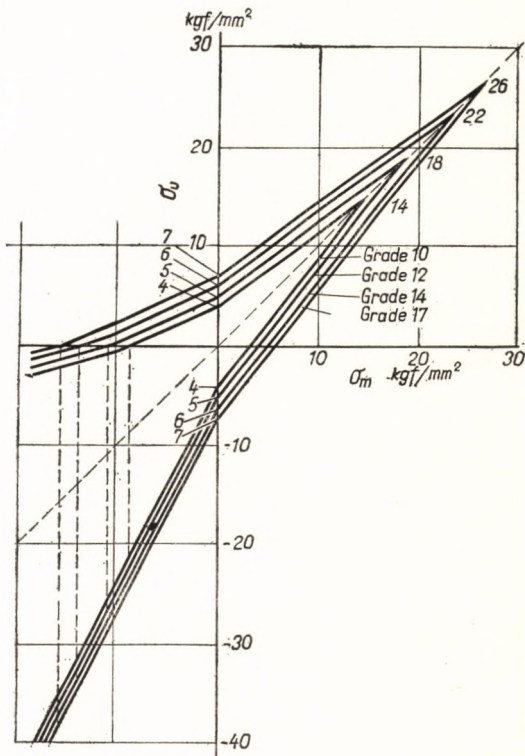


FIG. 22. Smith diagram of cast iron, BS 1452 : 1961, Grade 14

FIG. 23. Tension-compression fatigue strength of cast iron



Material: Cast iron, BS 1452 : 1961	Tensile strength σ_T	Compressive strength σ_C
	kgf/mm ²	
Grade 10	14	58
Grade 12	18	78
Grade 14	22	91
Grade 17	26	108

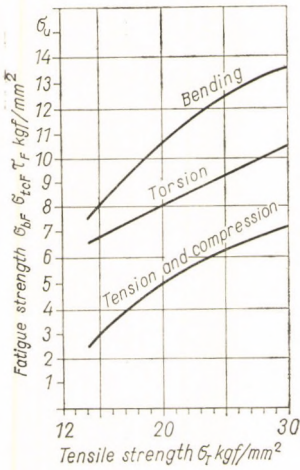


FIG. 24. Relationship between tensile strength and fatigue strength of cast iron

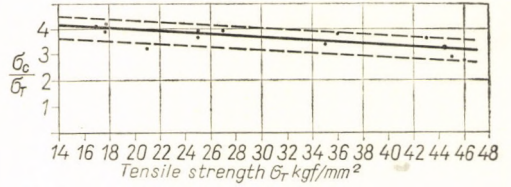


FIG. 25. Relationship between tensile and compressive strength of cast iron

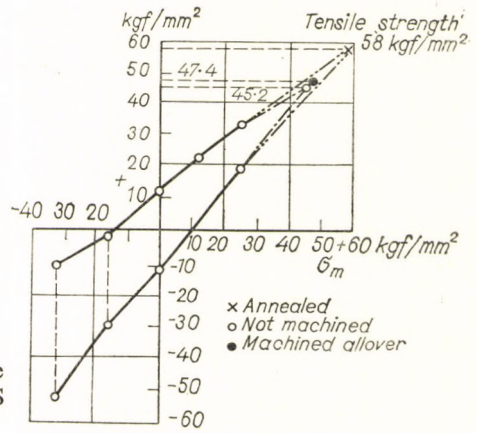


FIG. 26. Smith diagram for tensile-compressive loading of blackheart malleable cast iron, BS 310 : 1958, Grade B 22/14

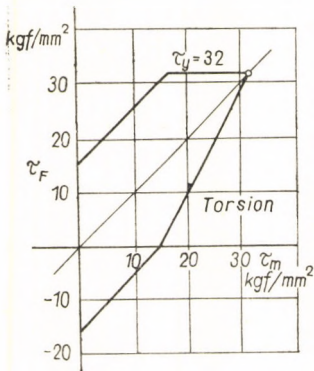


FIG. 27. Smith diagram for torsional stress of whiteheart malleable cast iron, BS 310 : 1958, Grade W 24/8

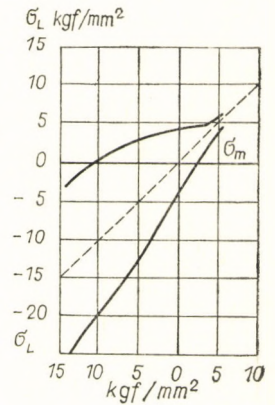


FIG. 28. Tension-compression fatigue limit diagram of sand-cast "Elektron", composition 5 to 6% Al, 2 to 3.5% Zn, 0.1 to 0.5% Mn

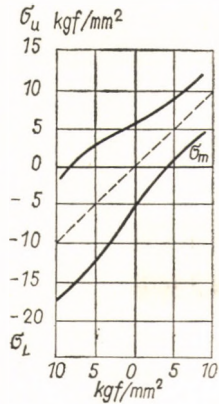


FIG. 29. Tension-compression fatigue limit diagram of sand-cast "Elektron", composition 7 to 11% Al, 0 to 1.5% Zn, 0.1 to 0.5% Mn

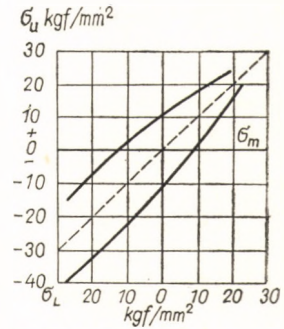


FIG. 30. Tension-compression fatigue limit diagram of "Elektron", composition 6.5 to 10% Al, 0 to 2% Zn, 0.05 to 0.5% Mn

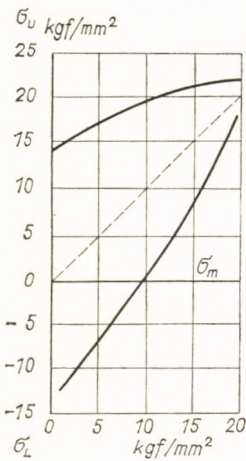


FIG. 31. Bending fatigue limit diagram of "Elektron", composition 6.5 to 10% Al, 0 to 2% Zn, 0.05 to 0.5% Mn

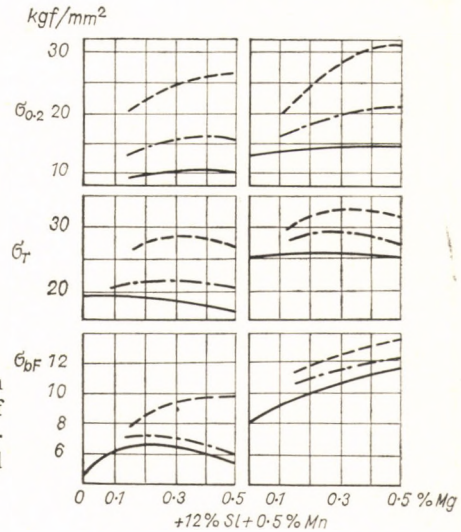


FIG. 32. Tensile strength and fatigue strength of various magnesium-containing sand-cast and chill-cast parts

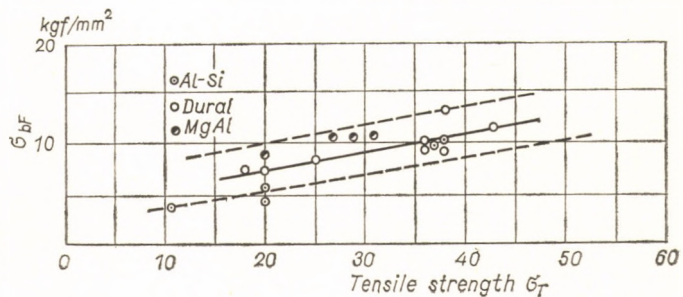


FIG. 33. Relationship between tensile strength and bending fatigue strength of aluminium alloys

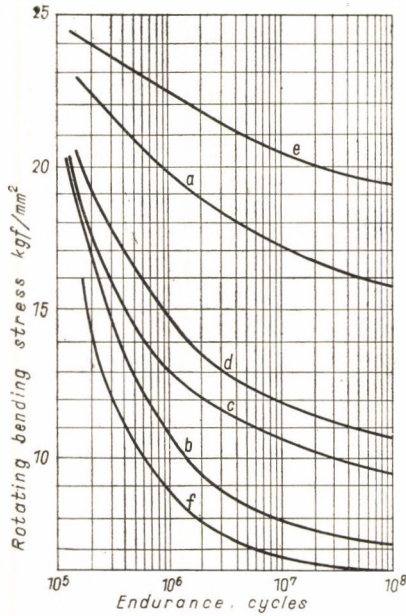


FIG. 34. Relative fatigue merits of shot peening, grit and vapour-blast treatments of Duralumin L 1

a — unnotched, and unnotched + vapour-blast; b — notched ($K_t = 1.76$); c — notched + vapour-blast; d — notched + grit-blast; e — notched + shot-peened; f — notched + shot-peened and heat treated (495°C for 3 hours, water quenched, aged at 70°C for 5 days)

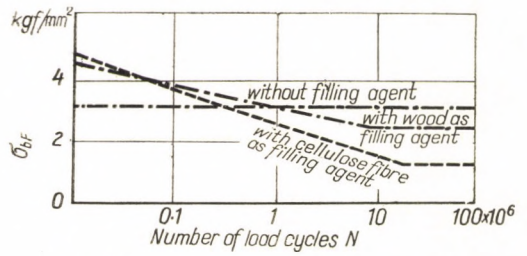


FIG. 35. S-N diagram of phenolic resins

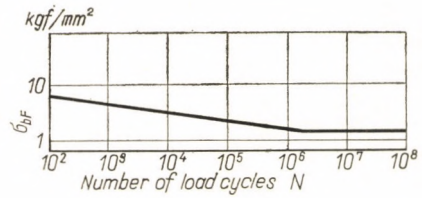


FIG. 36. S-N diagram of cellulose acetate

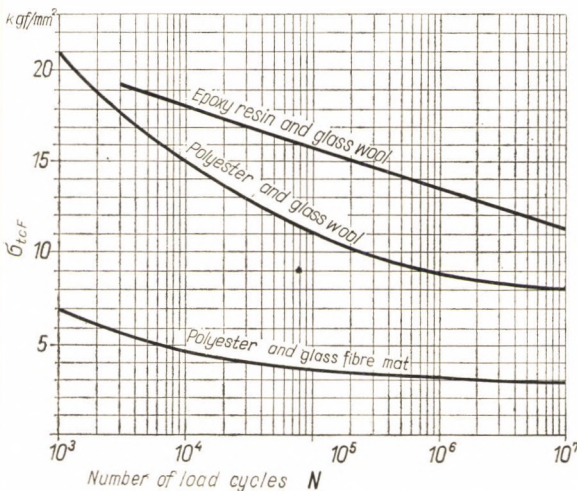


FIG. 37. S-N diagram of glass-fibre-reinforced plastics (smooth specimens, room temperature, fluctuating stress in tension and compression)

TABLE 2
 ROTATING-BENDING FATIGUE STRENGTH OF SOME PLASTICS
 (UNNOTCHED SPECIMEN, REPEATED CONSTANT STRAIN MACHINE,
 $n = 1500$ TO 1750 CYCLES/MIN)

Material	Specimen shape	Temperature	Tensile strength kgf/cm ²	Reversed bending fatigue strength		Ratio of fatigue strength to tensile strength
				Cycles × 10 ⁶	kgf/cm ²	
Phenolic resin with fine-grained woodflour	Flat, 5 mm thick	Room	750	20	255	0.34
Phenolic resin with shredded fabric	ditto	Room	550	20	245	0.43
Phenolic resin with cellulose fibres	ditto	Room	575	20	137	0.24
Phenolic resin with laminated cloth	ditto	Room	1370	20	305	0.24
Phenolic resin with long cloth or paper fibres	ditto	Room	1150	20	360	0.31
Phenolic resin without filler	ditto	Room	1050	20	320	0.31
Phenolic resin with felted asbestos filler	Flat	Room	1550	1.7	455	0.29
Phenolic resin with cotton fabric	Flat	Room	1500	1.6	490	0.33
Phenolic resin with cross-banded high-strength paper	Flat	Room	1920	0.6	560	0.29
Phenolic resin with unidirectional high-strength paper	Flat	30°C	—	1.2	600	—
Phenolic resin with laminated fabric, longitudinal loading	Round	27°C	1500	100	350	0.23
Phenolic resin with laminated fabric, transverse loading	Round	27°C	1280	100	280	0.22
Phenolic resin with paper, longitudinal loading	Round	27°C	1300	100	365	0.28
Phenolic resin with paper, transverse loading	Round	27°C	1130	100	365	0.32
Cast phenolic resin	Round	27°C	850	100	295	0.35
Phenolic resin with unidirectional glass fibre laminate	Flat	Room	4250	100	875	0.21
Cellulose acetate	Round	27°C	345	100	70	0.20
Methyl methacrylate	Round	27°C	800	10	140	0.18
ditto	Round	-35°C	1300	10	340	0.27
Polyester with glass laminate, fast cure		Room	3500	1	900	0.26
Ditto but slow cure		Room	4200	1	1100	0.26
Epoxy resin with glass fabric		Room	3000	0.1	1380	0.46
ditto		Room		1	1070	0.36
ditto		Room		10	770	0.26

(TABLE 2, CONT.)

Material	Specimen shape	Temperature	Tensile strength kgf/cm ²	Reversed bending fatigue strength		Ratio of fatigue strength to tensile strength
				Cycles × 10 ⁶	kgf/cm ²	
Silicone resin with glass fabric		Room	2480	0.1	880	0.35
ditto		Room		1	710	0.29
ditto		Room		10	550	0.22
Resin bonded birch plywood, in direction of fibres	Flat, 4 mm	Room	960		250	0.26
Ditto but at 45° to fibres	ditto	Room	360		200	0.52
Casein bonded birch plywood, in direction of fibres	Flat, 3.5 mm	Room	1220		300	0.25
Ditto but at 45° to fibres	ditto	Room	325		85	0.26
Phenol-formaldehyde glue, two-ply laminated birch	Flat	Room	1800	2	450	0.25
Ditto but three-ply	Flat	Room	1550	2	400	0.24
Urea-formaldehyde glue, three-ply birch plywood	Flat	Room	1320	2	305	0.25
23 per cent phenolic-resin impregnated laminated compressed wood	8 mm dia.	Room	3600	200	700	0.20
23 per cent phenolic-resin impregnated laminated compressed wood	25 mm dia.	Room	2680	100	530	0.20
35 per cent phenolic-resin impregnated laminated compressed wood	25 mm dia.	Room	2560	500	630	0.25

TABLE 3
ROTATING-BENDING FATIGUE STRENGTH OF SOME LIGHT ALLOYS

Identification	Form	Condition	Tensile strength kgf/mm ²	Rotating-bending fatigue strength kgf/mm ²				Ratio of fatigue strength ($N = 10^7$) to tensile strength
				$N = 10^5$	$N = 10^6$	$N = 10^7$	$N = 10^8$	
<i>Aluminium alloys</i>								
BS 1470 to 1477								
V1 C	1-inch extruded	M	8.5	6.3	5.0	4.7	—	0.55
NV 5	ditto	M	22.8	18.4	15.2	14.7	14.0	0.65
NV 6	ditto	M	29.0	19.6	15.0	15.0	—	0.52
NV 7	ditto	M	34.5	22.6	18.0	17.0	16.8	0.49
HV 9	ditto	W	17.3	14.1	11.5	9.7	8.5	0.56
HV 10	ditto	W	23.6	16.8	13.6	11.0	9.1	0.46
HV 11	ditto	W	37.6	21.6	17.6	15.0	13.3	0.40
HF 12	Forged bar	WP	45.0	—	21.2	16.5	13.8	0.37
HF 18	ditto	WP	45.0	—	21.5	17.0	14.5	0.38
BS 1490								
LM 8	Sand cast	M	12.5	—	7.9	6.2	5.8	0.50
		W	16.5	—	8.6	6.1	5.5	0.37
		WP	23.5	—	8.8	6.4	5.7	0.27
	Chill cast	M	16.8	—	9.4	8.6	8.3	0.51
		W	23.6	—	10.4	9.0	8.5	0.38
		WP	28.4	—	10.6	9.0	8.5	0.32
LM 10	Sand cast	W	31.5	—	7.2	6.4	6.3	0.20
		WP	25.2	—	8.0	6.4	6.3	0.25
LM 14	Sand cast	WP	23.6	—	—	8.6	6.3	0.36
	Chill cast	WP	30.0	—	—	11.0	9.4	0.36
LM 15	Sand cast	WP	29.0	—	9.1	7.9	7.7	0.27
LM 23	Sand cast	P	17.3	—	8.8	7.4	7.2	0.43
	Chill cast	P	20.5	—	10.7	8.8	8.6	0.43
<i>Magnesium alloys</i>								
BS 2970								
MAG 1	Cast	M	14.2 to 17.3	—	—	7.8 to 8.6	—	0.50 to 0.55
MAG 3	Cast	M	12.5 to 16.5	—	—	7.8 to 8.6	—	0.52 to 0.63
		W	20.5 to 25.2	—	—	7.8 to 9.4	—	0.37 to 0.38
		WP	20.5 to 26.0	—	—	7.1 to 7.8	—	0.30 to 0.35
MAG 5		P	23.6	—	—	—	12.0	0.51
MAG 7		M	12.5 to 17.3	—	—	7.5 to 8.1	—	0.47 to 0.60
		W	18.9 to 25.7	—	—	7.8 to 8.6	—	0.45 to 0.50
		WP	18.9 to 25.7	—	—	6.3 to 7.5	—	0.40

M = As manufactured

WP = Solution treated and precipitation hardened

W = Solution treated

P = Precipitation hardened

TABLE 4

FATIGUE STRENGTH OF LIGHT

	Denomination of material in the literature	Composition (%)						
		Al	Mg	Si	Mn	Cu	Cr	Zn
Aluminium alloys	G Al Si	main con- stituent		11...13.5	0.3...0.5			
	G Al Si Mg	main con- stituent	0.2...0.4	9...10	0.3...0.5			
	G Al Mg 3	main con- stituent	1.5...3.5 0...1.3	0...1.3	0...0.6		0...0.3	
	G Al Si 5 Mg	main con- stituent	0.2...0.4	9...10	0.3...0.5			
	Al Cu Mg	main con- stituent	0.2...1.8		0.3...1.5	2.5...5		
	Al Mg Si	main con- stituent	0.6...4	0.6...1.2	0.6...1		0...0.3	
	Al Mg 3	main con- stituent	2...4		0...0.4		0...0.3	
	Al Mg 5	main con- stituent	4...5.5		0...0.8		0...0.3	
	Al Mg 7	main con- stituent	5.5...7.5		0...0.8		0...0.3	

ALLOYS WITH $N = 50 \times 10^6$

Others	Strength values (kgf/mm ²)			Condition	Literature reference
	Tensile strength σ_T	Bending fatigue strength σ_{bF}	Torsional fatigue strength τ_F		
	16...22 16...26	4...6 6...8		Sand-cast Chill-cast	Hütte 28 Page 1008
	17...24 20...30 18...26 22...32	5...7 7...12 6...10 8...12		Sand-cast Heat-treated sand-cast Chill-cast Heat-treated chill-cast	Hütte 28 Page 1008
Ti 0...0.3	13...19 16...28 14...26 18...33	6...7 8...10 9...10 10...11		Sand-cast Heat-treated sand-cast Chill-cast Heat-treated chill-cast	Hütte 28 Page 1008
	11...18 14...30 13...20 17...30	6...6.5 6.5...7.5 6...7.5 7.5...8.5		Sand-cast Heat-treated sand-cast Chill-cast Heat-treated chill-cast	Hütte 28 Page 1008
	18...24 37...44	8...11 12...15	4...7 6...9	Soft Heat-treated	Hütte 28 Page 1008
	11...13 20...26 28...32	8...10 9...12 10...13	5...6 5...6 6...7	Soft Cold hardened Hardened	Hütte 28 Page 1008
	18...21 22...25	10...13 12...15	5...7 6...8	Soft Semi-hard	Hütte 28 Page 1008
	22...28 25...31	12...14 13...15	6...7 7...8	Soft Semi-hard	Hütte 28 Page 1008
	30...34 34...38	12...14 13...15	7...8 7...9	Soft Semi-hard	Hütte 28 Page 1008

TABLE 4

	Denomination of material in the literature	Composition (%)						
		Al	Mg	Si	Mn	Cu	Cr	Zn
	Al Mg Mn	main con- stituent	1.5...3		0.5...1.5		0...0.3	
	Al Cu Ni	main con- stituent	1.3...1.8			3.5...4.5		
	Silumin G Mg Al 3 Zn	2.5...3.5	the rest	13	0.1...0.5			0.5...1.5
Magnesium alloys	G Mg Al 4 Zn	3...4.5	the rest		0.1...0.5			2...3.5
	G Mg Al 6 Zn	5...6.5	the rest		0.1...0.5			2...3.5
	G Mg Al	7...11	the rest		0.1...0.5			0...1.5
	G Mg Al	7...11	the rest		0.1...0.5			0...1.5
	Mg Mn		the rest		1...2.5			
	Mg Al 2	1.5...4	the rest		0.05...0.5			0...1.5
	Mg Al 6	5...6.5	the rest		0.05...0.5			0...1.5
	Mg Al 9	5...10	the rest		0.05...0.5			0...2

(CONT.)

Others	Strength values (kgf/mm ²)			Condition	Literature reference
	Tensile strength σ_T	Bending fatigue strength σ_{bF}	Torsional fatigue strength τ_F		
	18...22 22...23 24...28	7...10 8...12 10...15	3...6 4...7 5...6	Soft Semi-hard Hard	Hütte 28 Page 1008
Ni 1.8...2.2	35...40	14...17	8...10	Hard	Hütte 28 Page 1008
	17...20 17		5.5	Sand-cast	Buchmann VDI-1941 Page 15
	19	6.5		Sand-cast	
	19	7...9.2		Sand-cast	
	27	8...12		Sand-cast	
	21	6.5...8.5		Chill-cast	
	30	7.5...11		Forgeable	
	27	11		Forgeable	
	32	14.5...17		Forgeable	
	34	14.5.. 17		Forgeable	

TABLE 5

FATIGUE STRENGTH OF COPPER AND SOME OF ITS ALLOYS

Identification	Source	Composition, % per cent						Condition	Ten- sile strength kgf/ mm ²	Rotating- bending fatigue strength kgf/mm ²			Ratio of fatigue strength ($N = 10^7$) to tensile strength		
		Cu	Zn	Sn	Si	Fe	Other			10 ⁶	10 ⁷	10 ⁸			
Electrolytic copper	BURGHOFF and BLANK	99.93						Drawn 30 per cent	30.8	17.6	13.7	11.5	0.44		
Cartridge brass		69.37	30.61					Drawn 21 per cent	40.0	22.0	14.8	10.6	0.37		
Free-cutting brass		61.78	34.81				Pb 3.31	Drawn 20 per cent	38.5	21.4	16.5	14.0	0.43		
Naval brass		59.88	39.31	0.68				Drawn 24 per cent	61.0	33.6	25.4	23.3	0.42		
ditto		59.74	39.39	0.71				Drawn 24 per cent	61.0	20.4	15.0	14.8	0.25		
1½% silicon bronze		97.18	1.35		1.43					28.5	14.3	11.9	10.5	0.42	
ditto		97.12	1.39		1.46			Drawn 21 per cent	38.0	23.1	19.6	19.6	0.51		
3% silicon bronze		95.88	1.05		3.01			Drawn 10 per cent	44.0	20.7	17.4	16.8	0.40		
ditto		95.88	1.05		3.01			Drawn 44 per cent	72.0	31.6	25.4	24.2	0.35		
Aluminium bronze		87.84					1.95 Al	9.65 Te	Drawn 10 per cent	65.0	32.4	23.0	20.0	0.35	
Cupro-nickel		68.04					0.49 Ni	30.67 Mn	0.53	Drawn 33 per cent	57.0	31.4	25.6	24.3	0.47
Phosphor-bronze		ANDERSON, SWAN and PALMER	88.35		9.31		1.36	Mn 0.78	Drawn 36 per cent	81.0	40.0	31.5	23.3	0.39	
Phosphor-bronze, Grade A	97.25			4.32			P 0.20	Annealed 550°C	35.5	22.7	21.0	20.4	0.59		
ditto							P 0.38	Drawn 15 per cent	39.7	24.0	20.7	19.7	0.52		
ditto								Drawn 30 per cent	49.0	25.6	21.6	21.0	0.44		
ditto								Drawn 50 per cent	67.5	30.2	24.5	23.2	0.36		
Electrolytic copper	<i>Metals Handbook 1948</i>	99.9						Flat, semi-hard	30			9.3	0.31		
								Flat, hard	36			9.3	0.26		
								Round bar, hard	34			12	0.35		

Tombak	The American Society for Metals	80	20				Flat, 1 mm thick, spring-hard	65	17	0.28		
		70	30				Hard wire, 2 mm ditto	78	16	0.20		
							Flat, 1 mm thick,	90	18	0.20		
							Flat, 1 mm thick, semi-hard	31	9	0.29		
							Flat, 1 mm thick, hard	44	13	0.30		
							Flat, 1 mm thick, spring-hard	55	15	0.27		
							Wire, spring-hard	67	16	0.24		
							25 mm rod, semi-hard	92	17	0.18		
		Flat, rolled	50	16	0.32							
		71	28	1				35	8.5	0.24		
						37	14	0.38				
Brass	The American Society for Metals	65	35				Flat, hard, rolled "Spring-hard"	53		10	0.19	
		60	39.3	0.7			Rod	65		14	0.21	
								43		11	0.26	
Silicon-bronze	The American Society for Metals	96					Si 3 Mn 1	Flat	47		11	0.23
		98.17		0.21	0.06	Si 1.41	Flat, hard	67		16	0.24	
							Flat, cold-rolled	65		24	0.37	
							Cold-rolled or hot-rolled	64		22	0.35	
Aluminium bronze	The American Society for Metals	89.71		0.38		0.64	Al 8.74 Ni 0.51	Hard	70		15.5	0.22
		89.5 89.81 90	1.40			0.15 0.13	Al 8.89 Al 10.06 Al 10	Drawn	57		22.5	0.39
								Drawn	55		24	0.43
									60		20	0.33

3. Effect of various factors on fatigue strength

3.1 Surface finish

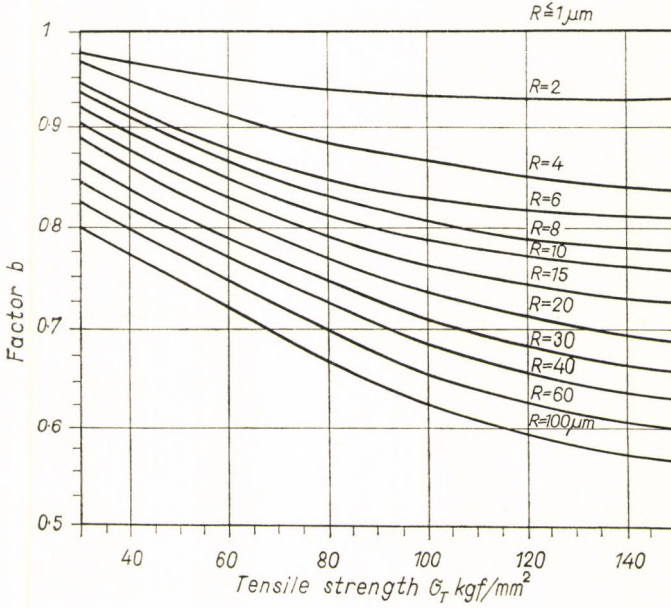


FIG. 38. Surface-finish factor b for bending fatigue strength in relation to tensile strength and surface finish

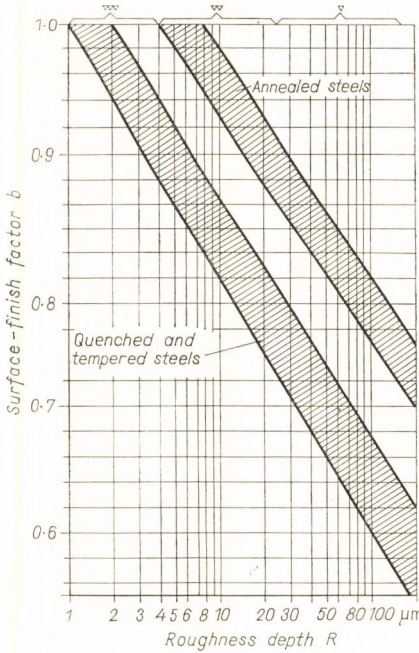


FIG. 39. Surface-finish factor b for fluctuating tensile stress

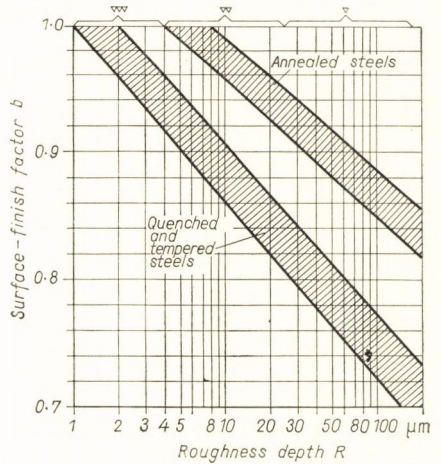
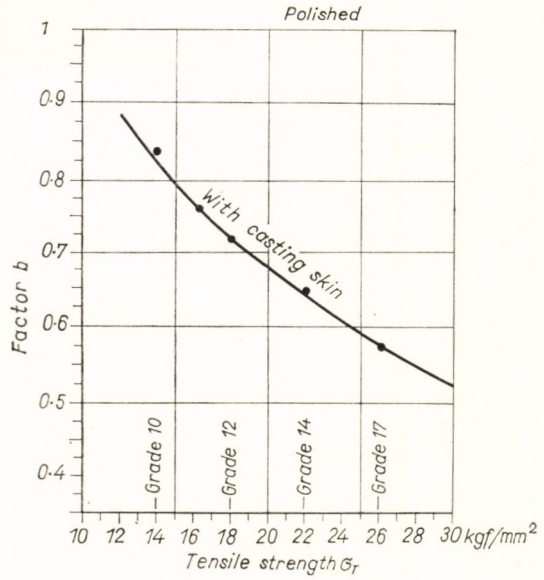


FIG. 40. Surface-finish factor b for tension-compression and rotating bending stress

FIG. 41. Decrease of the bending fatigue strength of cast-iron parts with the casting skin in comparison with that of a polished specimen



3.2 Shape and dimensions

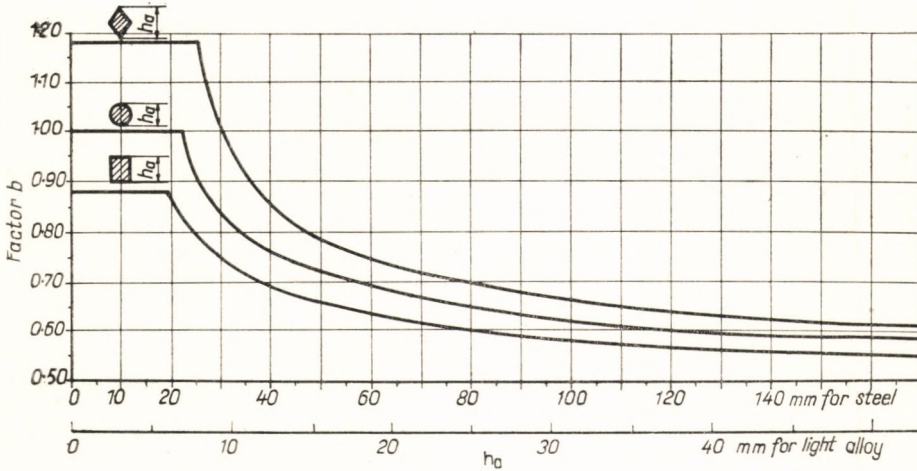
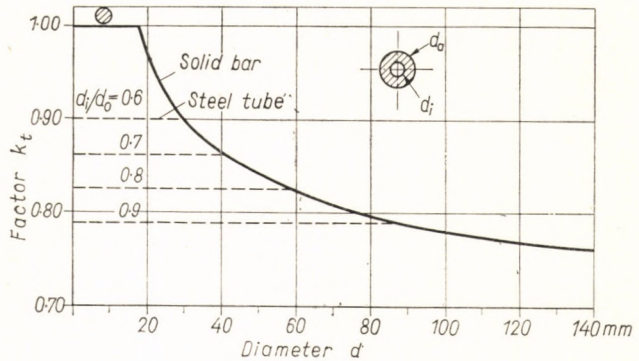


FIG. 42. Size factor b for bending of machine components of rectangular, circular, elliptical, and rhombic cross-section

FIG. 43. Size factor k_t for torsion of machine components of solid and hollow cross-section



3.3 Temperature

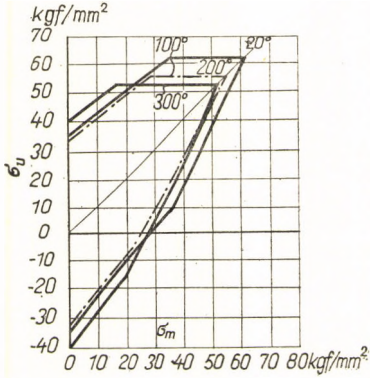


FIG. 44. Smith diagram for chromium-molybdenum steel at various temperatures

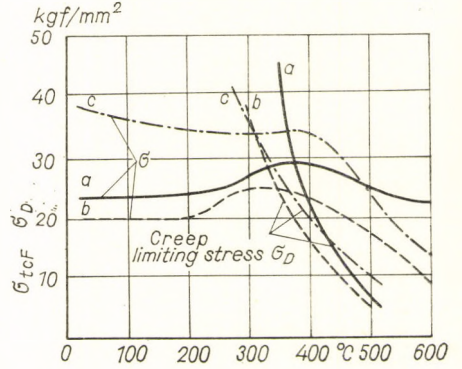


FIG. 45. Tension-compression fatigue strength and creep limiting stress of various steels in relation to temperature

- Curve a — C: 0.14%
Si: 0.19%
Mn: 0.68%
- b — C: 0.15%
Cr: 13.5%
- c — C: 0.38%
Cr: 13.5%

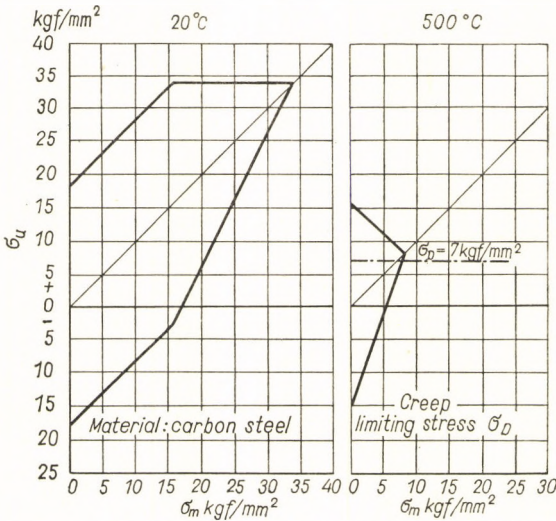


FIG. 46. Smith diagram for carbon steel at 20° and 500°C

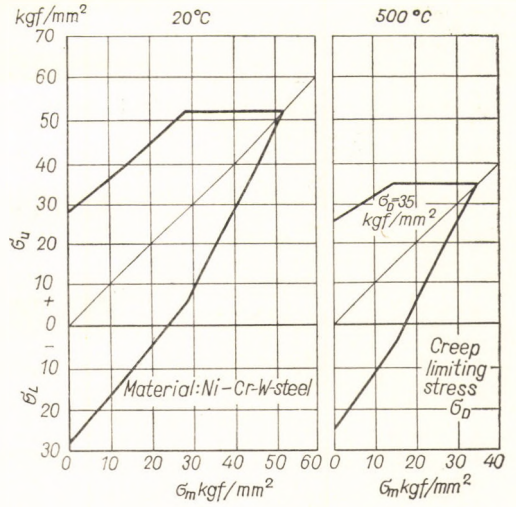
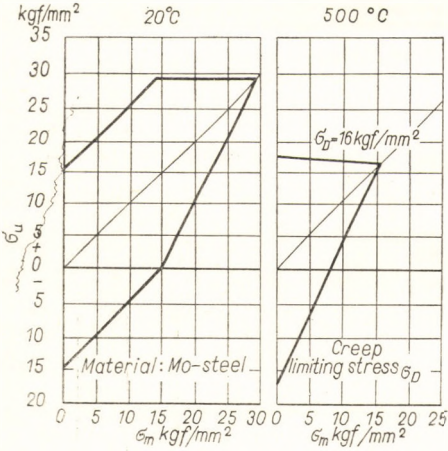


FIG. 47. Smith diagram for Mo steel at 20° and 500°C

FIG. 48. Smith diagram for NiCrW steel at 20° and 500°C

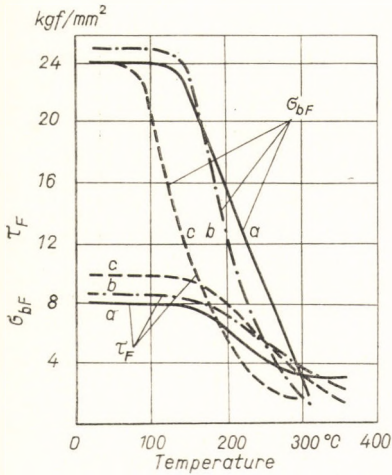


FIG. 49. Bending and torsion fatigue strength of light alloys in relation to temperature

Compositions: *a* 92.2% Al, 4% Cu, 2% Ni, 1.5% Mg, 0.3% Fe, heat treated
b 92% Al, 2.5% Cu, 1.3% Ni, 1.5% Mg, 1.2% Si, 1.4% Fe, 0.1% Ti, cast
c 86.9% Al, 12% Si, 0.4% Mg, 0.4% Mn, 0.3% Fe, heat treated

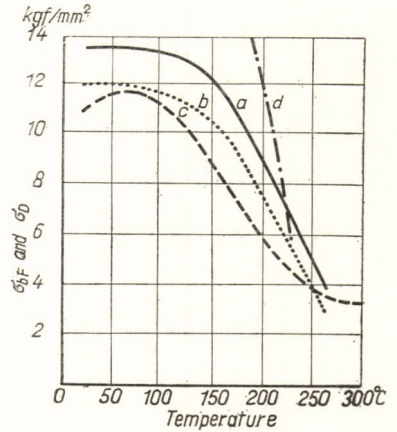


FIG. 50. Variation of bending fatigue strength and creep limiting stress with temperature for light alloys

a Al-Cu-Mg alloy with $N = 20 \times 10^6$
b Al-Cu-Mg alloy with $N = 100 \times 10^6$
c Al-Cu alloy with $N = 10 \times 10^6$
d Creep limiting stress of the Al-Cu-Mg alloy

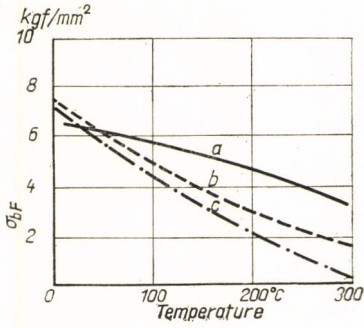


FIG. 51. Variation of bending fatigue strength and creep limiting stress with temperature for aluminium and copper

- a — Bending fatigue strength of 99.5% Al
- b — Creep limiting stress of Cu
- c — Creep limiting stress of 99.5% Al

FIG. 52. Increase of fatigue strength with decrease of temperature. Relationship between tension compression and bending fatigue strength and the temperature factor K_T

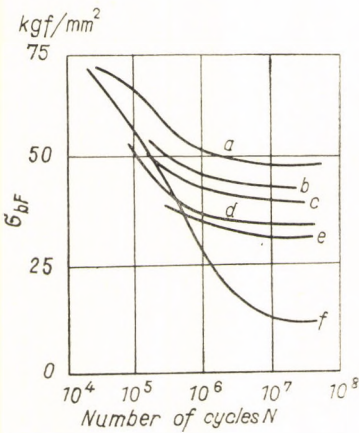
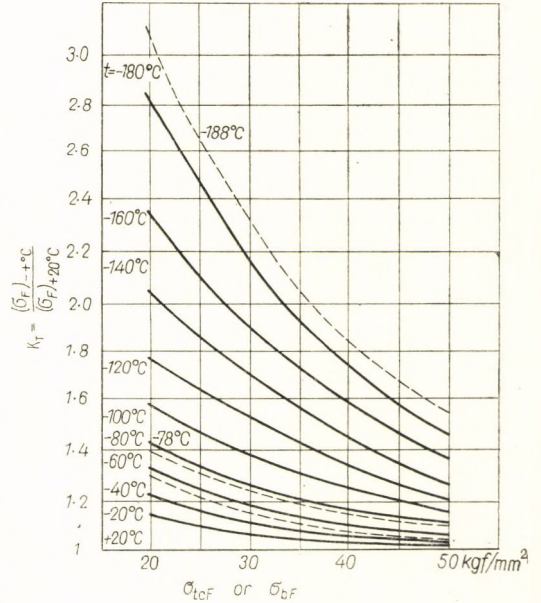


FIG. 53. Effect of corrosion on bending fatigue strength

- a Fatigue strength in air
- b Pre-corroded for one day in tap water
- c Pre-corroded for two days in tap water
- d Pre-corroded for six days in tap water
- e Pre-corroded for ten days in tap water
- f Bending fatigue test carried out in tap water

3.5 Corrosion

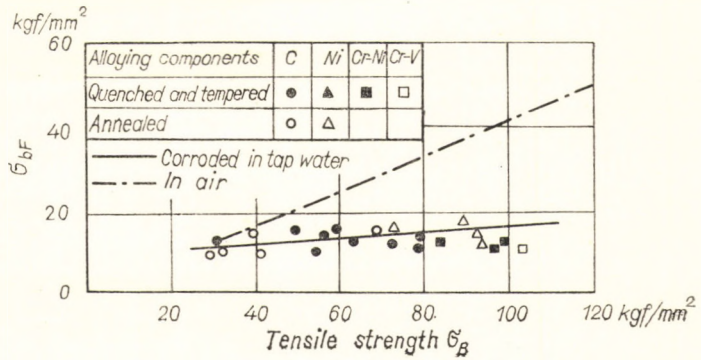


FIG. 54. Bending fatigue strength of various steels in air and corroded in tap water

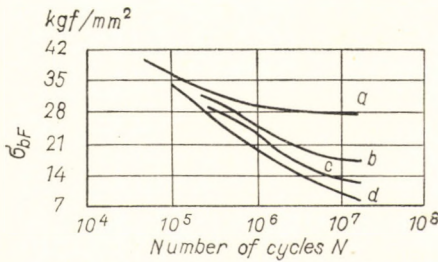


FIG. 55. Effect of the corrosive liquid on fatigue strength

- a Fatigue strength in air
- b Water + 25 mg/l. NaCl + 25 mg/l. Na₂SO₄
- c Water + 2 g/l. NaCl
- d Water + 30 g/l. NaCl

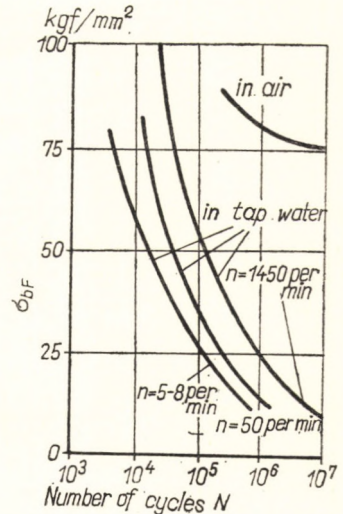


FIG. 56. Alteration in bending fatigue strength of Ni steel corroded in tap water at frequencies *n* between 5 per min and 1450 per min

FIG. 57. Alteration in bending and torsion fatigue strength of Cr-Va steel in corrosion-free and corroded condition

- a Bending fatigue strength in air
- b Torsion fatigue strength in air
- c Bending fatigue strength — corroded in tap water
- d Torsion fatigue strength — corroded in tap water

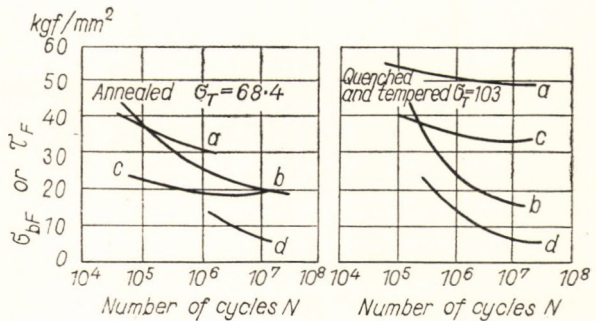


TABLE 6

EFFECT OF CORROSION ON CAST STEEL PARTS

Material DIN 17006 (BS 592)	Composition (%)			Investi- gated by	Tensile strength σ_T (kgf/mm ²)	Fatigue strength (kgf/mm ²)			N 10 ⁶
	C	Si	Mn			Bend- ing σ_{bF}	σ_{bF} cor- roded in tap water	σ_{bF} cor- roded in sea water	
GS 45.81 s (Grade A)	0.19	0.44	0.66	Thum and Ochs	46.3	20	12	4	50
GS 45.81 s (Grade A)	0.20	0.27	0.72	Thum and Ochs	48.9	21	16	—	10
GS 52.81 s (Grade B)	0.36	0.33	0.79	Thum and Ochs	56.1	23	15	—	10
GS 52.81 s (Grade B)	0.48	0.36	0.84	Thum and Ochs	64.5	22	12	4	50
Electric steel	—	—	—	Thoma and Föppl	65	24	14	—	10
Stainless cast steel	0.19	0.34	0.38 Mn 0.82 Ni 12.4 Cr	Thum and Ochs	69	32	16	8	50
Stainless cast steel	0.2	—	15 Cr	Roesch	61	26	20	—	—

TABLE 7

EFFECT OF CORROSION ON THE FATIGUE STRENGTH OF CAST IRON

Material		Composition (%)					Investi- gated by	Tensile strength σ_T (kgf/mm ²)	Fatigue strength (kgf/mm ²)			N 10 ⁶
DIN 17006	BS 1452	To- tal C	Com- bin- ed C	Si	Mn	P			Bend- ing σ_{bF}	σ_{bF} cor- roded in tap water	σ_{bF} cor- roded in sea water	
GG 14	10	3.66	1.02	1.75	0.54	1.93	Thum and Ochs	13.3	8	5	—	50
GG 22	14	—	—	—	—	—	Ludwig	24.8	14	—	7.5	10
GG 26	17	3.39	0.90	2.08	0.76	0.55	Thum and Ochs	29.8	18	14	—	50
GG 30	20	3.3	—	1.52	0.86	0.42	Linicus	30	13	9	8	50

TABLE 8
EFFECT OF CORROSION ON THE FATIGUE STRENGTH OF SOME
METALS AND ALLOYS

Alloy composition	Corroded in	Decrease of bending fatigue strength (%)
Nickel	Tap water	30...50
	Salt water	40...60
Monel-Metal 25...30% Cu, 65...70% Ni	Tap water	16...40
Brass	Tap water	8...30
	Salt water	23...45
Bronze (Cu-Sn-Zn)	Salt water	25
Cu-Sn alloy	Tap water	4...20
	Salt water	4...10
Cr-Ni	Tap water	0
	Salt water	8...50
	Sea water	
Aluminium	Tap water	50
	Salt water	50
Duralumin	Tap water	17...50
	Salt water	30...60
"Silumin" alloys	Tap water	0
	Salt water	10...25
"Elektron" and Mg alloys	Tap water	50
	Salt water	70

TABLE 9
BENDING FATIGUE STRENGTH OF STEELS IN VARIOUS KINDS OF WATER

Corrosive medium	0.3% Ni steel $\sigma_T = 50.2 \text{ kgf/mm}^2$	1.1% Cr, 0.12% V, 0.33% C steel $\sigma_T = 67.2 \text{ kgf/mm}^2$
In air, $N = 100 \times 10^6$	$\sigma_{bF} = 25 \text{ kgf/mm}^2$	$\sigma_{bF} = 35 \text{ kgf/mm}^2$
In hard water	16	16.5
In soft water	15.5	15
In sea water	5.5	6

TABLE 10

BENDING FATIGUE STRENGTH OF STEELS IN STEAM

Corrosive medium	3.5% Ni steel $\sigma_T = 74 \text{ kgf/mm}^2$	12.5% Cr steel $\sigma_T = 72 \text{ kgf/mm}^2$
In air, $N = 50 \times 10^6$	$\sigma_{bF} = 32 \text{ kgf/mm}^2$	$\sigma_{bF} = 43 \text{ kgf/mm}^2$
In steam, 4 atm at 149°C	25	39
In steam, 15 atm at 371°C	24	38
Steam condensed on surface (steam and air)	16	23

TABLE 11

EFFECT OF THE NUMBER OF LOAD CYCLES ON FATIGUE STRENGTH

Condition	Number of cycles N (10^6)				
	5	10	20	40	80
Fatigue strength in uncorroded condition (kgf/mm ²)	36	36	36	36	36
Corroded in tap water (kgf/mm ²)	26	23	21.5	19.5	18

4. Theoretical stress concentration factor

Form	Type of loading	Nominal stress	Scale $\sqrt{h/r}$	Curve $\sqrt{a/r}$	Curve $\sqrt{b/r}$	Serial No
	Tension F Bending M_b	$\frac{F}{2da}$ $\frac{3M_b}{2da^2}$	B	1		1
	Tension F Bending M_b	$\frac{F}{da}$ $\frac{6M_b}{da^2}$	B	3	4	2
	Tension F Bending M_b	$\frac{F}{2da}$ $\frac{3M_b h}{2d(e^3 - h^3)}$	B	A	5	3
	Tension F	$\frac{F}{\pi a^2}$	B	6		5
	Bending M_b	$\frac{4M_b}{\pi a^3}$	B	7		7
	Shear V	$\frac{1.23V}{\pi a^2}$	A	8		8
	Torsion M_t	$\frac{2M_t}{\pi a^3}$	A	9		9
	Tension F	$\frac{F}{\pi(b^2 - c^2)}$	B	5	1	11
	Bending M_t	$\frac{4M_b b}{\pi(b^4 - c^4)}$	B	5	2	12
	Shear V	$\frac{(1.23b^2 + 2.77c^2)V}{\pi(b^4 - c^4)}$	A	10	3	13
	Torsion M_t	$\frac{2M_t b}{\pi(b^4 - c^4)}$	A	10	4	14
	Tension F	$\frac{F}{\pi(e^2 - b^2)}$	B	5	5	15
	Bending M_t	$\frac{4M_b b}{\pi(e^4 - b^4)}$	B	5	6	16
	Shear V	$\frac{(2.77e^2 + 1.23b^2)V}{\pi(e^4 - b^4)}$	A	10	7	17
	Torsion M_t	$\frac{2M_t b}{\pi(e^4 - b^4)}$	A	10	8	18
	Shear V	$\frac{V}{\pi ab}$	A	10		19
	Torsion M_t	$\frac{M_t}{2\pi ab^2}$	A	10		20
	Shear V	$\frac{VS^*}{2aJ}$	A	10		21
	Torsion M_t	$\frac{M_t}{2aA^{**}}$	A	10		22

* S = Moment of the upper half in relation to the neutral surface
 * J = Moment of inertia
 ** A = Total area of section bounded by the centre line

FIG. 58. Table for Neuber's nomogram

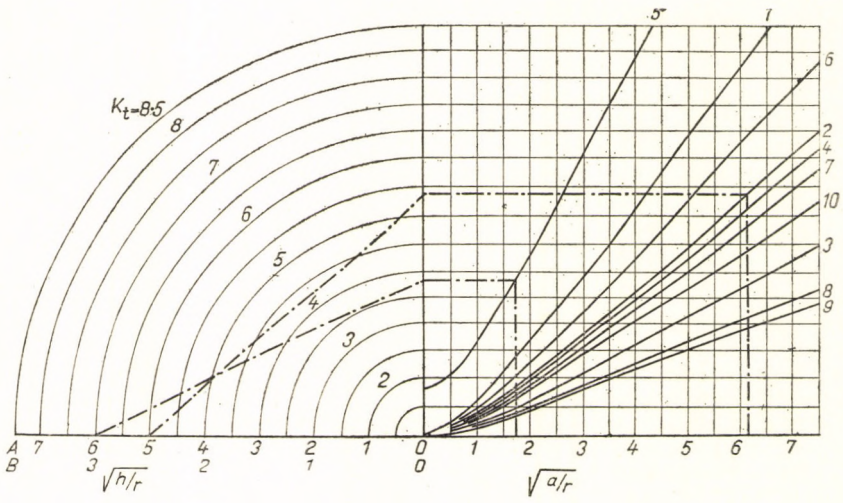


FIG. 59. Neuber's nomogram

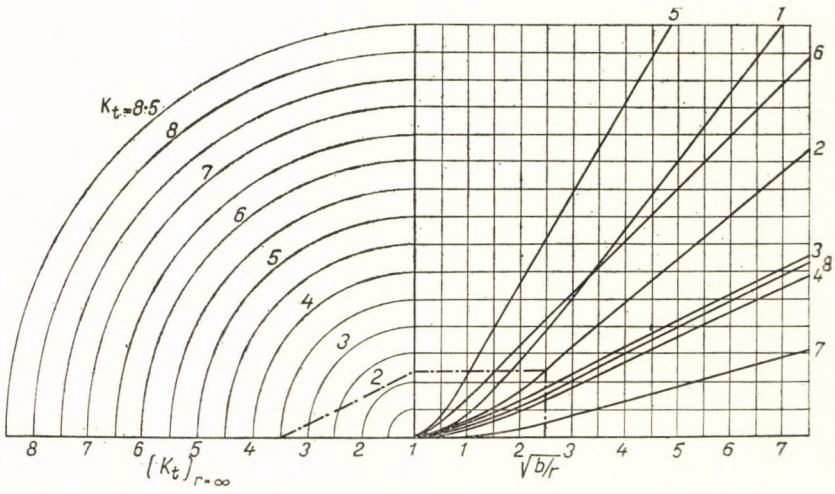


FIG. 60. Neuber's complementary nomogram for hollow workpieces

NOTES ON TABLE 12

Sub-tables 1 and 2. These give the theoretical stress concentration factors of flat pieces notched at both sides. Notch sides are parallel; $\gamma = 0^\circ$. Data according to NEUBER's formula [64].

Sub-table 3. The same as above, but notch sides are not parallel to each other.

Look for the K_t value in Sub-table 1 or 2, taking the notch sides as being parallel to each other. The required theoretical stress concentration factor is obtained in the column for this value of K_t and in the row corresponding to the angle of inclination of the sides. If $\gamma < 90^\circ$, assume $\gamma = 90^\circ$. When necessary, values can be interpolated.

Data from measurements by FROCHT and LEVEN [16].

Sub-tables 4 and 5. The same as with Sub-tables 1 and 2, but $r \gg d$. When the value of D/d becomes greater than 1.1, K_t shows hardly any further change.

Data according to NEUBER's formula [64].

Sub-table 6. This gives the K_t values for sheets subject to bending perpendicular to the plane of the sheet. The sheet thickness is considerably less than the notch depth.

Data based on the formulae of GOODIER, LEE, and NEUBER [17], [46], [64].

Sub-tables 7 and 8. These give K_t for unilaterally notched flat pieces, the notch sides being parallel to each other.

Data available only for bending. For tensile stress use the relevant values of Sub-table 1 increased by about 15 per cent.

Data from FROCHT and LEVEN [16].

Sub-table 9. This is for unilaterally notched flat pieces where the notch sides subtend an angle γ .

If $\gamma < 60^\circ$, use the values from Sub-table 8. For $\gamma > 60^\circ$, look for K_t in Sub-table 8 as if γ were equal to 0. Locate the row for which the first column of Sub-table 9 gives that value of K_t ; the required value of K_t will then be found in that row and in the column headed by the actual value of γ . When necessary, values can be interpolated.

Data from FROCHT and LEVEN [16].

Sub-tables 10 to 12. These are for notched shafts with the notch sides parallel to each other.

Data from NEUBER [64].

Sub-tables 13 to 15. The same as Sub-tables 10 to 12, but for relatively shallower "notches".

Data according to NEUBER's formula [64].

Sub-tables 16 and 17. These give K_t for flat pieces symmetrically reduced in width. The tensile forces are applied through the end faces. For bending, the two end faces are supported.

Data based on photo-elastic measurements carried out by FROCHT [12], [14], [117].

Sub-tables 18 to 21. These give K_t for pieces loaded in tension and supported at both shoulders.

The tables are for different values of r/d , so that triple interpolation may be necessary.

Data based on photo-elastic measurements carried out by HETÉNYI [26].

Sub-tables 22 to 24. These give K_t for stepped shafts.

Data based on photo-elastic measurements carried out by FROCHT [12], [14] and on the electrical analogy method of JACOBSEN [35].

Sub-tables 25 to 27. These give K_t for a flat beam (machine part) stressed in bending, thickened in the middle above or below (or all round). A separate table is given for each value of D/d , so that a triple interpolation may be necessary.

Data based on photo-elastic measurements carried out by LEVEN and HARTMANN [49].

Sub-tables 28 and 29. These give K_t for a sheet drilled at its centre. Data from HOWLAND's calculations [33].

Sub-table 30. This gives K_t for a sheet with an asymmetrical hole.

Data based on SJÖSTRÖM's calculations [87]. The formula for nominal stress is worthy of notice.

Sub-tables 31 and 32. These give K_t for a sheet having a slit bounded by semicircles at the ends.

Data based on photo-elastic measurements carried out by FROCHT and LEVEN.

Sub-table 33. This is for a sheet reinforced by a collar projection round the hole at each side. The table gives K_t for the point of greatest stress (point C), and the formula is only valid for the value $d/w = 0.2$. For other values of d/w , first determine K_t for a sheet without reinforcement from Sub-table 28 and then use the following formula:

$$K_{tm} = B(K_{ts} - 1) + 1$$

where K_{tm} is the theoretical stress concentration factor for the sheet with reinforcement and K_{ts} that for the unreinforced (smooth) sheet. Values for B are included in the table.

Data based on TIMOSHENKO's calculation [103].

Sub-tables 34 to 36. These give K_t for a very large sheet with two holes.

Data based on calculations by CHIH-BING LING [9].

Sub-tables 37 to 39. These give K_t for an infinite sheet with one row of holes. The values are for the inside holes.

Data from a mathematical derivation by SCHOUZ [81].

The values are not applicable for the first and last holes

Sub-tables 40 and 41. These give K_t for a shaft with a transverse hole.

Date based on strain measurements by THUM and KIRMSER [97].

Sub-table 42. This gives K_t for angle sections stressed in torsion.

Data based on calculations by HUTH [34].

Sub-tables 43 and 44. These give K_t for thick-walled pipes and rings loaded in tension and compression. The formulae for nominal stress are worthy of notice.

Data based on calculations and photo-elastic measurements by TIMOSHENKO [102] and HORGER [30].

Sub-table 45. This gives K_t for rectangular tubes stressed in torsion.

Data based on calculations by HUTH [34].

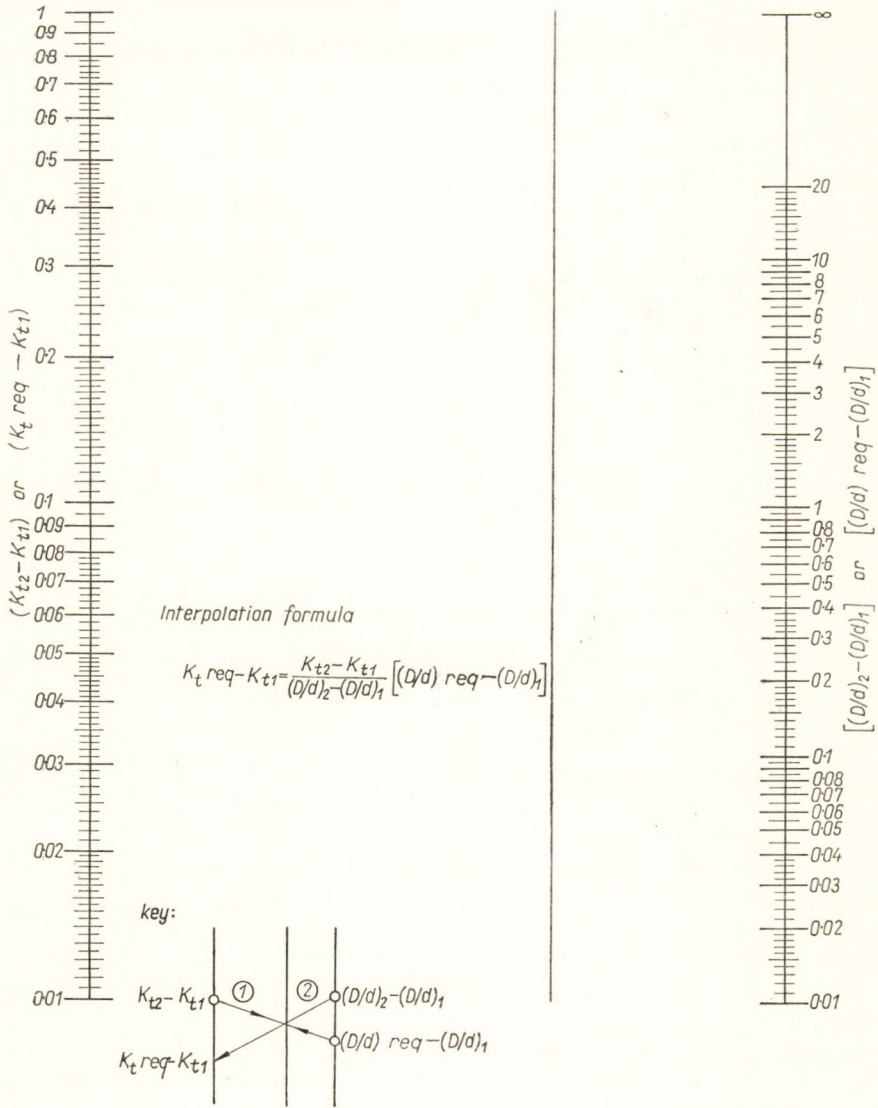


FIG. 61. Interpolation nomogram

TABLE 12
THEORETICAL STRESS CONCENTRATION FACTORS

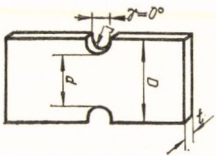
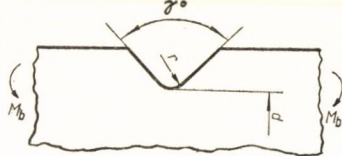
Form	Stress	Nominal stress	$\frac{\sigma_{\max}}{\sigma_n} = K_t$																																																																																							
 <p>Notched on both sides</p>	TENSION	$\sigma_n = \frac{P}{dt}$	$\frac{\sigma_{\max}}{\sigma_n} = K_t$																																																																																							
													<table border="1"> <thead> <tr> <th rowspan="2">r/d</th> <th colspan="10">D/d</th> </tr> <tr> <th>∞</th> <th>3</th> <th>2</th> <th>1.5</th> <th>1.3</th> <th>1.2</th> <th>1.1</th> <th>1.05</th> <th>1.02</th> <th>1.01</th> </tr> </thead> <tbody> <tr> <td>0-04</td> <td></td> <td></td> <td></td> <td></td> <td></td> <td></td> <td>2.90</td> <td>2.41</td> <td>2.00</td> <td>1.70</td> </tr> <tr> <td>0-10</td> <td>2.93</td> <td>2.89</td> <td>2.78</td> <td>2.65</td> <td>2.50</td> <td>2.38</td> <td>2.13</td> <td>1.89</td> <td>1.60</td> <td>1.42</td> </tr> <tr> <td>0-15</td> <td>2.44</td> <td>2.41</td> <td>2.35</td> <td>2.26</td> <td>2.17</td> <td>2.08</td> <td>1.90</td> <td>1.71</td> <td>1.49</td> <td>1.35</td> </tr> <tr> <td>0-20</td> <td>2.16</td> <td>2.14</td> <td>2.10</td> <td>2.03</td> <td>1.97</td> <td>1.90</td> <td>1.76</td> <td>1.60</td> <td>1.42</td> <td>1.30</td> </tr> <tr> <td>0-25</td> <td>1.98</td> <td>1.96</td> <td>1.93</td> <td>1.88</td> <td>1.84</td> <td>1.78</td> <td>1.65</td> <td>1.53</td> <td>1.37</td> <td>1.27</td> </tr> <tr> <td>0-30</td> <td>1.84</td> <td>1.83</td> <td>1.80</td> <td>1.77</td> <td>1.72</td> <td>1.68</td> <td>1.56</td> <td>1.47</td> <td>1.34</td> <td>1.25</td> </tr> </tbody> </table>	r/d	D/d										∞	3	2	1.5	1.3	1.2	1.1	1.05	1.02	1.01	0-04							2.90	2.41	2.00	1.70	0-10	2.93	2.89	2.78	2.65	2.50	2.38	2.13	1.89	1.60	1.42	0-15	2.44	2.41	2.35	2.26	2.17	2.08	1.90	1.71	1.49	1.35	0-20	2.16	2.14	2.10	2.03	1.97	1.90	1.76	1.60	1.42	1.30	0-25	1.98	1.96	1.93	1.88	1.84	1.78	1.65	1.53	1.37	1.27	0-30
r/d	D/d																																																																																									
	∞	3	2	1.5	1.3	1.2	1.1	1.05	1.02	1.01																																																																																
0-04							2.90	2.41	2.00	1.70																																																																																
0-10	2.93	2.89	2.78	2.65	2.50	2.38	2.13	1.89	1.60	1.42																																																																																
0-15	2.44	2.41	2.35	2.26	2.17	2.08	1.90	1.71	1.49	1.35																																																																																
0-20	2.16	2.14	2.10	2.03	1.97	1.90	1.76	1.60	1.42	1.30																																																																																
0-25	1.98	1.96	1.93	1.88	1.84	1.78	1.65	1.53	1.37	1.27																																																																																
0-30	1.84	1.83	1.80	1.77	1.72	1.68	1.56	1.47	1.34	1.25																																																																																
 <p>Notched on both sides</p>	BENDING	$\sigma_n = \frac{6M_b}{d^2 t}$	$\frac{\sigma_{\max}}{\sigma_n} = K_t$																																																																																							
													<table border="1"> <thead> <tr> <th rowspan="2">r/d</th> <th colspan="10">D/d</th> </tr> <tr> <th>∞</th> <th>3</th> <th>2</th> <th>1.5</th> <th>1.3</th> <th>1.2</th> <th>1.1</th> <th>1.05</th> <th>1.02</th> <th>1.01</th> </tr> </thead> <tbody> <tr> <td>0-04</td> <td></td> <td></td> <td></td> <td>2.95</td> <td>2.89</td> <td>2.80</td> <td>2.59</td> <td>2.28</td> <td>1.91</td> <td>1.67</td> </tr> <tr> <td>0-10</td> <td>2.19</td> <td>2.15</td> <td>2.13</td> <td>2.10</td> <td>2.06</td> <td>2.01</td> <td>1.90</td> <td>1.77</td> <td>1.56</td> <td>1.43</td> </tr> <tr> <td>0-15</td> <td>1.88</td> <td>1.86</td> <td>1.84</td> <td>1.83</td> <td>1.80</td> <td>1.77</td> <td>1.70</td> <td>1.60</td> <td>1.45</td> <td>1.35</td> </tr> <tr> <td>0-20</td> <td>1.71</td> <td>1.69</td> <td>1.68</td> <td>1.67</td> <td>1.65</td> <td>1.63</td> <td>1.57</td> <td>1.49</td> <td>1.39</td> <td>1.31</td> </tr> <tr> <td>0-25</td> <td>1.59</td> <td>1.58</td> <td>1.57</td> <td>1.57</td> <td>1.55</td> <td>1.54</td> <td>1.49</td> <td>1.43</td> <td>1.34</td> <td>1.28</td> </tr> <tr> <td>0-30</td> <td>1.51</td> <td>1.50</td> <td>1.49</td> <td>1.49</td> <td>1.48</td> <td>1.47</td> <td>1.44</td> <td>1.38</td> <td>1.30</td> <td>1.26</td> </tr> </tbody> </table>	r/d	D/d										∞	3	2	1.5	1.3	1.2	1.1	1.05	1.02	1.01	0-04				2.95	2.89	2.80	2.59	2.28	1.91	1.67	0-10	2.19	2.15	2.13	2.10	2.06	2.01	1.90	1.77	1.56	1.43	0-15	1.88	1.86	1.84	1.83	1.80	1.77	1.70	1.60	1.45	1.35	0-20	1.71	1.69	1.68	1.67	1.65	1.63	1.57	1.49	1.39	1.31	0-25	1.59	1.58	1.57	1.57	1.55	1.54	1.49	1.43	1.34	1.28	0-30
r/d	D/d																																																																																									
	∞	3	2	1.5	1.3	1.2	1.1	1.05	1.02	1.01																																																																																
0-04				2.95	2.89	2.80	2.59	2.28	1.91	1.67																																																																																
0-10	2.19	2.15	2.13	2.10	2.06	2.01	1.90	1.77	1.56	1.43																																																																																
0-15	1.88	1.86	1.84	1.83	1.80	1.77	1.70	1.60	1.45	1.35																																																																																
0-20	1.71	1.69	1.68	1.67	1.65	1.63	1.57	1.49	1.39	1.31																																																																																
0-25	1.59	1.58	1.57	1.57	1.55	1.54	1.49	1.43	1.34	1.28																																																																																
0-30	1.51	1.50	1.49	1.49	1.48	1.47	1.44	1.38	1.30	1.26																																																																																
BENDING	Instructions on p. 39 in the "Notes on Table 12"		K_t when $\gamma = 0^\circ$ <table border="1"> <thead> <tr> <th>p</th> <th>1.4</th> <th>1.6</th> <th>1.8</th> <th>2.0</th> <th>2.2</th> <th>2.4</th> <th>2.6</th> <th>2.8</th> <th>3.0</th> <th>3.2</th> </tr> </thead> <tbody> <tr> <td>90°</td> <td></td> <td></td> <td></td> <td></td> <td></td> <td>2.37</td> <td>2.56</td> <td>2.75</td> <td>2.93</td> <td>3.12</td> </tr> <tr> <td>120°</td> <td></td> <td></td> <td>1.76</td> <td>1.92</td> <td>2.08</td> <td>2.24</td> <td>2.40</td> <td>2.54</td> <td>2.68</td> <td>2.82</td> </tr> <tr> <td>140°</td> <td>1.39</td> <td>1.50</td> <td>1.64</td> <td>1.75</td> <td>1.86</td> <td>1.96</td> <td>2.07</td> <td>2.16</td> <td>2.26</td> <td>2.35</td> </tr> <tr> <td>150°</td> <td>1.36</td> <td>1.44</td> <td>1.54</td> <td>1.64</td> <td>1.72</td> <td>1.80</td> <td>1.88</td> <td>1.95</td> <td>2.00</td> <td>2.06</td> </tr> <tr> <td>160°</td> <td>1.26</td> <td>1.36</td> <td>1.42</td> <td>1.48</td> <td>1.53</td> <td>1.57</td> <td>1.62</td> <td>1.65</td> <td>1.69</td> <td>1.73</td> </tr> <tr> <td>170°</td> <td>1.20</td> <td>1.26</td> <td>1.30</td> <td>1.33</td> <td>1.35</td> <td>1.37</td> <td>1.39</td> <td>1.40</td> <td>1.42</td> <td>1.43</td> </tr> </tbody> </table>										p	1.4	1.6	1.8	2.0	2.2	2.4	2.6	2.8	3.0	3.2	90°						2.37	2.56	2.75	2.93	3.12	120°			1.76	1.92	2.08	2.24	2.40	2.54	2.68	2.82	140°	1.39	1.50	1.64	1.75	1.86	1.96	2.07	2.16	2.26	2.35	150°	1.36	1.44	1.54	1.64	1.72	1.80	1.88	1.95	2.00	2.06	160°	1.26	1.36	1.42	1.48	1.53	1.57	1.62	1.65	1.69	1.73	170°	1.20	1.26	1.30	1.33	1.35	1.37	1.39	1.40	1.42	1.43	3
p	1.4	1.6	1.8	2.0	2.2	2.4	2.6	2.8	3.0	3.2																																																																																
90°						2.37	2.56	2.75	2.93	3.12																																																																																
120°			1.76	1.92	2.08	2.24	2.40	2.54	2.68	2.82																																																																																
140°	1.39	1.50	1.64	1.75	1.86	1.96	2.07	2.16	2.26	2.35																																																																																
150°	1.36	1.44	1.54	1.64	1.72	1.80	1.88	1.95	2.00	2.06																																																																																
160°	1.26	1.36	1.42	1.48	1.53	1.57	1.62	1.65	1.69	1.73																																																																																
170°	1.20	1.26	1.30	1.33	1.35	1.37	1.39	1.40	1.42	1.43																																																																																

TABLE 12 (CONT.)

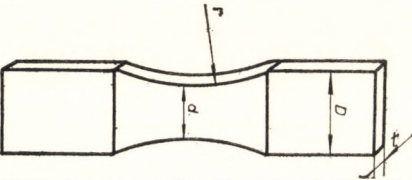
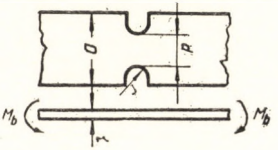
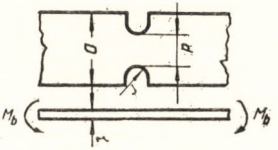
Form	Stress	Nominal stress	$\frac{\sigma_{max}}{\sigma_n} = K_t$										
	TENSION	$\sigma_n = \frac{P}{dt}$	D/d										
			r/d										
			∞	1.1	1.05	1.02	1.01						
			0.4	1.47	1.39	1.28	1.21						
	BENDING	$\sigma_n = \frac{6M_b}{d^2t}$	D/d										
			r/d										
			∞	1.1	1.05	1.02	1.01						
			0.4	1.40	1.35	1.32	1.26	1.21					
			0.5	1.33	1.29	1.27	1.22	1.18					
			0.6	1.28	1.25	1.23	1.19	1.15					
			0.8	1.22	1.19	1.17	1.15	1.12					
			1.0	1.17	1.16	1.15	1.12	1.10					
			2.0	1.09	1.09	1.08	1.07	1.06					
			<p style="text-align: center;">$\frac{t}{r/d}$</p> 	BENDING PERPENDICULAR TO PLANE OF SHEET	$\sigma_n = \frac{6M_b}{dt^2}$	D/d							
r/d													
∞	2.0	1.50				1.25	1.10	1.05	1.02				
0.02	2.96	2.77				2.61	2.41	2.10	1.85	1.58			
0.04	2.20	2.11				2.04	1.93	1.74	1.58	1.43			
0.06	1.88	1.82				1.78	1.71	1.59	1.47	1.35			
0.08	1.70	1.66				1.64	1.59	1.49	1.40	1.30			
0.10	1.60	1.57				1.54	1.51	1.43	1.37	1.27			

TABLE 12 (CONT.)

Form	Stress	Nominal stress	$\frac{\sigma_{\max}}{\sigma_n} = K_t$													
	TENSION	$\sigma_n = \frac{4P}{d^2\pi}$	D/d													
			r/d	∞	2.00	1.50	1.30	1.20	1.10	1.05	1.03	1.02	1.01			
			0.04						2.70	2.37	2.15	1.94	1.70			
			0.10	2.45	2.39	2.33	2.27	2.18	2.01	1.81	1.68	1.58	1.42			
			0.15	2.08	2.04	1.99	1.95	1.90	1.78	1.64	1.55	1.47	1.33			
			0.20	1.86	1.83	1.80	1.77	1.73	1.65	1.54	1.46	1.40	1.28			
			0.25	1.72	1.69	1.67	1.65	1.62	1.55	1.46	1.40	1.34	1.24			
			0.30	1.61	1.59	1.58	1.55	1.53	1.47	1.40	1.36	1.31	1.22	1.10		
						D/d										
r/d	∞	2.00	1.50	1.30	1.20	1.10	1.05	1.03	1.02	1.01						
0.04	2.83	2.79	2.74	2.70	2.61	2.45	2.22	2.02	1.88	1.66						
0.10	1.99	1.98	1.96	1.92	1.89	1.81	1.70	1.61	1.53	1.41						
0.15	1.75	1.74	1.72	1.70	1.69	1.63	1.56	1.49	1.42	1.33						
0.20	1.61	1.59	1.58	1.57	1.56	1.51	1.46	1.40	1.34	1.27						
0.25	1.49	1.48	1.47	1.46	1.45	1.42	1.38	1.34	1.29	1.23						
0.30	1.41	1.41	1.40	1.39	1.38	1.36	1.33	1.29	1.24	1.21	1.11					
			D/d													
r/d	∞	2.00	1.30	1.20	1.10	1.05	1.02	1.01								
0.04	1.97	1.93	1.89	1.85	1.74	1.61	1.45	1.33								
0.10	1.52	1.51	1.48	1.46	1.41	1.35	1.27	1.20								
0.15	1.39	1.38	1.37	1.35	1.32	1.27	1.21	1.16								
0.20	1.32	1.31	1.30	1.28	1.26	1.22	1.18	1.14								
0.25	1.27	1.26	1.25	1.24	1.22	1.19	1.16	1.13								
0.30	1.22	1.22	1.21	1.20	1.19	1.17	1.15	1.12								
			D/d													
r/d	∞	2.00	1.30	1.20	1.10	1.05	1.02	1.01								
0.04	1.97	1.93	1.89	1.85	1.74	1.61	1.45	1.33								
0.10	1.52	1.51	1.48	1.46	1.41	1.35	1.27	1.20								
0.15	1.39	1.38	1.37	1.35	1.32	1.27	1.21	1.16								
0.20	1.32	1.31	1.30	1.28	1.26	1.22	1.18	1.14								
0.25	1.27	1.26	1.25	1.24	1.22	1.19	1.16	1.13								
0.30	1.22	1.22	1.21	1.20	1.19	1.17	1.15	1.12								

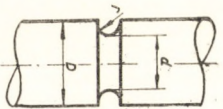


TABLE 12 (CONT.)

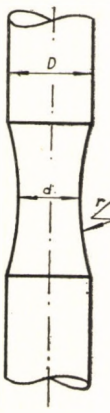
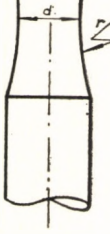


Form	Stress	Nominal stress	$\frac{\sigma_{\max}}{\sigma_n} = K_t$													
	TENSION	$\sigma_n = \frac{4P}{d^2\pi}$	D/d													
			r/d	∞	1.1	1.05	1.02	1.01								
			0.4	1.47	1.37	1.33	1.26	1.20								
			0.5	1.39	1.33	1.29	1.23	1.18								
			0.6	1.34	1.28	1.25	1.20	1.16								
			0.8	1.26	1.23	1.20	1.17	1.13								
			1.0	1.22	1.18	1.17	1.14	1.12								
			2.0	1.11	1.10	1.09	1.08	1.07								
			13													
				BENDING	$\sigma_n = \frac{32M_b}{d^3\pi}$	D/d										
						r/d	∞	1.1	1.05	1.02	1.01					
						0.4	1.32	1.29	1.27	1.20	1.17					
						0.5	1.27	1.24	1.22	1.18	1.15					
0.6	1.22	1.21				1.19	1.16	1.13								
0.8	1.17	1.16				1.15	1.12	1.11								
1.0	1.14	1.13				1.12	1.10	1.09								
2.0	1.07	1.07				1.06	1.06	1.05								
14																
	TORSION	$\tau_n = \frac{16M_t}{d^3\pi}$				D/d										
						r/d	∞	1.1	1.05	1.02	1.01					
						0.4	1.18	1.16	1.14	1.12	1.09					
						0.5	1.14	1.13	1.12	1.10	1.08					
			0.6	1.12	1.11	1.10	1.08	1.07								
			0.8	1.09	1.08	1.08	1.07	1.06								
			1.0	1.08	1.08	1.07	1.06	1.05								
			2.0	1.04	1.04	1.03	1.03	1.02								
			15													

TABLE 12 (CONT.)

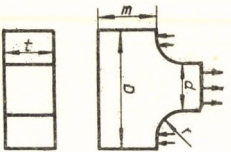
Form	Stress	Nominal stress	$\frac{\sigma_{max}}{\sigma_n} = K,$												
 <p>T-shaped head The two shoulders resist the tensile forces</p>	TENSION the forces are applied through the two end faces	$\sigma_n = \frac{P}{dt}$	D/d												
			r/d	3.0	2.0	1.5	1.30	1.20	1.15	1.10	1.10	1.05	1.02	1.01	
			0.04		2.88	2.61	2.43	2.31	2.10	1.85	1.60	1.42			
			0.10		2.28	2.10	1.93	1.80	1.72	1.63	1.55	1.49	1.34		
			0.15		2.0	1.86	1.72	1.63	1.56	1.50	1.40	1.27	1.18		
			0.20		1.87	1.83	1.72	1.62	1.53	1.47	1.42	1.35	1.23	1.15	
			0.25		1.75	1.72	1.63	1.54	1.47	1.42	1.37	1.31	1.21	1.14	
			0.30		1.66	1.63	1.56	1.49	1.43	1.38	1.34	1.28	1.19	1.13	
			D/d												
			r/d	6.0	3.0	2.0	1.30	1.20	1.10	1.05	1.03	1.02	1.01		
			0.04	2.85	2.69	2.51	2.37	2.20	2.08	1.92	1.84	1.75	1.62		
			0.10	2.04	1.94	1.85	1.78	1.71	1.65	1.57	1.52	1.46	1.37		
			0.15	1.74	1.68	1.63	1.60	1.55	1.52	1.46	1.41	1.36	1.28		
			0.20	1.57	1.53	1.50	1.48	1.46	1.43	1.38	1.34	1.30	1.23		
			0.25	1.47	1.44	1.42	1.40	1.38	1.37	1.34	1.30	1.26	1.20		
			0.30	1.40	1.38	1.37	1.35	1.34	1.33	1.30	1.27	1.24	1.18		
			$r/d = 0.05$												
			m/d												
			D/d	0.50	0.55	0.60	0.70	0.80	0.90	1.0	1.20	1.50	3.0		
			1.5	9.50	8.90	8.45	7.55	6.95	6.50	6.30	6.25	6.20	6.10		
			1.8	10.85	10.05	9.40	8.20	7.25	6.40	5.85	5.70	5.50	5.30		
			2.1	12.20	11.20	10.30	8.90	7.70	6.65	5.90	5.60	5.20	4.85		
			2.4	13.60	12.30	11.30	9.55	8.20	7.0	6.20	5.65	5.0	4.55		
			2.7	15.0	13.45	12.20	10.20	8.70	7.50	6.55	5.80	5.0	4.30		
			3.0	16.40	14.55	13.15	10.90	9.20	7.90	6.95	6.0	5.10	4.10		
			$r/d = 0.05$												
			m/d												
			D/d	0.50	0.55	0.60	0.70	0.80	0.90	1.0	1.20	1.50	3.0		
			1.5	9.50	8.90	8.45	7.55	6.95	6.50	6.30	6.25	6.20	6.10		
			1.8	10.85	10.05	9.40	8.20	7.25	6.40	5.85	5.70	5.50	5.30		
			2.1	12.20	11.20	10.30	8.90	7.70	6.65	5.90	5.60	5.20	4.85		
			2.4	13.60	12.30	11.30	9.55	8.20	7.0	6.20	5.65	5.0	4.55		
			2.7	15.0	13.45	12.20	10.20	8.70	7.50	6.55	5.80	5.0	4.30		
			3.0	16.40	14.55	13.15	10.90	9.20	7.90	6.95	6.0	5.10	4.10		

17

16

TABLE 12 (CONT.)

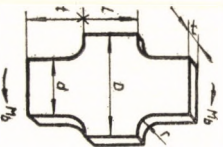
Form	Stress	Nominal stress	$\frac{\sigma_{\max}}{\sigma_n} = K_t$										
	TENSION	$\sigma_n = \frac{P}{dt}$	$r/d = 0.075$										
			m/d										
			D/d	0.50	0.55	0.60	0.70	0.80	0.90	1.0	1.20	1.50	3.0
			1.5	6.85	6.50	6.25	5.90	5.62	5.40	5.25	5.07	5.0	4.90
			1.8	8.20	7.40	6.80	5.90	5.40	5.05	4.80	4.50	4.25	4.15
			2.1	9.45	8.40	7.60	6.45	5.65	5.10	4.70	4.40	4.10	3.80
			2.4	10.70	9.40	8.60	7.20	6.25	5.55	5.05	4.60	4.10	3.65
			2.7	12.0	10.60	9.70	8.15	6.95	6.20	5.55	4.90	4.20	3.55
			3.0	13.25	11.85	10.90	9.10	7.80	6.90	6.10	5.40	4.55	3.50
			$r/d = 0.100$										
			m/d										
			D/d	0.50	0.55	0.60	0.70	0.80	0.90	1.0	1.20	1.50	3.0
			1.5	6.85	6.45	6.10	5.60	5.40	5.20	5.05	4.90	4.75	4.70
			1.8	7.80	7.10	6.55	5.55	4.80	4.45	4.20	3.95	3.75	3.65
			2.1	8.70	7.90	7.10	7.0	5.05	4.55	4.10	3.80	3.50	3.20
			2.4	9.60	8.70	7.85	6.65	5.55	4.90	4.35	3.95	3.55	3.10
			2.7	10.55	9.45	8.70	7.40	6.20	5.50	4.80	4.30	3.75	3.0
			3.0	11.45	10.30	9.50	8.10	7.0	6.20	5.40	4.80	4.10	3.10
			$r/d = 0.200$										
			m/d										
			D/d	0.50	0.55	0.60	0.70	0.80	0.90	1.0	1.20	1.50	3.0
			1.5										
			1.8	3.85	3.70	3.60	3.40	3.30	3.25	3.20	3.10	3.05	3.0
			2.1	5.15	4.70	4.40	3.85	3.45	3.15	2.95	2.80	2.65	2.50
			2.4	6.80	6.05	5.55	4.70	4.10	3.65	3.20	2.90	2.65	2.35
			2.7	7.60	6.80	6.15	5.25	4.50	4.0	3.65	3.25	2.90	2.40
			3.0	8.70	7.80	7.20	6.10	5.30	4.70	4.20	3.75	3.20	2.50



T-shaped head
The two shoulders
resist the tensile
forces

TABLE 12 (CONT.)

Form	Stress	Nominal stress	$\frac{\sigma_{\max}}{\sigma_n} = K_t$																					
Rectangular beam with narrow shoulders on both sides at the middle of the length	BENDING	$\sigma_n = \frac{6M_b}{d^2t}$	$D/d = 1.25$																					
			r/d																					
			0.02	0.03	0.04	0.06	0.10	0.20	0.30	0.40	0.60	1.0	0.02	0.03	0.04	0.06	0.10	0.20	0.30	0.40	0.60	1.0		
			0.1	2.32	2.14	2.02	1.83	1.59	1.40	1.31	1.26	1.20	1.11	0.1	2.32	2.14	2.02	1.83	1.59	1.40	1.31	1.26	1.20	1.11
			0.3	2.73	2.52	2.37	2.12	1.77	1.46	1.35	1.29	1.21	1.12	0.3	2.73	2.52	2.37	2.12	1.77	1.46	1.35	1.29	1.21	1.12
			0.5	2.92	2.66	2.48	2.21	1.85	1.49	1.36	1.30	1.22	1.12	0.5	2.92	2.66	2.48	2.21	1.85	1.49	1.36	1.30	1.22	1.12
			1.0		2.82	2.60	2.30	1.91	1.51	1.38	1.31	1.23	1.12	1.0		2.82	2.60	2.30	1.91	1.51	1.38	1.31	1.23	1.12
			1.5		2.88	2.66	2.34	1.93	1.52	1.38	1.31	1.23	1.12	1.5		2.88	2.66	2.34	1.93	1.52	1.38	1.31	1.23	1.12
			2.0		2.91	2.67	2.35	1.94	1.53	1.39	1.32	1.23	1.12	2.0		2.91	2.67	2.35	1.94	1.53	1.39	1.32	1.23	1.12
			$D/d = 2$																					
			r/d																					
			0.02	0.03	0.04	0.06	0.10	0.20	0.30	0.40	0.60	1.0	0.02	0.03	0.04	0.06	0.10	0.20	0.30	0.40	0.60	1.0		
			0.1	2.20	1.94	1.81	1.68	1.58	1.36	1.28	1.25	1.19	1.11	0.1	2.20	1.94	1.81	1.68	1.58	1.36	1.28	1.25	1.19	1.11
			0.3	2.50	2.30	2.16	1.93	1.67	1.44	1.33	1.28	1.20	1.11	0.3	2.50	2.30	2.16	1.93	1.67	1.44	1.33	1.28	1.20	1.11
			0.5	2.70	2.47	2.30	2.04	1.74	1.47	1.35	1.29	1.21	1.12	0.5	2.70	2.47	2.30	2.04	1.74	1.47	1.35	1.29	1.21	1.12
			1.0	2.93	2.65	2.43	2.14	1.81	1.49	1.36	1.30	1.22	1.12	1.0	2.93	2.65	2.43	2.14	1.81	1.49	1.36	1.30	1.22	1.12
			1.5	3.02	2.71	2.48	2.18	1.84	1.50	1.37	1.31	1.23	1.12	1.5	3.02	2.71	2.48	2.18	1.84	1.50	1.37	1.31	1.23	1.12
			2.0		2.73	2.50	2.20	1.85	1.51	1.37	1.31	1.23	1.12	2.0		2.73	2.50	2.20	1.85	1.51	1.37	1.31	1.23	1.12
			$D/d = 3$																					
			r/d																					
			0.02	0.03	0.04	0.06	0.10	0.20	0.30	0.40	0.60	1.0	0.02	0.03	0.04	0.06	0.10	0.20	0.30	0.40	0.60	1.0		
			0.1	2.32	2.14	2.02	1.83	1.59	1.40	1.31	1.26	1.20	1.11	0.1	2.32	2.14	2.02	1.83	1.59	1.40	1.31	1.26	1.20	1.11
			0.3	2.73	2.52	2.37	2.12	1.77	1.46	1.35	1.29	1.21	1.12	0.3	2.73	2.52	2.37	2.12	1.77	1.46	1.35	1.29	1.21	1.12
			0.5	2.92	2.66	2.48	2.21	1.85	1.49	1.36	1.30	1.22	1.12	0.5	2.92	2.66	2.48	2.21	1.85	1.49	1.36	1.30	1.22	1.12
			1.0		2.82	2.60	2.30	1.91	1.51	1.38	1.31	1.23	1.12	1.0		2.82	2.60	2.30	1.91	1.51	1.38	1.31	1.23	1.12
			1.5		2.88	2.66	2.34	1.93	1.52	1.38	1.31	1.23	1.12	1.5		2.88	2.66	2.34	1.93	1.52	1.38	1.31	1.23	1.12
			2.0		2.91	2.67	2.35	1.94	1.53	1.39	1.32	1.23	1.12	2.0		2.91	2.67	2.35	1.94	1.53	1.39	1.32	1.23	1.12



Rectangular beam with narrow shoulders on both sides at the middle of the length

TABLE 12 (CONT.)


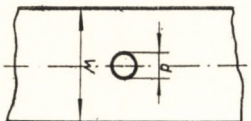
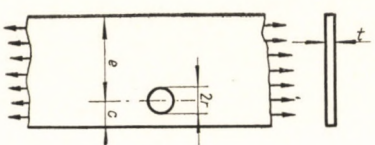
Form	Stress	Nominal stress	$\frac{\sigma_{\max}}{\sigma_n} = K_t$																																																																																													
	TENSION	$\sigma_n = \frac{P}{(w-d)t}$	<table border="1"> <tr> <td>d/w</td> <td></td> <td></td> <td></td> <td></td> <td></td> <td></td> <td></td> <td></td> <td></td> <td></td> <td></td> </tr> <tr> <td>0</td> <td>3.0</td> <td></td> <td></td> <td></td> <td></td> <td></td> <td></td> <td></td> <td></td> <td></td> <td></td> </tr> <tr> <td>0.1</td> <td>2.72</td> <td></td> <td></td> <td></td> <td></td> <td></td> <td></td> <td></td> <td></td> <td></td> <td></td> </tr> <tr> <td>0.2</td> <td>2.51</td> <td></td> <td></td> <td></td> <td></td> <td></td> <td></td> <td></td> <td></td> <td></td> <td></td> </tr> <tr> <td>0.3</td> <td>2.46</td> <td></td> <td></td> <td></td> <td></td> <td></td> <td></td> <td></td> <td></td> <td></td> <td></td> </tr> <tr> <td>0.4</td> <td>2.25</td> <td></td> <td></td> <td></td> <td></td> <td></td> <td></td> <td></td> <td></td> <td></td> <td></td> </tr> <tr> <td>0.5</td> <td>2.16</td> <td></td> <td></td> <td></td> <td></td> <td></td> <td></td> <td></td> <td></td> <td></td> <td></td> </tr> </table>										d/w												0	3.0											0.1	2.72											0.2	2.51											0.3	2.46											0.4	2.25											0.5	2.16										
													d/w																																																																																			
0	3.0																																																																																															
0.1	2.72																																																																																															
0.2	2.51																																																																																															
0.3	2.46																																																																																															
0.4	2.25																																																																																															
0.5	2.16																																																																																															
	BENDING PERPENDICULAR TO PLANE OF SHEET	$\sigma_n = \frac{6M_b}{(w-d)t^2}$	<table border="1"> <tr> <td>d/w</td> <td></td> <td></td> <td></td> <td></td> <td></td> <td></td> <td></td> <td></td> <td></td> <td></td> <td></td> </tr> <tr> <td>0</td> <td>3.0</td> <td>2.74</td> <td>2.50</td> <td>2.25</td> <td>2.12</td> <td>2.04</td> <td>1.85</td> <td></td> <td></td> <td></td> <td></td> </tr> <tr> <td>0.1</td> <td>2.72</td> <td>2.48</td> <td>2.27</td> <td>2.06</td> <td>1.94</td> <td>1.86</td> <td>1.68</td> <td></td> <td></td> <td></td> <td></td> </tr> <tr> <td>0.2</td> <td>2.51</td> <td>2.30</td> <td>2.11</td> <td>1.91</td> <td>1.79</td> <td>1.71</td> <td>1.56</td> <td></td> <td></td> <td></td> <td></td> </tr> <tr> <td>0.3</td> <td>2.36</td> <td>2.16</td> <td>1.98</td> <td>1.79</td> <td>1.67</td> <td>1.60</td> <td>1.46</td> <td></td> <td></td> <td></td> <td></td> </tr> <tr> <td>0.4</td> <td>2.25</td> <td>2.04</td> <td>1.88</td> <td>1.69</td> <td>1.57</td> <td>1.51</td> <td>1.37</td> <td></td> <td></td> <td></td> <td></td> </tr> <tr> <td>0.5</td> <td>2.17</td> <td>1.95</td> <td>1.79</td> <td>1.60</td> <td>1.50</td> <td>1.44</td> <td>1.30</td> <td></td> <td></td> <td></td> <td></td> </tr> </table>										d/w												0	3.0	2.74	2.50	2.25	2.12	2.04	1.85					0.1	2.72	2.48	2.27	2.06	1.94	1.86	1.68					0.2	2.51	2.30	2.11	1.91	1.79	1.71	1.56					0.3	2.36	2.16	1.98	1.79	1.67	1.60	1.46					0.4	2.25	2.04	1.88	1.69	1.57	1.51	1.37					0.5	2.17	1.95	1.79	1.60	1.50	1.44	1.30				
													d/w																																																																																			
0	3.0	2.74	2.50	2.25	2.12	2.04	1.85																																																																																									
0.1	2.72	2.48	2.27	2.06	1.94	1.86	1.68																																																																																									
0.2	2.51	2.30	2.11	1.91	1.79	1.71	1.56																																																																																									
0.3	2.36	2.16	1.98	1.79	1.67	1.60	1.46																																																																																									
0.4	2.25	2.04	1.88	1.69	1.57	1.51	1.37																																																																																									
0.5	2.17	1.95	1.79	1.60	1.50	1.44	1.30																																																																																									
	TENSION	$\sigma_n = \frac{P}{(e+c)t} \frac{\sqrt{1-\left(\frac{r}{c}\right)^2}}{\left(1-\frac{r}{c}\right)\left[1-\frac{c}{e}\sqrt{1-\left(\frac{r}{c}\right)^2}\right]}$	<table border="1"> <tr> <td>e/c</td> <td></td> <td></td> <td></td> <td></td> <td></td> <td></td> <td></td> <td></td> <td></td> <td></td> <td></td> </tr> <tr> <td>1</td> <td>3.0</td> <td>2.72</td> <td>2.51</td> <td>2.38</td> <td>2.29</td> <td>2.22</td> <td></td> <td></td> <td></td> <td></td> <td></td> </tr> <tr> <td>2.4</td> <td>3.0</td> <td>2.72</td> <td>2.50</td> <td>2.36</td> <td>2.26</td> <td>2.16</td> <td></td> <td></td> <td></td> <td></td> <td></td> </tr> <tr> <td>∞</td> <td>3.0</td> <td>2.72</td> <td>2.50</td> <td>2.34</td> <td>2.23</td> <td>2.13</td> <td></td> <td></td> <td></td> <td></td> <td></td> </tr> </table>										e/c												1	3.0	2.72	2.51	2.38	2.29	2.22						2.4	3.0	2.72	2.50	2.36	2.26	2.16						∞	3.0	2.72	2.50	2.34	2.23	2.13																																									
													e/c																																																																																			
1	3.0	2.72	2.51	2.38	2.29	2.22																																																																																										
2.4	3.0	2.72	2.50	2.36	2.26	2.16																																																																																										
∞	3.0	2.72	2.50	2.34	2.23	2.13																																																																																										
			<table border="1"> <tr> <td>r/c</td> <td></td> <td></td> <td></td> <td></td> <td></td> <td></td> <td></td> <td></td> <td></td> <td></td> <td></td> </tr> <tr> <td>0</td> <td>0.1</td> <td>0.2</td> <td>0.3</td> <td>0.4</td> <td>0.5</td> <td></td> <td></td> <td></td> <td></td> <td></td> <td></td> </tr> </table>										r/c												0	0.1	0.2	0.3	0.4	0.5																																																																		
r/c																																																																																																
0	0.1	0.2	0.3	0.4	0.5																																																																																											

TABLE 12 (CONT.)

Form	Stress	Nominal stress	$\frac{\sigma_{\max}}{\sigma_n} = K_t$

TENSION	$\sigma_n = \frac{P}{dt}$	r/d												
		t/r	0.05	0.10	0.20	0.30	0.40	0.50	0.60	0.70				
		1	2.62	2.46	2.32	2.23	2.18	2.14	2.11	2.08				
		2	3.20	2.87	2.55	2.41	2.33	2.26	2.22	2.16				
		4	3.53	3.15	2.67	2.46	2.36	2.29	2.24	2.18				

31

BENDING PERPENDICULAR TO PLANE OF SHEET	$\sigma_n = \frac{24M_b D}{dt [d^3 + 1.5(2D - d)^2]}$	r/d														
		t/r	0.05	0.10	0.20	0.30	0.40	0.50	0.60	0.70	0.80	1.0				
		1							1.08	1.15	1.21	1.30				
		2			1.0	1.20	1.34	1.45	1.52	1.57	1.61	1.63				
		4		1.17	1.56	1.71	1.78	1.82	1.85	1.87	1.88	1.89				

32

TENSION	For σ_n see below the table	$d/w = 0.2$														
		f	0.1	0.2	0.3	0.4	0.5	0.6	0.7	0.8	0.9	1.0				
		At point C	2.28	2.13	2.00	1.91	1.83	1.76	1.70	1.64	1.58	1.53				
		Value B (see "Notes on Table 12")	0.84	0.75	0.66	0.60	0.55	0.50	0.46	0.42	0.39	0.36				

$$\sigma_n = \frac{P}{wt} \left[\frac{1}{1 - \frac{d}{w}(1-f)} \right] \quad f = \frac{(D-d)(H-t)}{d \cdot t}$$

33

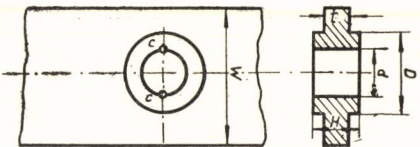


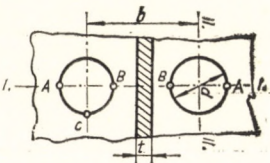
TABLE 12 (CONT.)

Form

Stress

Nominal stress

$$\frac{\sigma_{\max}}{\sigma_n} = K.$$



TENSION IN THE DIRECTION I - I OF THE COMMON AXIS OF THE HOLES

$$\sigma_n = \frac{P}{A}$$

	b/d								∞	
	1	1.5	2	3	4	5	6	7		8
At point C	2.57	2.62	2.71	2.82	2.89	2.92	2.94	2.96	2.97	3.0
At point A										

34

TENSION IN THE DIRECTION II - II PERPENDICULAR TO THE COMMON AXIS OF THE HOLES

$$\sigma_n = \frac{\sigma_{\text{full}}}{1 - \frac{d}{b}}$$

	b/d								∞	
	1	1.5	2	3	4	5	6	7		8
Point B	1.0	1.10	1.52	2.0	2.22	2.40	2.50	2.56	2.62	3.0
At point A	3.88	3.15	3.06	3.04						3.0

35

TENSION IN BOTH DIRECTIONS

$$\sigma_n = \frac{\sigma_{\text{full}}}{1 - \frac{d}{b}}$$

	b/d								∞	
	1	1.5	2	3	4	5	6	7		8
At point B		1.0	1.22	1.44	1.56	1.64	1.68	1.73	1.78	2.0
At point A	2.90	2.26	2.16	2.08	2.06					2.0

36

K_t for a very large sheet with two holes $\sigma_{\text{full}} = F/A$ where A denotes the unreduced cross-section

Note: The peak stresses at the points A and B are given in the table. Peak stresses must not be added

TABLE 12 (CONT.)

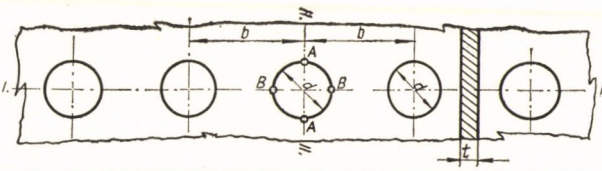
Form	Stress	Nominal stress	$\frac{\sigma_{max}}{\sigma_n} = K_t$																						
<p>$\sigma_{full} = P/A$ where A denotes the unreduced cross-section</p> 	<p>TENSION IN THE DIRECTION I - I OF THE COMMON AXIS OF THE HOLES</p>	$\sigma_n = \frac{P}{A}$	<p>At point A</p> <table border="1"> <thead> <tr> <th>b/d</th> <th>1</th> <th>1.5</th> <th>2</th> <th>3</th> <th>4</th> <th>5</th> <th>6</th> <th>7</th> <th>8</th> <th>∞</th> </tr> </thead> <tbody> <tr> <td></td> <td>1.72</td> <td>1.83</td> <td>2.15</td> <td>2.48</td> <td>2.65</td> <td>2.74</td> <td>2.80</td> <td>2.84</td> <td>2.88</td> <td>3.0</td> </tr> </tbody> </table>	b/d	1	1.5	2	3	4	5	6	7	8	∞		1.72	1.83	2.15	2.48	2.65	2.74	2.80	2.84	2.88	3.0
b/d	1	1.5	2	3	4	5	6	7	8	∞															
	1.72	1.83	2.15	2.48	2.65	2.74	2.80	2.84	2.88	3.0															
<p>TENSION IN THE DIRECTION II - II PERPENDICULAR TO THE COMMON AXIS OF THE HOLES</p>	<p>TENSION IN THE DIRECTIONS I - I AND II - II</p>	$\sigma_n = \frac{\sigma_{full}}{1 - \left(\frac{d}{b}\right)}$	<p>At point B</p> <table border="1"> <thead> <tr> <th>b/d</th> <th>1</th> <th>1.5</th> <th>2</th> <th>3</th> <th>4</th> <th>5</th> <th>6</th> <th>7</th> <th>8</th> <th>∞</th> </tr> </thead> <tbody> <tr> <td></td> <td>1.0</td> <td>1.30</td> <td>1.63</td> <td>2.05</td> <td>2.26</td> <td>2.42</td> <td>2.52</td> <td>2.58</td> <td>2.64</td> <td>3.0</td> </tr> </tbody> </table>	b/d	1	1.5	2	3	4	5	6	7	8	∞		1.0	1.30	1.63	2.05	2.26	2.42	2.52	2.58	2.64	3.0
b/d	1	1.5	2	3	4	5	6	7	8	∞															
	1.0	1.30	1.63	2.05	2.26	2.42	2.52	2.58	2.64	3.0															
<p>Row of holes in a very large sheet</p>			<p>At point B</p> <table border="1"> <thead> <tr> <th>b/d</th> <th>1</th> <th>1.5</th> <th>2</th> <th>3</th> <th>4</th> <th>5</th> <th>6</th> <th>7</th> <th>8</th> <th>∞</th> </tr> </thead> <tbody> <tr> <td></td> <td>1.0</td> <td>1.24</td> <td>1.48</td> <td>1.55</td> <td>1.64</td> <td>1.70</td> <td>1.74</td> <td>1.78</td> <td>1.80</td> <td>2.0</td> </tr> </tbody> </table>	b/d	1	1.5	2	3	4	5	6	7	8	∞		1.0	1.24	1.48	1.55	1.64	1.70	1.74	1.78	1.80	2.0
b/d	1	1.5	2	3	4	5	6	7	8	∞															
	1.0	1.24	1.48	1.55	1.64	1.70	1.74	1.78	1.80	2.0															

TABLE 12 (CONT.)



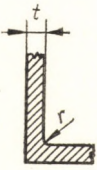
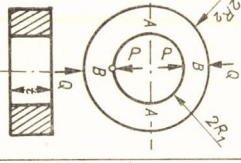
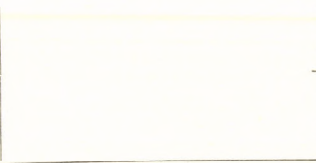
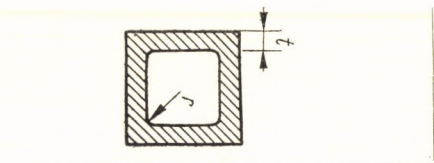
Form	Stress	Nominal stress	$\frac{\sigma_{max}}{\sigma_n} = K_t$																						
	BENDING	$\sigma_n = \frac{M_b}{\left(\frac{D^3\pi}{32}\right) - \left(\frac{dD^3}{6}\right)}$	<i>d/D</i>										40												
			<table border="1" style="width: 100%; text-align: center;"> <tr> <td>0.0</td><td>0.05</td><td>0.10</td><td>0.15</td><td>0.20</td><td>0.25</td><td>0.30</td><td></td><td></td><td></td><td></td><td></td> </tr> <tr> <td>3</td><td>2.46</td><td>2.25</td><td>2.13</td><td>2.03</td><td>1.96</td><td>1.89</td><td></td><td></td><td></td><td></td><td></td> </tr> </table>	0.0	0.05	0.10	0.15	0.20	0.25	0.30							3	2.46	2.25	2.13	2.03	1.96	1.89		
0.0	0.05	0.10	0.15	0.20	0.25	0.30																			
3	2.46	2.25	2.13	2.03	1.96	1.89																			
	TORSION	$\tau_n = \frac{M_t}{\left(\frac{\pi D^3}{16}\right) - \left(\frac{dD^2}{6}\right)}$	<i>d/D</i>										41												
			<table border="1" style="width: 100%; text-align: center;"> <tr> <td>0</td><td>0.05</td><td>0.10</td><td>0.15</td><td>0.20</td><td>0.25</td><td>0.30</td><td></td><td></td><td></td><td></td><td></td> </tr> <tr> <td>2.0</td><td>1.78</td><td>1.66</td><td>1.57</td><td>1.50</td><td>1.46</td><td>1.42</td><td></td><td></td><td></td><td></td><td></td> </tr> </table>	0	0.05	0.10	0.15	0.20	0.25	0.30							2.0	1.78	1.66	1.57	1.50	1.46	1.42		
0	0.05	0.10	0.15	0.20	0.25	0.30																			
2.0	1.78	1.66	1.57	1.50	1.46	1.42																			
	TORSION	$\tau_n = \frac{M_t}{A}$	<i>r/t</i>										42												
			<table border="1" style="width: 100%; text-align: center;"> <tr> <td>0.1</td><td>0.2</td><td>0.3</td><td>0.4</td><td>0.6</td><td>0.8</td><td>1.0</td><td>1.2</td><td>1.4</td><td>1.5</td><td></td><td></td> </tr> <tr> <td>2.95</td><td>2.20</td><td>1.84</td><td>1.70</td><td>1.59</td><td>1.56</td><td>1.56</td><td>1.56</td><td>1.58</td><td>1.60</td><td></td><td></td> </tr> </table>	0.1	0.2	0.3	0.4	0.6	0.8	1.0	1.2	1.4		1.5			2.95	2.20	1.84	1.70	1.59	1.56	1.56	1.56	1.58
0.1	0.2	0.3	0.4	0.6	0.8	1.0	1.2	1.4	1.5																
2.95	2.20	1.84	1.70	1.59	1.56	1.56	1.56	1.58	1.60																

TABLE 12 (CONT.)

Form	Stress	Nominal stress	$\frac{\sigma_{max}}{\sigma_n} = K_t$																														
	INNER PAIR OF TENSILE FORCES P - P ACTING IN OPPOSITE DIRECTIONS	$\sigma_n = \frac{P}{2t(R_2 - R_1)} \left[1 + \frac{3(R_2 + R_1) \left(1 - \frac{2}{\pi} \right)}{R_2 - R_1} \right]$ <table border="1" data-bbox="1102 451 1478 1083"> <thead> <tr> <th colspan="2">At point A</th> </tr> <tr> <th>R_1/R_2</th> <th></th> </tr> </thead> <tbody> <tr><td>0.05</td><td>0.10</td></tr> <tr><td>0.15</td><td>0.20</td></tr> <tr><td>0.25</td><td>0.30</td></tr> <tr><td>0.30</td><td>0.40</td></tr> <tr><td>0.40</td><td>0.50</td></tr> <tr><td>0.50</td><td>0.60</td></tr> <tr><td>0.60</td><td>0.70</td></tr> <tr><td>2.68</td><td>2.40</td></tr> <tr><td>2.18</td><td>1.98</td></tr> <tr><td>1.82</td><td>1.79</td></tr> <tr><td>1.48</td><td>1.33</td></tr> <tr><td>1.23</td><td>1.17</td></tr> </tbody> </table>	At point A		R_1/R_2		0.05	0.10	0.15	0.20	0.25	0.30	0.30	0.40	0.40	0.50	0.50	0.60	0.60	0.70	2.68	2.40	2.18	1.98	1.82	1.79	1.48	1.33	1.23	1.17	43		
At point A																																	
R_1/R_2																																	
0.05	0.10																																
0.15	0.20																																
0.25	0.30																																
0.30	0.40																																
0.40	0.50																																
0.50	0.60																																
0.60	0.70																																
2.68	2.40																																
2.18	1.98																																
1.82	1.79																																
1.48	1.33																																
1.23	1.17																																
	PAIR OF COMPRESSIVE FORCES Q-Q ACTING IN OPPOSITE DIRECTIONS	$\sigma_n = \frac{3Q(R_2 + R_1)}{\pi t(R_2 - R_1)^2}$ <table border="1" data-bbox="654 451 1039 1083"> <thead> <tr> <th colspan="2">At point B</th> </tr> <tr> <th>R_1/R_2</th> <th></th> </tr> </thead> <tbody> <tr><td>0.05</td><td>0.10</td></tr> <tr><td>0.15</td><td>0.20</td></tr> <tr><td>0.25</td><td>0.30</td></tr> <tr><td>0.30</td><td>0.40</td></tr> <tr><td>0.40</td><td>0.50</td></tr> <tr><td>0.50</td><td>0.60</td></tr> <tr><td>0.60</td><td>0.70</td></tr> <tr><td>1.70</td><td>1.50</td></tr> <tr><td>1.39</td><td>1.32</td></tr> <tr><td>1.26</td><td>1.22</td></tr> <tr><td>1.16</td><td>1.11</td></tr> <tr><td>1.11</td><td>1.07</td></tr> <tr><td>1.07</td><td>1.03</td></tr> </tbody> </table>	At point B		R_1/R_2		0.05	0.10	0.15	0.20	0.25	0.30	0.30	0.40	0.40	0.50	0.50	0.60	0.60	0.70	1.70	1.50	1.39	1.32	1.26	1.22	1.16	1.11	1.11	1.07	1.07	1.03	44
At point B																																	
R_1/R_2																																	
0.05	0.10																																
0.15	0.20																																
0.25	0.30																																
0.30	0.40																																
0.40	0.50																																
0.50	0.60																																
0.60	0.70																																
1.70	1.50																																
1.39	1.32																																
1.26	1.22																																
1.16	1.11																																
1.11	1.07																																
1.07	1.03																																
	TORSION	$\tau_n = \frac{M_t}{A}$ <table border="1" data-bbox="206 451 591 1083"> <thead> <tr> <th colspan="2">r/t</th> </tr> </thead> <tbody> <tr><td>0.1</td><td>0.2</td></tr> <tr><td>0.3</td><td>0.4</td></tr> <tr><td>0.6</td><td>0.8</td></tr> <tr><td>1.0</td><td>1.2</td></tr> <tr><td>1.4</td><td>1.5</td></tr> <tr><td>2.75</td><td>2.22</td></tr> <tr><td>1.91</td><td>1.56</td></tr> <tr><td>1.37</td><td>1.25</td></tr> <tr><td>1.16</td><td>1.10</td></tr> <tr><td>1.10</td><td>1.08</td></tr> </tbody> </table>	r/t		0.1	0.2	0.3	0.4	0.6	0.8	1.0	1.2	1.4	1.5	2.75	2.22	1.91	1.56	1.37	1.25	1.16	1.10	1.10	1.08	45								
r/t																																	
0.1	0.2																																
0.3	0.4																																
0.6	0.8																																
1.0	1.2																																
1.4	1.5																																
2.75	2.22																																
1.91	1.56																																
1.37	1.25																																
1.16	1.10																																
1.10	1.08																																

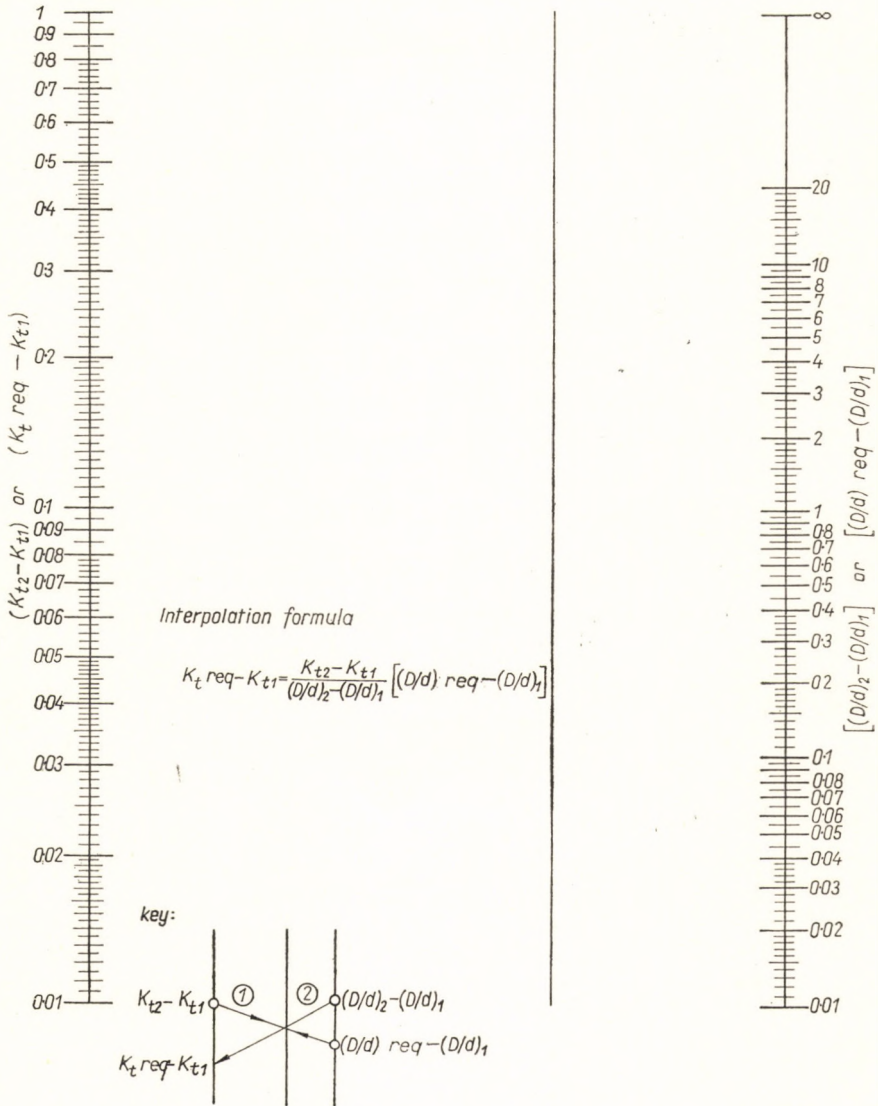


FIG. 61. Interpolation nomogram

TABLE 12

THEORETICAL STRESS CONCENTRATION FACTORS

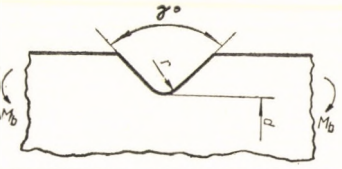
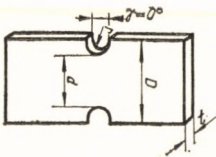
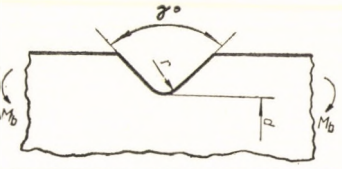
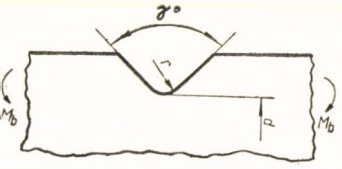
Form	Stress	Nominal stress	$\frac{\sigma_{\max}}{\sigma_n} = K_t$																																																																																										
 <p>Notched on both sides</p>	BENDING	Instructions on p. 39 in the "Notes on Table 12"	<table border="1"> <thead> <tr> <th colspan="13">K_t when $\gamma = 0^\circ$</th> </tr> <tr> <th>r/d</th> <th>1.4</th> <th>1.6</th> <th>1.8</th> <th>2.0</th> <th>2.2</th> <th>2.4</th> <th>2.6</th> <th>2.8</th> <th>3.0</th> <th>3.2</th> </tr> </thead> <tbody> <tr> <td>90°</td> <td></td> <td></td> <td></td> <td></td> <td></td> <td>2.37</td> <td>2.56</td> <td>2.75</td> <td>2.93</td> <td>3.12</td> </tr> <tr> <td>120°</td> <td></td> <td></td> <td>1.76</td> <td>1.92</td> <td>2.08</td> <td>2.24</td> <td>2.40</td> <td>2.54</td> <td>2.68</td> <td>2.82</td> </tr> <tr> <td>140°</td> <td>1.39</td> <td>1.50</td> <td>1.64</td> <td>1.75</td> <td>1.86</td> <td>1.96</td> <td>2.07</td> <td>2.16</td> <td>2.26</td> <td>2.35</td> </tr> <tr> <td>150°</td> <td>1.36</td> <td>1.44</td> <td>1.54</td> <td>1.64</td> <td>1.72</td> <td>1.80</td> <td>1.88</td> <td>1.95</td> <td>2.00</td> <td>2.06</td> </tr> <tr> <td>160°</td> <td>1.26</td> <td>1.36</td> <td>1.42</td> <td>1.48</td> <td>1.53</td> <td>1.57</td> <td>1.62</td> <td>1.65</td> <td>1.69</td> <td>1.73</td> </tr> <tr> <td>170°</td> <td>1.20</td> <td>1.26</td> <td>1.30</td> <td>1.33</td> <td>1.35</td> <td>1.37</td> <td>1.39</td> <td>1.40</td> <td>1.42</td> <td>1.43</td> </tr> </tbody> </table>	K_t when $\gamma = 0^\circ$													r/d	1.4	1.6	1.8	2.0	2.2	2.4	2.6	2.8	3.0	3.2	90°						2.37	2.56	2.75	2.93	3.12	120°			1.76	1.92	2.08	2.24	2.40	2.54	2.68	2.82	140°	1.39	1.50	1.64	1.75	1.86	1.96	2.07	2.16	2.26	2.35	150°	1.36	1.44	1.54	1.64	1.72	1.80	1.88	1.95	2.00	2.06	160°	1.26	1.36	1.42	1.48	1.53	1.57	1.62	1.65	1.69	1.73	170°	1.20	1.26	1.30	1.33	1.35	1.37	1.39	1.40	1.42	1.43
				K_t when $\gamma = 0^\circ$																																																																																									
r/d	1.4	1.6	1.8	2.0	2.2	2.4	2.6	2.8	3.0	3.2																																																																																			
90°						2.37	2.56	2.75	2.93	3.12																																																																																			
120°			1.76	1.92	2.08	2.24	2.40	2.54	2.68	2.82																																																																																			
140°	1.39	1.50	1.64	1.75	1.86	1.96	2.07	2.16	2.26	2.35																																																																																			
150°	1.36	1.44	1.54	1.64	1.72	1.80	1.88	1.95	2.00	2.06																																																																																			
160°	1.26	1.36	1.42	1.48	1.53	1.57	1.62	1.65	1.69	1.73																																																																																			
170°	1.20	1.26	1.30	1.33	1.35	1.37	1.39	1.40	1.42	1.43																																																																																			
 <p>Notched on both sides</p>	BENDING	$\sigma_n = \frac{6M_b}{d^2 t}$	<table border="1"> <thead> <tr> <th colspan="13">K_t when $\gamma = 0^\circ$</th> </tr> <tr> <th>r/d</th> <th>1.4</th> <th>1.6</th> <th>1.8</th> <th>2.0</th> <th>2.2</th> <th>2.4</th> <th>2.6</th> <th>2.8</th> <th>3.0</th> <th>3.2</th> </tr> </thead> <tbody> <tr> <td>90°</td> <td></td> <td></td> <td></td> <td></td> <td></td> <td>2.37</td> <td>2.56</td> <td>2.75</td> <td>2.93</td> <td>3.12</td> </tr> <tr> <td>120°</td> <td></td> <td></td> <td>1.76</td> <td>1.92</td> <td>2.08</td> <td>2.24</td> <td>2.40</td> <td>2.54</td> <td>2.68</td> <td>2.82</td> </tr> <tr> <td>140°</td> <td>1.39</td> <td>1.50</td> <td>1.64</td> <td>1.75</td> <td>1.86</td> <td>1.96</td> <td>2.07</td> <td>2.16</td> <td>2.26</td> <td>2.35</td> </tr> <tr> <td>150°</td> <td>1.36</td> <td>1.44</td> <td>1.54</td> <td>1.64</td> <td>1.72</td> <td>1.80</td> <td>1.88</td> <td>1.95</td> <td>2.00</td> <td>2.06</td> </tr> <tr> <td>160°</td> <td>1.26</td> <td>1.36</td> <td>1.42</td> <td>1.48</td> <td>1.53</td> <td>1.57</td> <td>1.62</td> <td>1.65</td> <td>1.69</td> <td>1.73</td> </tr> <tr> <td>170°</td> <td>1.20</td> <td>1.26</td> <td>1.30</td> <td>1.33</td> <td>1.35</td> <td>1.37</td> <td>1.39</td> <td>1.40</td> <td>1.42</td> <td>1.43</td> </tr> </tbody> </table>	K_t when $\gamma = 0^\circ$													r/d	1.4	1.6	1.8	2.0	2.2	2.4	2.6	2.8	3.0	3.2	90°						2.37	2.56	2.75	2.93	3.12	120°			1.76	1.92	2.08	2.24	2.40	2.54	2.68	2.82	140°	1.39	1.50	1.64	1.75	1.86	1.96	2.07	2.16	2.26	2.35	150°	1.36	1.44	1.54	1.64	1.72	1.80	1.88	1.95	2.00	2.06	160°	1.26	1.36	1.42	1.48	1.53	1.57	1.62	1.65	1.69	1.73	170°	1.20	1.26	1.30	1.33	1.35	1.37	1.39	1.40	1.42	1.43
				K_t when $\gamma = 0^\circ$																																																																																									
r/d	1.4	1.6	1.8	2.0	2.2	2.4	2.6	2.8	3.0	3.2																																																																																			
90°						2.37	2.56	2.75	2.93	3.12																																																																																			
120°			1.76	1.92	2.08	2.24	2.40	2.54	2.68	2.82																																																																																			
140°	1.39	1.50	1.64	1.75	1.86	1.96	2.07	2.16	2.26	2.35																																																																																			
150°	1.36	1.44	1.54	1.64	1.72	1.80	1.88	1.95	2.00	2.06																																																																																			
160°	1.26	1.36	1.42	1.48	1.53	1.57	1.62	1.65	1.69	1.73																																																																																			
170°	1.20	1.26	1.30	1.33	1.35	1.37	1.39	1.40	1.42	1.43																																																																																			
 <p>Notched on both sides</p>	TENSION	$\sigma_n = \frac{P}{dt}$	<table border="1"> <thead> <tr> <th colspan="13">K_t when $\gamma = 0^\circ$</th> </tr> <tr> <th>r/d</th> <th>1.4</th> <th>1.6</th> <th>1.8</th> <th>2.0</th> <th>2.2</th> <th>2.4</th> <th>2.6</th> <th>2.8</th> <th>3.0</th> <th>3.2</th> </tr> </thead> <tbody> <tr> <td>90°</td> <td></td> <td></td> <td></td> <td></td> <td></td> <td>2.37</td> <td>2.56</td> <td>2.75</td> <td>2.93</td> <td>3.12</td> </tr> <tr> <td>120°</td> <td></td> <td></td> <td>1.76</td> <td>1.92</td> <td>2.08</td> <td>2.24</td> <td>2.40</td> <td>2.54</td> <td>2.68</td> <td>2.82</td> </tr> <tr> <td>140°</td> <td>1.39</td> <td>1.50</td> <td>1.64</td> <td>1.75</td> <td>1.86</td> <td>1.96</td> <td>2.07</td> <td>2.16</td> <td>2.26</td> <td>2.35</td> </tr> <tr> <td>150°</td> <td>1.36</td> <td>1.44</td> <td>1.54</td> <td>1.64</td> <td>1.72</td> <td>1.80</td> <td>1.88</td> <td>1.95</td> <td>2.00</td> <td>2.06</td> </tr> <tr> <td>160°</td> <td>1.26</td> <td>1.36</td> <td>1.42</td> <td>1.48</td> <td>1.53</td> <td>1.57</td> <td>1.62</td> <td>1.65</td> <td>1.69</td> <td>1.73</td> </tr> <tr> <td>170°</td> <td>1.20</td> <td>1.26</td> <td>1.30</td> <td>1.33</td> <td>1.35</td> <td>1.37</td> <td>1.39</td> <td>1.40</td> <td>1.42</td> <td>1.43</td> </tr> </tbody> </table>	K_t when $\gamma = 0^\circ$													r/d	1.4	1.6	1.8	2.0	2.2	2.4	2.6	2.8	3.0	3.2	90°						2.37	2.56	2.75	2.93	3.12	120°			1.76	1.92	2.08	2.24	2.40	2.54	2.68	2.82	140°	1.39	1.50	1.64	1.75	1.86	1.96	2.07	2.16	2.26	2.35	150°	1.36	1.44	1.54	1.64	1.72	1.80	1.88	1.95	2.00	2.06	160°	1.26	1.36	1.42	1.48	1.53	1.57	1.62	1.65	1.69	1.73	170°	1.20	1.26	1.30	1.33	1.35	1.37	1.39	1.40	1.42	1.43
				K_t when $\gamma = 0^\circ$																																																																																									
r/d	1.4	1.6	1.8	2.0	2.2	2.4	2.6	2.8	3.0	3.2																																																																																			
90°						2.37	2.56	2.75	2.93	3.12																																																																																			
120°			1.76	1.92	2.08	2.24	2.40	2.54	2.68	2.82																																																																																			
140°	1.39	1.50	1.64	1.75	1.86	1.96	2.07	2.16	2.26	2.35																																																																																			
150°	1.36	1.44	1.54	1.64	1.72	1.80	1.88	1.95	2.00	2.06																																																																																			
160°	1.26	1.36	1.42	1.48	1.53	1.57	1.62	1.65	1.69	1.73																																																																																			
170°	1.20	1.26	1.30	1.33	1.35	1.37	1.39	1.40	1.42	1.43																																																																																			
 <p>Notched on both sides</p>	TENSION	$\sigma_n = \frac{P}{dt}$	<table border="1"> <thead> <tr> <th colspan="13">K_t when $\gamma = 0^\circ$</th> </tr> <tr> <th>r/d</th> <th>1.4</th> <th>1.6</th> <th>1.8</th> <th>2.0</th> <th>2.2</th> <th>2.4</th> <th>2.6</th> <th>2.8</th> <th>3.0</th> <th>3.2</th> </tr> </thead> <tbody> <tr> <td>90°</td> <td></td> <td></td> <td></td> <td></td> <td></td> <td>2.37</td> <td>2.56</td> <td>2.75</td> <td>2.93</td> <td>3.12</td> </tr> <tr> <td>120°</td> <td></td> <td></td> <td>1.76</td> <td>1.92</td> <td>2.08</td> <td>2.24</td> <td>2.40</td> <td>2.54</td> <td>2.68</td> <td>2.82</td> </tr> <tr> <td>140°</td> <td>1.39</td> <td>1.50</td> <td>1.64</td> <td>1.75</td> <td>1.86</td> <td>1.96</td> <td>2.07</td> <td>2.16</td> <td>2.26</td> <td>2.35</td> </tr> <tr> <td>150°</td> <td>1.36</td> <td>1.44</td> <td>1.54</td> <td>1.64</td> <td>1.72</td> <td>1.80</td> <td>1.88</td> <td>1.95</td> <td>2.00</td> <td>2.06</td> </tr> <tr> <td>160°</td> <td>1.26</td> <td>1.36</td> <td>1.42</td> <td>1.48</td> <td>1.53</td> <td>1.57</td> <td>1.62</td> <td>1.65</td> <td>1.69</td> <td>1.73</td> </tr> <tr> <td>170°</td> <td>1.20</td> <td>1.26</td> <td>1.30</td> <td>1.33</td> <td>1.35</td> <td>1.37</td> <td>1.39</td> <td>1.40</td> <td>1.42</td> <td>1.43</td> </tr> </tbody> </table>	K_t when $\gamma = 0^\circ$													r/d	1.4	1.6	1.8	2.0	2.2	2.4	2.6	2.8	3.0	3.2	90°						2.37	2.56	2.75	2.93	3.12	120°			1.76	1.92	2.08	2.24	2.40	2.54	2.68	2.82	140°	1.39	1.50	1.64	1.75	1.86	1.96	2.07	2.16	2.26	2.35	150°	1.36	1.44	1.54	1.64	1.72	1.80	1.88	1.95	2.00	2.06	160°	1.26	1.36	1.42	1.48	1.53	1.57	1.62	1.65	1.69	1.73	170°	1.20	1.26	1.30	1.33	1.35	1.37	1.39	1.40	1.42	1.43
				K_t when $\gamma = 0^\circ$																																																																																									
r/d	1.4	1.6	1.8	2.0	2.2	2.4	2.6	2.8	3.0	3.2																																																																																			
90°						2.37	2.56	2.75	2.93	3.12																																																																																			
120°			1.76	1.92	2.08	2.24	2.40	2.54	2.68	2.82																																																																																			
140°	1.39	1.50	1.64	1.75	1.86	1.96	2.07	2.16	2.26	2.35																																																																																			
150°	1.36	1.44	1.54	1.64	1.72	1.80	1.88	1.95	2.00	2.06																																																																																			
160°	1.26	1.36	1.42	1.48	1.53	1.57	1.62	1.65	1.69	1.73																																																																																			
170°	1.20	1.26	1.30	1.33	1.35	1.37	1.39	1.40	1.42	1.43																																																																																			

TABLE 12 (CONT.)

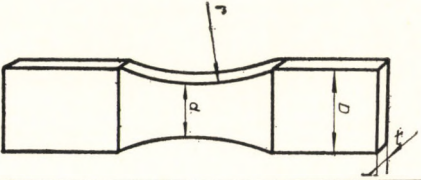
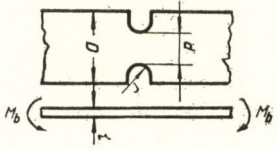
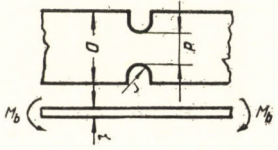
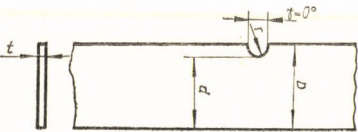
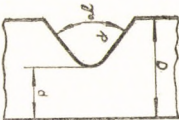
Form	Stress	Nominal stress	$\frac{\sigma_{\max}}{\sigma_n} = K_t$												
	TENSION	$\sigma_n = \frac{P}{dt}$	<i>D/d</i>												
			<i>r/d</i>												
			∞	1.1	1.05	1.02	1.01								
			0.4		1.47	1.39	1.28	1.21							
			0.5		1.41	1.34	1.25	1.18							
			0.6	1.46	1.36	1.31	1.22	1.16							
			0.8	1.36	1.30	1.25	1.18	1.13							
			1.0	1.30	1.25	1.21	1.16	1.11							
			2.0	1.16	1.14	1.12	1.09	1.07							
				BENDING	$\sigma_n = \frac{6M_b}{d^2t}$	<i>D/d</i>									
						<i>r/d</i>									
						∞	1.1	1.05	1.02	1.01					
0.4	1.40	1.35				1.32	1.26	1.21							
0.5	1.33	1.29				1.27	1.22	1.18							
0.6	1.28	1.25				1.23	1.19	1.15							
0.8	1.22	1.19				1.17	1.15	1.12							
1.0	1.17	1.16				1.15	1.12	1.10							
2.0	1.09	1.09				1.08	1.07	1.06							
	BENDING PERPENDICULAR TO PLANE OF SHEET	$\sigma_n = \frac{6M_b}{dt^2}$				<i>D/d</i>									
						<i>r/d</i>									
						∞	2.0	1.50	1.25	1.10	1.05	1.02			
			0.02	2.96	2.77	2.61	2.41	2.10	1.85	1.58					
			0.04	2.20	2.11	2.04	1.93	1.74	1.58	1.43					
			0.06	1.88	1.82	1.78	1.71	1.59	1.47	1.35					
			0.08	1.70	1.66	1.64	1.59	1.49	1.40	1.30					
			0.10	1.60	1.57	1.54	1.51	1.43	1.37	1.27					

TABLE 12 (CONT.)

Form	Stress	Nominal stress	$\frac{\sigma_{max}}{\sigma_n} = K_t$																																																																																																																
 <p>Angle subtended by notch sides $\gamma^\circ = 0$</p>	TENSION	$\sigma_n = \frac{P}{dt}$	No data available as yet																																																																																																																
	BENDING	$\sigma_n = \frac{6M_b}{d^2t}$																																																																																																																	
 <p>Notched on one side</p>	BENDING	Instructions on p. 39 in the "Notes on Table 12"	<table border="1"> <thead> <tr> <th rowspan="2">K_t</th> <th colspan="11">γ</th> </tr> <tr> <th>$\gamma = 0$</th> <th>60°</th> <th>90°</th> <th>100°</th> <th>110°</th> <th>120°</th> <th>130°</th> <th>140°</th> <th>150°</th> <th>160°</th> <th>170°</th> </tr> </thead> <tbody> <tr> <td>0.04</td> <td></td> <td></td> <td></td> <td></td> <td></td> <td></td> <td></td> <td></td> <td></td> <td></td> <td></td> <td></td> </tr> <tr> <td>0.08</td> <td></td> <td></td> <td>2.84</td> <td>2.78</td> <td>2.71</td> <td>2.54</td> <td>2.38</td> <td>2.08</td> <td>1.70</td> <td>1.42</td> <td></td> <td></td> </tr> <tr> <td>0.12</td> <td>2.42</td> <td>2.38</td> <td>2.34</td> <td>2.27</td> <td>2.13</td> <td>2.03</td> <td>1.82</td> <td>1.54</td> <td>1.27</td> <td></td> <td></td> <td></td> </tr> <tr> <td>0.20</td> <td>1.99</td> <td>1.97</td> <td>1.94</td> <td>1.90</td> <td>1.80</td> <td>1.72</td> <td>1.56</td> <td>1.35</td> <td>1.18</td> <td></td> <td></td> <td></td> </tr> <tr> <td>0.40</td> <td>1.60</td> <td>1.60</td> <td>1.59</td> <td>1.58</td> <td>1.50</td> <td>1.43</td> <td>1.30</td> <td>1.20</td> <td>1.11</td> <td></td> <td></td> <td></td> </tr> <tr> <td>0.60</td> <td>1.42</td> <td>1.42</td> <td>1.42</td> <td>1.41</td> <td>1.38</td> <td>1.31</td> <td>1.20</td> <td>1.12</td> <td>1.06</td> <td></td> <td></td> <td></td> </tr> </tbody> </table>												K_t	γ											$\gamma = 0$	60°	90°	100°	110°	120°	130°	140°	150°	160°	170°	0.04													0.08			2.84	2.78	2.71	2.54	2.38	2.08	1.70	1.42			0.12	2.42	2.38	2.34	2.27	2.13	2.03	1.82	1.54	1.27				0.20	1.99	1.97	1.94	1.90	1.80	1.72	1.56	1.35	1.18				0.40	1.60	1.60	1.59	1.58	1.50	1.43	1.30	1.20	1.11				0.60	1.42	1.42	1.42	1.41	1.38	1.31	1.20	1.12	1.06			
			K_t	γ																																																																																																															
$\gamma = 0$	60°	90°		100°	110°	120°	130°	140°	150°	160°	170°																																																																																																								
0.04																																																																																																																			
0.08			2.84	2.78	2.71	2.54	2.38	2.08	1.70	1.42																																																																																																									
0.12	2.42	2.38	2.34	2.27	2.13	2.03	1.82	1.54	1.27																																																																																																										
0.20	1.99	1.97	1.94	1.90	1.80	1.72	1.56	1.35	1.18																																																																																																										
0.40	1.60	1.60	1.59	1.58	1.50	1.43	1.30	1.20	1.11																																																																																																										
0.60	1.42	1.42	1.42	1.41	1.38	1.31	1.20	1.12	1.06																																																																																																										
			<table border="1"> <thead> <tr> <th rowspan="2">K_t</th> <th colspan="11">γ</th> </tr> <tr> <th>$\gamma = 0$</th> <th>60°</th> <th>90°</th> <th>100°</th> <th>110°</th> <th>120°</th> <th>130°</th> <th>140°</th> <th>150°</th> <th>160°</th> <th>170°</th> </tr> </thead> <tbody> <tr> <td>3.4</td> <td>3.38</td> <td>3.27</td> <td>3.22</td> <td>3.10</td> <td>2.95</td> <td>2.70</td> <td>2.45</td> <td>2.11</td> <td>1.78</td> <td>1.44</td> <td></td> <td></td> </tr> </tbody> </table>												K_t	γ											$\gamma = 0$	60°	90°	100°	110°	120°	130°	140°	150°	160°	170°	3.4	3.38	3.27	3.22	3.10	2.95	2.70	2.45	2.11	1.78	1.44																																																																			
K_t	γ																																																																																																																		
	$\gamma = 0$	60°	90°	100°	110°	120°	130°	140°	150°	160°	170°																																																																																																								
3.4	3.38	3.27	3.22	3.10	2.95	2.70	2.45	2.11	1.78	1.44																																																																																																									

7

8

9

TABLE 12 (CONT.)

Form	Stress	Nominal stress	$\frac{\sigma_{\max}}{\sigma_n} = K_t$												
TENSION	$\sigma_n = \frac{4P}{d^2\pi}$	$\sigma_n = \frac{32M_b}{d^3\pi}$	<i>D/d</i>												
			<i>r/d</i>	∞	2.00	1.50	1.30	1.20	1.10	1.05	1.02	1.01			
			0.04					2.70	2.37	2.15	1.94	1.70			
			0.10	2.45	2.39	2.33	2.27	2.18	2.01	1.81	1.68	1.58	1.42		
			0.15	2.08	2.04	1.99	1.95	1.90	1.78	1.64	1.55	1.47	1.33		
			0.20	1.86	1.83	1.80	1.77	1.73	1.65	1.54	1.46	1.40	1.28		
			0.25	1.72	1.69	1.67	1.65	1.62	1.55	1.46	1.40	1.34	1.24		
			0.30	1.61	1.59	1.58	1.55	1.53	1.47	1.40	1.36	1.31	1.22	10	
						<i>D/d</i>									
<i>r/d</i>	∞	2.00	1.50	1.30	1.20	1.10	1.05	1.03	1.02	1.01					
0.04	2.83	2.79	2.74	2.70	2.61	2.45	2.22	2.02	1.88	1.66					
0.10	1.99	1.98	1.96	1.92	1.89	1.81	1.70	1.61	1.53	1.41					
0.15	1.75	1.74	1.72	1.70	1.69	1.63	1.56	1.49	1.42	1.33					
0.20	1.61	1.59	1.58	1.57	1.56	1.51	1.46	1.40	1.34	1.27					
0.25	1.49	1.48	1.47	1.46	1.45	1.42	1.38	1.34	1.29	1.23					
0.30	1.41	1.41	1.40	1.39	1.38	1.36	1.33	1.29	1.24	1.21	11				
			<i>D/d</i>												
<i>r/d</i>	∞	2.00	1.30	1.20	1.10	1.05	1.02	1.01							
0.04	1.97	1.93	1.89	1.85	1.74	1.61	1.45	1.33							
0.10	1.52	1.51	1.48	1.46	1.41	1.35	1.27	1.20							
0.15	1.39	1.38	1.37	1.35	1.32	1.27	1.21	1.16							
0.20	1.32	1.31	1.30	1.28	1.26	1.22	1.18	1.14							
0.25	1.27	1.26	1.25	1.24	1.22	1.19	1.16	1.13							
0.30	1.22	1.22	1.21	1.20	1.19	1.17	1.15	1.12							
			<i>D/d</i>												
<i>r/d</i>	∞	2.00	1.30	1.20	1.10	1.05	1.02	1.01							
0.04	1.97	1.93	1.89	1.85	1.74	1.61	1.45	1.33							
0.10	1.52	1.51	1.48	1.46	1.41	1.35	1.27	1.20							
0.15	1.39	1.38	1.37	1.35	1.32	1.27	1.21	1.16							
0.20	1.32	1.31	1.30	1.28	1.26	1.22	1.18	1.14							
0.25	1.27	1.26	1.25	1.24	1.22	1.19	1.16	1.13							
0.30	1.22	1.22	1.21	1.20	1.19	1.17	1.15	1.12							

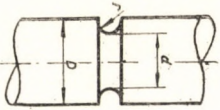
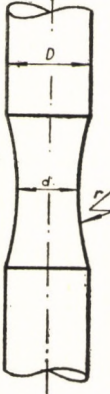


TABLE 12 (CONT.)

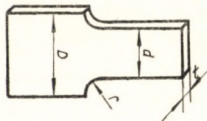
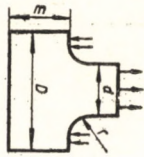
Form	Stress	Nominal stress	$\frac{\sigma_{\max}}{\sigma_n} = K_t$										
	TENSION	$\sigma_n = \frac{4P}{d^2\pi}$	<i>D/d</i>										
			<i>r/d</i>	∞	1.1	1.05	1.02	1.01					
			0.4	1.47	1.37	1.33	1.26	1.20					
			0.5	1.39	1.33	1.29	1.23	1.18					
			0.6	1.34	1.28	1.25	1.20	1.16					
			0.8	1.26	1.23	1.20	1.17	1.13					
			1.0	1.22	1.18	1.17	1.14	1.12					
	2.0	1.11	1.10	1.09	1.08	1.07							
	BENDING	$\sigma_n = \frac{32M_b}{d^3\pi}$	<i>D/d</i>										
			<i>r/d</i>	∞	1.1	1.05	1.02	1.01					
			0.4	1.32	1.29	1.27	1.20	1.17					
			0.5	1.27	1.24	1.22	1.18	1.15					
			0.6	1.22	1.21	1.19	1.16	1.13					
			0.8	1.17	1.16	1.15	1.12	1.11					
			1.0	1.14	1.13	1.12	1.10	1.09					
	2.0	1.07	1.07	1.06	1.06	1.05							
	TORSION	$\tau_n = \frac{16M_t}{d^3\pi}$	<i>D/d</i>										
			<i>r/d</i>	∞	1.1	1.05	1.02	1.01					
0.4			1.18	1.16	1.14	1.12	1.09						
0.5			1.14	1.13	1.12	1.10	1.08						
0.6			1.12	1.11	1.10	1.08	1.07						
0.8			1.09	1.08	1.08	1.07	1.06						
1.0			1.08	1.08	1.07	1.06	1.05						
2.0	1.04	1.04	1.03	1.03	1.02								

13

14

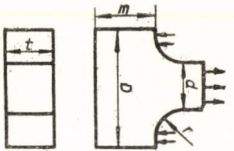
15

TABLE 12 (CONT.)

Form	Stress	Nominal stress	$\frac{\sigma_{max}}{\sigma_n} = K,$																									
	TENSION the forces are applied through the two end faces	$\sigma_n = \frac{P}{dt}$	D/d																									
			r/d	3.0	2.0	1.5	1.30	1.20	1.15	1.10	1.10	1.05	1.02	1.01	0.04		2.88	2.61	2.43	2.31	2.10	1.85	1.60	1.42				
	BENDING with support at the two end surfaces	$\sigma_n = \frac{6M_b}{d^2t}$	D/d																									
			r/d	6.0	3.0	2.0	1.30	1.20	1.10	1.05	1.03	1.02	1.01	0.04	2.85	2.69	2.51	2.37	2.20	2.08	1.92	1.84	1.75	1.62				
				0.10	2.04	1.94	1.85	1.78	1.71	1.65	1.57	1.52	1.46	1.37	0.10	2.04	1.94	1.85	1.78	1.71	1.65	1.57	1.52	1.46	1.37			
				0.15	1.74	1.68	1.63	1.60	1.55	1.52	1.46	1.41	1.36	1.28	0.15	1.74	1.68	1.63	1.60	1.55	1.52	1.46	1.41	1.36	1.28			
				0.20	1.57	1.53	1.50	1.48	1.46	1.43	1.38	1.34	1.30	1.23	0.20	1.57	1.53	1.50	1.48	1.46	1.43	1.38	1.34	1.30	1.23			
				0.25	1.47	1.44	1.42	1.40	1.38	1.37	1.34	1.30	1.26	1.20	0.25	1.47	1.44	1.42	1.40	1.38	1.37	1.34	1.30	1.26	1.20			
				0.30	1.40	1.38	1.37	1.35	1.34	1.33	1.30	1.27	1.24	1.18	1.17	0.30	1.40	1.38	1.37	1.35	1.34	1.33	1.30	1.27	1.24	1.18		
			$r/d = 0.05$																									
			m/d																									
					D/d	0.50	0.55	0.60	0.70	0.80	0.90	1.0	1.20	1.50	3.0													
TENSION		$\sigma_n = \frac{P}{dt}$																										
				1.5	9.50	8.90	8.45	7.55	6.95	6.50	6.30	6.25	6.20	6.10														
				1.8	10.85	10.05	9.40	8.20	7.25	6.40	5.85	5.70	5.50	5.30														
				2.1	12.20	11.20	10.30	8.90	7.70	6.65	5.90	5.60	5.20	4.85														
				2.4	13.60	12.30	11.30	9.55	8.20	7.0	6.20	5.65	5.0	4.55														
				2.7	15.0	13.45	12.20	10.20	8.70	7.50	6.55	5.80	5.0	4.30														
	3.0	16.40	14.55	13.15	10.90	9.20	7.90	6.95	6.0	5.10	4.10																	

T-shaped head
The two shoulders
resist the tensile
forces

TABLE 12 (CONT.)

Form	Stress	Nominal stress	$\frac{\sigma_{\max}}{\sigma_n} = K_t$										
 <p>T-shaped head The two shoulders resist the tensile forces</p>	TENSION	$\sigma_n = \frac{P}{dt}$	$r/d = 0.075$										
			m/d										
			D/d	0.50	0.55	0.60	0.70	0.80	0.90	1.0	1.20	1.50	3.0
			1.5										
			1.8	3.85	3.70	3.60	3.40	3.30	3.25	3.20	3.10	3.05	3.0
			2.1	5.15	4.70	4.40	3.85	3.45	3.15	2.95	2.80	2.65	2.50
			2.4	6.80	6.05	5.55	4.70	4.10	3.65	3.20	2.90	2.65	2.35
			2.7	7.60	6.80	6.15	5.25	4.50	4.0	3.65	3.25	2.90	2.40
			3.0	8.70	7.80	7.20	6.10	5.30	4.70	4.20	3.75	3.20	2.50
			$r/d = 0.100$										
			m/d										
			D/d	0.50	0.55	0.60	0.70	0.80	0.90	1.0	1.20	1.50	3.0
			1.5	6.85	6.45	6.10	5.60	5.40	5.20	5.05	4.90	4.75	4.70
			1.8	7.80	7.10	6.55	5.55	4.80	4.45	4.20	3.95	3.75	3.65
			2.1	8.70	7.90	7.10	7.0	5.05	4.55	4.10	3.80	3.50	3.20
			2.4	9.60	8.70	7.85	6.65	5.55	4.90	4.35	3.95	3.55	3.10
			2.7	10.55	9.45	8.70	7.40	6.20	5.50	4.80	4.30	3.75	3.0
			3.0	11.45	10.30	9.50	8.10	7.0	6.20	5.40	4.80	4.10	3.10
			$r/d = 0.200$										
m/d													
D/d	0.50	0.55	0.60	0.70	0.80	0.90	1.0	1.20	1.50	3.0			
1.5													

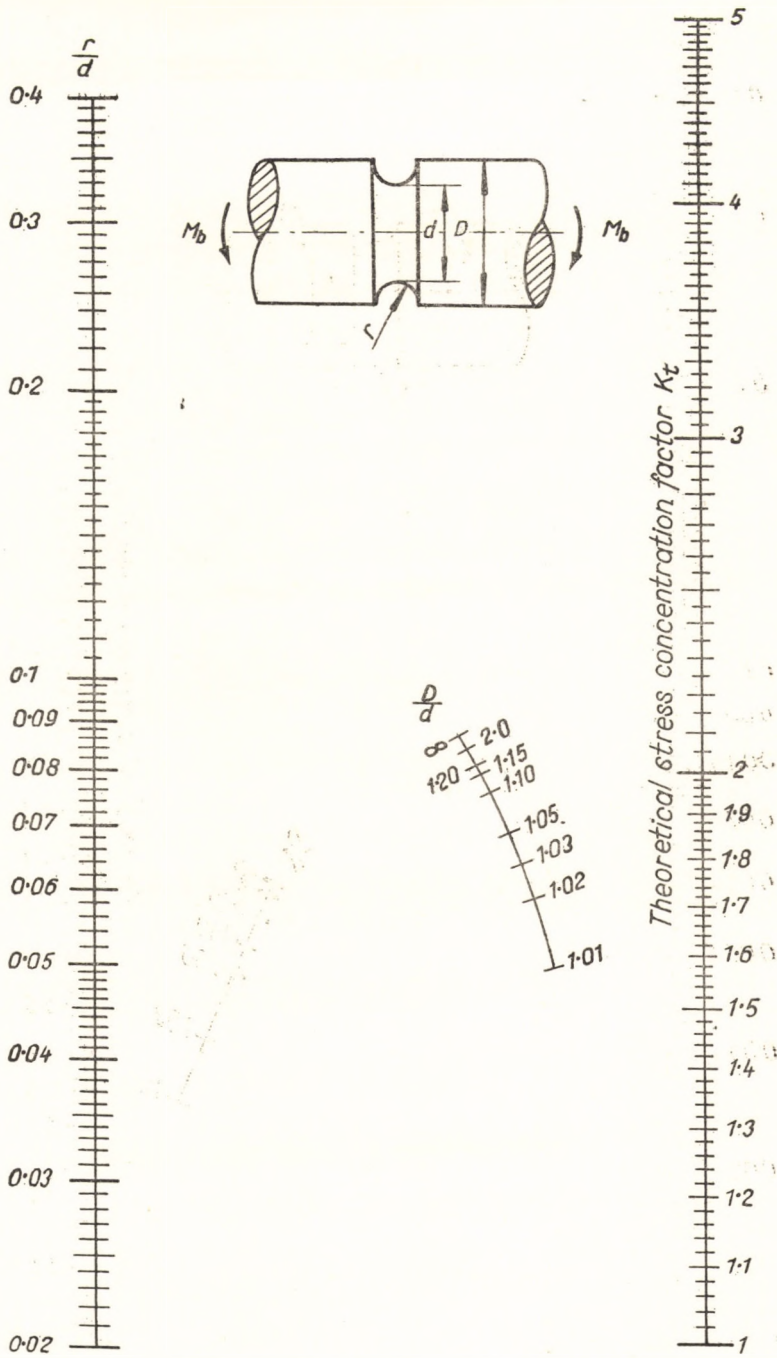


FIG. 72. Nomogram for K_t ; use in conjunction with Fig. 88 (in pocket inside cover of book)

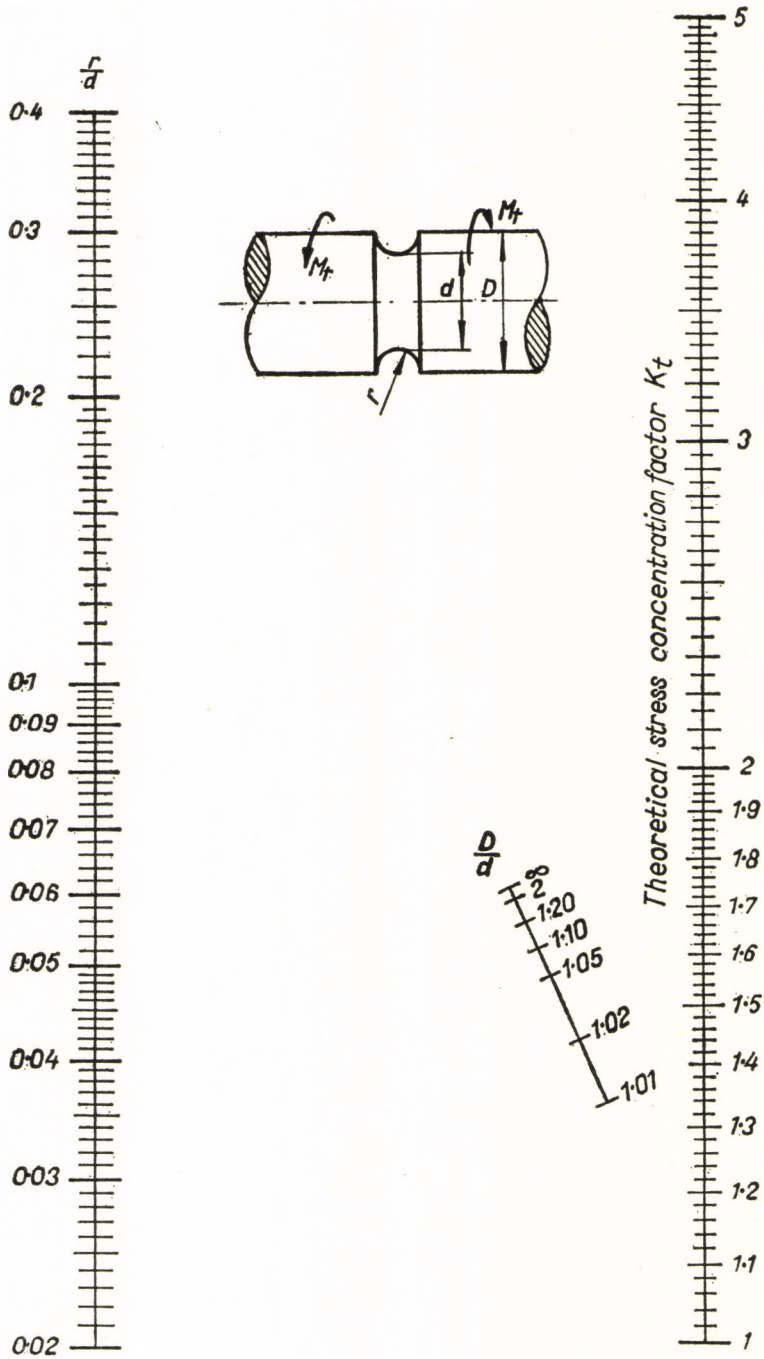


FIG. 73. Nomogram for K_t ; use in conjunction with Fig. 88 (in pocket inside cover of book)

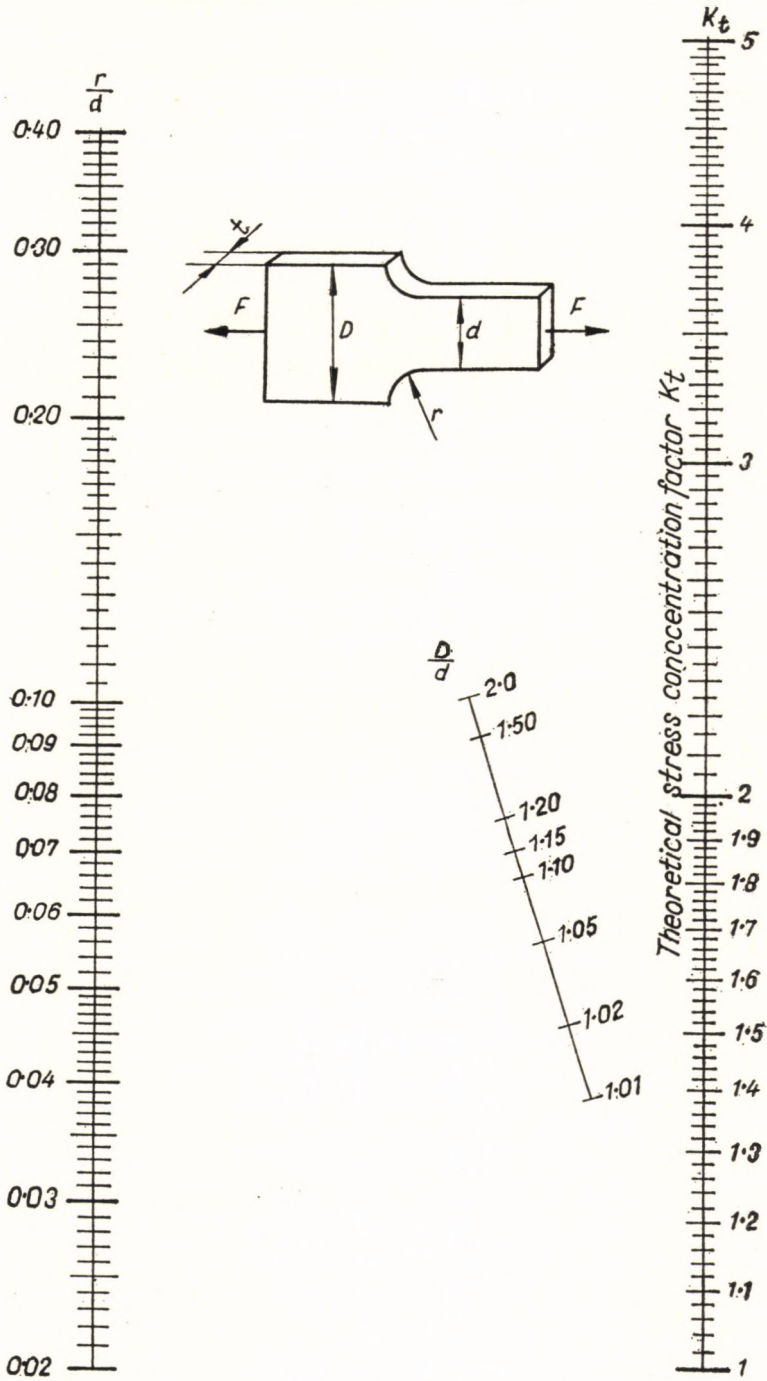


FIG. 74. Nomogram for K_t ; use in conjunction with Fig. 88 (in pocket inside cover of book)

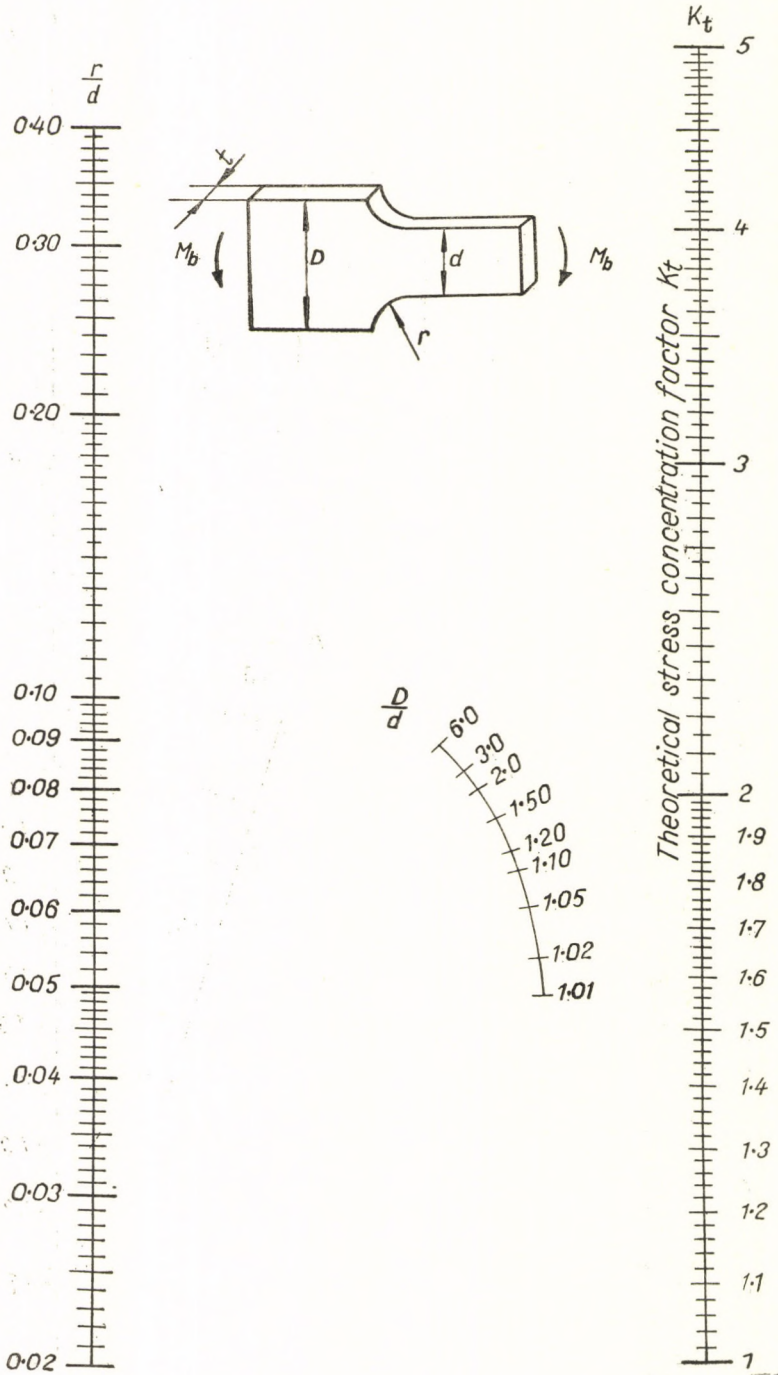


Fig. 75. Nomogram for K_t ; use in conjunction with Fig. 88
(in pocket inside cover of book)

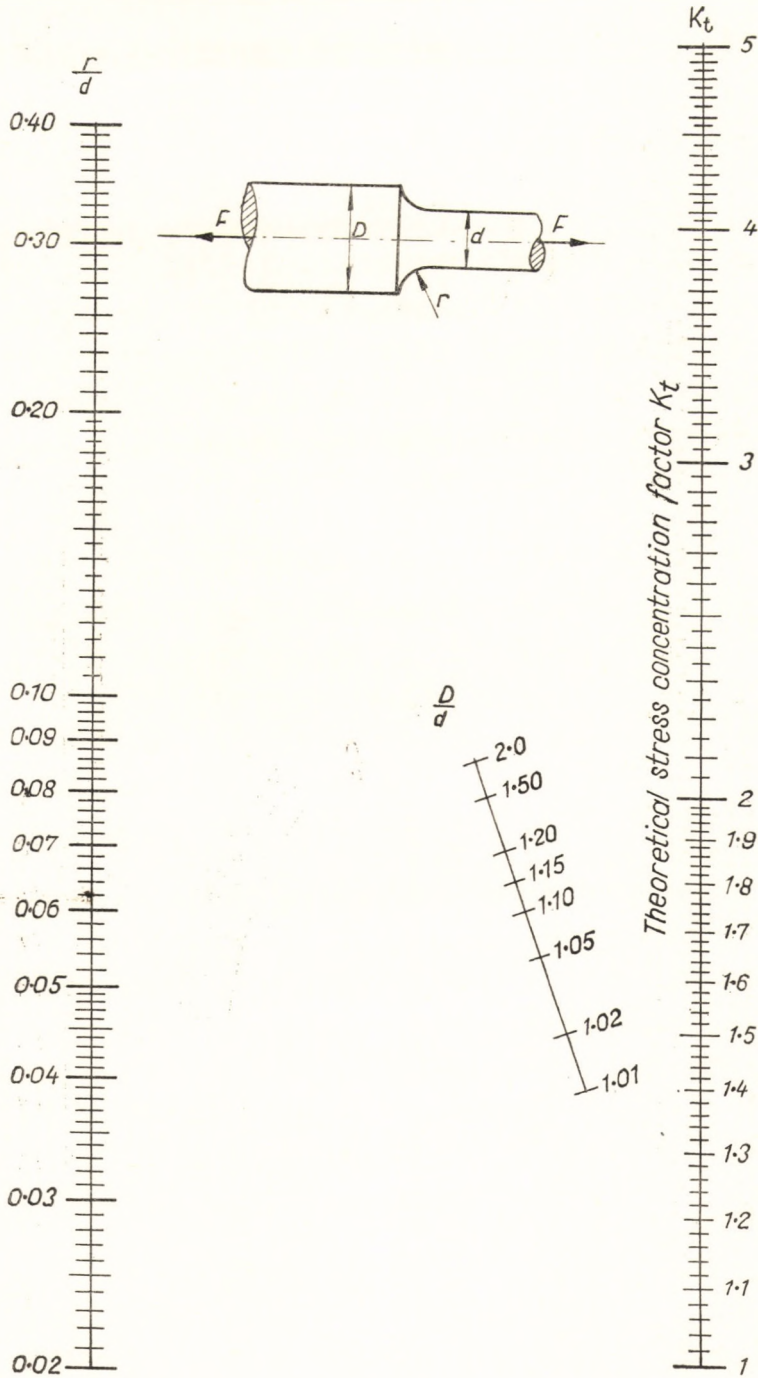


FIG. 76. Nomogram for K_t ; use in conjunction with Fig. 88 (in pocket inside cover of book)

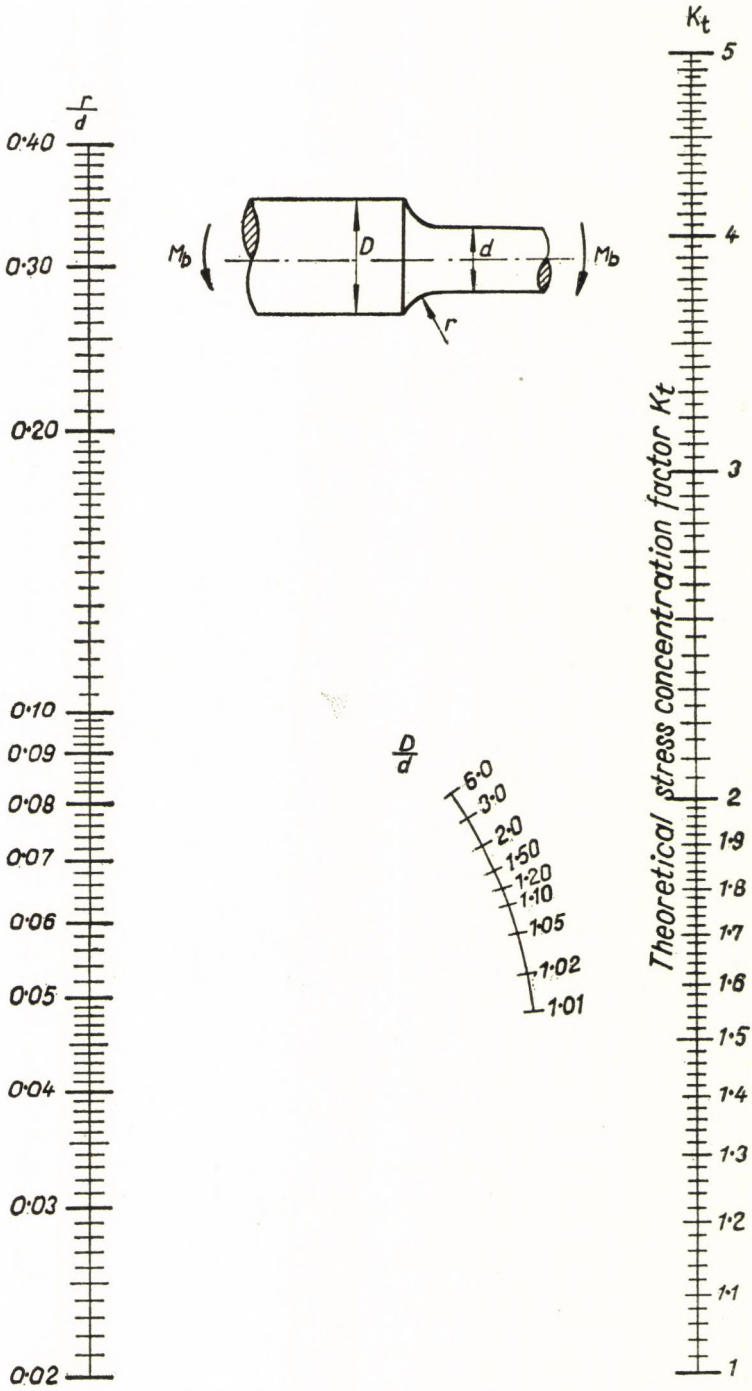


FIG. 77. Nomogram for K_t ; use in conjunction with Fig. 88 (in pocket inside cover of book)

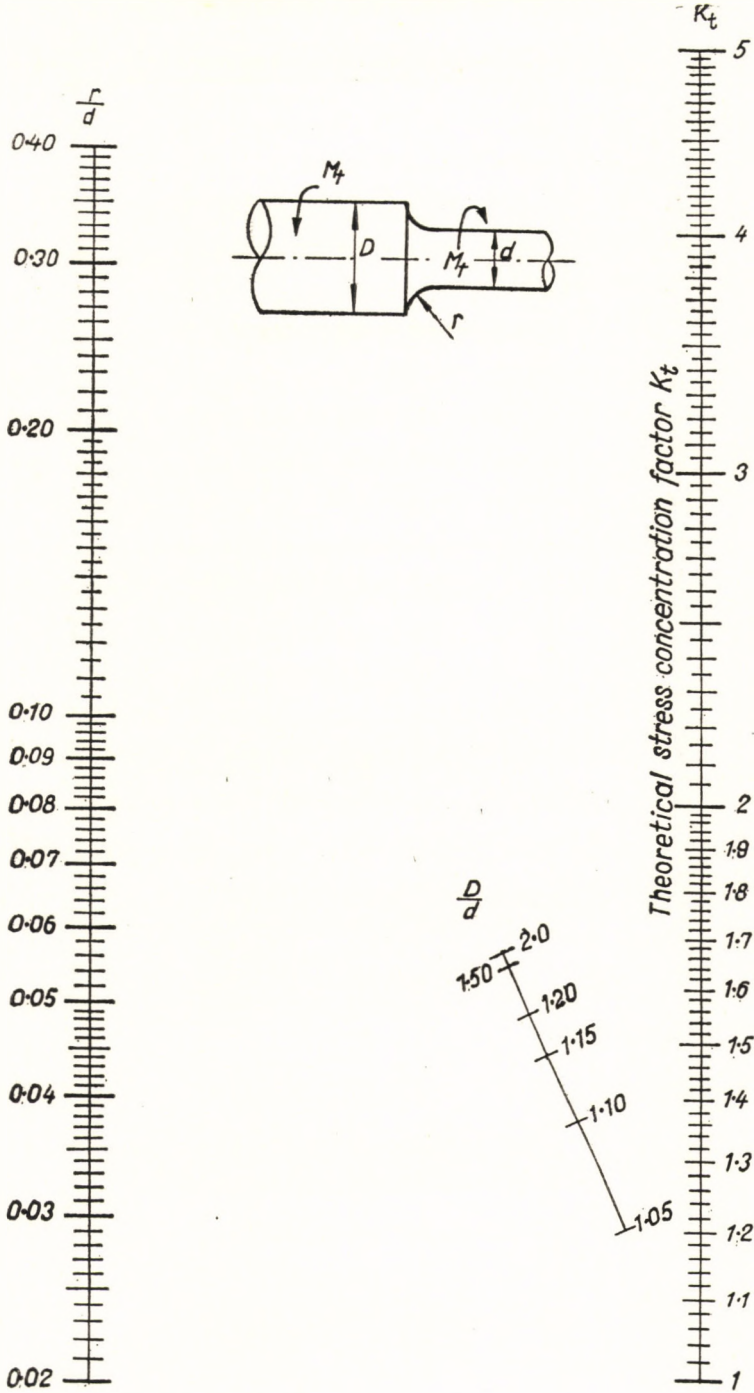


FIG. 78. Nomogram for K_t ; use in conjunction with Fig. 88 (in pocket inside cover of book)

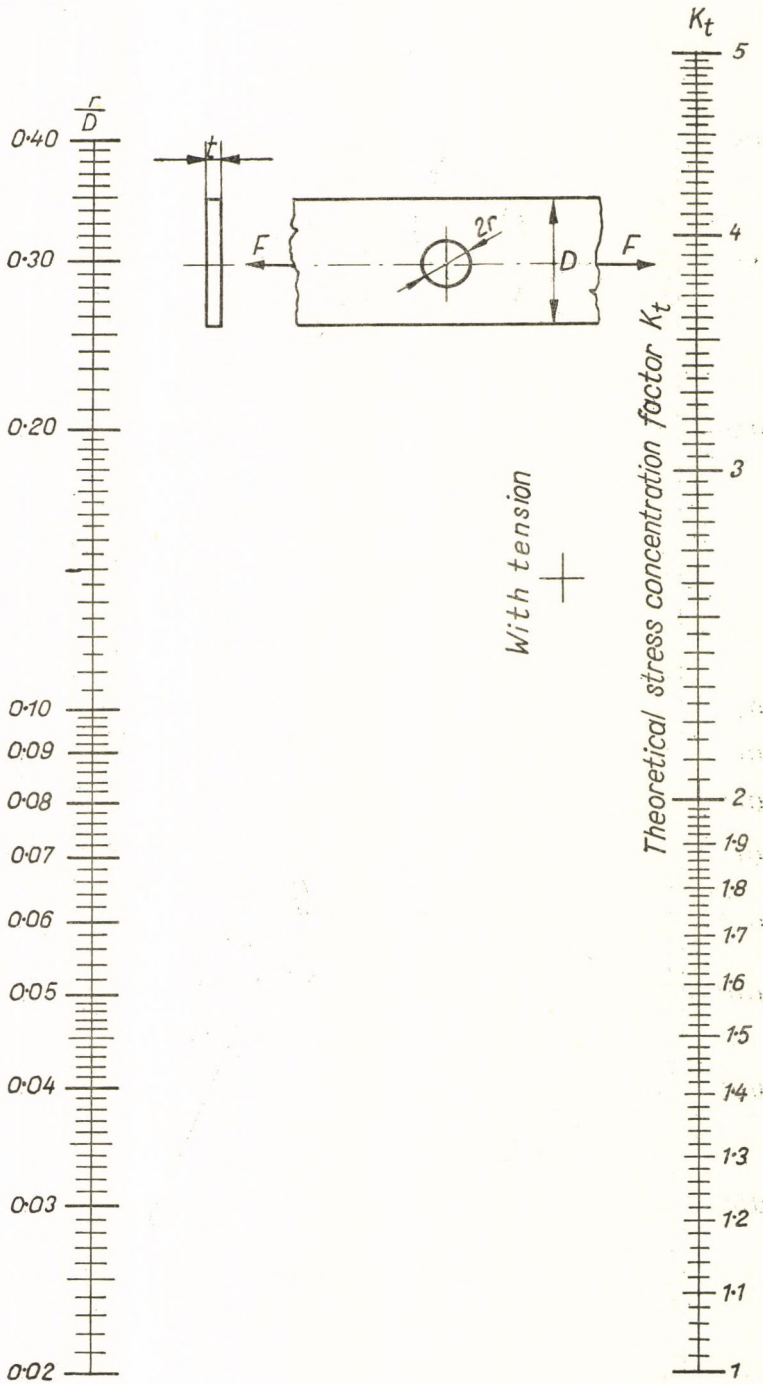


FIG. 79. Nomogram for K_t ; use in conjunction with Fig. 88
(in pocket inside cover of book)

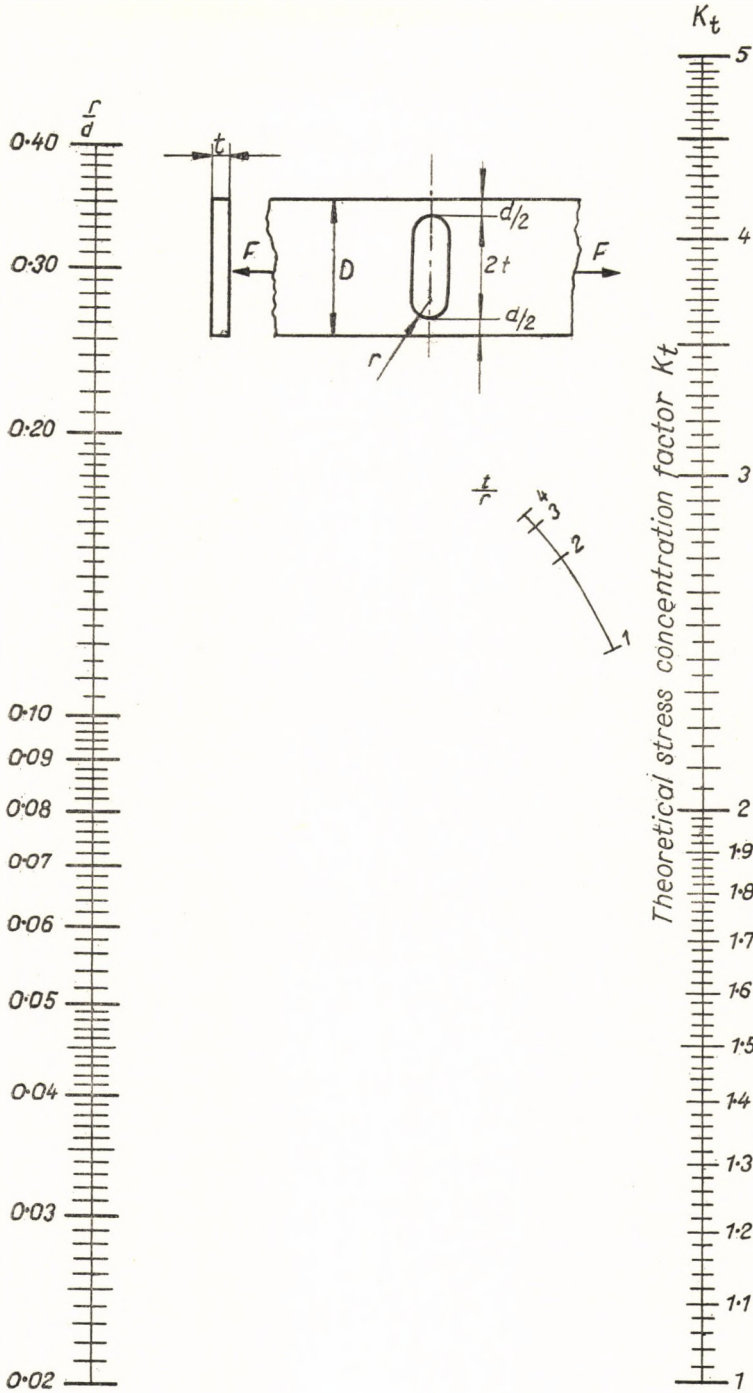


FIG. 80. Nomogram for K_t ; use in conjunction with Fig. 88 (in pocket inside cover of book)

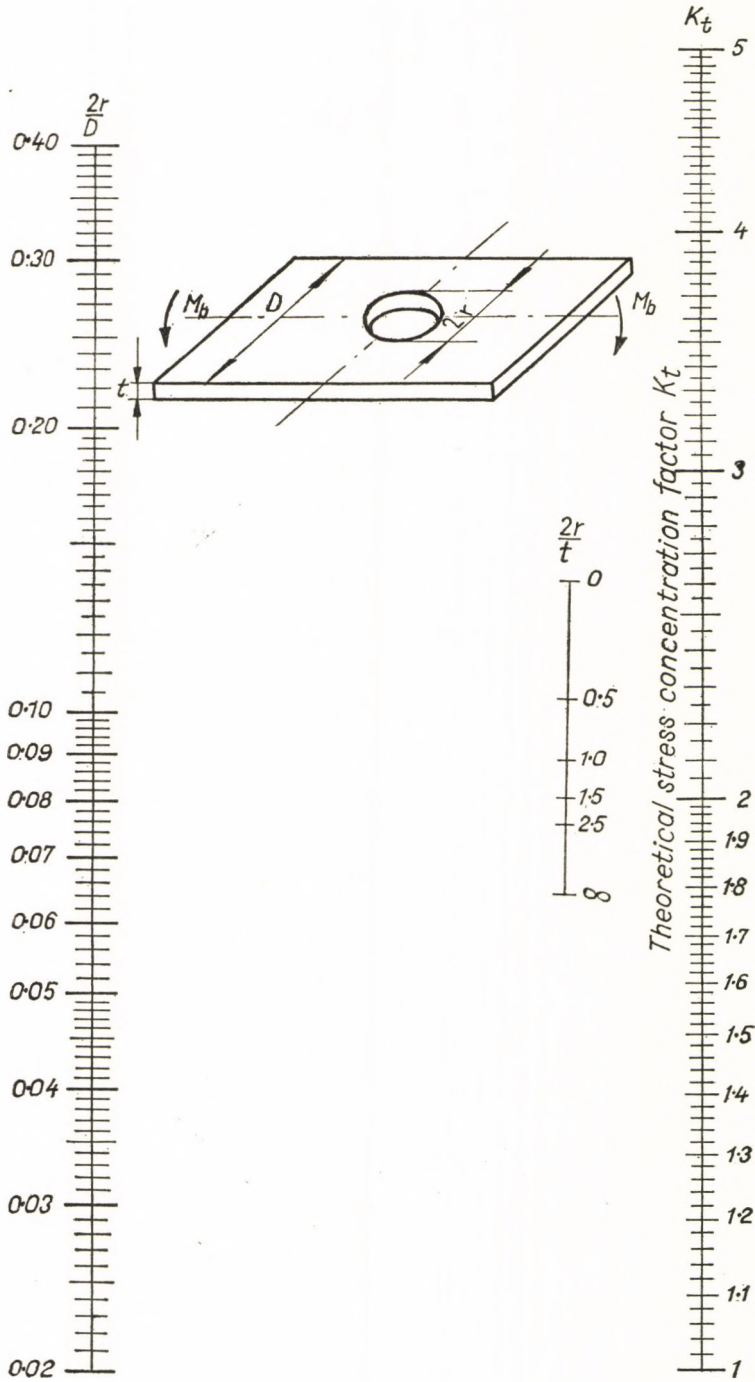


FIG. 81. Nomogram for K_t ; use in conjunction with Fig. 88
(in pocket inside cover of book)

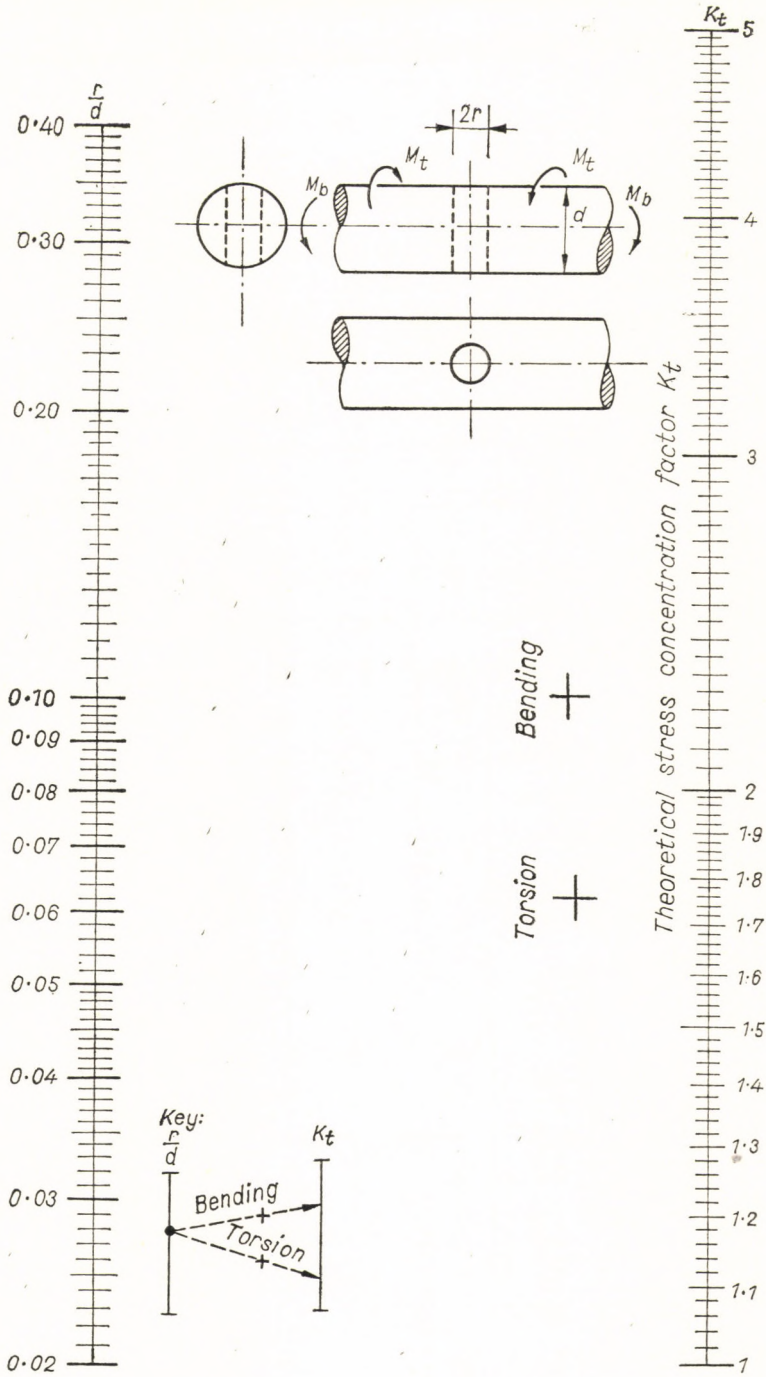


FIG. 82. Nomogram for K_t ; use in conjunction with Fig. 88 (in pocket inside cover of book)

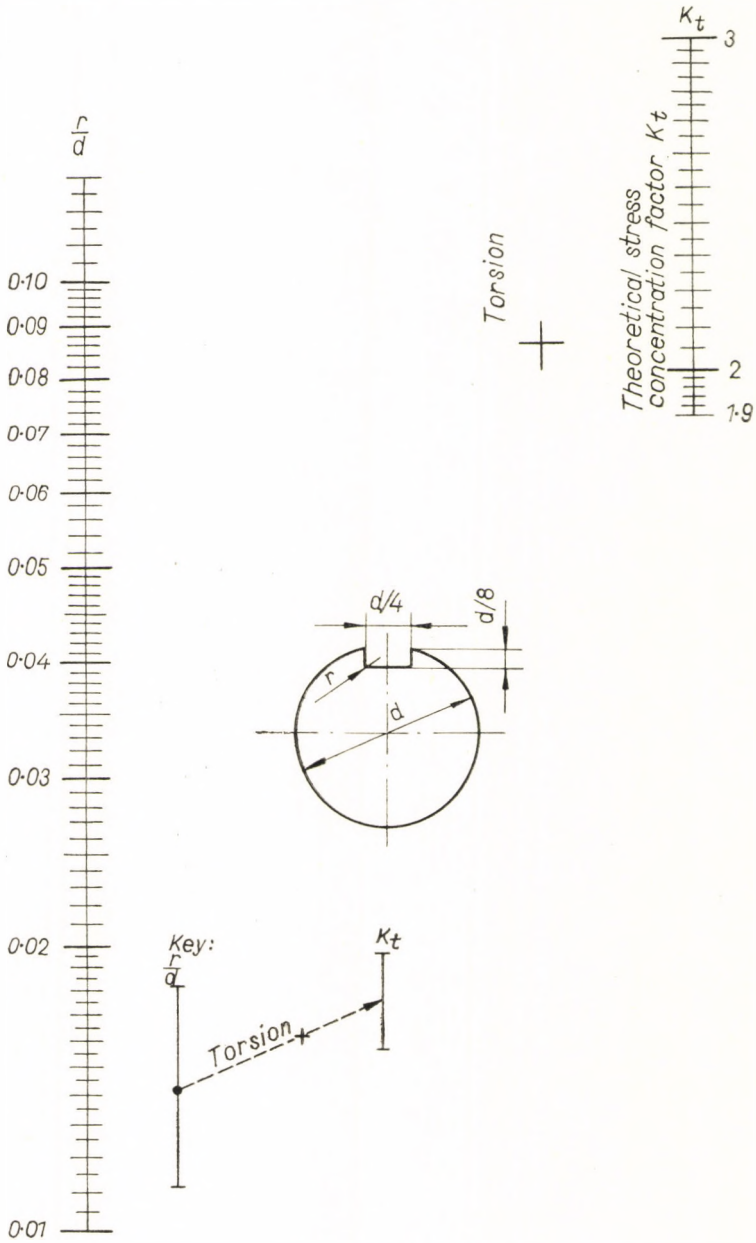


FIG. 83. Nomogram for K_t ; use in conjunction with Fig. 88
(in pocket inside cover of book)

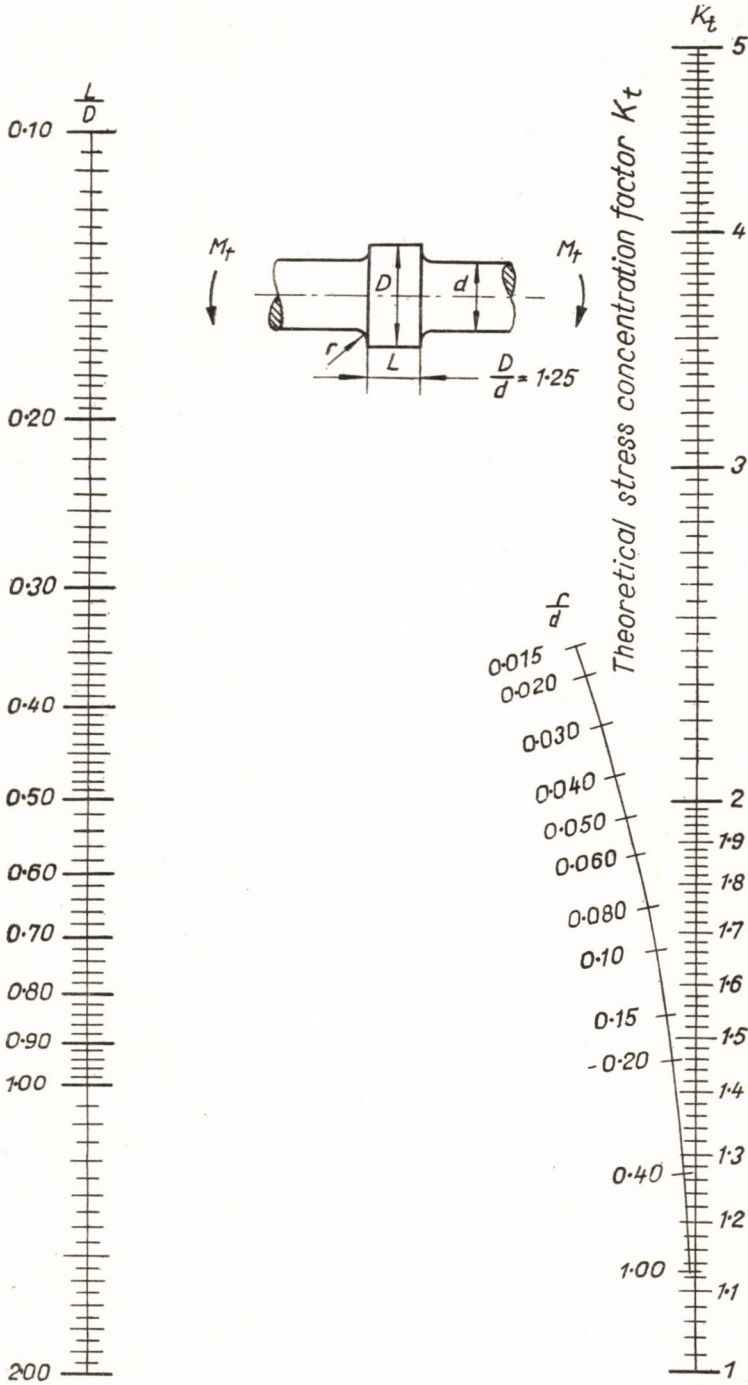


FIG. 84. Nomogram for K_t ; use in conjunction with Fig. 88 (in pocket inside cover of book)

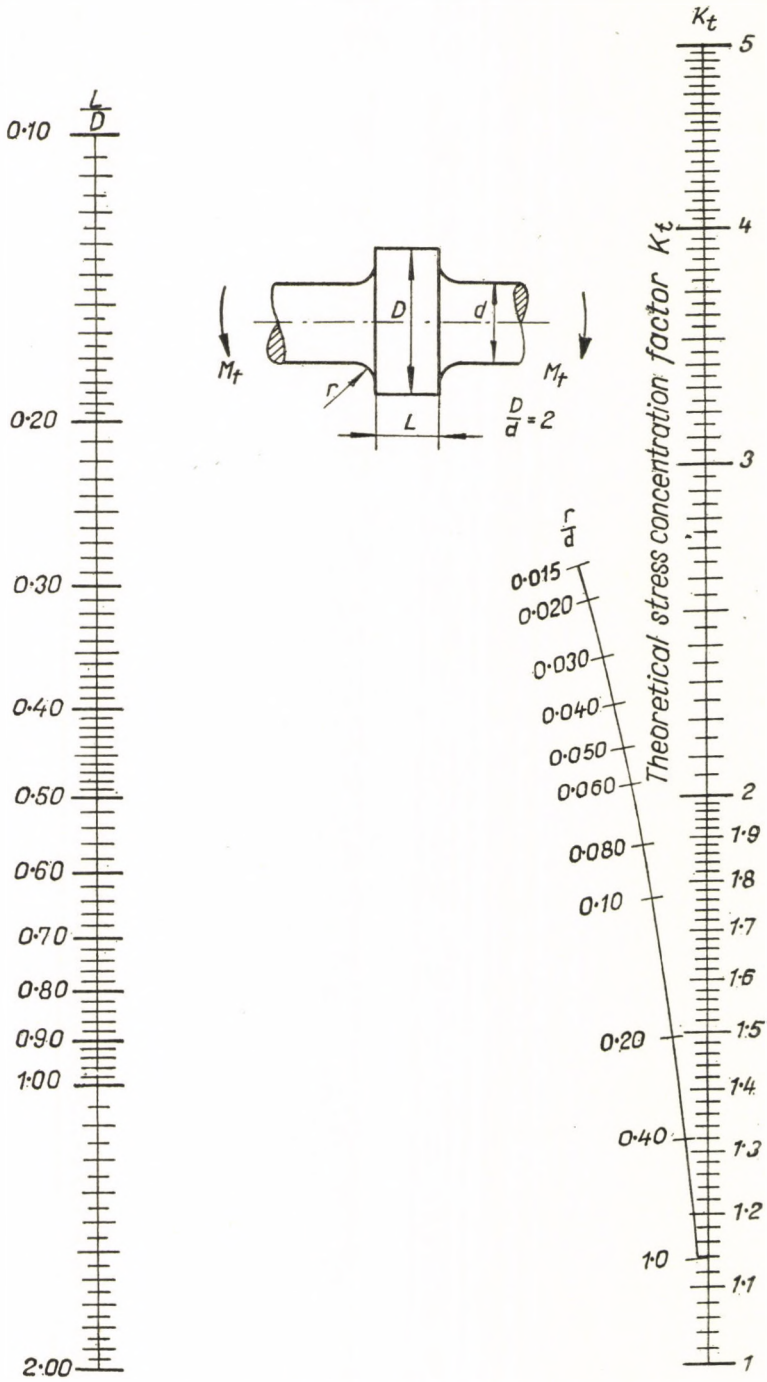


FIG. 85. Nomogram for K_t ; use in conjunction with Fig. 88
(in pocket inside of book)

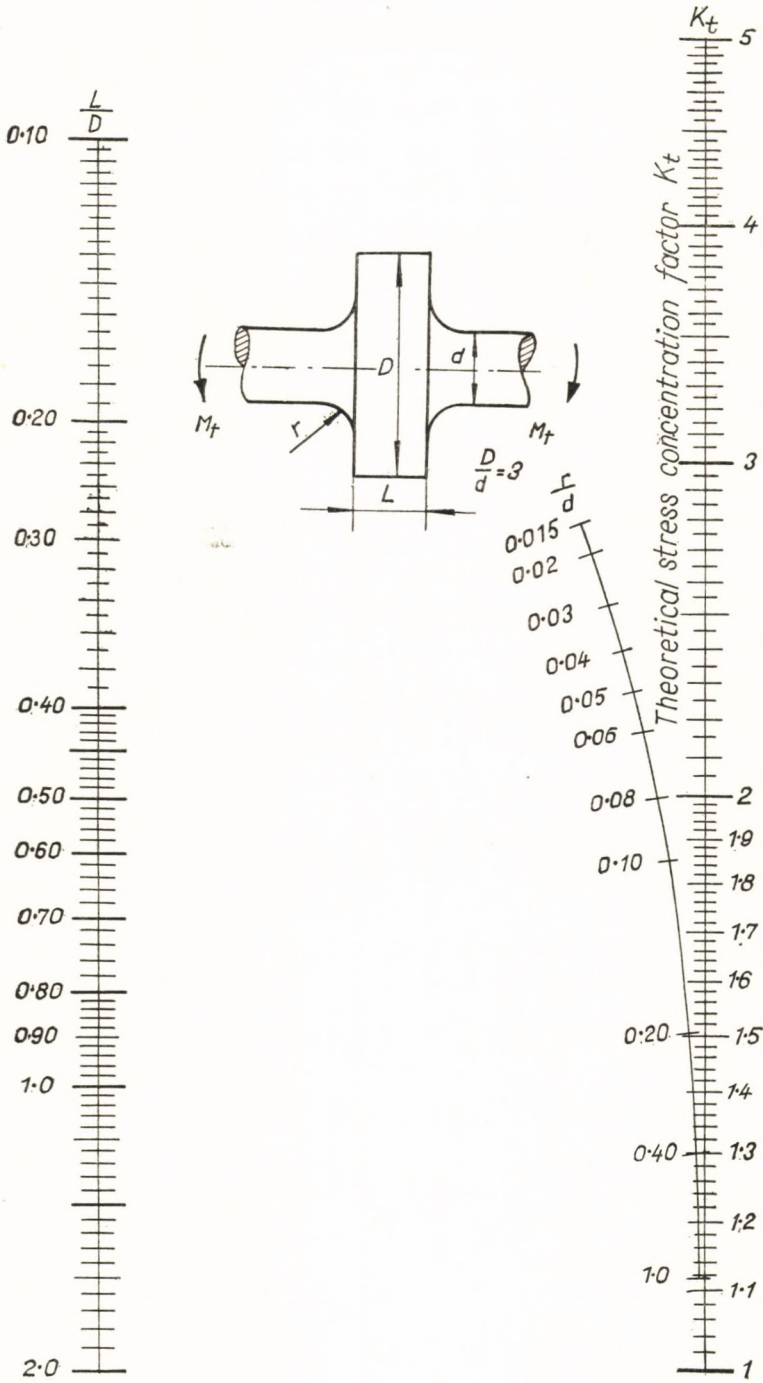


FIG. 86. Nomogram for K_t ; use in conjunction with Fig. 88 (in pocket inside cover of book)

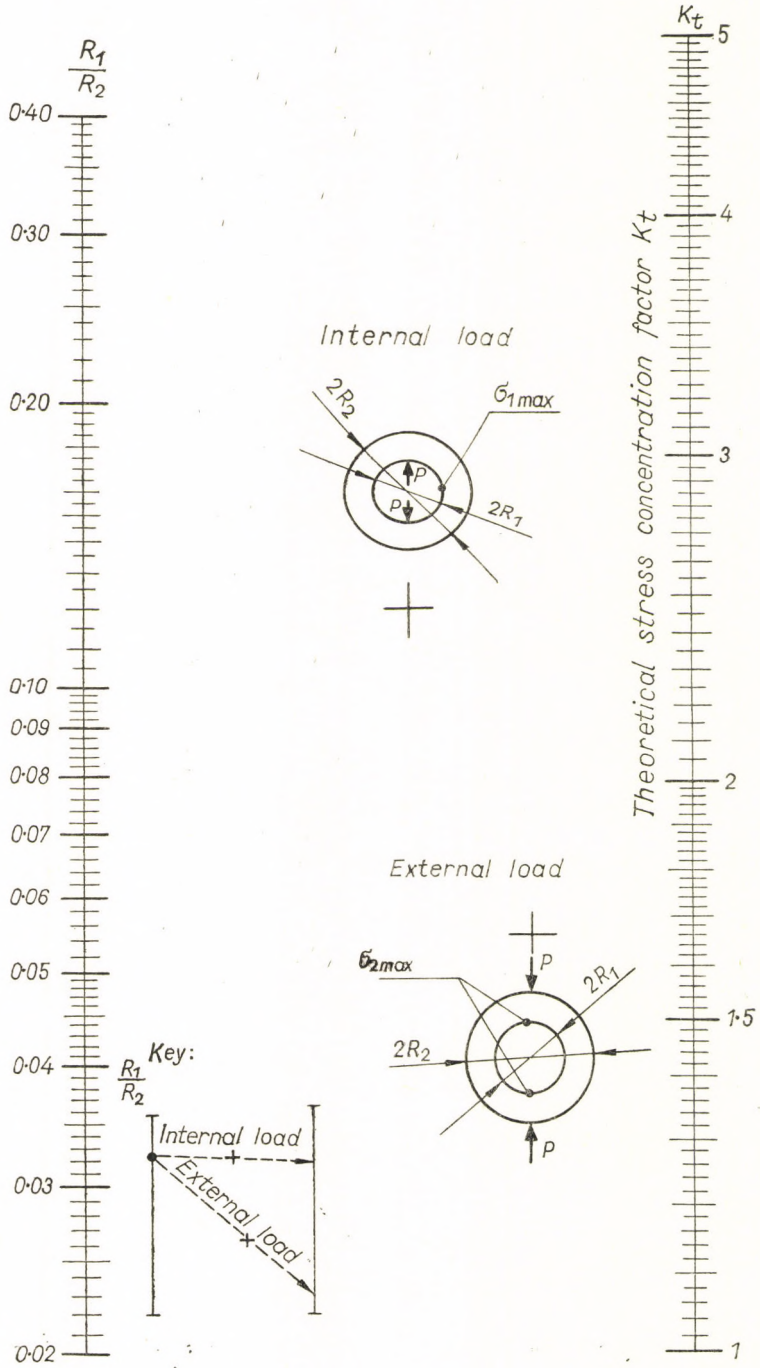


FIG. 87. Nomogram for K_t ; use in conjunction with Fig. 88 (in pocket inside cover of book)

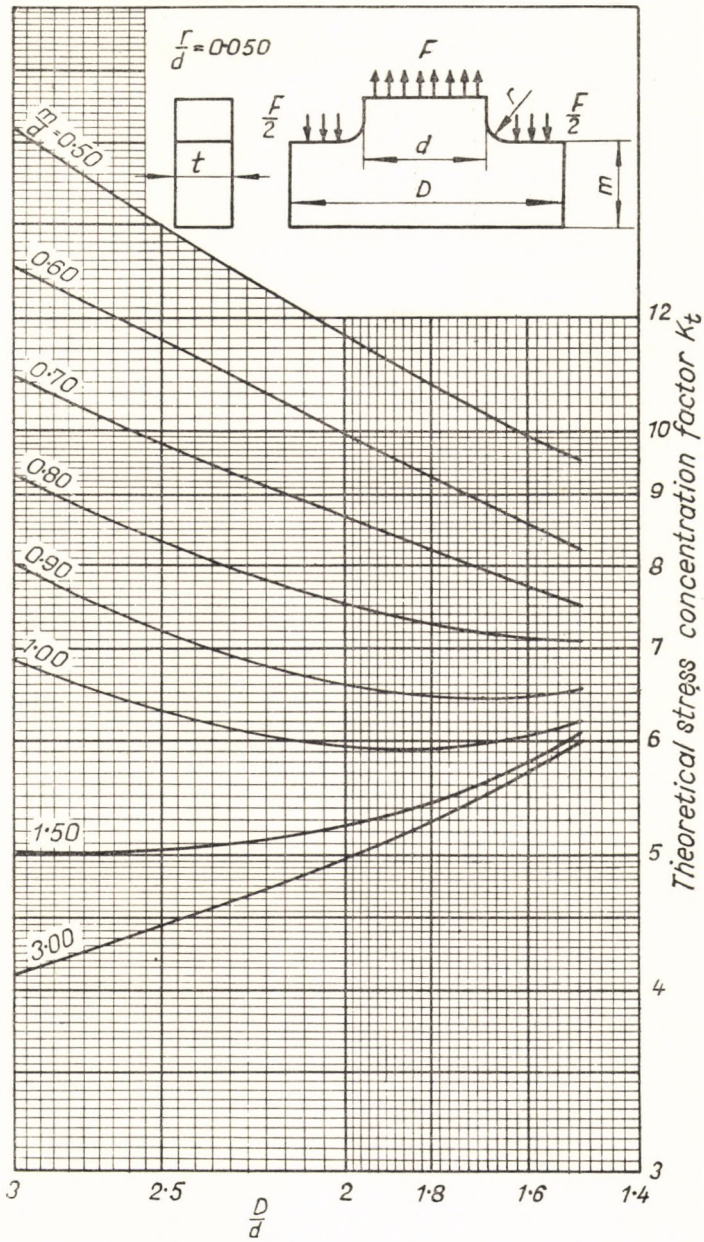


FIG. 89. Theoretical stress concentration factor

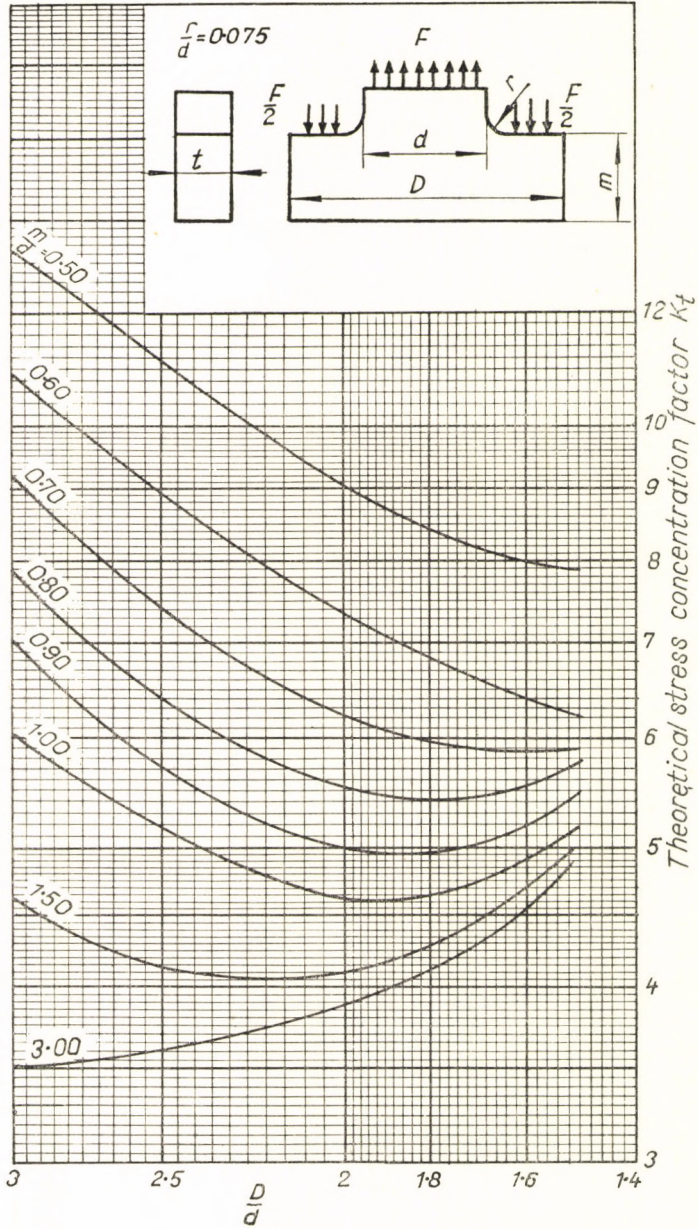


FIG. 90. Theoretical stress concentration factor

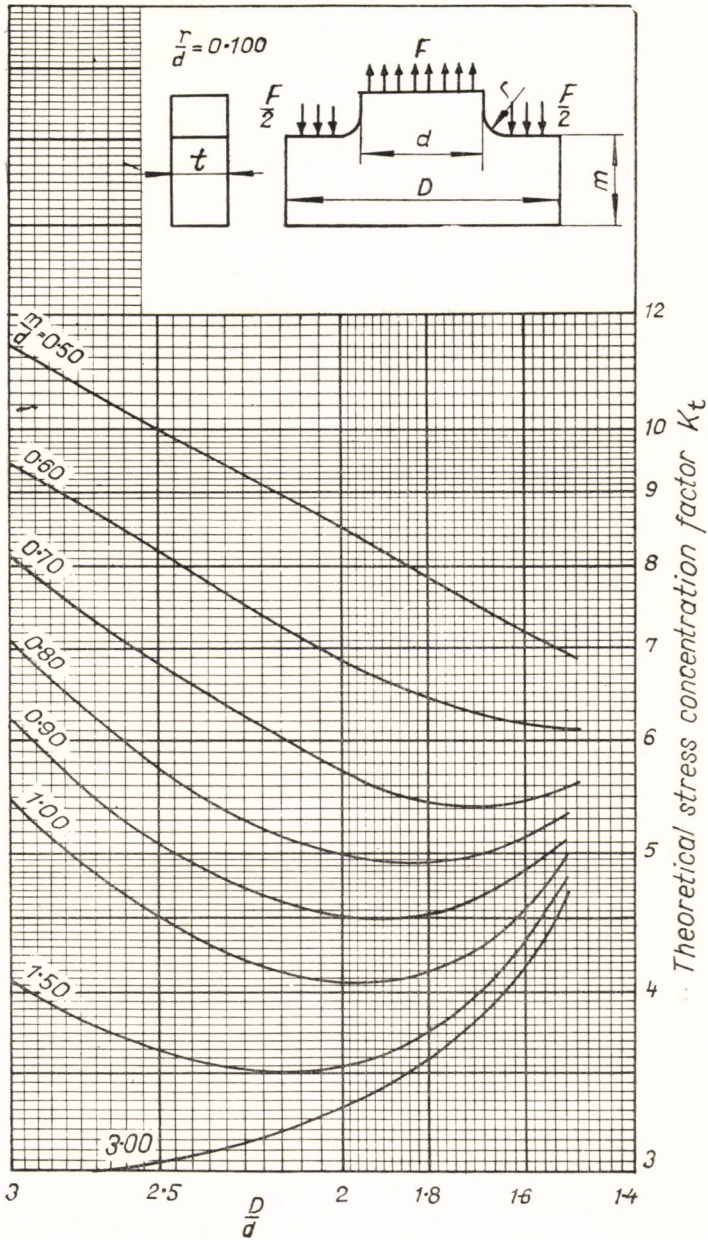


FIG. 91. Theoretical stress concentration factor

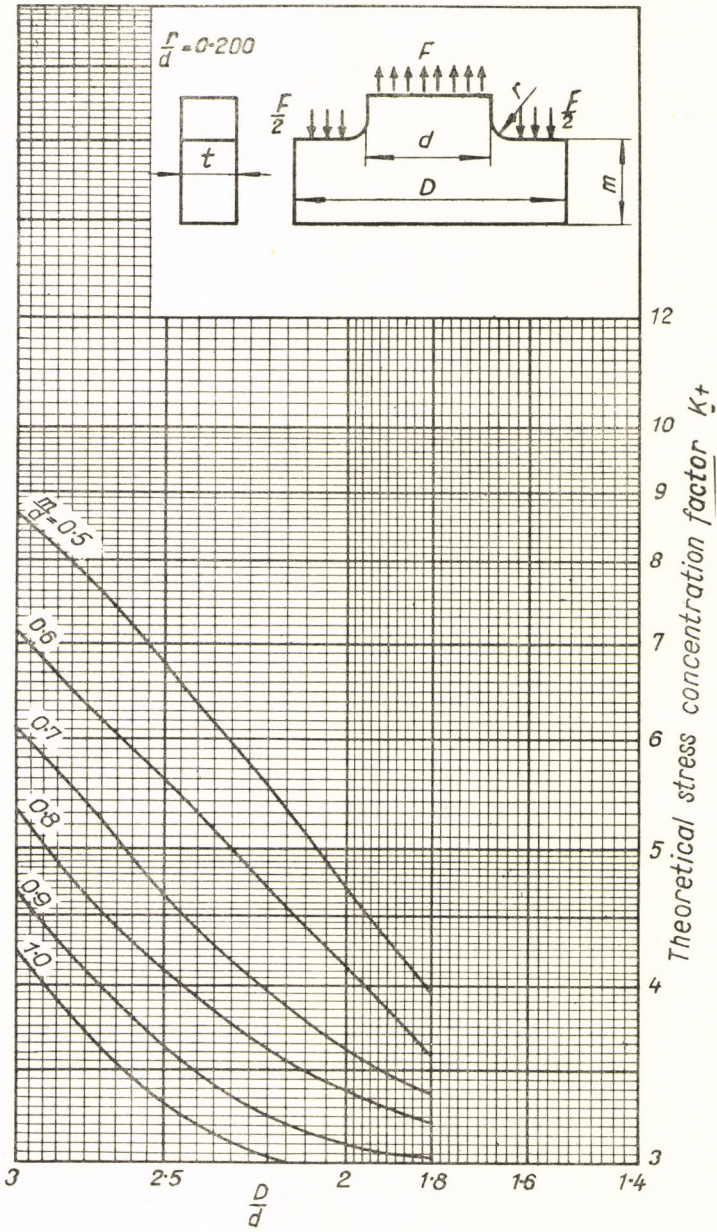


FIG. 92. Theoretical stress concentration factor

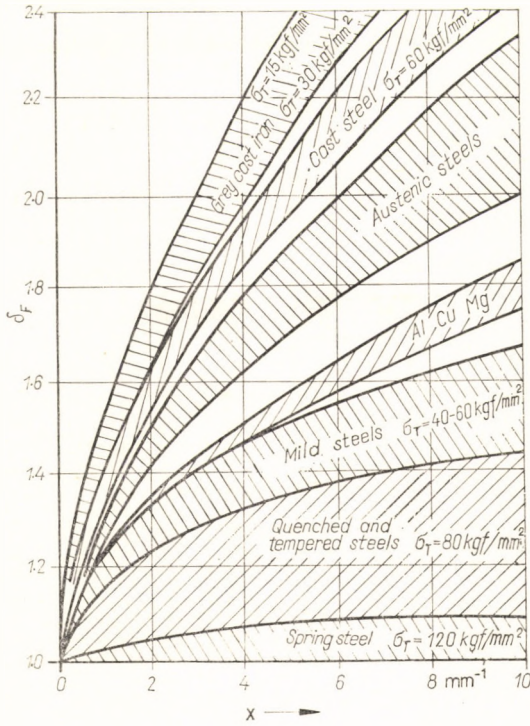


FIG. 93. Siebel diagram

Stress	Form of component	$X [mm^{-1}]$
Tension and compression	 Flat specimen with external notch	$X = \frac{2}{r}$
	 Flat specimen with internal notch	
	 Round specimen with external notch	
Bending	 Flat specimen with external notch	$X = \frac{2}{d} + \frac{2}{r}$
	 Round specimen with external notch	
Torsion	 Round specimen with longitudinal notch	$X = \frac{2}{d} + \frac{1}{r}$
	 Round specimen with circumferential notch	
	 Round specimen with transverse hole	

FIG. 94. Values of X for various forms of stress raisers

6. Factor of safety

TABLE 13
FACTOR OF SAFETY

Type of stress	Factor of safety
Reversed and fluctuating stress	1.5...2
As above, if it is important for the machine component to be light and if the probability of deviation from the calculated values is slight	1.2...1.5

TABLE 14
MULTIPLYING COEFFICIENTS FOR THE FACTOR OF SAFETY

Condition	Multiplying coefficient	
The multiplying coefficients for the factor of safety must be applied along or in combination (cumulatively) according to the number of the conditions shown that are present	If failure can cause an accident or represents a danger to life	1.2...1.5
	If the component can be easily overloaded	1.2...1.3
	For shock loading, when only small shocks occur; applies especially to starting-up conditions (steam and water turbines, grinding machines, etc.)	1...1.1
	If fairly small shocks occur in operation (plunger-type die-casting machines, planing machines, etc.)	1.2...1.5
	If fairly large shocks occur in operation (section shearing machines, blanking presses, etc.)	1.5...2.0
	For hammers, stone crushers, rolling mills and the like	2.0...3.0

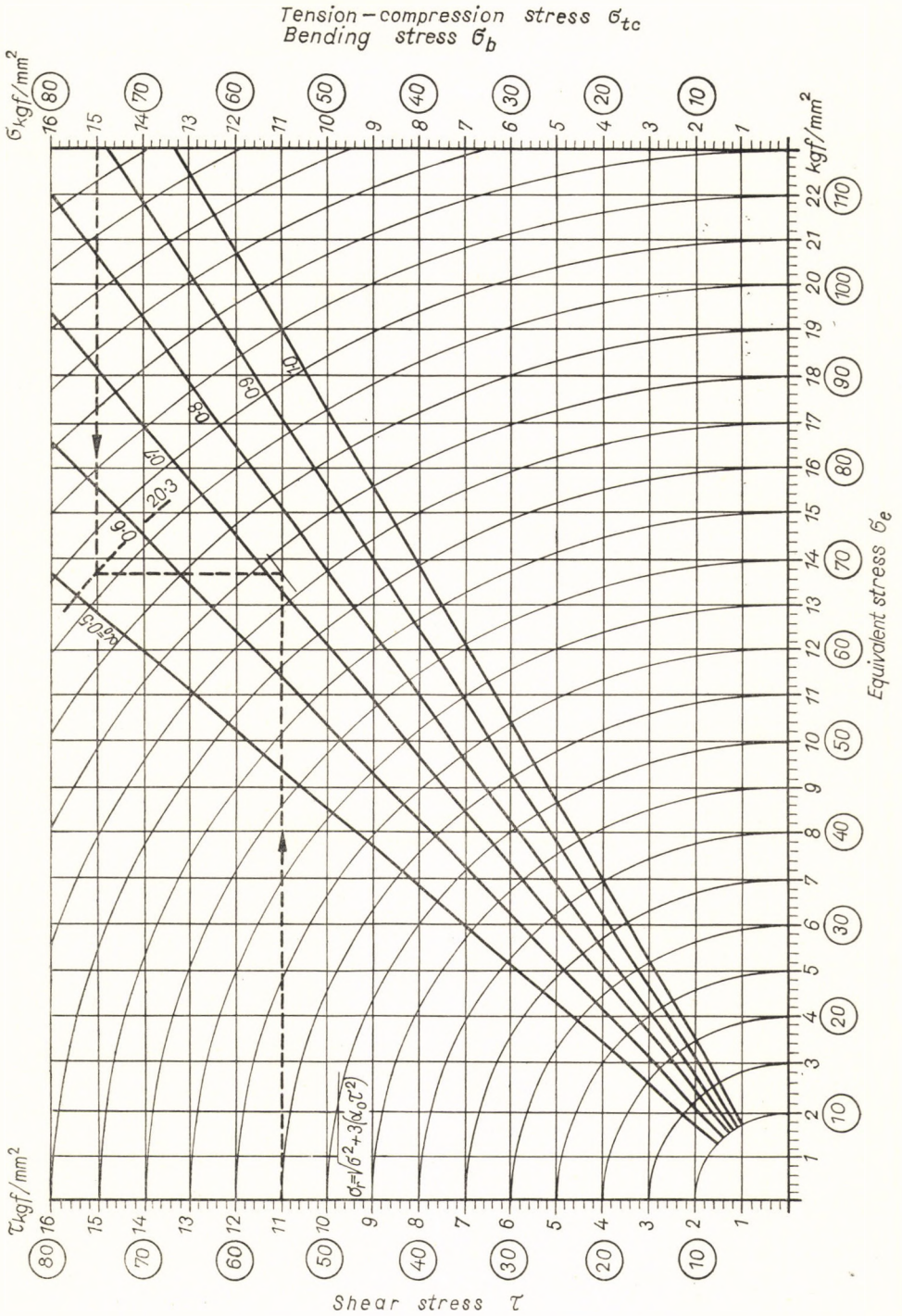


FIG. 95. Nomogram for determination of equivalent stress σ_e

8. Fatigue design of some machine components

8.1 Shafts and journals

TABLE 15

FATIGUE STRENGTH REDUCTION FACTOR K_f FOR FLANGED SHAFTS (THUM AND BRUDER [93])

Form	Stress	Ma- terial	K_f	Remarks	
<p>Fatigue fracture</p> <p>$\phi 85$</p> <p>$\phi 55$</p> <p>$\phi 70$</p> <p>$\phi 75$</p> <p>4 or 8 bolt holes</p>	Bending and torsion	Number of cycles $N = 10 \times 10^6$	1.62 1.45 1.34 1.27 1.26 1.48 1.32	4 bolt holes, $S = 8$ mm 8 bolt holes } $S = 8$ mm } $S = 12$ mm	
<p>Fatigue fracture</p> <p>$\phi 85$</p> <p>$\phi 55$</p> <p>$\phi 70$</p> <p>$\phi 75$</p>	Bending and torsion		1.27 0.97	Not rolled Rolled	} $S = 18$ mm
<p>Fatigue fracture</p> <p>$\phi 15$</p> <p>$\phi 30$</p> <p>$\phi 85$</p> <p>$\phi 55$</p> <p>$\phi 70$</p> <p>$\phi 75$</p>	Bending and torsion		1.62 1.32	Without washer With washer 12 mm thick } $S = 8$ mm	
<p>Fatigue fracture</p> <p>$\phi 85$</p> <p>$\phi 55$</p> <p>$\phi 70$</p> <p>$\phi 75$</p>	Bending and torsion		1.62 1.66	Not bored Bore 8 mm in diameter } $S = 8$ mm	
<p>Fatigue fracture</p> <p>$\phi 85$</p> <p>$\phi 8 \pm 0.07$</p> <p>$\phi 55$</p> <p>$\phi 70$</p> <p>$\phi 75$</p>	Bending and torsion		St C 60.61	1.27 1.42	Not bored Bore 8 mm in diameter } $S = 18$ mm

TABLE 15 (CONT.)

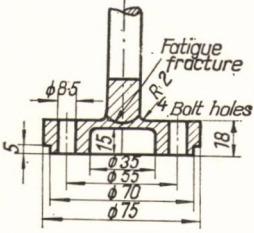
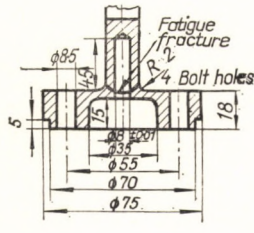
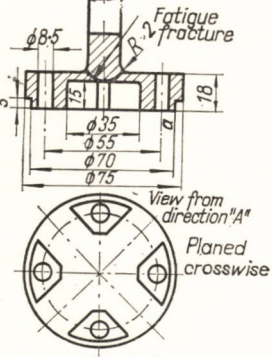
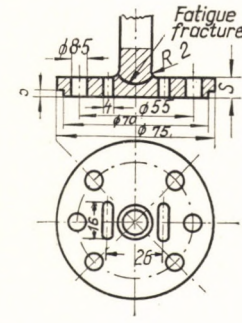
Form	Stress	Material	K_f	Remarks
	Bending and torsion	Number of cycles $N = 10 \times 10^6$	1.27 2.4	Full flange Turned recess in flange 35 mm in diameter \times 15 mm } $S = 18$ mm
	Bending and torsion		1.27 2.29	Full flange Turned recess in flange 35 mm in diameter \times 15 mm Bore 8 mm in diameter } $S = 18$ mm
	Bending and torsion		1.27 3.74	Full flange Flange planed crosswise } $S = 18$ mm
	Bending and torsion		St C 60.64	1.82 1.63

TABLE 16

FATIGUE STRENGTH REDUCTION FACTOR K_f FOR SPLINED SHAFT IN TORSION (HEROLD [25])

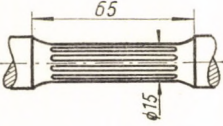
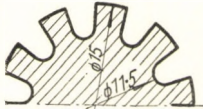
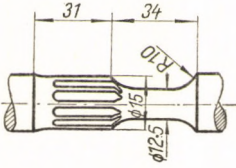
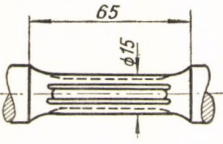
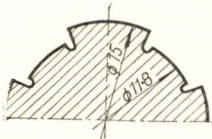
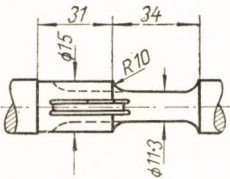
Form	Material	K_f	Remarks
	<p>VCN 15 $\sigma_T = 85.5 \text{ kgf/mm}^2$</p>	<p>1.09</p>	<p>10 splines as shown in the sketch below</p> 
	<p>VCN 15 $\sigma_T = 85.5 \text{ kgf/mm}^2$</p>	<p>1.04</p>	<p>Bottom of groove rounded off with a large radius</p>
	<p>VCN 15 $\sigma_T = 85.5 \text{ kgf/mm}^2$</p>	<p>1.92</p>	<p>4 splines as shown in the sketch below</p> 
	<p>VCN 15 $\sigma_T = 85.5 \text{ kgf/mm}^2$</p>	<p>2.33</p>	<p>Bottom of groove rounded off with a small radius only</p>

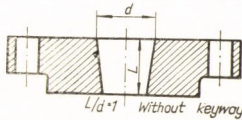
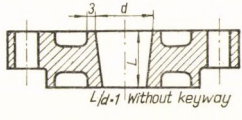
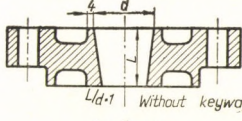
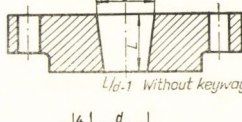
TABLE 17

NOMENCLATURE FOR THE MATERIALS USED IN THE DETERMINATION OF THE FATIGUE
STRENGTH REDUCTION FACTOR OF THE VARIOUS WHEEL HUBS

	Sym- bol	Chemical composition, per cent								Mechanical properties						Blank diam- eter (mm)	Ma- chined diam- eter (mm)
		C	Si	Mn	Ni	Mo	Cr	P	S	σ_T (kgf/ mm ²)	σ_y (kgf/ mm ²)	Elonga- tion % $L=10d_0$	Re- duction of area, %	σ_F (kgf/ mm ²)	τ_F (kgf/ mm ²)		
Shaft	W ₁	0.28	0.39	0.71	—	0.025	0.1	0.061	0.02	56.2	35.9	24.1	58.7	—	22.2	30	20
	W ₂	0.20	0.29	0.49	—	—	—	0.018	0.02	52.2	36.9	21.7	57.1	32.5	—	23	
	W ₃	0.23	0.25	0.67	0.29	0.23	0.95	0.021	0.012	86.6	77.1	12.5	64.1	33.5	22.4	30	
	W ₄	0.25	—	—	—	—	—	—	—	60.0	34.9	22.0	52.6	28.0	20.5	32	
	W ₅	0.28	0.30	0.66	—	—	—	0.020	0.020	56.2	32.7	29.0	—	30.5	18.0	32	
Hub	N ₁	0.22	0.28	0.60	—	—	—	0.021	0.020	48.1	26.1	$L=5d_0$ 26.4	42.3	—	—	125	115
	N ₂	0.34	0.30	0.60	—	0.01	0.2	0.067	0.023	57.0	31.8	14.0	18.0	—	—	120	
	N ₃	0.42	0.24	0.72	—	0.30	1.03	0.015	0.020	81.5	64.3	8.6	8.9	—	—	130	
	N ₄	0.21	0.25	0.71	—	—	—	0.031	0.023	40.0	—	—	—	—	—	130	
	N ₅	0.28	0.30	0.66	—	—	—	0.020	0.020	51.5	26.4	24.1	36.8	—	—	130	

TABLE 18

SUMMARY OF THE RESULTS OF TESTS CARRIED OUT BY A. THUM TO DETERMINE
THE FATIGUE STRENGTH REDUCTION FACTORS OF WHEEL HUBS [94]

Form of hub	Shrinking temperature (°C)	Shaft compressed by λ mm	Torsion fatigue strength			K_f	Torsion fatigue strength			K_f	Object of test
			Material		σ_{bF} (kgf/mm ²)		Material		τ_F (kgf/mm ²)		
			Shaft	Hub			Shaft	Hub			
 $L/d = 1$ Without keyway	100		W_4	N_1	13.6	2.06					Determination of shrinking pressure in relation to shrinking temperature
	130		W_4	N_1	13.0	2.15	W_4	N_2	13.2	1.56	
	150		W_4	N_1	16.4	1.71					
	200		W_4	N_1	16.6	1.69	W_4	N_2	12.2	1.68	
	300		W_4	N_1	16.4	1.71					
 $L/d = 1$ Without keyway	100		W_4	N_1	15.0	1.87					
	130		W_4	N_1	14.0	2.0	W_4	N_2	13.2	1.55	
	150		W_4	N_1	17.2	1.63					
	200		W_4	N_1	17.4	1.61					
	300		W_4	N_1	17.7	1.58					
 $L/d = 1$ Without keyway	150	$s = 2$	W_5	N_3	18.8	1.62	W_5	N_3	14.4	1.25	
	150	$s = 4$	W_5	N_3	16.8	1.81	W_5	N_3	14.1	1.27	
	150	$s = 8$	W_5	N_3	16.0	1.91	W_5	N_3	13.9	1.29	
 $L/d = 1$ Without keyway	150		W_5	N_3	16.0	1.91	—	—	—	—	Form of hub
	150		W_5	N_3	18.4	1.66	W_5	N_3	13.2	1.36	

	$L/d = 1$	150		W_5	N_4	15.5	1.97	W_5	N_1	13.7	1.31	Material of hub	
	Without keyway	150		W_5	N_5	15.0	2.03	W_5	N_5	13.3	1.35		
	With keyway but without key	100		W_3	N_1	18.0	1.86	W_1	N_1	17.2	1.29	Effect of key and keyway	
	With keyway and key	100		W_3	N_1	14.8	2.27	W_1	N_1	16.4	1.35		
	Keyway in hub only	100		W_3	N_1	14.2	2.36	W_1	N_1	16.0	1.39		
		100		W_3	N_1	14.6	2.3						
	Without keyway	150						W_3	N_2	17.5	1.65		
	With keyway and key		0.3	W_5	N_3	14.2	2.15						
		150						W_3	N_2	17.5	1.28		
	Groove in hub only		0.3	W_5	N_3	12.0	2.54						
		150						W_3	N_2	12.7	1.76		
	Groove in shaft only	150						W_3	N_2	16.5	1.36		
	$L/d = 1$	150						W_5	N_3	14.1	1.27		Length of wheel hub
	$L/d = 1$		0.3	W_5	N_3	14.2	2.15						
		150						W_5	N_3	14.0	1.28		
	$L/d = 1.25$		0.3	W_5	N_3	14.9	2.05	W_5	N_3	14.7	1.22		
			0.3	W_5	N_3	18.0	1.69						
	$L/d = 1.8$		0.3	W_5	N_3	15.5	1.95						

8.3 Ball and roller bearings

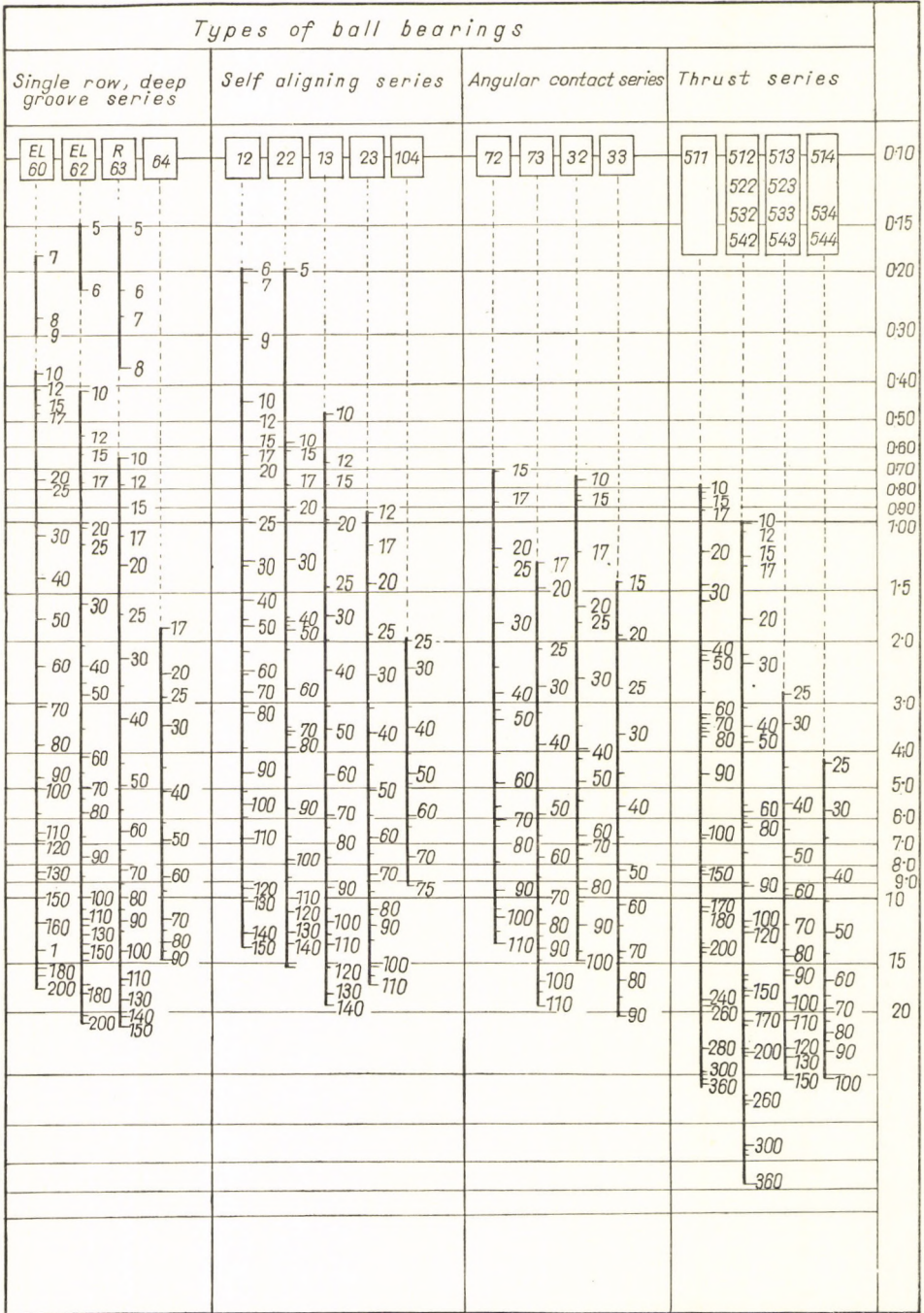
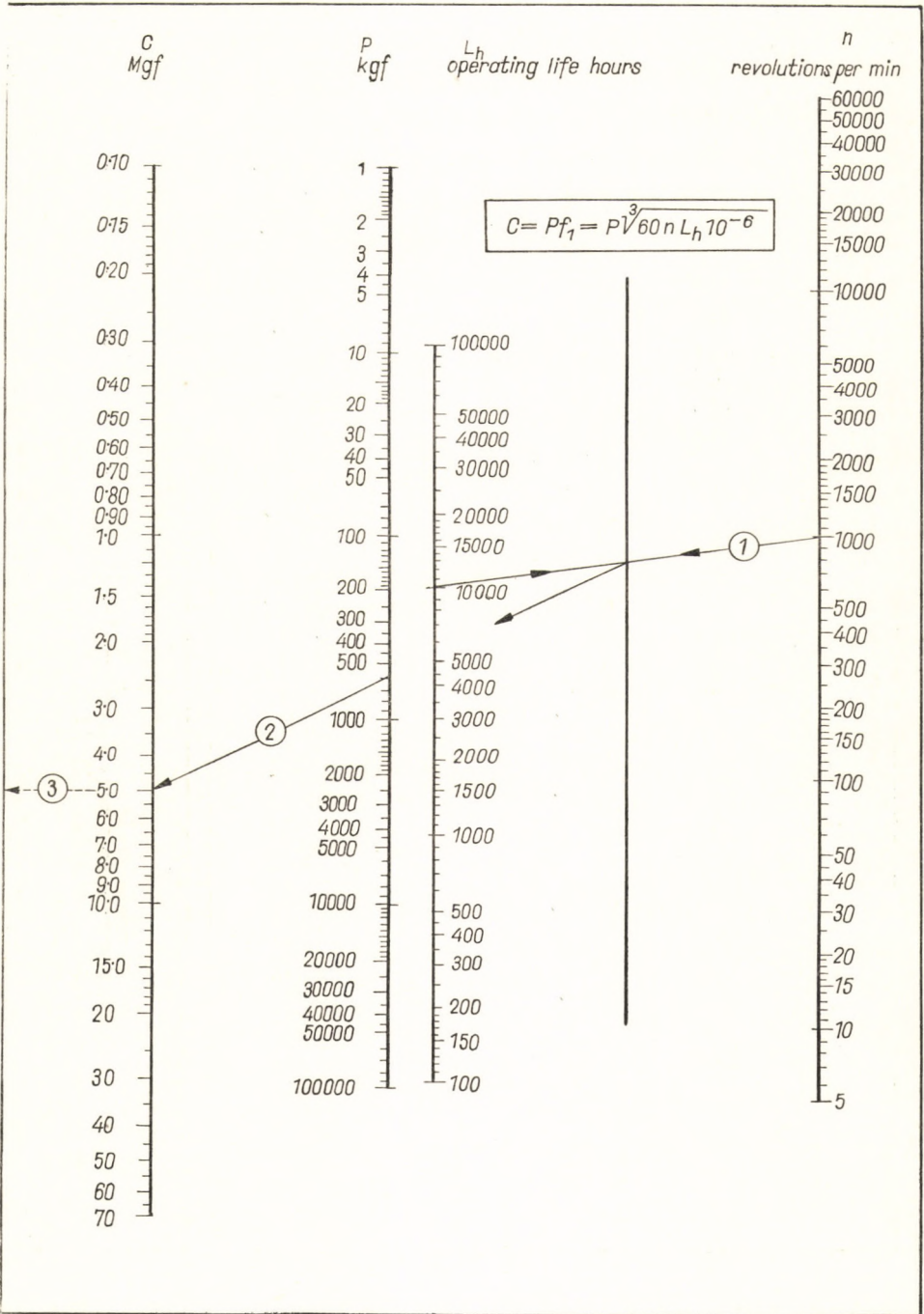


FIG. 96. Nomogram for selection of ball bearings



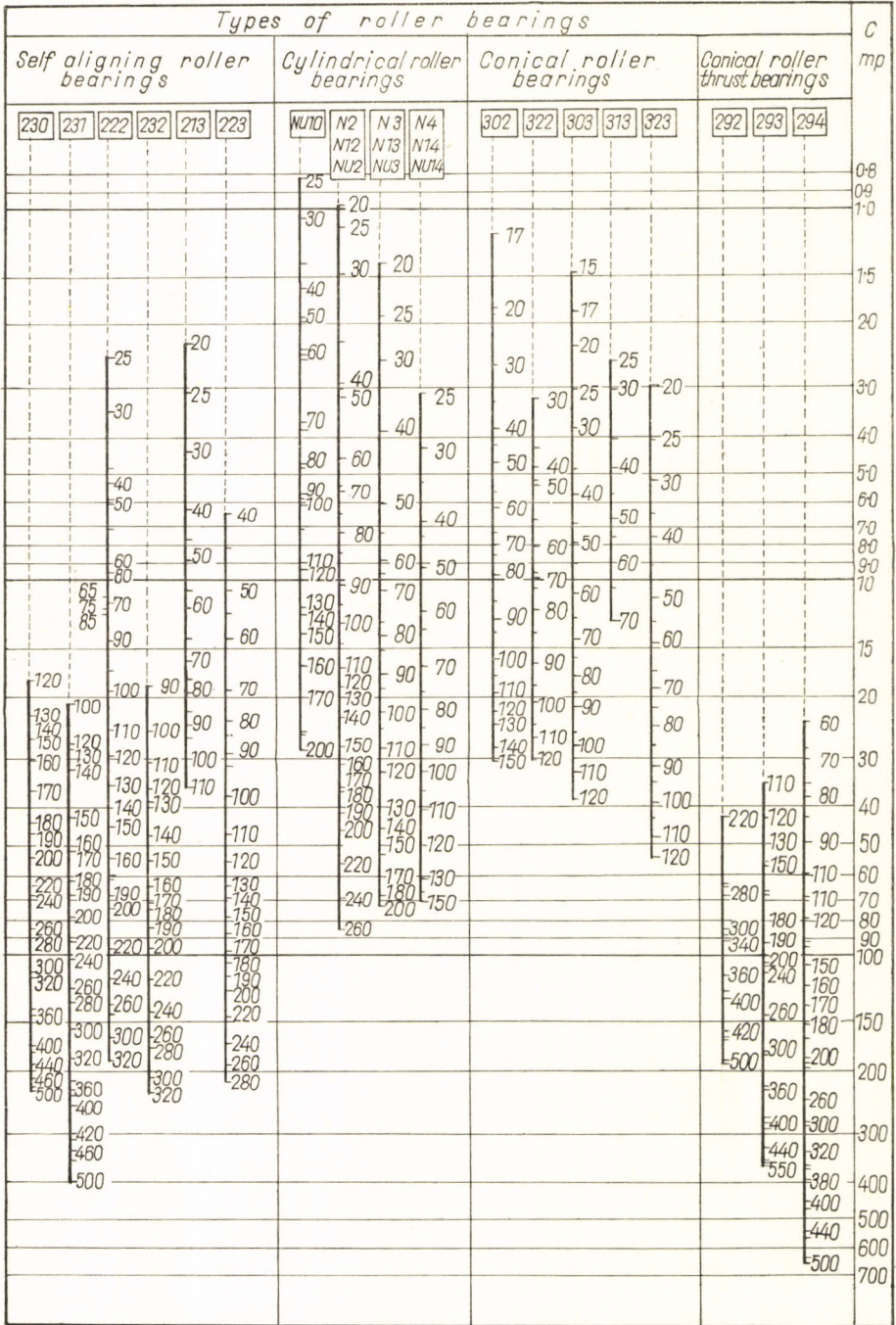
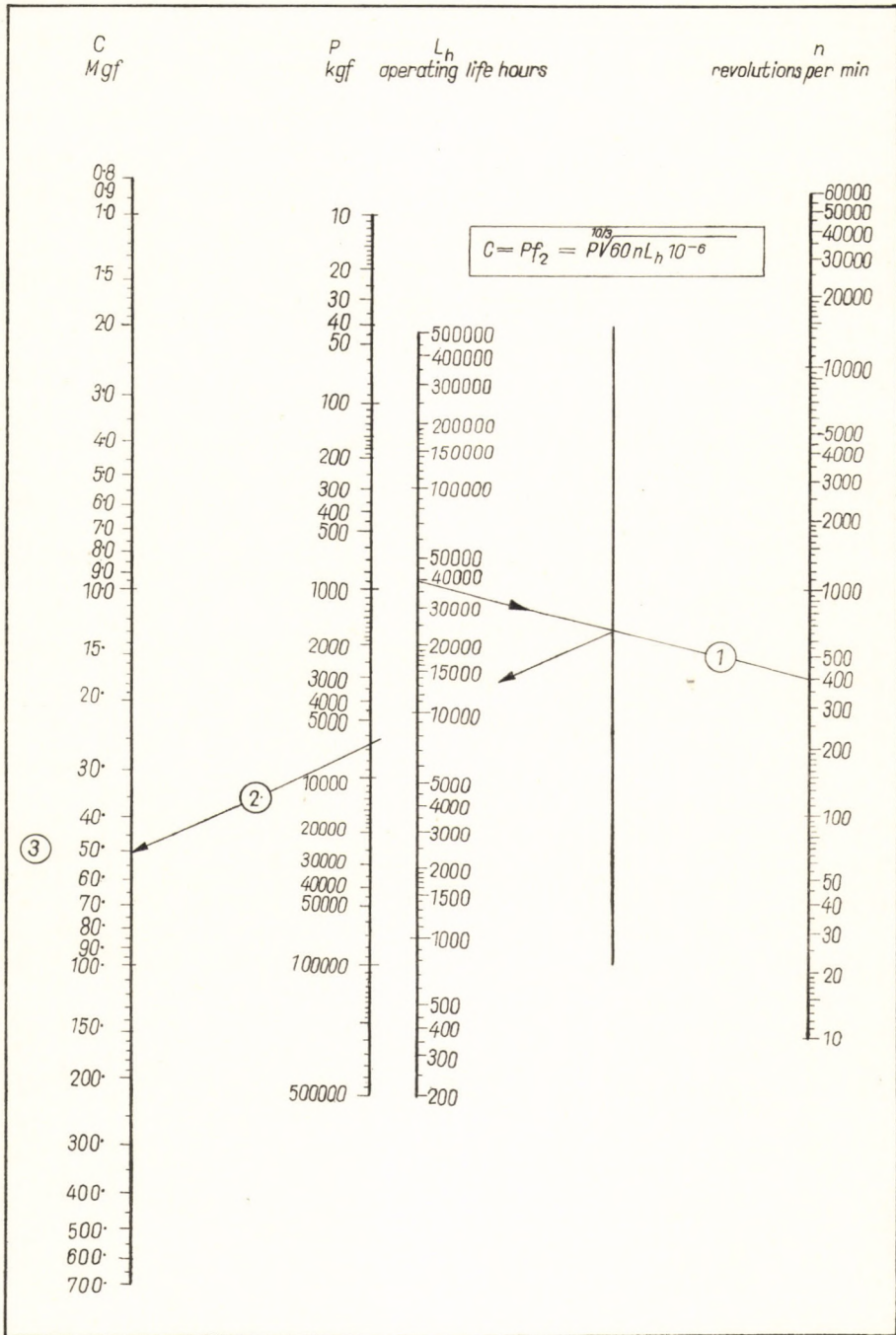


FIG. 97. Nomogram for selection of roller bearings



8.4 Bolts

TABLE 19
FATIGUE STRENGTH REDUCTION FACTOR K_f FOR BOLTS

Description of thread	K_f	
Whitworth thread, rounded at root,	carbon steel	3.2...3.8
	heat treated alloy steel	5.4...6.0
Metric thread,	carbon steel	4.4...5.0
	heat treated alloy steel	5.6...6.4
With rolled threads reduce the K_f value		
for ordinary carbon steel by	14...18%	
for ductile alloy steel by	20...24%	
for hard alloy steel by	30...40%	

8.5 Springs

TABLE 20
FLUCTUATING TORSION FATIGUE STRENGTH OF PIANO WIRES
OF VARIOUS SIZES
FOR $\sigma_l/\sigma_u = 0.5$ AND $N = 10^4$

Diameter, mm	Torsion fatigue strength, kgf/mm ²	Diameter, mm	Torsion fatigue strength, kgf/mm ²
0.10	100.0	2.00	82.0
0.15	99.0	2.30	80.0
0.20	98.5	2.40	79.0
0.25	98.0	2.75	77.5
0.30	97.0	3.00	77.0
0.35	96.5	3.20	76.0
0.40	96.0	3.40	75.5
0.45	95.0	3.75	73.5
0.50	94.0	4.00	73.0
0.55	93.5	4.50	71.0
0.60	93.0	4.75	70.5
0.65	92.0	5.00	70.0
0.70	92.0	5.25	69.0
0.75	91.5	5.50	68.5
0.80	91.5	5.75	68.0
0.85	91.0	6.00	67.0
0.90	90.0	6.30	66.5
0.95	89.5	6.70	65.0
1.00	89.0	7.00	64.0
1.20	88.0	8.00	62.0
1.40	87.0	8.50	61.5
1.60	85.0	9.00	60.5
1.80	84.0	9.50	60.0

TABLE 21

FACTORS OF VARIOUS ENDURANCES FOR SOME SPRING MATERIALS

Material	$R = \frac{\sigma_l}{\sigma_u}$	10^3	10^4	10^5	∞ 10^6
Pianino wires	0.75	1.220	1.120	1.020	0.952
	0.50	1.150	1.000	0.862	0.764
	0.25	1.120	0.944	0.785	0.650
	0	1.100	0.910	0.695	0.550
Spring wire, oil quenched	0.75	1.100	1.040	0.970	0.926
	0.50	1.063	0.944	0.834	0.752
	0.25	1.040	0.870	0.705	0.595
	0	1.000	0.800	0.606	0.458
Chrome-vanadium steel, hardened	0.75	0.944	0.877	0.826	0.787
	0.50	0.910	0.787	0.675	0.606
	0.25	0.862	0.725	0.588	0.485
	0	0.834	0.675	0.524	0.414
Stainless steel	0.75	0.877	0.834	0.800	0.770
	0.50	0.840	0.764	0.690	0.636
	0.25	0.813	0.700	0.588	0.518
	0	0.780	0.641	0.507	0.413
Phosphor-Bronze	0.75	0.513	0.476	0.431	0.392
	0.50	0.472	0.404	0.350	0.303
	0.25	0.435	0.357	0.286	0.239
	0	0.394	0.318	0.239	0.183
Beryllium-Bronze	0.75	0.752	0.725	0.705	0.685
	0.50	0.725	0.675	0.625	0.588
	0.25	0.695	0.625	0.550	0.505
	0	0.670	0.578	0.485	0.413

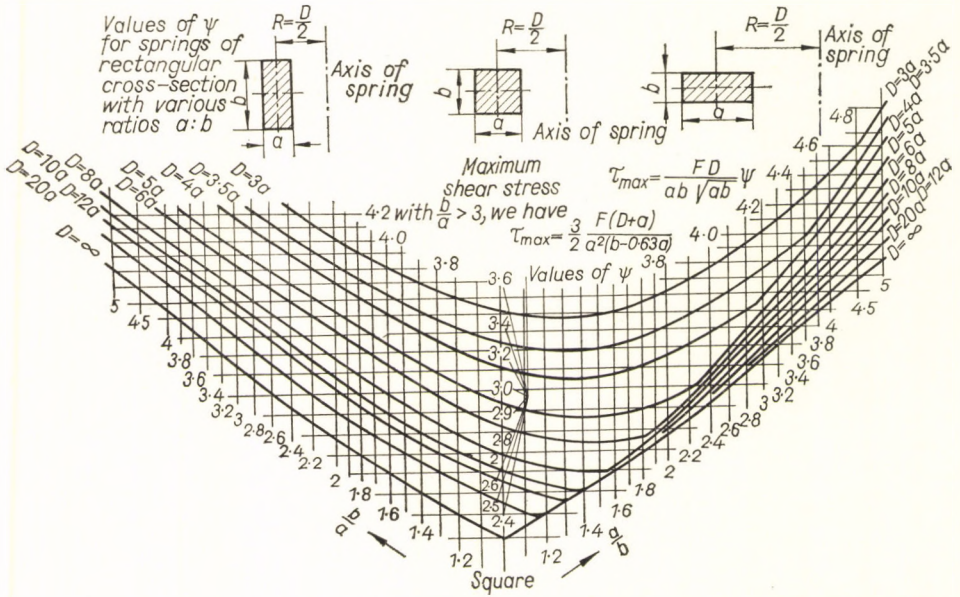


FIG. 98. Values of ψ for determination of maximum torsional stress in springs of rectangular cross-section

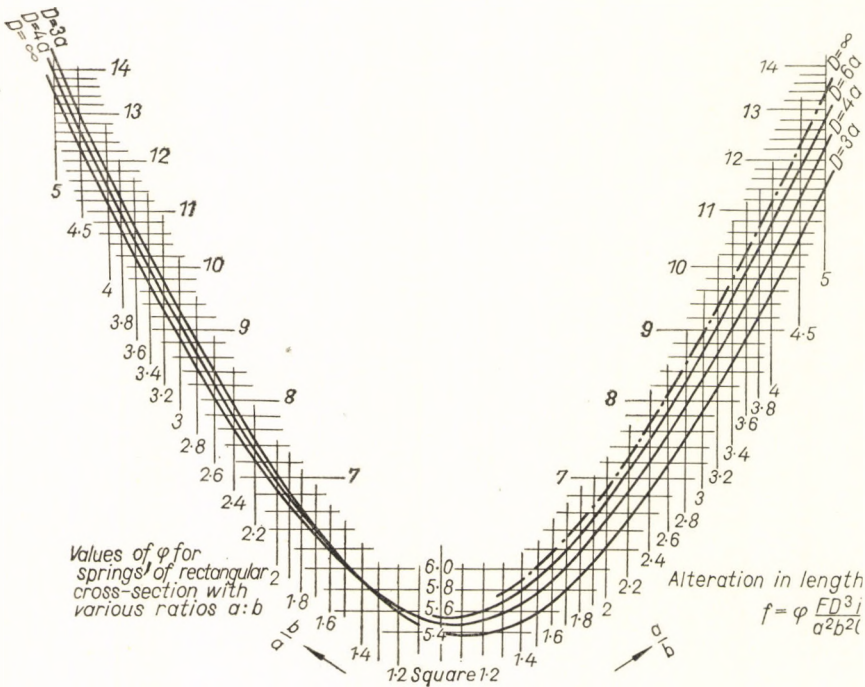


FIG. 99. Values of ϕ for determination of the extension of springs of rectangular cross-section

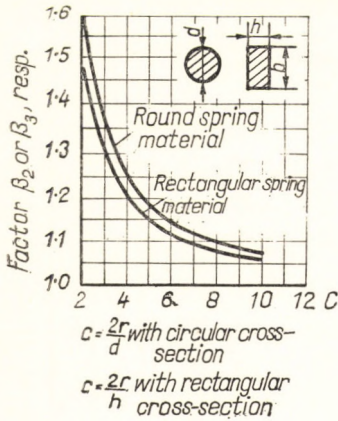


FIG. 100. Values of β_2 and β_3 for determination of maximum shear stress in springs of circular and rectangular cross-section stressed in torsion

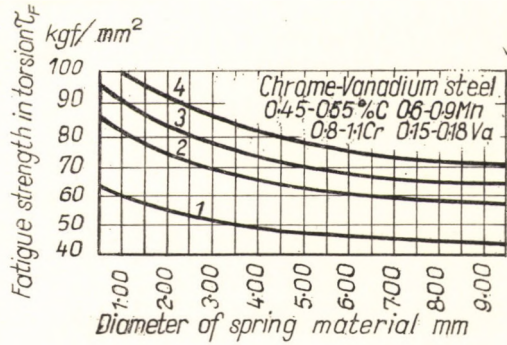


FIG. 101.

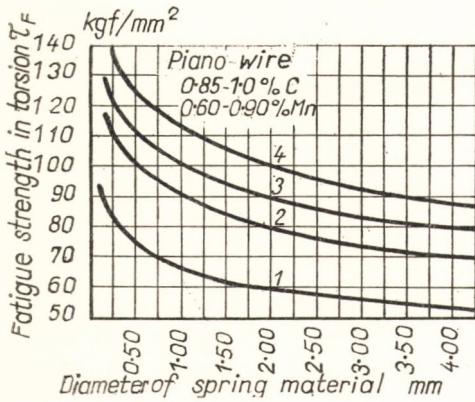


FIG. 102

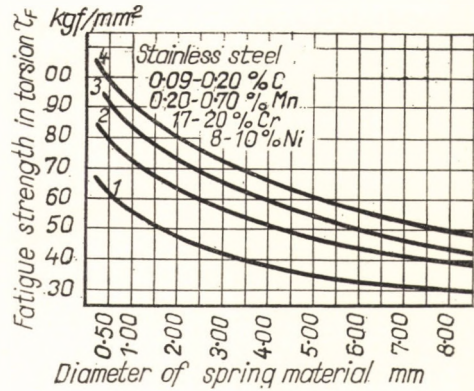


FIG. 103

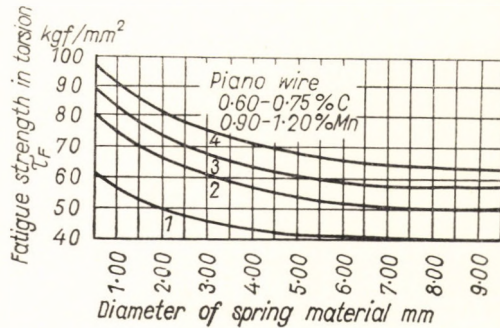


FIG. 104

Figs. 101 to 104.

Permissible torsional stress in spring steel

- 1 for endurance 10^6 to 10×10^6
- 2 for endurance 10^5 to 10^6
- 3 for endurance 10^3 to 10^4
- 4 for static loading

8.6 Welded joints

TABLE 22

FORMULAE FOR THE DETERMINATION OF NOMINAL STRESS FOR VARIOUS TYPES OF WELDED JOINTS

Pictorial representation of joint	$\sigma_n (\tau_n)$	Pictorial representation of joint	$\sigma_n (\tau_n)$	Pictorial representation of joint	$\sigma_n (\tau_n)$
	$\sigma_n = \frac{F}{n \cdot a \cdot l}$		$\sigma_n = \frac{6M}{l^2 a}$		$\sigma_b = \sqrt{\sigma^2 + 3\alpha^2 \tau^2}$ $\sigma = \frac{F}{n \cdot a \cdot l}$ $\tau = \frac{F}{2 \cdot a \cdot l}$
	$\sigma_n = \frac{F}{n \cdot a \cdot l}$		$\sigma_n = \frac{6M}{l^2 a}$		$\sigma_b = \sqrt{\sigma^2 + 3\alpha^2 \tau^2}$ $\sigma = \frac{6Fc}{l^2 a}$ $\tau = \frac{3 \times F}{2 \times 2 \cdot a \cdot l}$
	$\sigma_n = \frac{F}{n \cdot a \cdot l}$		$\sigma_n = \frac{6M}{l^2 a}$		$\sigma_b = \sqrt{\sigma^2 + 3\alpha^2 \tau^2}$ $\sigma = \frac{6Fc}{l^2 r}$ $\tau = \frac{3 \times F}{2 \times l \cdot r}$
	$\sigma_n = \frac{F}{n \cdot a \cdot l}$		$\sigma_n = \frac{6M}{l^2 a}$		$\sigma_b = \sqrt{\sigma^2 + 3\alpha^2 \tau^2}$ $\sigma = \frac{6Fc}{l^2 r}$ $\tau = \frac{3 \times F}{2 \times l \cdot r}$
	$\sigma_n = \frac{F}{n \cdot 2 \cdot a \cdot l}$		$\sigma_n = \frac{6M}{l^2 a}$		$\tau = \frac{M(3l + 7.8a)}{l^2 a^2}$
	$\sigma_n = \frac{F}{n \cdot 2 \cdot a \cdot l}$		$\sigma_b = \sqrt{\sigma^2 + 3\alpha^2 \tau^2}$ $\sigma = \frac{3Fc}{l^2 a}$ $\tau = \frac{3 \times F}{2 \times l \cdot a}$		$\tau = \frac{M(3l + 7.8a)}{l^2 a^2}$
	$\sigma_n = \frac{6M}{n \cdot a^2}$		$\sigma_b = \sqrt{\sigma^2 + 3\alpha^2 \tau^2}$ $\sigma = \frac{6Fc}{l^2 a}$ $\tau = \frac{3 \times F}{2 \times l \cdot t}$		$\tau = \frac{M}{2(l-a)(t-a)a}$
	$\sigma_n = \frac{6M}{n \cdot a^2}$		$\sigma_b = \sqrt{\sigma^2 + 3\alpha^2 \tau^2}$ $\sigma = \frac{6Fc}{l^2 a}$ $\tau = \frac{3 \times F}{2 \times l \cdot t}$		$\tau = \frac{M}{2(l-a)(t-a)a}$
	$\sigma_n = \frac{6M}{n \cdot a^2}$				$\tau = \frac{M}{2 \cdot a^2 \left(\frac{\pi(l-d+a)}{32} + \frac{\pi x a^4}{32} \right)}$
	$\sigma_n = \frac{6M}{n \cdot a^2}$				

TABLE 23

"z TO s" LINES FOR WELDED JOINTS

Line	Types of welded joint
z	Parent metal
y	Butt weld, special quality, plate machined smooth
x	Tension-compression specimen with gusset plate burnt out of solid, rounded off Beam with continuous "K" and fillet welds
w	Tension-compression specimen with transverse fillet weld, machined Tension-compression specimen with longitudinal fillet weld, machined Parent metal at the end of a welded-on chamfered strap, transition machined Tension-compression specimen (beam) with gusset plate, welded, rounded off, and machined Butt weld, normal quality, not machined (100 per cent radiography)
v	Tension-compression specimen with transverse fillet weld, not machined Bend test specimen with transverse fillet weld, not machined Beam with welded stiffeners, not machined Tension-compression specimen with longitudinal fillet weld, not machined Bend test specimen with longitudinal fillet weld, not machined Parent metal at the end of a welded-on strap, front fillet weld, transition not machined "K" weld, not machined, free of defects (100 per cent radiography)
u	Parent metal at the end of a welded-on strap, no front fillet weld Butt weld, not machined, vertical or overhead welding, no radiography Beam with non-continuous fillet welds "K" weld, not machined, no radiography Shear, general
t	Tension-compression specimen (beam) with welded-on rectangular gusset plate, not machined Front fillet weld (cross plate), calculated on design cross-section Fillet in parallel shear (fish-plate), calculated on design cross-section
s	Front fillet weld (cross plate), calculated on weld cross-section Fillet in parallel shear (fish-plate), calculated on weld cross-section

TABLE 24

VALUES OF Φ_k FOR STEELS ST 37 (0.15% C STEEL)
AND ST 52 (EN 7 APPROX.)

Line	Value of Φ_k	
	0.15% C steel	En 7 steel
z	1.00	1.00
y	0.90	0.85
x	0.80	0.70
w	0.70	0.58
v	0.60	0.47
u	0.50	0.40
t	0.40	0.30
s	$0.27 \sigma_T$	

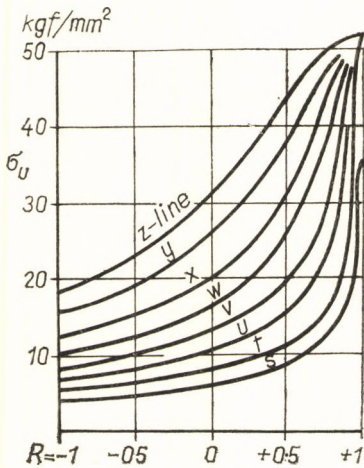


FIG. 106. "z to s" lines for welded joints of St 52 (En 7 approx.)

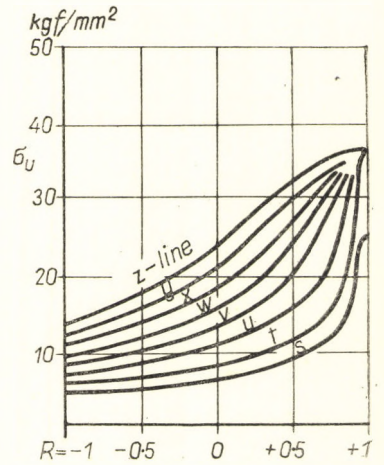


FIG. 105. "z to s" lines for welded joints of St 37 (0.15% C steel)

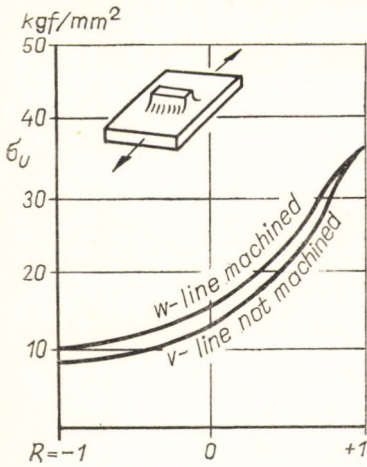


FIG. 107. Transverse weld, St 37 (0.15% C steel) (tension-compression and bending)

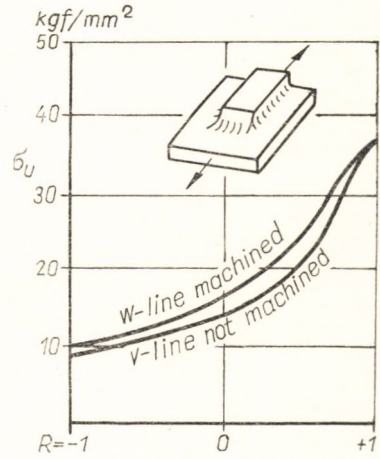


FIG. 108. Welded-on strap (tension compression and bending)

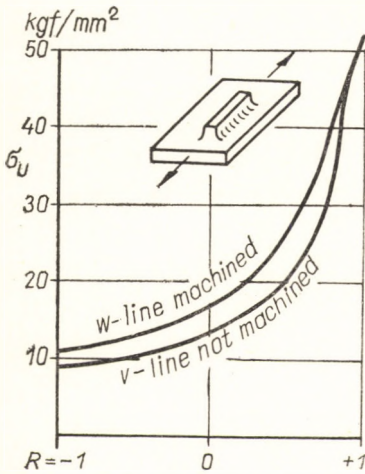


FIG. 109. Longitudinal weld, St 52 (En 7 approx.) (tension-compression and bending)

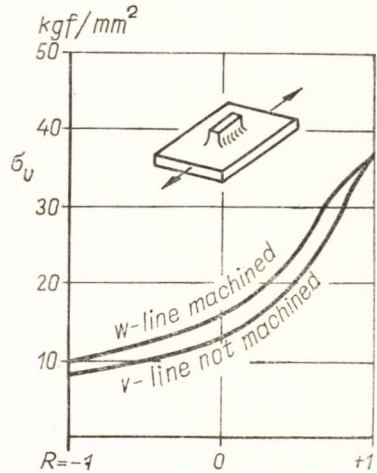


FIG. 110. Longitudinal weld, St 37 (0.15% C steel) (tension-compression and bending)

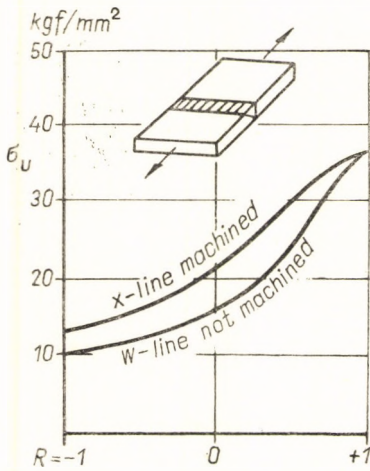


FIG. 111. Butt weld, St 37 (0.15% C steel), horizontal welding, 100 per cent radiography (tension-compression and bending)

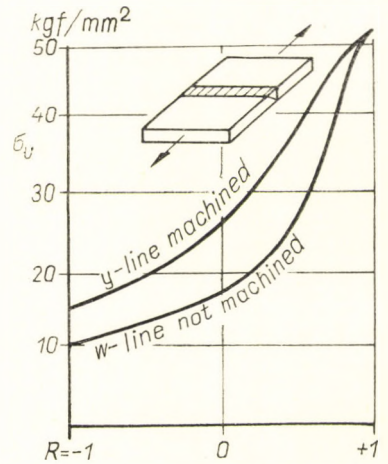


FIG. 112. Butt weld, St 52 (En 7 approx.) horizontal welding, 100 per cent radiography (tension-compression and bending)

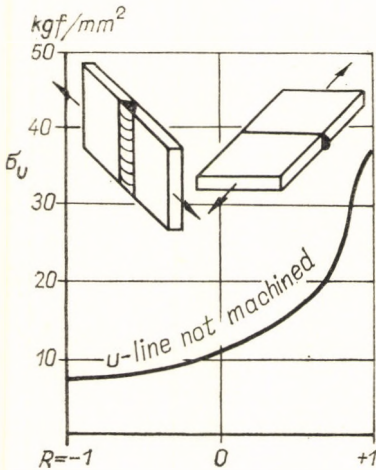


FIG. 113. Butt weld, overhead or vertical welding, St 37 (0.15% C), 100 per cent radiography (tension and compression)

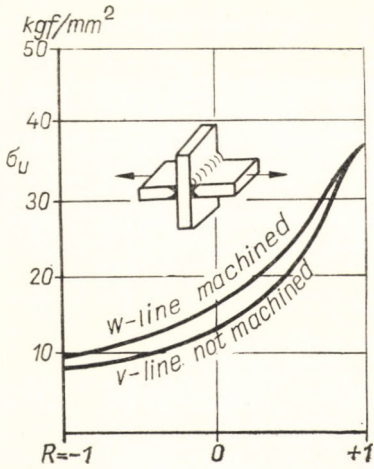


FIG. 114. Cross plate, St 37 (0.15% C steel) (tension and compression)

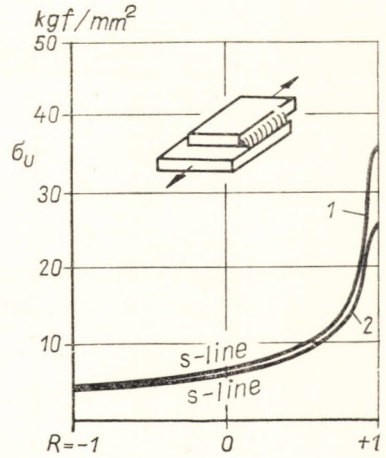


FIG. 115. Front fillet welds, St 37 (0.15% C steel) (tension and compression)
 1 calculated on design cross-section
 2 calculated on weld cross-section

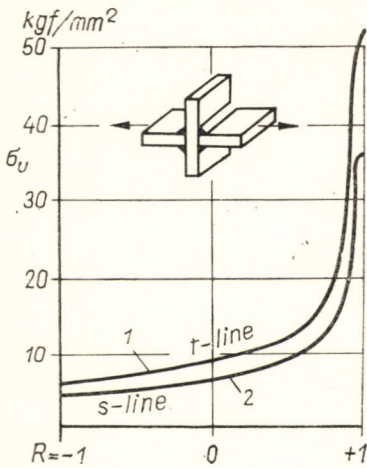


FIG. 116. Front fillet welds, St 52 (En 7 approx.) (tension and compression)
 1 calculated on design cross-section
 2 calculated on weld cross-section

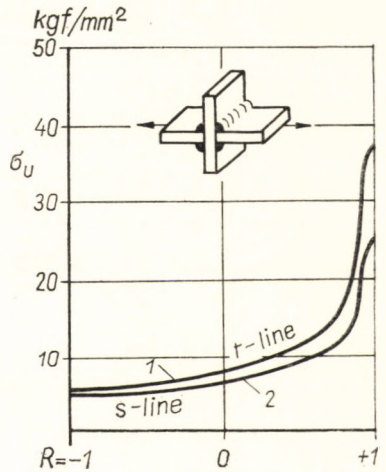


FIG. 117. Fillet welds in parallel shear
 1 St 52 (En 7 approx.) } calculated on design cross-section
 2 St 37 (0.15% C steel) }

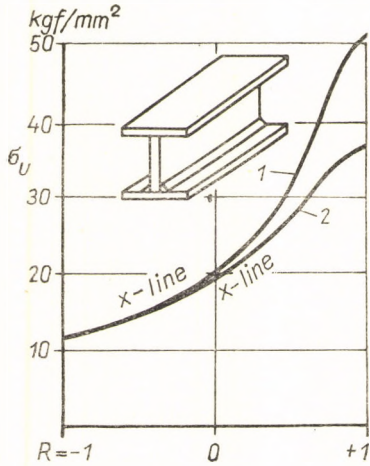


FIG. 118. Continuous fillet welds in beams, not machined, calculated on beam cross-section
 1 St 52 (En 7 approx.)
 2 St 37 (0.15% C steel)

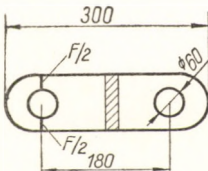
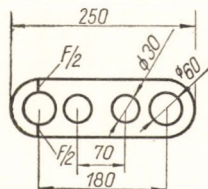
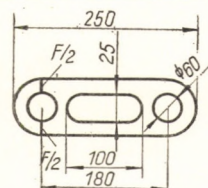
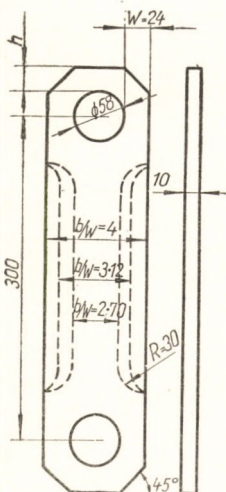
8.7 Plates with holes at each end

TABLE 25

FATIGUE STRENGTH REDUCTION FACTORS
 (THUM AND BRUDER [92]) OF BARS AND VARIOUS SHAPES,
 DRILLED AT BOTH ENDS (BUSH ROLLER CHAIN LINKS).
 LOADING: TENSION-COMPRESSION

Sketch	Material	K_f	Remarks
	St 70.11 (En 9)	3.42	
	St 70.11 (En 9)	2.5	
	St 70.11 (En 9)	2.78	

TABLE 25 (CONT.)

Sketch	Material	K_f	Remarks																																						
	St 70.11 (En 9)	2.48																																							
	St 70.11 (En 9)	3...3.13	The holes are too close, and consequently ineffective for relief																																						
	St 70.11 (En 9)	2.68	The relieving hole makes K_f smaller than in Case 3																																						
	St 42-11 (0.25% C steel) $\sigma_T = 41.2 \text{ kgf/mm}^2$ $\epsilon = 29.8\%$	Values of K_f in "Remarks" column	<p>Values of K_f for hole with sliding fit</p> <table border="1" data-bbox="620 913 1053 1120"> <thead> <tr> <th rowspan="2">b/w</th> <th colspan="3">h/w</th> </tr> <tr> <th>1.92</th> <th>1.58</th> <th>1.00</th> </tr> </thead> <tbody> <tr> <td>4.1</td> <td>2.02</td> <td>2.18</td> <td>2.98</td> </tr> <tr> <td>3.12</td> <td>2.40</td> <td>2.68</td> <td>3.50</td> </tr> <tr> <td>2.7</td> <td>2.58</td> <td>2.94</td> <td>3.95</td> </tr> </tbody> </table> <p>Values of K_f for 1 mm clearance between pin and hole</p> <table border="1" data-bbox="620 1236 1053 1442"> <thead> <tr> <th rowspan="2">b/w</th> <th colspan="3">h/w</th> </tr> <tr> <th>1.92</th> <th>1.58</th> <th>1.00</th> </tr> </thead> <tbody> <tr> <td>4.1</td> <td>2.45</td> <td>—</td> <td>2.98</td> </tr> <tr> <td>3.12</td> <td>2.55</td> <td>—</td> <td>3.40</td> </tr> <tr> <td>2.7</td> <td>2.51</td> <td>—</td> <td>3.68</td> </tr> </tbody> </table>	b/w	h/w			1.92	1.58	1.00	4.1	2.02	2.18	2.98	3.12	2.40	2.68	3.50	2.7	2.58	2.94	3.95	b/w	h/w			1.92	1.58	1.00	4.1	2.45	—	2.98	3.12	2.55	—	3.40	2.7	2.51	—	3.68
b/w	h/w																																								
	1.92	1.58	1.00																																						
4.1	2.02	2.18	2.98																																						
3.12	2.40	2.68	3.50																																						
2.7	2.58	2.94	3.95																																						
b/w	h/w																																								
	1.92	1.58	1.00																																						
4.1	2.45	—	2.98																																						
3.12	2.55	—	3.40																																						
2.7	2.51	—	3.68																																						

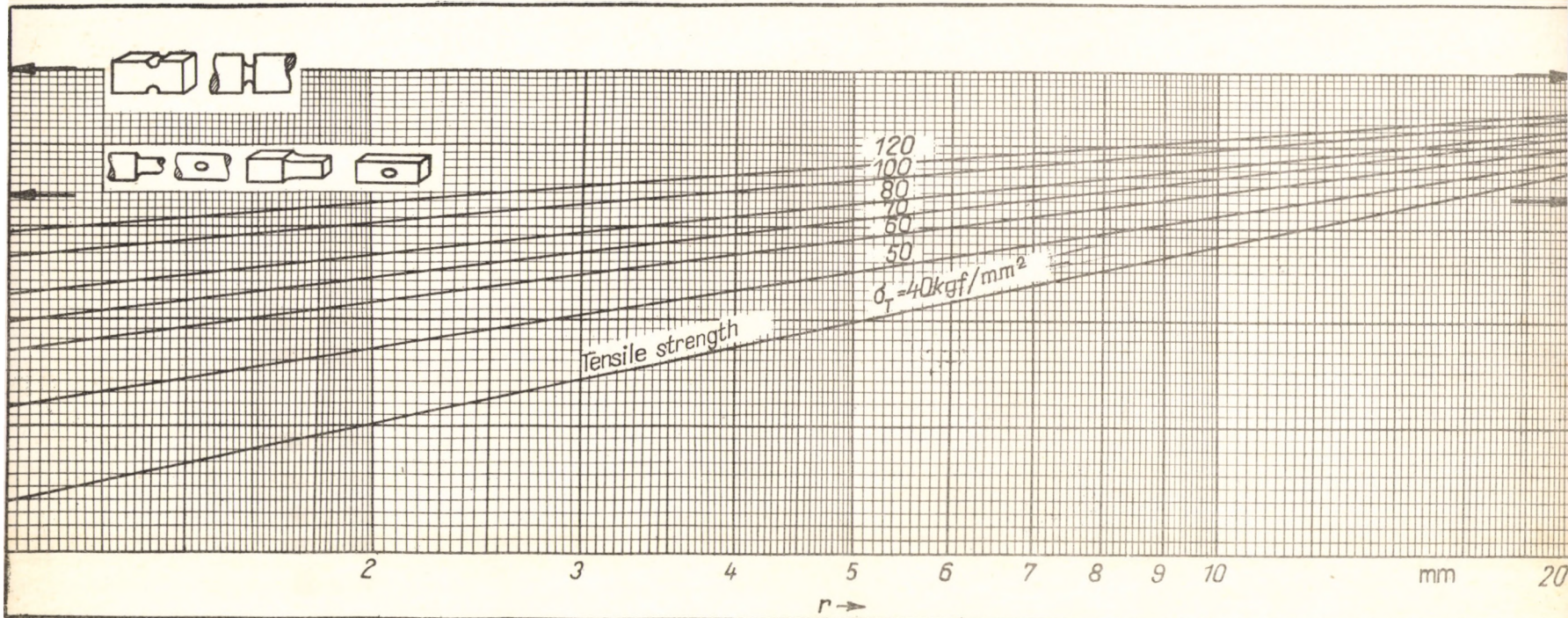


FIG. 88. Movable nomogram for use in conjunction with Figs. 68 to 87

